# Petrology and Provenance of the Upper Cretaceous Strata in Central Utah

**Mette Lundberg**

Thesis for Master degree in Geodynamics


Department of Earth Science

University of Bergen

2015

# ABSTRACT

The reservoir quality of sandstones is primarily controlled by the primary composition of the rock volume and the effects of later diagenetic processes. Much work has been done to improve the understanding of diagenetic processes, but the controls and influence of primary composition has not been studied as extensively. The objective of this thesis is to use the world-class exposures and stratigraphic framework of the Mesaverde Group in the Wasatch Plateau and Book Cliffs, Utah, USA to investigate how petrological properties vary temporarily and spatially within a paralic clastic wedge.

Sandstone composition, porosity and permeability have been studied through thin section analysis and in-field permeability measurements. The results were analysed based on facies associations, and stratigraphic and lateral position in the basin.

Results show that the facies association is the dominant control on the composition, especially within wave-dominated shallow marine sandstones. The proportion of carbonate grains and carbonate-cement increase palaeoseaward, while the proportion of quartz-cement and porosity decrease along with permeability. Cluster analysis shows that the carbonate grains and carbonate-cements have a high positive correlation, which indicates that the amount of carbonate-cement formed in the samples is primarily related to the amount of detrital carbonate grains. Further, the analyses of the point counting results indicate that carbonate-cement rather that quartz-cement is the controlling factor on reservoir quality of these sandstones, as the maximum burial depth was too low for extensive quartz cementation to develop. Samples with a high amount of carbonate cement typically exhibit poor reservoir quality.

Lateral variations in composition within one parasequence, the Kenilworth K4 parasequence of the Kenilworth Mb., were also investigated in this study, and the results indicate no lateral variation in the sandstone composition over the 60 km long and 60 km wide study area. This represents effective redistribution of sediments along the shoreline, together with lateral homogeneity in the source area.

Temporal variations on composition can also be recognised in this study. The strongest variation occurs within the Panther Tongue Mb. This member is distinct from the other members with a high proportion of chert, which implies an abrupt change in provenance during the deposition of this unit. Another significant stratigraphic trend is seen in the amount of detrital carbonate content in the Mesaverde Group. The content is gradually decreasing upwards in the stratigraphy from the Storrs Mb. of the Star Point Fm. to the Castlegate Mb. of the Price River Fm. This indicates a gradual change in provenance over time.

# ACKNOWLEDGEMENTS

This thesis is a part of a Master Degree in geodynamics at the University of Bergen, to which I owe gratitude for funding my field work.

First of all, I would like to express my gratitude for being introduced to this exciting project by my supervisor Professor John Anthony Howell. He is especially thanked for guidance in the field and for his review of my thesis. My co-supervisor, Professor Haakon Fossen is also thanked for arranging the administrative parts of this thesis.

I would like to express my profound appreciation to Christian Haug Eide who has given me valuable advice, knowledge and inspiration through the course of this thesis. He is also thanked for editing the manuscript and providing constructive criticism.

Romain Meyer is thanked for his help showing the operations of the point-counter.

My field assistant, Margrethe Bøyum, is thanked for taking time out of her busy schedule to help out during my field work.

I would like to thank my family and friends for all their support and encouragement during the five years I have spent at the University. A special thanks to my dear friends in "Chalcopyrite" (Merethe, Heidi Synnøve, Elin, Heidi Ims, Andreas, Fredrik and Thomas). Fellow students at the University and at "Hovedkarteret" are also thanked for making these years fly by.

Finally, a very special thanks to my boyfriend Jostein, for his help and support during my Master Degree. Especially in the last few weeks prior to the deadline, you have been essential.

Mette Lundberg

Bergen, June 2015

# CONTENTS


1 Introduction ..... 1
1.1 Aim of study ..... 1
1.2 Study Area ..... 2
1.2.1 Book Cliffs ..... 3
1.2.2 Wasatch Plateau ..... 3
2 Geological Background ..... 5
2.1 Tectonic History and Palaeogeography ..... 5
2.1.1 Sevier Orogeny ..... 7
2.1.2 Laramide Orogeny ..... 10
2.2 Sedimentology and Palaeoclimate ..... 10
2.2.1 Palaeoclimate ..... 10
2.2.2 Mesozoic Sedimentology- A summary ..... 10
2.3 Late Cretaceous Stratigraphy and Sedimentology ..... 12
2.3.1 The Mancos Shale Formation ..... 15
2.3.2 The Star Point Formation ..... 19
2.3.3 The Blackhawk Formation ..... 20
2.3.4 Price River Formation ..... 24
2.3.5 Controls on the stratigraphic architecture ..... 26
2.4 Provenance of Late Cretaceous sediments ..... 27
3 Methods ..... 29
3.1 Field Work ..... 29
3.1.1 Sampling and sampling strategy ..... 29
3.1.2 Outcrop sedimentology – Sedimentary logging ..... 29
3.1.3 TinyPerm II measurements ..... 30
3.2 Laboratory Work ..... 34
3.2.1 Microscopy Lab – Mineral description ..... 34
3.2.2 Microscopy Lab – Point counting ..... 37
3.2.3 Laboratory for Electron Microscopy – (SEM) ..... 39
3.3 Statistical Methods ..... 40
3.3.1 Analysis of multivariate populations – Cluster analysis ..... 40
4 Sedimentology ..... 41

4.1 Facies and Facies Associations ..... 41
4.1.1 Facies Association A – Shelf Turbidites (ST) ..... 41
4.1.2 Facies Association B – Offshore mud (OS) ..... 43
4.1.3 Facies Association C – Distal delta front (dDF) ..... 43
4.1.4 Facies Association D – Proximal delta front (pDF) ..... 44
4.1.5 Facies Association E – Mouth bar (MB) ..... 46
4.1.6 Facies Association F – Distributary Channel fill (DC) ..... 46
4.1.7 Facies Association G – Transgressive lag (LAG) ..... 48
4.1.8 Facies Association H – Offshore transition zone (OTz) ..... 49
4.1.9 Facies Association I – Lower shoreface deposits (LSF) ..... 50
4.1.10 Facies Association J – Middle shoreface deposits (MSF) ..... 51
4.1.11 Facies Association K – Upper shoreface deposits (USF) ..... 52
4.1.12 Facies Association L – Foreshore deposits (FS) ..... 53
4.1.13 Facies Association M – Lagoonal deposits (CP/L) ..... 54
4.1.14 Facies Association N – Mire and peat swamp coal (C) ..... 54
4.1.15 Facies Association O – Meandering channel fill (MC) ..... 55
4.1.16 Facies Association P–Crevasse splay, floodplain (CS/F) ..... 56
4.1.17 Facies Association Q – Braided channel bar (BC) ..... 57
4.2 Depositional Systems ..... 58
4.2.1 Offshore mud and Shelf turbidites ..... 58
4.2.2 Wave-dominated shoreface shallow marine systems ..... 58
4.2.3 River-dominated deltaic depositional system ..... 59
4.2.4 Coastal plain depositional system ..... 60
4.2.5 Alluvial plain depositional system ..... 60
5 Results ..... 61
5.1 Description of Formations and Members ..... 63
5.1.1 Mancos Shale Formation ..... 63
5.1.2 Star Point Formation ..... 71
5.1.3 Blackhawk Formation ..... 76
5.1.4 Price River Formation ..... 84
5.2 Permeability data ..... 86
5.3 Petrographic data ..... 90
5.3.1 Electron microscope - SEM data ..... 94
6 Analysis of results ..... 103

6.1 Cluster Analysis ..... 103
6.2 Analysis by facies associations and stratigraphic position ..... 105
6.2.1 Analysis of results by facies associations ..... 107
6.2.2 Analysis of results by stratigraphic units ..... 112
6.3 Lateral variation within a member ..... 119
6.3.1 Kenilworth Mb. ..... 119
7 Discussion ..... 121
7.1 Trends controlled by Facies associations ..... 121
7.1.1 Petrographic and petrophysical trends ..... 121
7.1.2 Trends within depositional environments ..... 125
7.2 Trends controlled by stratigraphic units ..... 130
7.2.1 Mancos Shale Fm. ..... 130
7.2.2 Star Point Fm.: Panther Tongue Mb. ..... 130
7.2.3 Blackhawk Fm. and Castlegate Mb. ..... 132
7.3 Lateral change within the Kenilworth Mb. ..... 134
7.4 Summary ..... 135
7.4.1 Facies association controls ..... 135
7.4.2 Stratigraphic controls ..... 136
7.5 Further work ..... 139
7.5.1 Studies on the collected samples ..... 139
7.5.2 Further field study ..... 140
8 Conclusions ..... 141
9 References ..... 143
Appendix I ..... 151
Tables ..... 151
Appendix II ..... 177
Figures ..... 177
Appendix III ..... 181
Thin section photos and SEM results ..... 181

# 1 INTRODUCTION

## 1.1 AIM OF STUDY

The Book Cliffs and the Wasatch Plateau, located in east-central Utah, contain extensive high quality outcrops that stretch for hundreds of kilometres. The sandstones exposed in these outcrops are amongst the most well-studied and well-understood examples of sedimentary rocks in the World, and a large number of stratigraphic and sedimentological studies have been undertaken (e.g. Young, 1955; Balsley, 1980; Van Wagoner et al., 1990; Van Wagoner, 1995; Edwards et al., 2005; Pattison et al., 2007; Bhattacharya and MacEachern, 2009; Hampson, 2010; Olariu et al., 2010; Deveugle et al., 2011; Hampson et al., 2014 and numerous others). The Late Cretaceous units are commonly used as analogues for numerous subsurface petroleum reservoirs such as the paralic deposits of the Gulf of Mexico, the Niger Delta,the Brent Group and and many others (Howell and Flint, 2003; Olariu et al., 2010; Holgate et al., 2014).

Previous studies have contributed to a robust stratigraphic framework and good understanding of the facies architecture, but very little research has focused on the petrography or provenance of the sedimentary rocks. This provides an excellent opportunity to ask questions about what controls mineralogy and petrophysical properties in these systems, especially the importance of facies associations (depositional environments) versus provenance changes. It also provides an opportunity to investigate the sediment routing to the clastic wedge.

In this study, petrographic composition, porosity and permeability in sandstones have been compared for eight stratigraphic intervals and the related facies associations. Field work was carried out during 4 weeks in May and June 2014. Rock samples were collected and in-field permeability measurements were taken. The collected samples were later analysed using the petrographic microscope and SEM at the University of Bergen.

The aims of this study are fourfold: to (1) examine if there are facies association controls on the petrographic content and petrophysical parameters; (2) to examine if parts of the petrographic content and the petrophysical parameters varies between the stratigraphic units; (3) to examine if the lateral position in the basin affected the petrographic content, and (4) to discuss possible mechanisms responsible for these variations.

## 1.2 STUDY AREA

The study area is located in the central/south-eastern part of Utah, within Carbon, Sanpete, Emery and Sevier counties. It covers more than 10 000 km$^2$, and consists of Late Cretaceous rocks. These rocks are well exposed in escarpments along the Wasatch Plateau and the Book Cliffs, which surround the San Rafael Swell (**Fig. 1.1**). The age of these rocks ranges from the Turonian for the Ferron Sandstone to Campanian for the Castlegate Sandstone (e.g. Young, 1955; McLaurin and Steel, 2007; Bhattacharya and MacEachern, 2009)


**Fig. 1.1:** The study area is situated in central and southeastern Utah. The dashed lines represent the cliff escarpments of the Book Cliffs and the Wasatch Plateau. Satellite images © Google 2015.

### 1.2.1 BOOK CLIFFS

The NNW-SSE trending Book Cliffs are approximately 300 km long and extends from Helper in eastern Utah to Grand Junction in western Colorado. The cliffs consist of Late Cretaceous (Santonian–Campanian) deposits, and the thickness varies from 300 m to 600 m. The Star Point Fm., Blackhawk and Price River Fm. are exposed in these cliffs (**Fig. 1.2**) (e.g. O'Byrne and Flint, 1993; Pattison, 1995; Van Wagoner, 1995; Howell and Flint, 2003; North et al., 2005). The strata dip shallowly toward the north and east, depositional dip was primarily towards the east and the deposits were laid down on a ramp type margin with no shelf break. (Howell and Flint, 2003).

### 1.2.2 WASATCH PLATEAU

The Wasatch Plateau is located in south-central Utah, southwest of Price. The plateau represents the northeastern part of the High Plateaus of Utah, and surrounds the eastern flank of the San Rafael Swell. The Wasatch Plateau is located south and west of the Book Cliffs. Proximal deposits of the Blackhawk Fm., sandstone members of the Star Point Fm. and Mancos Shale Fm. are superbly exposed in the eastern cliffs of the Wasatch Plateau (**Fig. 1.2**) (e.g. Spieker and Reeside, 1925; Spieker, 1931; Young, 1955; Newman and Chan, 1991).

The Mancos Shale is much more susceptible to erosion than the intertonguing sand bodies, and the extensive lowland areas in eastern Utah are a result of erosion down to this level. The escarpments of the Wasatch Plateau and the Book Cliffs are primarily a result of river erosion of marine sandstone and mudstone of Cretaceous age (Stokes, 1986; Hintze, 2005).

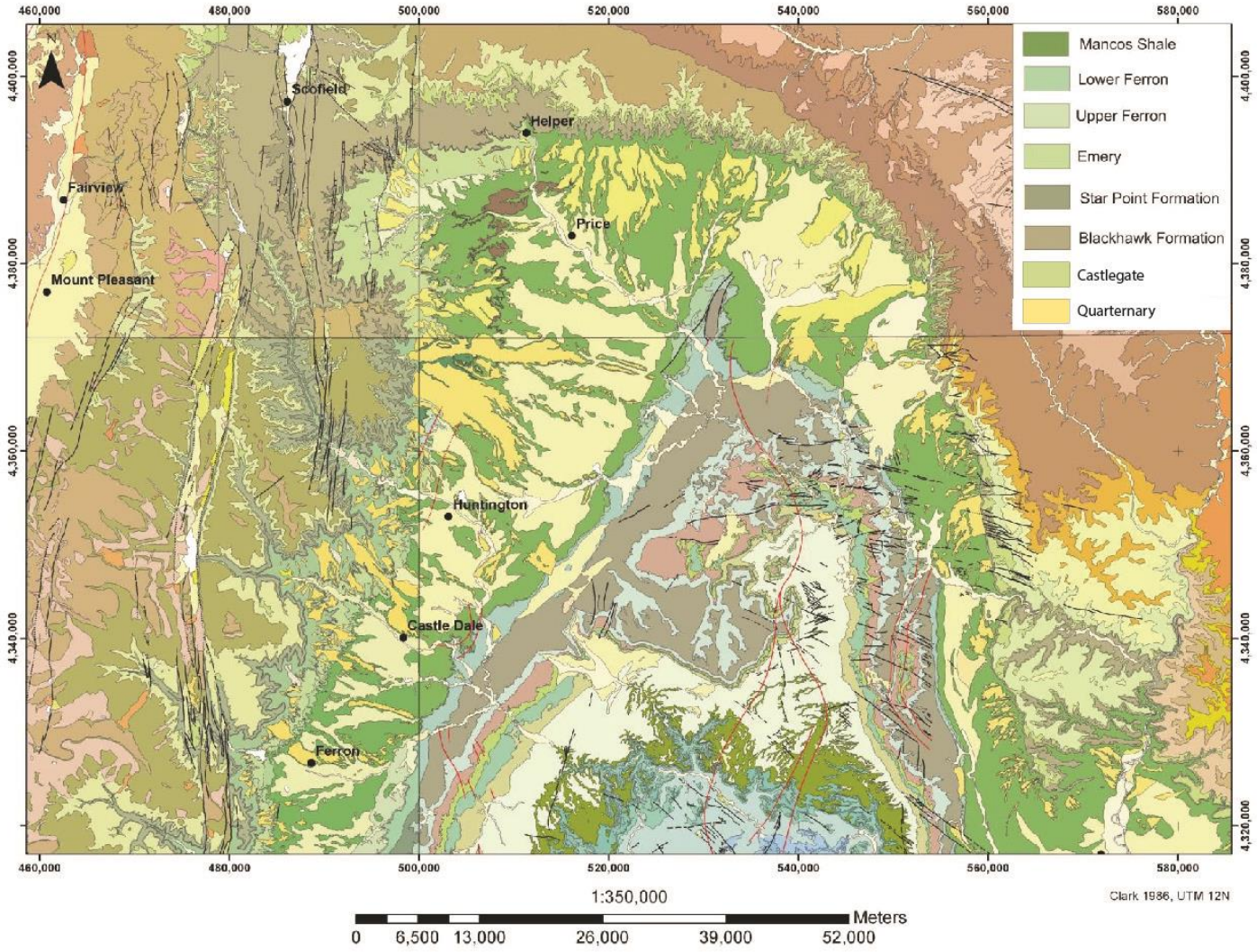


**Fig. 1.2:** Geological map of the study area, from Geological survey of Utah, edited by Knudsen (2008).

# 2 GEOLOGICAL BACKGROUND

## 2.1 TECTONIC HISTORY AND PALAEOGEOGRAPHY

During the Triassic the supercontinent of Pangea started to break up. The North American Plate separated from Europe and Africa, and started to drift towards the west. The area that is now the Colorado Plateau lay slightly above sea level through the Triassic and Jurassic (Blakey and Ranney, 2008). During the Jurassic subduction was initiated in the area that is now California, and the Pacific Farallon Plate was forced below the North American Plate creating the Cordilleran retroarc fold and thrust belt on the western margin of North America (Howell and Flint, 2003; DeCelles, 2004). This orogenic belt stretched over 6,000 km from Southern Mexico to Arctic Canada (DeCelles, 2004). The Sevier Orogeny is considered as a frontal segment of the larger Cordillerian retroarc fold and thrust belt (**Fig. 2.1**).

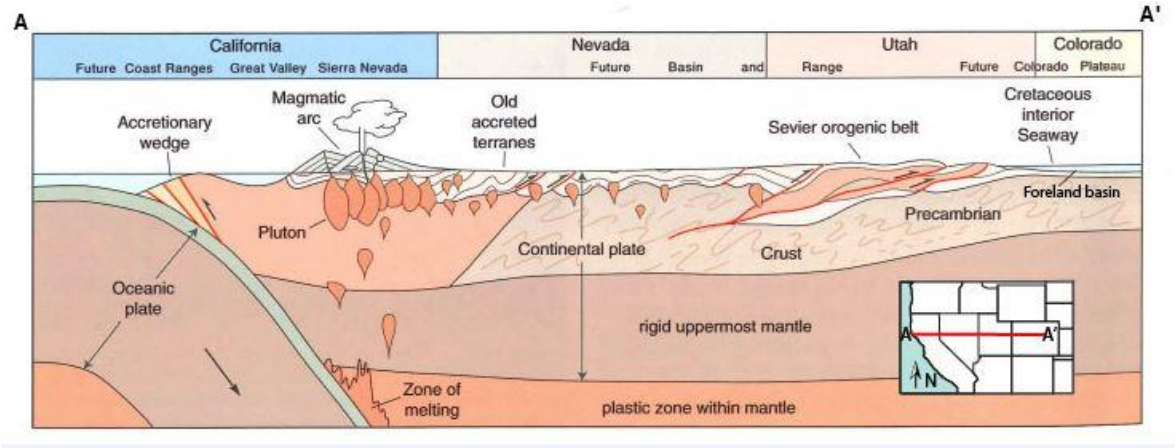


**Fig. 2.1:** The subduction zone in the west, caused uplift of the western region of the North American Plate and the formation of the fold and thrust belt known as the Sevier Orogeny. Note the foreland basin that formed in eastern Utah and Colorado as a result of subsidence due to the western uplift. This basin was flooded forming the Cretaceous interior Seaway. Figure from Hintze (2005).

A regional unconformity between Jurassic and Cretaceous deposits represents an early Cretaceous uplift with slow sedimentation rates and erosion of the Jurassic strata. The uplifted areas were located south and west of the Wasatch line. The Wasatch line represents the western edge of the Colorado Plateau. This line has also represented the collapsed Basin and Range Province's eastern margin since middle Cenozoic times. Along this line some of North America's longest faults have been mapped (Stokes, 1986; Blakey and Ranney, 2008) , see section 2.1.1.

The Sevier Orogeny reached its maximum intensity during the Late Cretaceous, about 80 Ma (Blakey and Ranney, 2008). The maximum deformation was along or west of the Wasatch Line (Stokes, 1986).The uplift in the west caused subsidence of the Colorado Plateau region in the east, and a foreland basin developed (Blakey and Ranney, 2008). A cross-section through the western North America during this time is shown in **Fig. 2.1**.

As a result of subsidence combined with an increase in eustatic sea-level the Western Interior Seaway formed (Blakey and Ranney, 2008). The sea flooded the North American continent from both the north and south creating and epi-continental seaway (**Fig. 2.2**). West of the seaway comprised a tectonically active and growing mountain belt. This land area was younger than the inactive lowlands to the east (Hintze, 2005). The flooding of Utah was enabled by the erosion of the Ancestral Rockies, and Utah was flooded mainly from the east (Stokes, 1986). The Western Interior Seaway covered large areas (**Fig. 2.2 A & B**), at most it reached from the Gulf of Mexico in the south to Alaska and Arctic Canada in the north. It had a width of 700- 1200 km (Kauffman, 1984; Hampson and Howell, 2005). The interior seaway withdrew at the end of the Cretaceous due to a combination of falling global sea-levels, uplift and filling with clastic sediment (**Fig. 2.2 C & D)** (Stokes, 1986).

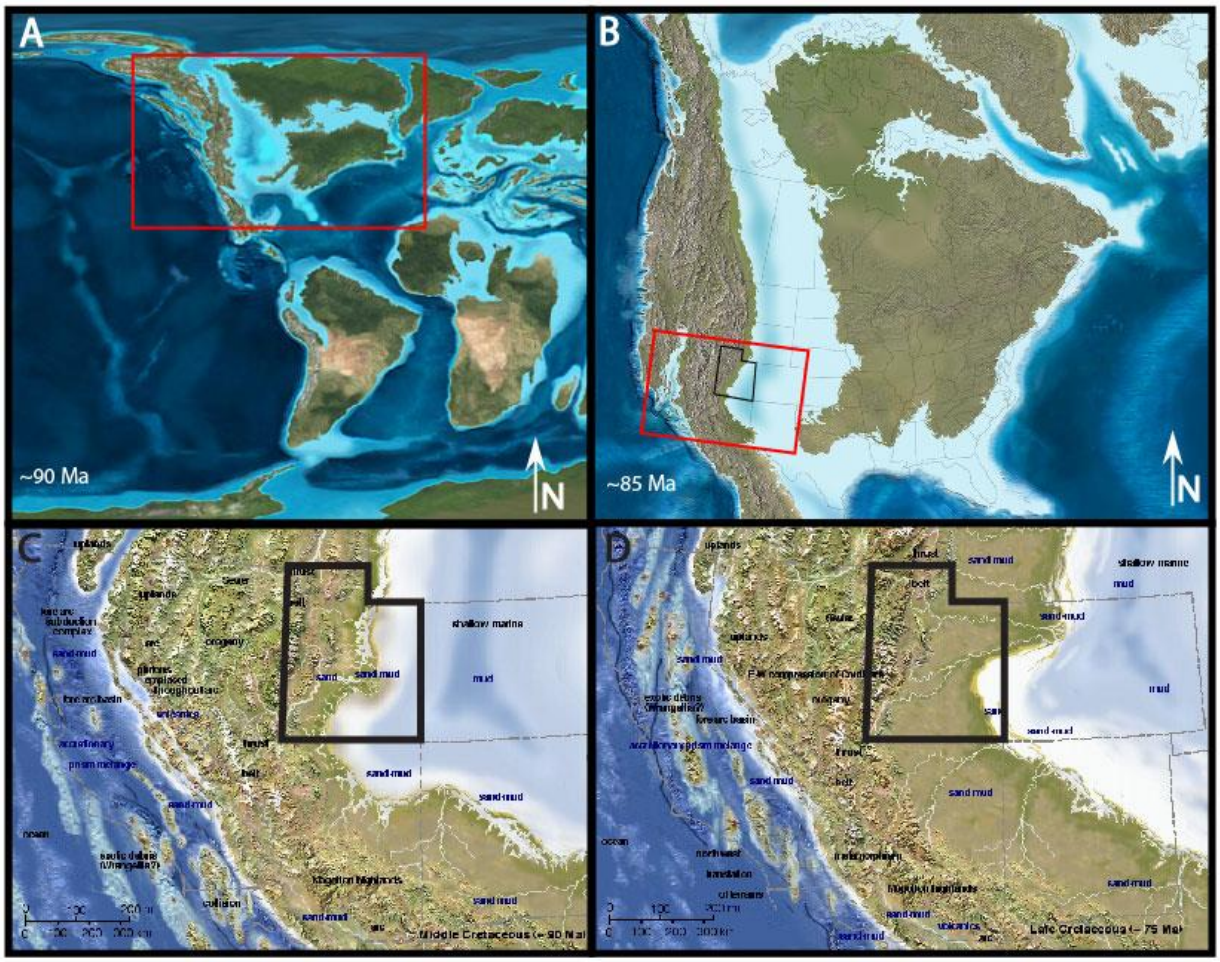


**Fig. 2.2:** The North American Plate during the Late Cretaceous (90-75 Ma). The red boxes represent the area for the following map, and Utah is marked with a black outline. A) A palaeogeographic World map from the Turonian (~90 Ma). B) The Western Interior Seaway (WIS) in the Santonian (~85 Ma). The seaway divided the North American continent in two. The western part comprised the Sevier Orogen. C) Southwestern USA during the Turonian (~90 Ma), sediments prograded eastward into the WIS. D) Southwestern USA during the Campanian (~75 Ma), the shoreline has gradually retreated during the Late Cretaceous. Maps from Blakey (2011).

### 2.1.1 SEVIER OROGENY

The Sevier orogenic belt stretches from Nevada into northwestern Canada and consists of numerous folds and thrust faults (**Fig. 2.3 A)** (DeCelles and Coogan, 2006). During Early Cretaceous mega-thrusting of Proterozoic to Palaeozoic rocks occurred within the Sevier Orogeny. Followed by multiple and more closely spaced thrusting of Palaeozoic to Mesozoic rocks during Late Cretaceous/ Palaeocene (DeCelles, 2004).

The Sevier Orogeny in north- central Utah was dominated by the Charleston-Nebo salient, a westward-oriented, triangular protrusion of the orogenic front. This major eastward curving salient comprises clastic and carbonate rocks of the Pennsylvanian-Permian Oqurrim Group (DeCelles, 2004; Horton et al., 2004). Several thrusts bound this salient, the Charleston thrust

in the north, the Nebo thrust in the south and the eastern part of the salient is bound by several unnamed thrusts in the frontal triangle zone of Jurassic and Cretaceous rocks. West of the Charleston-Nebo salient the Sheeprock, Tintic Valley, Stockton and Midas thrusts are recognised (DeCelles, 2004; Horton et al., 2004). The location of these thrusts is shown in **Fig. 2.3 B**.

The Charleston-Nebo salient also carried Precambrian basement rocks as well as the Oqurrim Group. The Sheeprock thrust sheet comprises sedimentary rocks from Proterozoic, and Palaeozoic rocks which are also found within the Tintic Valley-, Stockton- and Midas- thrust systems (DeCelles, 2004; Horton et al., 2004).

In south-central Utah the Sevier Orogeny can be divided into four major trust complexes: the Canyon Range- (~145-110 Ma), Pavant- (~110-86 Ma), Paxton (~86-75 Ma) and Gunnison- (~75-65 Ma) thrust systems (**Fig. 2.3 B**). The Canyon Range thrust system comprises a ~12 km thick series of sedimentary rocks. The age of these rocks varies from Neoproterozoic to Triassic. The other three thrust- systems comprise Lower Cambrian to Cretaceous rocks (DeCelles, 2004; DeCelles and Coogan, 2006). The Canyon Range thrust- system has often been considered as the dominant factor for sediment supply during the shortening of the Sevier belt (DeCelles and Coogan, 2006).

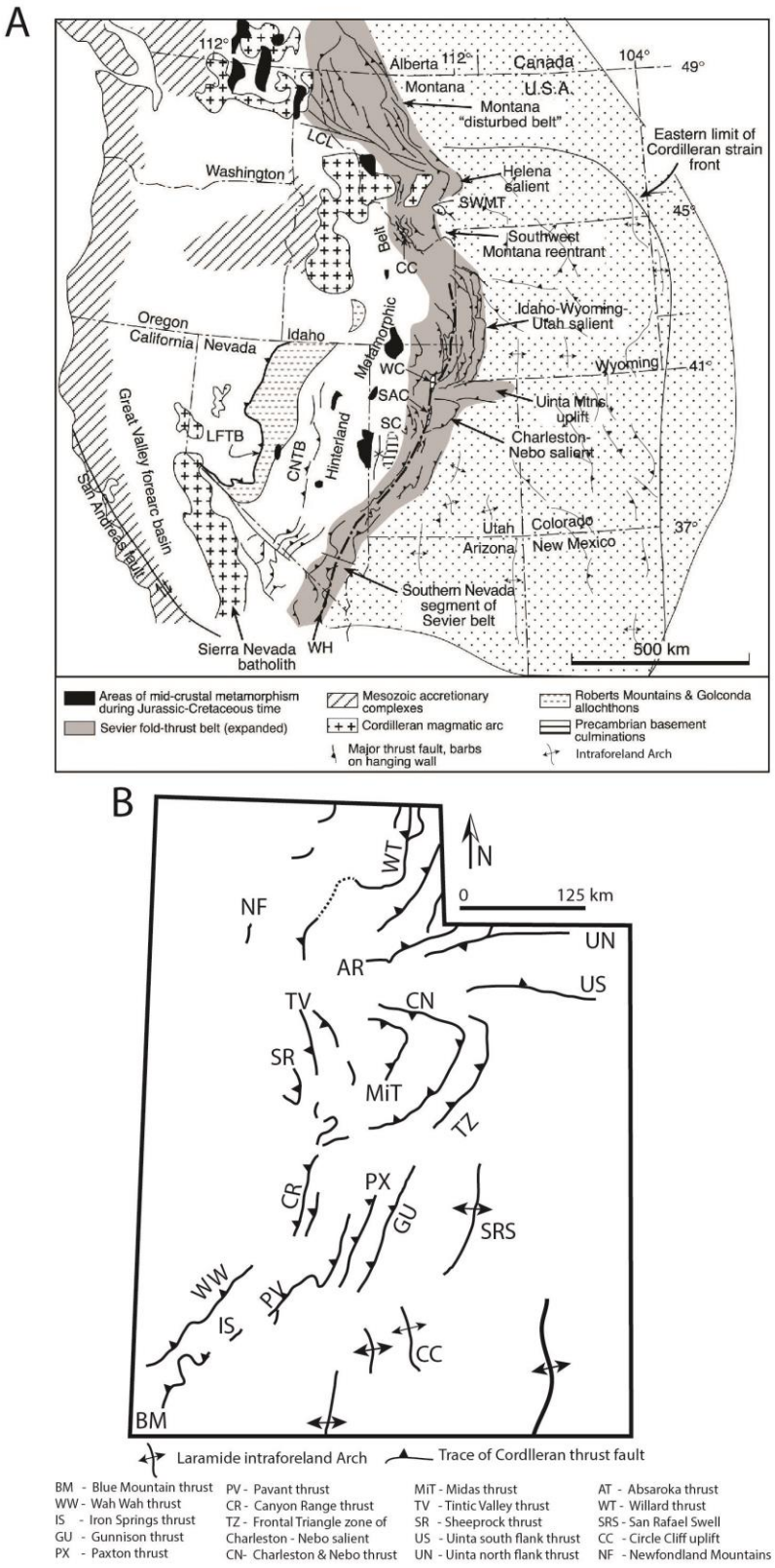


**Fig. 2.3: A)** Illustration of some of the major tectonic features in the Cordilleran retroarc fold and thrust belt, showing the Sevier thrust belt as a segment of the larger Cordilleran retroarc fold and thrust belt. From DeCelles (2004) **B)** Illustrating major tectonic structures of the Cordilleran retroarc fold and thrust belt in Utah. Abbreviations are explained below the figure. Modified from DeCelles (2004).

### 2.1.2 LARAMIDE OROGENY

The Laramide Orogeny is also referred to as the Rocky Mountain Orogeny. This event mainly impacted areas east of the Wasatch Line, and involved the uplift of the Uinta Mountains and a series of intraforeland structures, such as the San Rafael Swell (Stokes, 1986; Horton et al., 2004). Crystalline basement was uplifted along steeply dipping reverse faults creating this orogeny (Armstrong, 1968). At this time a wedge of asenosphere percolated between the sinking plate and the lithospheric base, resulting in a isostatic rebound of the crust. This rebound in the wide spread, regional uplift that is typical of the Laramide orogeny (Cross and Pilger Jr., 1978).

## 2.2 SEDIMENTOLOGY AND PALAEOCLIMATE

### 2.2.1 PALAEOCLIMATE

The climate in Early and Middle Jurassic times was very dry, and the study area was covered by a desert (Blakey and Ranney, 2008). During the Cretaceous the climate changed from arid to gradually more humid with greenhouse conditions. Central Utah had throughout Late Cretaceous times a subtropical climate and a palaeolatitude of approximately 42°N (Howell and Flint, 2003; Blakey and Ranney, 2008)

### 2.2.2 MESOZOIC SEDIMENTOLOGY- A SUMMARY

The Triassic and Jurassic sedimentary systems were predominantly arid continental with minor marine incursions from the west. The Early and Middle Jurassic deposits are characterised by aeolian dunes of the Entrada and Navajo sandstones interbedded with arid fluvial systems such as the Kayenta and Morrison formations developed during wetter periods (Blakey and Ranney, 2008). Early Cretaceous deposits are minor in comparison to their Late Cretaceous counterparts. The majority of the Cretaceous succession was deposited during the Late Cretaceous (Stokes, 1986). The Early Cretaceous rocks are very coarse grained fluvial deposits of the Cedar Mountain Formation which pass upward into the estuarine deposits of the Dakota Formation which represent the onset of marine conditions (Joeckel et al., 2005; Stikes, 2007). The rapid erosion of the Sevier Orogeny during the Late Cretaceous resulted in large volumes of sediment being supplied to the prograding wedge on the western side of the Interior Seaway (Stokes, 1986). The sedimentology and stratigraphy of the Late Cretaceous deposits are described in more detail in the sections below. A satellite image of present-day

Utah and a modern analogue for the Late Cretaceous depositional environment are shown in **Fig. 2.4.** These photos illustrate how the topography and environment has changed in Utah from Late Cretaceous times. The architectural relationship between the mountains in the source area and the coastline during the Late Cretaceous deposition was probably similar to the Costa de Nayarit, even though the Costa de Nayarit represents a peripheral foreland basin, while the Western Interior Sea represents a retro-arc foreland basin.

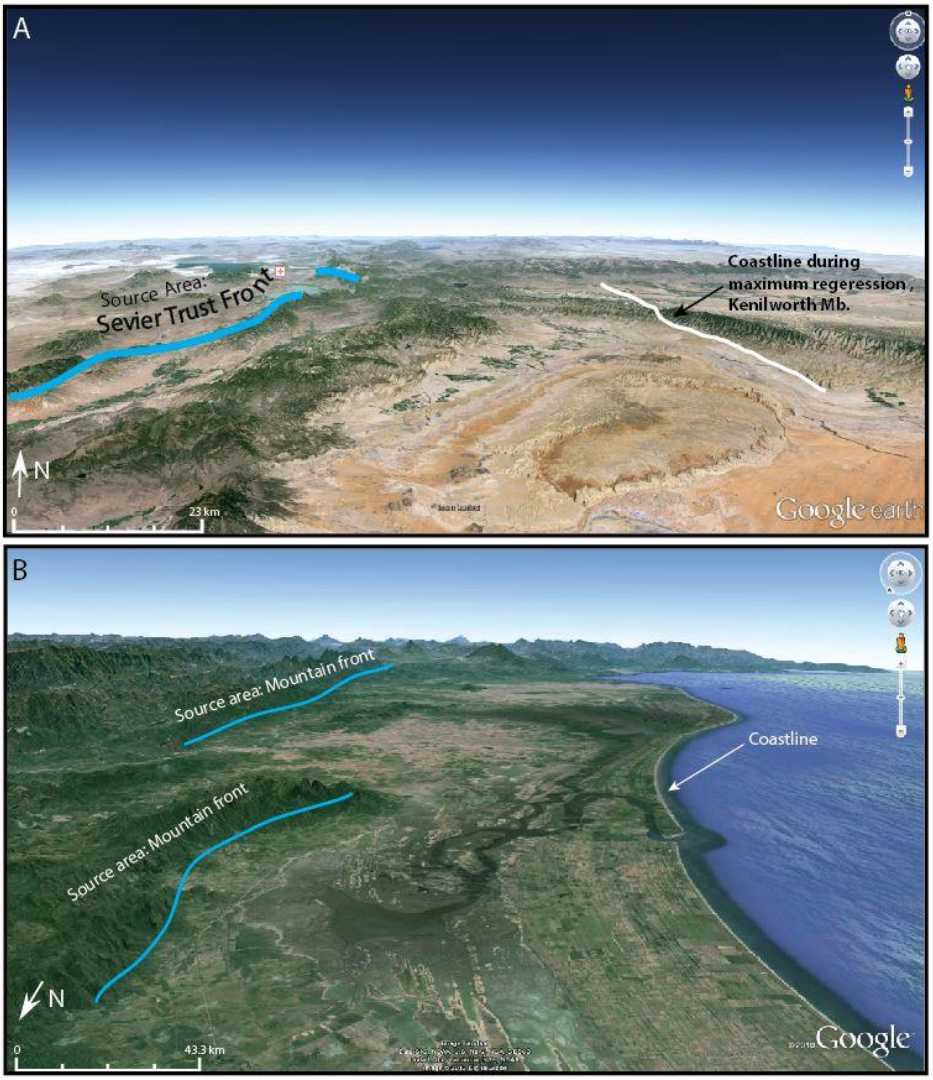


**Fig. 2.4: A)** A satellite photo of the study area in southeastern Utah. The main image shows the San Rafael Swell, a Laramide uplift. The centre of the anticline is Triassic and Jurassic deposits. The Swell is rimmed by Cretaceous offshore deposits which pass upward into shallow marine and coastal plain deposits which make up the Wasatch Plateau in the west and the Book Cliffs in the east. The approximate position of the Sevier Thrust front is marked by the blue line. The white line represents the approximate position of the coastline during the maximum regression of the Kenilworth Mb. **B)** .A modern day analogue for the Late Cretaceous depositional systems of Utah. This satellite image is from Costa de Nayarit in Western Mexico, showing a wave-dominated shoreline located relative close to the sediment source in the adjacent mountain belt. The architectural relations are similar, despite the fact that the Costa de Nayarit represents a peripheral foreland basin, while the Western Interior Sea represents a retro-arc foreland basin. Satellite photos © Google 2015

The present-day topography (**Fig. 2.4 B**) was formed during the late Cenozoic Era. Stream erosion cut down into the uplifted plateau as a result of the gradient difference between the uplifted area and the down-faulted neighbouring areas south and west of the plateau (Blakey and Ranney, 2008). The Monument Uplift, the San Rafael Swell and the Canyonlands landscape in south-eastern Utah, were created by the Colorado River and its tributaries. The rivers have removed all the Cretaceous strata from these uplifts (Hintze, 2005).

## 2.3 LATE CRETACEOUS STRATIGRAPHY AND SEDIMENTOLOGY

The Cretaceous Stratigraphy in Utah consists of clastic sedimentary rocks. Sediments were eroded from the active Sevier Orogeny in the west and deposited eastward into the Western Interior Basin (Stokes, 1986). The eastward movement of the shoreline trajectory through time was a result of sediments prograding into the basin, and the basin fill sediments became progressively non- marine upwards in the stratigraphy (**Fig. 2.5**) (Howell and Flint, 2003).

The stratigraphic units range in age from Turonian to Campanian (**Fig. 2.6**) and can be divided into four formations; the Mancos Shale Fm., the Star Point Fm., the Blackhawk Fm. and the Price River Fm. Each formation is divided into several members, which are described in more details in the sections below and illustrated in **Fig. 2.6**(Howell and Flint, 2003). The Mesaverde Group comprises the shallow marine deposits of the three youngest formations. The Panther Tongue Mb. Of the Star Point Fm. represents the base of this group. The uppermost part is represented by the Castlegate Sandstone Mb. of the Price River Fm. (Young, 1955; Swift et al., 1987; Miall, 1993; Howell and Flint, 2003).

The late Cretaceous stratigraphy consists of fluvial and shallow marine sandstones that inter-tonguing with the offshore deposits of the Mancos Shale Fm. (**Fig. 2.5 & Fig. 2.6)**. The shallow marine depositional system are predominantly wave-dominated although there are several distinct fluvial dominated intervals such as the Panther Tongue Mb. (Howell and Flint, 2003; Edwards et al., 2005). These changes were caused by variations in sediment supply and creation of accommodation space. The bathymetry of the Western Interior Basin can be characterised as a ramp-style, as the basin profile dipped gently in the palaeoseaward direction with no clear shelf break and no abyssal plain (Howell and Flint, 2003). However, a compound clinoform-geometry was likely developed reflecting the differential progradation rates of a nearshore shoreface and a subaqueous nearshore mudstone belt (Hampson, 2010). Also a change in fluvial style is reported between the two uppermost formations. The fluvial

depositional system changed from being mainly a low net-to-gross meandering river system during the deposition of the Blackhawk Fm. to being mainly a high net-to-gross braided river system during the deposition of the Castlegate Mb. of the Price River Fm. (Van Wagoner, 1995). However, new research shows that deposits from a braided river system can be found within the non-marine Blackhawk Fm. (Hampson et al., 2013), and deposits from a meandering river system can be found within the Castlegate Mb (McLaurin and Steel, 2007).

A box diagram of the Late Cretaceous depositional systems is shown in **Fig. 2.5.**

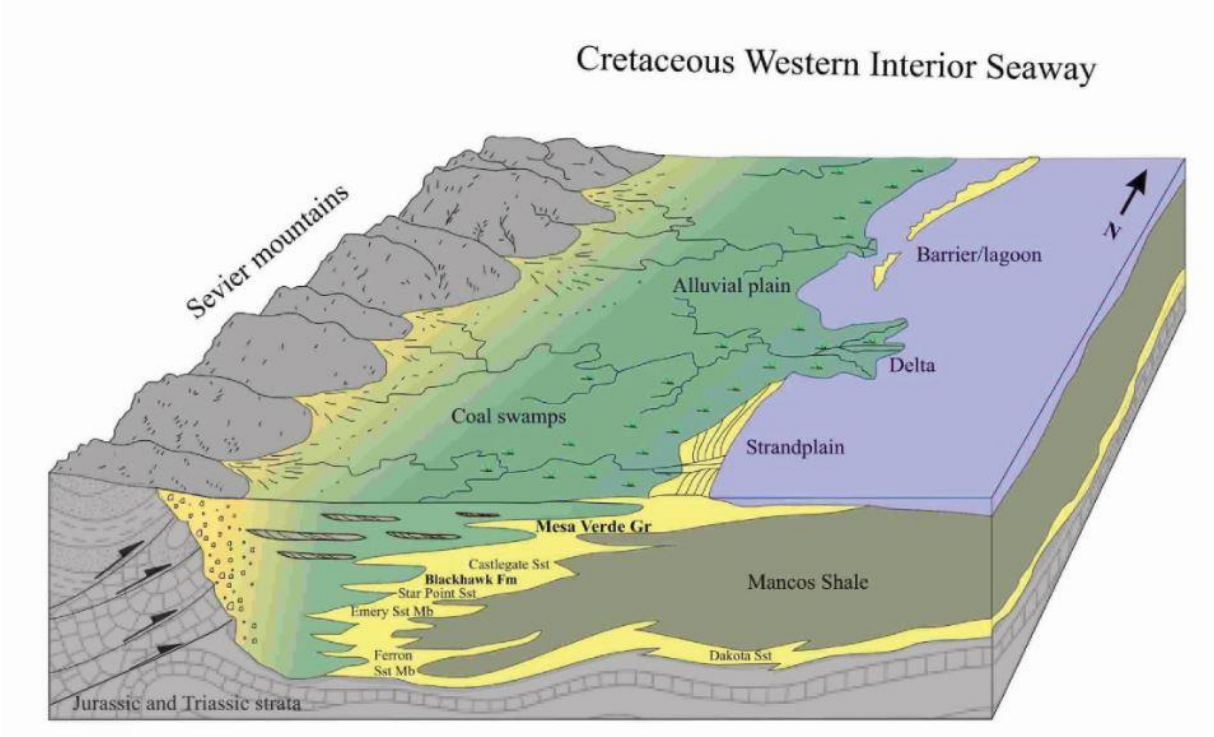


**Fig. 2.5:** This block diagram shows the Late Cretaceous depositional environments in Utah. The depositional environments varied between alluvial plain, coastal plain, river- dominated delta, wave-dominated strandplain and offshore environment. The shallow- marine members and formations are listed in stratigraphic order within this figure. This figure is modified from Hintze, (2005) by Knudsen (2008).

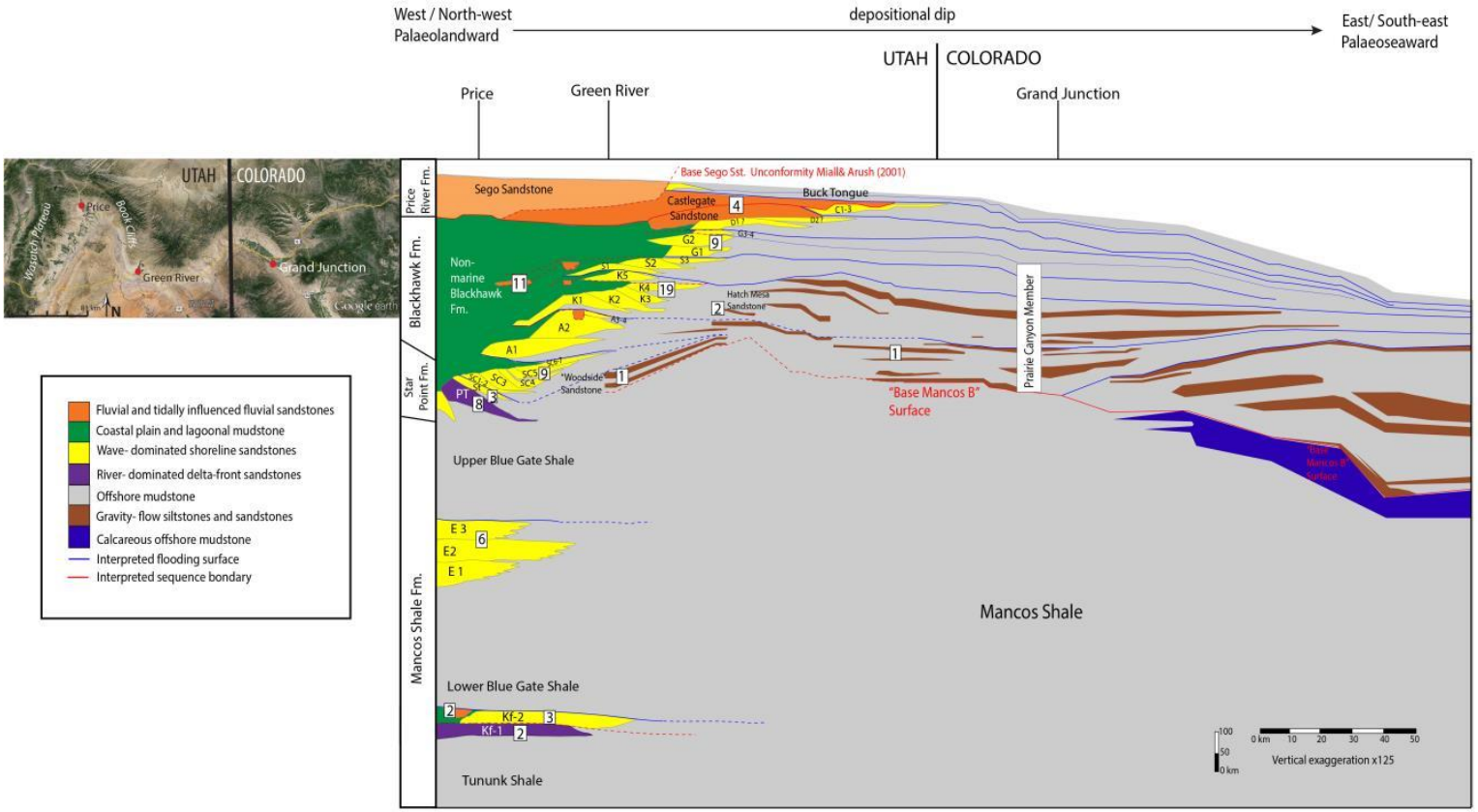


**Fig. 2.6:** An illustration of Late Cretaceous sequence architecture, modified from Hampson et al. (2014). The Star Point Fm., Blackhawk Fm. and Price River Fm. are copied from the correlation panel of Hampson et al. (2014). The extent of the Emery Sandstone Mb. is based on work by Knudsen (2008).The Ferron Sandstone Mb. is based on the schematic cross-sections of the Ferron Last Chance Delta in Deveugle et al. (2011). In this figure the Emery and Ferron sandstone units are not set to scale, the reason for including them is to give an overview of all the studied sequences and the sampling strategy. The number in the white boxes represents the amount of samples collected in that specific stratigraphic unit. The abbreviations for the different members are Kf, Ferron Mb.; E, Emery Mb.; PT, Panther Tongue Mb.; St, Storrs Mb.; SC, Spring Canyon Mb.; A, Aberdeen Mb.; K, Kenilworth Mb.; S, Sunnyside Mb.; G, Grassy Mb.; D, Dessert Mb.; C, Castlegate Mb.

### 2.3.1 THE MANCOS SHALE FORMATION

The Mancos Shale Fm. is predominantly comprised of the Late Cretaceous offshore deposits of the Western Interior Seaway. This formation can locally be more than 1.6 km thick. The lower part of the Mancos Shale Fm. includes two shallow marine members (the Ferron Sst. Mb. and the Emery Sst. Mb) while the upper part interfingers with the shallow marine and coastal plain deposits of the Star Point and Blackhawk formations (Young, 1955; Hintze, 2005).

The lower members of the Mancos Shale Fm. are, in stratigraphic order: Tununk Shale Member, Ferron Sandstone Member, Lower Blue Gate Shale Member, Emery Sandstone Member and Upper Blue Gate Member (Edwards et al., 2005). The upper part of the Mancos Shale Fm. which intertongues with the sandstones of the Mesaverde Group. This part of the Mancos Shale can be divided into the Buck Tongue and the Anchor Mine Tongue (Young, 1955; Hettinger and Kirschbaum, 2002).

This formation also comprises some marine-sandstone unit. The Prairie Canyon Member consists of several shelf turbidite complexes, such as Hatch Mesa Sandstone and Mancos B Sandstone. The Mancos B Sandstone consists of shelf turbidites which are viable hydrocarbon play; this is indicated by gas production from this member in western Colorado (Kellogg, 1977; Hettinger and Kirschbaum, 2002; Pattison et al., 2007). In Woodside Canyon some subaqueous channel deposits characterised as the Woodside Sandstone can be observed. These subaqueous channels connect the shelf turbidites of the Prairie Canyon Member to the shallow marine tongues of the Blackhawk Fm. (Hampson, 2010; Hampson et al., 2014; Eide et al., 2015). The stratigraphic architecture of these deposits is illustrated in **Fig. 2.6**.

The extensive badland areas in eastern Utah occur because the shale members of the Mancos Shale are soft and weathers easily (Hintze, 2005) The studied Ferron and Emery sandstones are described in more detail below.

**FERRON SANDSTONE MEMBER**

The Ferron Sst. Mb. of The Mancos Shale Fm. is of Turonian Age (93 Ma- 89.8 Ma). The formation can be divided into two sub-members. The Lower Ferron member comprises thin sheet like sandstones, and has been interpreted as shelf deposits at outcrop, although thick, shallow marine and coastal plain deposits exists in the subsurface in the Drunkards Wash coal bed methane-field in the northwest of the study area (Klausen, 2010). The Upper Ferron member comprises a wedge of sandstone, shale and coal, which coarsens and thickens towards the south, and this is interpreted as fluvial and deltaic deposits (Cotter, 1975). This sub-member consists of three separate delta systems each with its separate drainage area. These deltas from north to south were the Vernal, Last Chance and Notom. (**Fig. 2.7**) (Bhattacharya and MacEachern, 2009). The Ferron sandstone studied in this thesis was the Last Chance delta system (**Fig. 2.7 B**) of the Upper Ferron member. The sequence stratigraphy of the Last Chance Delta is complex with numerous different interpretations (Garrison Jr and Van den Bergh, 2004; Bhattacharya and MacEachern, 2009; Deveugle et al., 2011; Li et al., 2011) The samples used in this study were taken from the two different parasequence sets (Kf1 & 2) of Deveugle et al. (2011) (**Fig. 2.6**)

The Ferron deltas were deposited by relatively small rivers (max discharge 1500 $m^3/s$) during a subtropical climate with a palaeolatitude between 45-55° (**Fig. 2.7 A)**. The source area for these deltas was located in the active Sevier Orogen, and was relatively modest (50 000 $km^2$). The transport distance from source to sink was estimated to approximately 100 km (Bhattacharya and MacEachern, 2009). Palaeogeographic reconstructions from the Turonian and the Last Chance Delta are shown in **Fig. 2.7**.

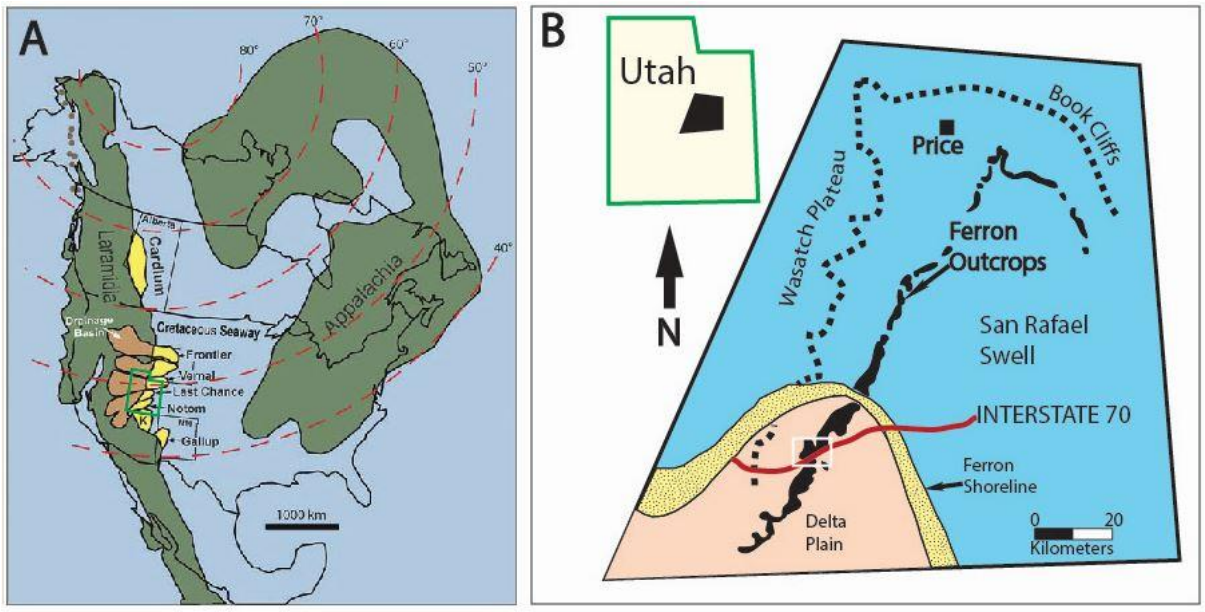


**Fig. 2.7: A)** Shows the Turonian palaeogeography of North America. The three Ferron deltas are illustrated on this map. Green represents undifferentiated terrestrial landscapes, brown represents drainage areas for the different deltaic units of the Ferron Mbr. and yellow represents delta front/shoreline deposits. The green outline shows the Utah state border. From Bhattacharya and MacEachern (2009). **B)** Shows a palaeogeographic reconstruction of the Last Chance delta, the white box represents the area studies and logged along I-70 in this thesis. Modified from Bhattacharya and MacEachern (2009).

The Last Chance Delta includes both wave dominated and river dominated shallow marine systems. The succession is interpreted to have been mainly wave dominated but with local areas of fluvial dominance around the mouths of trunk channels. The lowermost parasequence shows fluvial dominance in the studied outcrops (Li et al., 2011). Garrison Jr and Van den Bergh (2006) described the Last Chance Delta as "a wave-modified, river- dominated deltaic system".

Further interpretation of the river-dominated deposits of Kf-1 suggests that they have been deposited from hyperpycnal flows in a sheltered interdistributary bay during a normal regressive system (Bhattacharya and MacEachern, 2009; Enge et al., 2010).

### EMERY SANDSTONE MEMBER

The Santonian aged Emery Sandstone Member of the Mancos Shale consists of continental to shallow marine sandstones deposited in the Western Interior Seaway. The source area of these sandstones has been interpreted to be the Sevier Orogen, which fed the shoreline into a subsiding foreland basin. The Emery Member can be divided into 17 progradational to aggradational parasequences arranged into three parasequence sets (E1-3) (**Fig. 2.6)**.

Erosional sequence boundaries are lacking within these parasequence sets, which is most likely due to deposition in a region of high subsidence close to the thrust belt during a period ofrelatively high accommodation rates. These parasequences were deposited during highstand- and transgressive- system tracts (Edwards et al., 2005).

Edwards et al. (2005) suggest that the shoreline of these sandstone units were aligned approximately parallel to the cliffs making up the eastern edge of today's Wasatch Plateau. Based on the observed thinning and thickening of the sand units along these cliffs they interpreted the Emery Sandstones to have been deposited during two separate deltaic depositional systems (**Fig. 2.8 B**). These delta systems were strongly wave dominated and had a symmetrical shoreline. A good modern day analogue (**Fig. 2.8 A**) to these wave dominated deltaic shorelines is the Coast of Nayarit in Mexico (Bhattacharya and Giosan, 2003; Edwards et al., 2005).

The Emery sandstone was most likely transported from the source area through a cluster of several small rivers and deposited as deltas at the river mouth. The delta sediments were then reworked and redistributed by waves and strong longshore currents, creating strandplains which stretched tens of kilometres away from the delta lobes (Edwards et al., 2005).

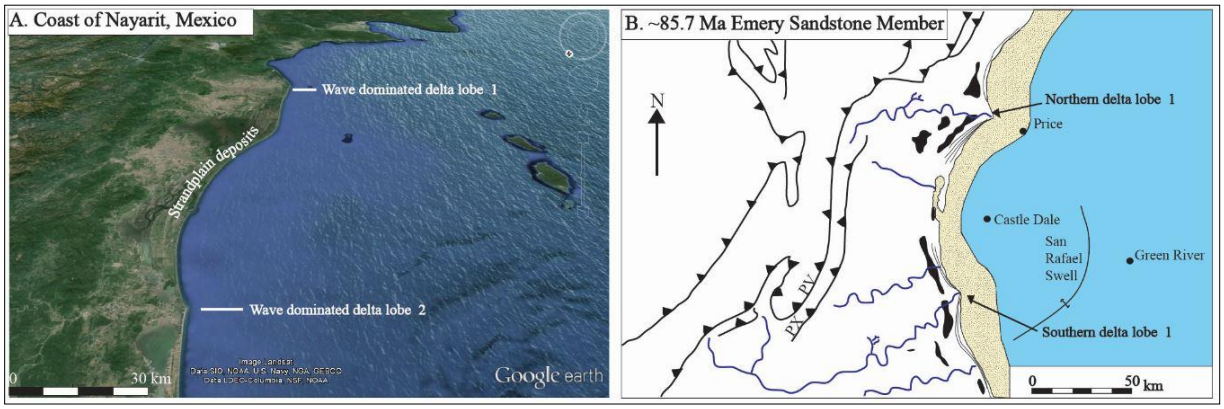


**Fig. 2.8: A)** A satellite photo of the coast of Nayarit in Mexico. This photo represents a modern day analogue for the Emery Sandstone Member's depositional system, showing a wave-dominated delta and strandplain environment. **B)** A palaeogeographic reconstruction of the shoreline along the Wasatch Plateau during the deposition of the Emery Sandstone Member, modified from Edwards et al. (2005). The white area represents the coastal- and delta plain, the black shapes represent coal- forming swamps, the yellow area represents shallow marine delta front and the blue area represents the offshore sea. PV= Pavant thrust and PX= Paxton thrust

### 2.3.2 THE STAR POINT FORMATION

The Star Point Fm. is well exposed in outcrops along the eastern flank of the Wasatch Plateau and extends into the north-western part of the Book Cliff. This formation is separated from the underlying the Emery Sandstone Mb. by a thick succession of Mancos Shale. The formation can be divided in to two members. The oldest member is the Panther Tongue Mb. of Santonian age, and comprises coarsening upwards river-dominated delta deposits (**Fig. 2.9 A**) with minor wave modification. The younger Storrs Mb. is of early Campanian age and is comprised of wave-dominated shoreface deposits (**Fig. 2.9 B**) (Young, 1955; Hwang and Heller, 2002; Howell and Flint, 2003; Edwards et al., 2005; Hampson et al., 2011).

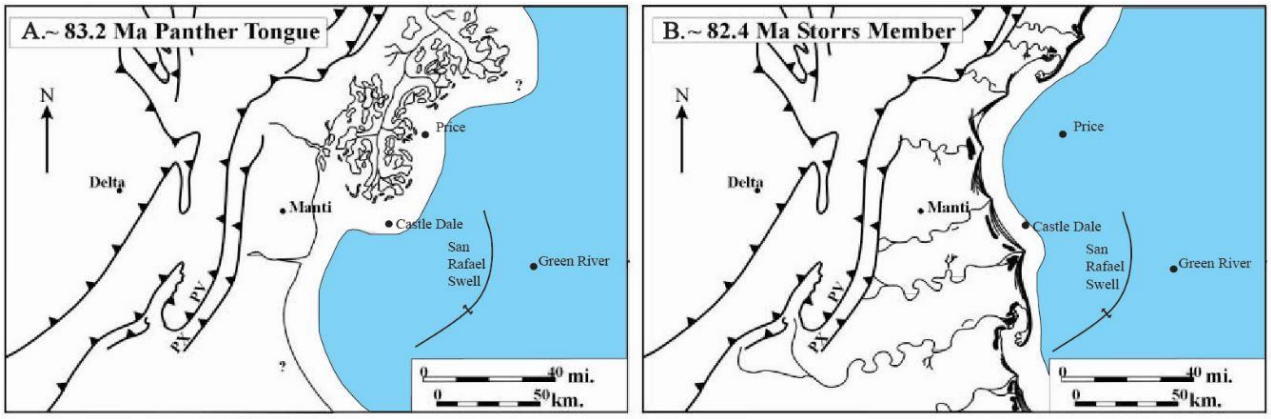


**Fig. 2.9: A)** A palaeogeographic reconstruction of the Panther Tongue Mb. The river dominated delta progrades from north to south. **B)** A palaeogeographic reconstruction of the wave-dominated shoreline of the Storrs Mb. These wave-dominated deltas have an east/ south-eastward and east/ north-eastward progradational trend. PV= Pavant thrust and PX= Paxton thrust. These two figured are modified from Edwards et al. (2005)

#### PANTHER TONGUE MEMBER

During the deposition of the Star Point Fm. the shoreline generally had a north-south orientation. However, the palaeocurrent measurements in the Panther Tongue Mb. indicate a southward sediment progradation (**Fig. 2.9 A**) (Newman and Chan, 1991; Edwards et al., 2005; Olariu et al., 2010; Hampson et al., 2011).

The deposits of the Panther Tongue Mb. are interpreted to have been deposited during a single sea-level fall event, The interval lacks coastal plain deposits, is capped by a thick and extensive transgressive lag, and progrades abnormally far into the basin (Hwang and Heller, 2002). The Panther Tongue is interpreted as a forced regressive deposits (Hwang and Heller, 2002; Howell and Flint, 2003).

Enge et al. (2010) compared the river dominated deposits of the Ferron Mb. to the younger Panther Tongue Mb. of the Star Point Formation, and concluded that Panther Tongue deposits were deposited in a more open basin during a falling stage to lowstand system tract.

There are several different theories for the change in depositional direction between the Panther Tongue Mb. and other systems in the Cretaceous of the study area. These were summarised by Olariu et al. (2010) as follows; 1) The transport direction switched from being parallel with the orogeny to becoming transverse. This switch happened as a result of the partial infilling of newly created small topographic basins due rapid and episodic uplift in the orogen (Balsley (1980) cited in Olariu et al. (2010)). 2) The depositional area was protected by an north-south trending structural high east of the shoreline, this resulted in a southward progradation of the delta and protection from waves causing the delta to be predominantly river dominated (Morris et al. (1995); Posamentier et al. (1995) cited in Olariu et al. (2010)). 3) The local progradation towards the south in the Panther Tongue Member was sheltered by a spit with N-S orientation. The spit was later eroded during the following transgression (Olariu et al., 2010).

#### STORRS MEMBER

While the progradational direction of Panther Tongue was towards the south, the overlying Storrs Mb. shows a more typical eastwards progradation (**Fig. 2.9 B**) (Newman and Chan, 1991; Edwards et al., 2005; Olariu et al., 2010; Hampson et al., 2011).

(Hampson et al., 2011) proposed that the Storrs Mb. can be divided into five parasequences, consisting predominately of wave dominated shoreface deposits. These parasequences have a progradational to aggradational stacking pattern(Eide et al., 2014), indicating deposition during a normal regression. The Storrs Mb. extends a relatively short distance basinward, and pinches out into the Mancos Shale just east of the town Helper (Hampson et al., 2011).

### 2.3.3 THE BLACKHAWK FORMATION

The Blackhawk Fm. is well exposed in the Book Cliffs and in the eastern part of the Wasatch Plateau. The formation consists of up to 400 m of aggradational to progradational parasequences, deposited between 82,5 and 79 Ma based on radiometric and palaentological age dating (Young, 1955; Fouch et al., 1983; Hampson et al., 2001). During this time the

shorelines were wave-dominated. The depositional environments observed with in the parasequences of the Blackhawk Fm. are coastal plain, foreshore, upper, middle and lower shoreface and offshore transition (Taylor and Lovell, 1995; Howell and Flint, 2003).

This formation is divided into several members. The coastal plain environment is informally called the non-marine Blackhawk. This non-marine portion consists of fluvial-, overbank-, lagoonal- and coal deposits (Howell and Flint, 2003; Hampson, 2010). The extensive and laterally continuous coal seams were formed in large raised mires which were developed parallel to the shoreline. Several of these coal seams have been mined in Utah for more than a 100 years. (Kalkreuth and Leckie, 1989; Davies et al., 2005).

The shallow marine deposits are divided into six sandstone dominated members, which are separated by the offshore Mancos Shale. The sandstone members are the Spring Canyon-, Aberdeen-, Kenilworth-, Sunnyside-, Grassy- and Desert members (Young, 1955; Taylor et al., 1995; Hampson et al., 2001; Howell and Flint, 2003). In this thesis the Spring Canyon-, Kenilworth- and Grassy- Member were studied. These three members are described in some more details below.

During the deposition of the Blackhawk Fm. the parasequence staking pattern changed from aggradational in the older members (Spring Canyon, Aberdeen member) to a more progradational trend in the younger members (Grassy, Dessert member). The Blackhawk Fm. consists of sediments deposited predominantly during a high stand system tract (Taylor and Lovell, 1995; Howell and Flint, 2003). Hampson et al. (2001) suggest that the deposition of this formation occurred during a relative rise in sea- level over a large period of time. This interpretation is summarised in **Fig. 2.6**.

### SPRING CANYON MEMBER

Spring Canyon Mb. consists of 7 progradational to aggradational parasequences (SC1-7), and represents the oldest member of the Blackhawk Fm. (**Fig. 2.6**) (Hampson and Howell, 2005; Hampson, 2010). The palaeoshoreline for this member was oriented in the north - south direction, and the parasequences prograded in an east-southeast direction.

The Spring Canyon Mb. was deposited in a wave-dominated depositional environment (Kamola and Van Wagoner, 1995). Kamola and Van Wagoner (1995) recognised three sub-environments within these parasequences: (1) marine, (2) marine to non-marine/ marginal transition and (3) non- marine (**Fig. 2.10)**. Maximum thickness of the marine part within one parasequence is 25 m in the part proximal to the palaeoshoreline and 10-15 m in the more distal part. The Spring Canyon Mb. is well exposed in the west/ northwestern part of the Book Cliffs and pinches out in the palaeobasinward direction (east of the Soldier Creek location). No major erosive unconformities are recognised in the Spring Canyon Mb. The Spring Canyon Mb. is bound by major marine flooding surfaces above and below (Kamola and Van Wagoner, 1995; Taylor et al., 2004).

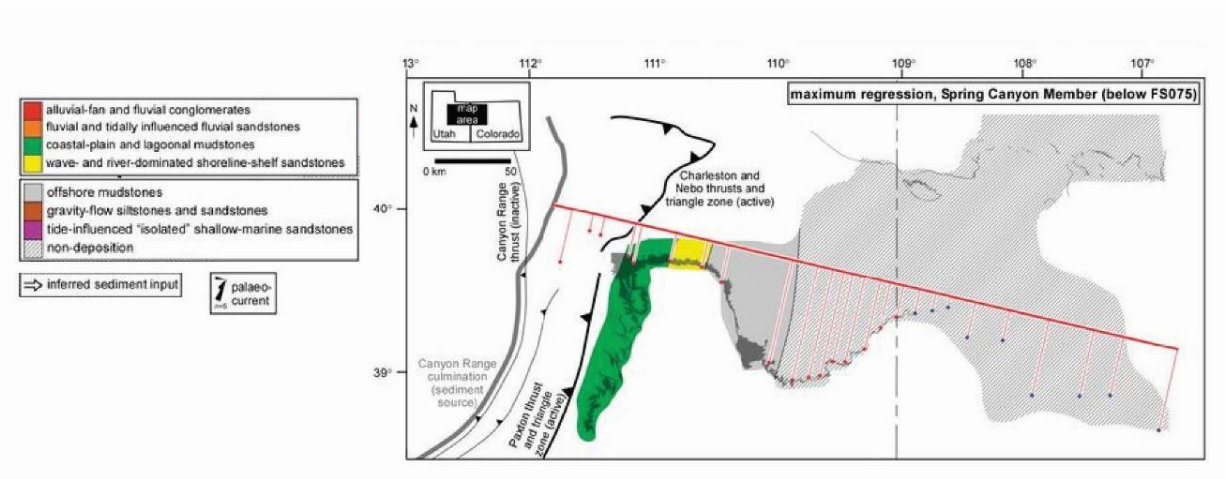


**Fig. 2.10:** Facies-belt extent of the Spring Canyon Mb. shoreline during maximum regression. The orange line trending NW-SE represents the section and corresponding study areas that Hampson et al. (2014) used to create the schematic illustration of the Mesaverde Group in Fig. 2.6. This figure is from Hampson et al. (2014)

### KENILWORTH MEMBER

The Kenilworth Mb. is well exposed in the Book cliffs with an average thickness of 100 m. Taylor and Lovell (1995) divided this member into five parasequences (**Fig. 2.6**).

The first four parasequence represent deposition in a high stand system tract. The upper most parasequence (K4) has also been interpreted as a forced regressive system tract because it is sharped based and extends a long way into the basin (Pattison, 1995). The boundary between the fourth (K4) and fifth (K5) parasequence represents a relative rise in sea-level, the shoreline was moved palaeolandward creating a retrogradational shoreline trajectory between K4 and K5. This rise in sea-level is coincident with a change in the overall shoreline trajectory of the Blackhawk Fm. from an aggradational to a more progradational trend (Taylor and Lovell, 1995; Hampson et al., 2001; Howell and Flint, 2003). A palaeogographic reconstruction of the Kenilworth wave-dominated shoreline during deposition is illustrated in **Fig. 2.11**.

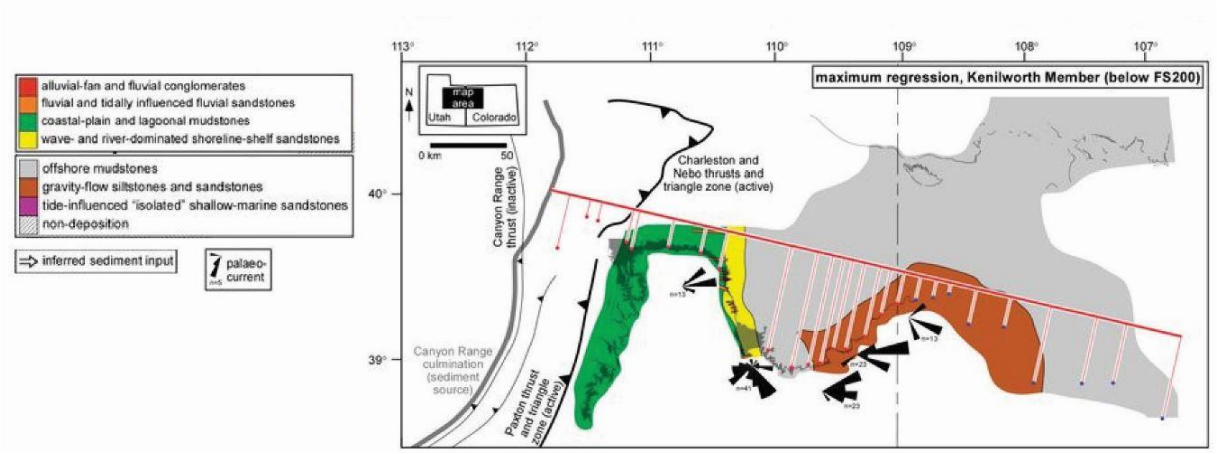


**Fig. 2.11:** Facies-belt extent of the Kenilworth shoreline during maximum regression. Figure from Hampson et al. (2014)

### GRASSY MEMBER

The Grassy Mb. can be divided into four parasequences (G1-4) (**Fig. 2.6**) (Hampson, 2010). These parasequences consist of deposits from strandplain and barrier island – lagoonal depositional systems. The wave dominated and microtidal palaeoshoreline for this member was oriented in the NE-SW direction (**Fig. 2.12)**, and palaeocurrent measurements indicate alongshore sediment transport in the S/SE direction.

The parasequence set in the Grassy formation shows a strongly progradational trajectory and well developed erosional fluvial channels. No major erosive unconformities are associated with the Spring Canyon Mb., but there are two major erosive unconformities described within the Grassy Mb. (GSB2 and GSB3), the Grassy Mb is also bound below by a major erosive unconformity at the top of the Sunnyside Member (GSB1) (O'Byrne and Flint, 1995).

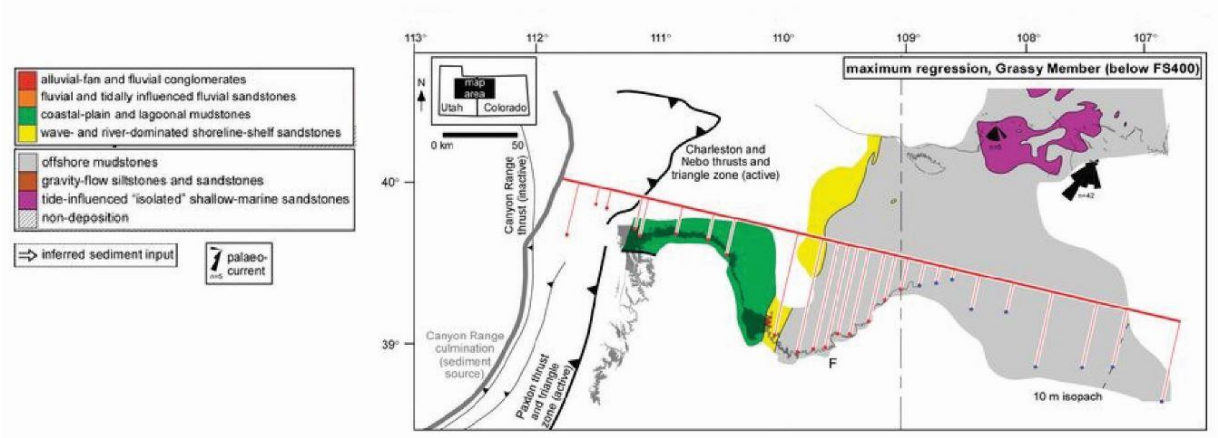


**Fig. 2.12:** Facies-belt extent of the Grassy shoreline during maximum regression. Figure from Hampson et al. (2014)

### 2.3.4 PRICE RIVER FORMATION

This formation is the uppermost part of the Mesaverde Group. The Price River Fm. exposed in the Neslen Canyon, Utah can be divided into 5 members. In stratigraphic order the members are; Castlegate-, Sego-, Corcoran-, Cozzette- and Cameo- Member (Young, 1955). The Castlegate Sandstone Mb. of the Mesa Verde Group is the only member of the Price River Fm. studied in this thesis.

#### CASTLEGATE SANDSTONE MEMBER

The Castlegate Sandstone is of Campanian age. This sandstone member consists of amalgamated braided fluvial sandstones, which thins eastward and pinches out into the Mancos Shale around West Salt Creek. East of the town Green River in the Book Cliffs the Castelegate Sandstone Member is separated from the overlying Sego Sandstone Member by the Buck Tongue Member of the Mancos shale. To the west this marine shale member is erosionally truncated below the Sego Sandstone Mb. (Young, 1955; Yoshida et al., 1996).

The Castlegate around Price is approximately 160 m thick, and can informally be divided into two or three sequences (**Fig. 2.6)**. The erosional sequence boundaries were caused by thrust loading and unloading of the basin (Miall and Arush, 2001; McLaurin and Steel, 2007). McLaurin and Steel (2007) divided the Castlegate sandstone into (1) the Lower-, (2) the Middle- and (3) Upper- Castlegate Member. For the purpose of this thesis the Lower Castlegate Member was studied. It has an approximately thickness of 60 m and consists of amalgamated fluvial channel-belt sandstones, and continuous overbank mudstone deposits are absent (McLaurin and Steel, 2007). The tidal influence is strongest in the Middle and Upper Member (Miall and Arush, 2001; McLaurin and Steel, 2007)

The Castlegate Sandstone is interpreted to have been deposited during a falling stage system by rivers with low to intermediate sinuosity with various influence of tidal processes (Young, 1955; Miall and Arush, 2001; Adams and Bhattacharya, 2005; McLaurin and Steel, 2007; Bhattacharya, 2011). During this time of deposition the regional subsidence rate of the foreland basin was reduced, resulting in low accommodation (Yoshida et al., 1996; Miall and Arush, 2001; Lynds and Hajek, 2006; McLaurin and Steel, 2007). A palaeogeographic reconstruction of the Castlegate shoreline is illustrated in **Fig. 2.13**.

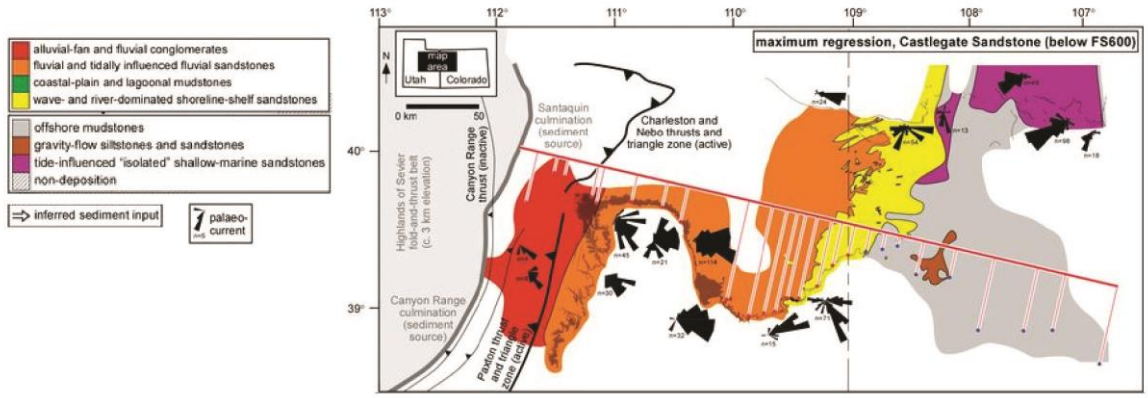


**Fig. 2.13:** Facies-belt extent during maximum regression of the Castlegate Sandstone Member. Figure from Hampson et al. (2014)

### 2.3.5 CONTROLS ON THE STRATIGRAPHIC ARCHITECTURE

Different factors have been suggested as controlling mechanisms for the large scale stratigraphic architecture of the Late Cretaceous sediments in Utah. Some of these controls are described below.

#### EUSTATIC SEA-LEVEL CHANGES

Edwards et al. (2005) suggest that the increase in accommodation and progradation of the Emery Member could have been controlled by Santonian glacio-eustatic sea-level changes, but they also mentions tectonic control of the progradation as suggested by Kamola and Huntoon (1995) as another possibility. Van Wagoner (1995) also interpreted eustatic changes to be the driving mechanism for deposition of high-frequency sequences in the Book Cliffs. He also proposed that the control on lithofacies and low-frequency sequences can be driven by tectonics, such as thrust sheet emplacement and erosion.

#### INTERNAL (AUTOGENIC) CONTROLS IN THE DEPOSITIONAL SYSTEMS

During relative sea-level rise, or stillstand space is created in the coastal plain due to the aggradation and expansion of the fluvial profile. The shoreline progradation is reduced as more of the sediment is deposited in the coastal plain. Eventually this leads to retreat (autoretreat) of the shoreline and flooding of coastal plain deposits (Muto et al., 2007; Hampson, 2010).

Concave landward shoreline trajectories are characteristically associated with autoretreat of the shoreline. The lower aggradational members of the Blackhawk Fm. (Spring Canyon Mb. and Aberdeen Mb.) have a typical concave landward shoreline trajectory. These members are bounded by flooding surfaces (Hampson, 2010). These members may represent deposition controlled by internal autogenic factors such as autoretreat of the shoreline (Hampson, 2010), and not controlled by tectonics of the thrust sheet as suggested in previous studies (Kamola and Huntoon, 1995).

#### TECTONIC CONTROLS

Numerous authors (e.g. Kamola and Huntoon, 1995; Yoshida et al., 1998; DeCelles, 2004; Horton et al., 2004; DeCelles and Coogan, 2006) suggest that tectonic changes are the major

driving mechanism for sequence development in the Book Cliffs. The progradational upper members of the Blackhawk Fm. (Grassy Mb. and Dessert Mb.) have a concave seaward shoreline trajectory, which can be explained by a slowing of the tectonic subsidence resulting in a decrease in the Late Cretaceous relative sea-level rise in Utah (Hampson, 2010).

It has been suggested by several authors (e.g., Yoshida et al., 1996; Miall and Arush, 2001; Horton et al., 2004; Hampson, 2010) that tectonic mechanisms such as flexural loading and unloading have been the main controlling factors for the deposition of the Upper Blackhawk Fm. and Castlegate Mb. There is no independent evidence supporting climate changes or changes in the eustatic sea-level to be the controlling factors.

Horton et al. (2004) suggest that the progradation of the Castlegate Sandstone Mb. can be tied to the tectonic shortening of the Charleston- Nebo salient. They also acknowledge that Laramide basement uplift (involving the formation of the San Rafael Swell) reduced the subsidence and accommodation rates and could have influenced the progradation.

## 2.4 PROVENANCE OF LATE CRETACEOUS SEDIMENTS

Very few provenance studies have been previously published from the Late Cretaceous deposits in southeastern Utah. Horton et al. (2004) suggested a change in provenance between the Blackhawk Fm. and the Castlegate Sandstone Mb. based on palaeocurrent data, conglomerate clast count and petrographic data from sandstones deposited in the foreland basin.

The Blackhawk Fm. studied by Horton et al. (2004) contains Precambrian-Mesozoic clasts (**Fig. 2.14**) and palaeocurent data indicated a southeastward sediment transport direction. The source area for this formation is interpreted to be the Midas and Sheeprock thrust sheets bounding the western part of the Charleston-Nebo salient, due to the observation of Precambrian clasts (Mitra, 1997; Constenius et al., 2003; Horton et al., 2004).

The Castlegate Sandstone contains Pennsylvanian-Permian clasts (**Fig. 2.14**), and palaeocurrent data indicate an east-southeast sediment transport direction. The source area is interpreted to be the Oquirrh Group exposed in the roof sheet of the Santaquin culmination within the Charleston- Nebo salient (Horton et al., 2004).

Horton et al. (2004) suggest that the provenance area for the Book Cliff sediments was not the commonly cited Canyon Range and Pavant thrusts (DeCelles et al., 1995; DeCelles, 2004; DeCelles and Coogan, 2006), but the more proximal Charleston- Nebo salient. They also state that the progradation of Campanian sediments was linked to the shortening of this salient (location of the thrust systems in the provenance area are illustrated in Fig. 2.3). It has been suggested by DeCelles (2004) that the Charleston- Nebo salient had a minimum shortening of 105 km. The tectonic activity within the Charleston-Nebo salient was also a driving mechanism for flexural accommodation created in the foreland basin (Horton et al., 2004).

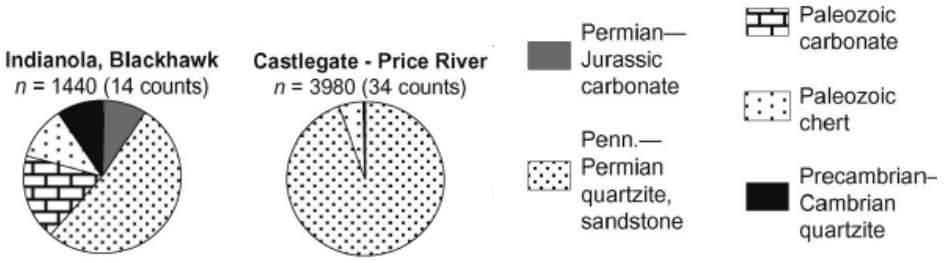


**Fig. 2.14:** Clast composition provenance data from Horton et al. (2004). Note the difference age and carbonate content. The source area for the Castlegate sandstone contains less carbonates and have a low abundance in Precambrian rocks.

# 3 METHODS

The results presented in this thesis are based on data gathered from field work and laboratory work. The workflow consisted of the following steps:

- Synthesising published data about the field area from papers, field guides etc.
- Field work including sampling rocks, TinyPerm II measurements and logging.
- Thin section descriptions and Point counting
- SEM work to get a better idea of the chemical composition of the different minerals.
- Comparing and synthesising the collected data.

## 3.1 FIELD WORK

The field work was conducted during four weeks in May and June 2014. Numerous locations were visited along the Wasatch Plateau and Book Cliffs in south-eastern Utah, USA (**Fig. 1.1**).

### 3.1.1 SAMPLING AND SAMPLING STRATEGY

A total of 81 rock samples were collected in the field using hammer and chisel. The rock samples had a typical size of 8-12 cm long, 6-10 cm wide and 4-7 cm thick. They were selected from fresh, unweathered surfaces.

### 3.1.2 OUTCROP SEDIMENTOLOGY – SEDIMENTARY LOGGING

Traditional sedimentary logging was conducted at five sections (**Table 3.1**) in the study area. Grain size distribution, bed thickness, nature of bed contacts, sedimentary structures and lithology were described in lithostratigraphic logs, and facies associations were interpreted from these data along with the large-scale architecture from the exposures. The location, lithostragographic unit and scale of the logs are displayed in, the GPS coordinates for these locations are listed in **Table 1** in **Appendix I**. The Cretaceous formations in this area have been logged several times by previous workers and are relatively well-understood. Detailed logs were collected to calibrate the published works and to provide an overview of where the rock samples and TinyPerm II measurements were taken. In Gentile Wash a log acquired by John Howell (**Fig.1** in **Appendix II**) were used for the Storrs Mb. and Spring Canyon Mb.

**Table 3.1**: Overview of the location, formation and scale of the sedimentary logs conducted during the field work.

| Log # | Location | Formations (Fm.)/ Members (Mb.) | Scale |
|---|---|---|---|
| *Log 1* | *Ivie Creek, along Interstate 70* | Ferron Fm. | 1:200 |
| *Log 2* | *Quitchupah Creek, West of State 10* | Emery Fm. | 1:50 |
| *Log 3* | *Joe's Valley* | Price River Fm. (Castlegate Mb.) | 1:50 |
| *Log 4* | *Horse Canyon* | Blackhawk Fm. (Kenilworth Mb.) | 1:50 |
| *Log 5* | *Gray Canyon* | Blackhawk Fm. (Grassy Mb.) | 1:50 |

### 3.1.3 TINYPERM II MEASUREMENTS

Permeability of sandstone units was measured in the field with a TinyPerm II permeameter (**Fig. 3.1**). The permeameter works by creating a vacuum close to the rock surface, and measuring the time (or rate of pressure change) it takes for air to seep in through the rock to equilibrate the pressure. This is used to estimate the permeability of the rock. As the system is pulling air through the rock it is critical that no air is able to enter the permeameter via the nozzle, therefore the measured surface needs to be planar and clean. The measured surface must also be unweathered, as weathered surface may give a different permeability measurement than a clean surface. Geological hammer and chisel were used to create these clean planar surfaces (**Fig. 3.2**). The process of using the permeameter is described below:

1. The surface to be measured is cleaned with a hammer to remove the weathering crust
2. Then the surface needs to be cleaned of sand and dust. This is done by sucking air out of the outcrop surface with the permeameter. The handle is pulled out as the permeameter is moved away from the surface.
3. When the surface is ready to be measured the handle needs to be pulled all the way out and the display has to say “Push + Hold”.
4. The nozzle is then pushed firmly against the surface and the handle is pushed all the way in. The permeameter now starts counting down until the vacuum is 0 and the measurement is completed.
5. The result appears on the screen and can be written into the notebook. The permeameter has no memory, so the result needs to be systematically listed.
6. Absolute permeability can be found by cross-referencing the measurement with the calibration curve from the user manual (**Fig. 3.3**)

Several readings are taken on any given surfaces to ensure that they are consistent and the seal has not been breached. Once 3 to 6 consistent measurements are achieved the data are recorded. .


**Fig. 3.1:** This picture shows the components of permeameter. 1) Handle and plunger 2) Vacuum cylinder 3) Pressure transducer enclosure 4) Field notebook 5) Microprocessor and control unit 6) Electrical cable 7) Spare nozzle 8) Silly Putty 9) Artist's eraser 10) Carrying Case. 8 and 9 were not used in this study. The picture and description is from the TinyPerm II User's Manual provided by New England Research Inc.

All together 194 surfaces were measured in different formations and localities, and each surface was measured 3-6 times, to get a consistent reading. Detailed permeability transects were acquired in the Spring Canyon Mb. (Gentile Wash), the Kenilworth Mb. (Horse Canyon) and the Grassy Mb. (Gray Canyon), where the permeability was measured every meter within one parasequence. For the other formations and members at least one surface was measured within each facies association (**Table 2** in **Appendix I**)

**Fig. 3.2:** Permeability measurement on a clean and planar surface. This measurement is from a LSF sandstone in Spring Canyon Mb. of the Blackhawk Fm. located in Gentile Wash.

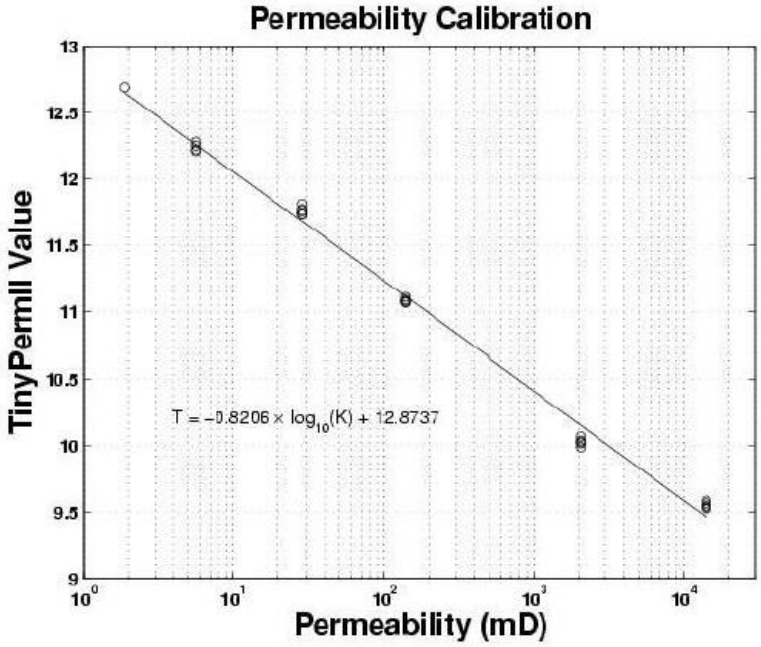


**Fig. 3.3:** Permeability Calibration Curve for the TinyPerm II measurement, the curve is provided by the TinyPerm II User's Manual provided by New England Research Inc.

Filomena et al. (2014) and Fossen et al. (2011) conducted a studies were they compared TinyPerm II measurements with gas driven plug measurements (**Fig. 3.4**). Filomena et al. (2014) found that TinyPerm II measurements almost correlate in a one-to-one

ratio with the ErgoTech Hassler cell measurements (HET) of the plugs, with a coefficient of determination ($R^2$) of 0.955. The correlation between outcrop permeameter measurements and gas driven permeability measurements on plugs depends on the measurement methods used, and needs to be corrected. They concluded that permeameters such as TinyPermII can give relative accurate outcrop measurements compared to gas driven plug measurements.

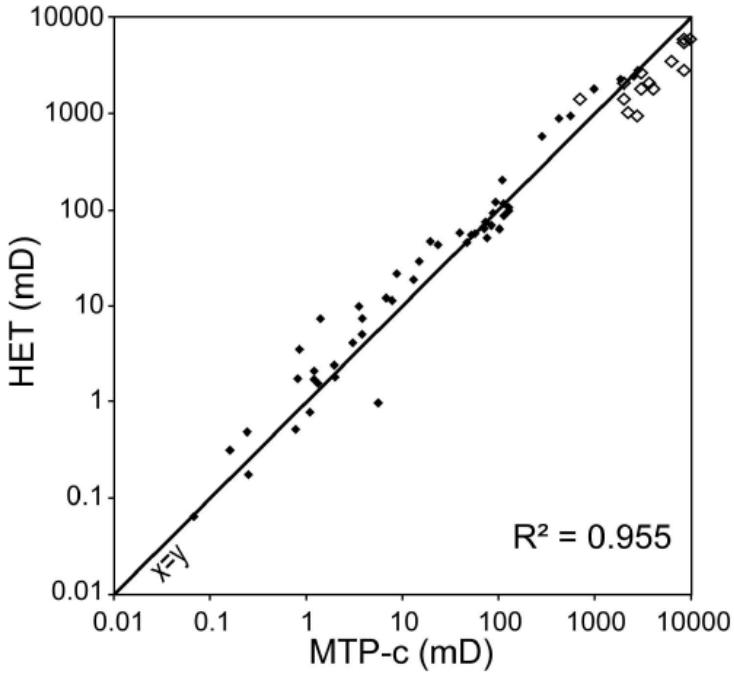


**Fig. 3.4:** The filled boxes represent TinyPerm II measurements (MTP-c) plotted against ErgoTech Hassler cell measurements (HET). The MTP-c measurements are TniyPerm II measurements from plugs, which have been corrected for the discrepancy between plug and outcrop measurements. This data is from the study done by Filomena et al. (2014). The open boxes represent TinyPerm II field measurements from outcrops plotted against laboratory gas (Helium) measurements of permeability of plugs, done by (Fossen et al., 2011). The figure is from Filomena et al. (2014)

## 3.2 LABORATORY WORK

Samples collected in the field formed the base for the laboratory work, which were conducted at the Microscopy Lab and the Laboratory for Electron Microscopy at the University of Bergen. Thin sections were made from the samples collected in the field. The thin sections were provided by the Preparation Lab for thin sections at the Department of Earth Science, University of Bergen. All the samples were impregnated with blue proxy in order to highlight the porosity. The four samples used in the electron microscope were polished, the rest of the samples were sprayed with "Spray Lacquer". In the Microscopy Lab the thin sections were both described and point counted.

### 3.2.1 MICROSCOPY LAB – MINERAL DESCRIPTION

The description of the thin sections included observed mineral content, grain size, sorting, grain roundness and type of grain contacts.

**MINERAL CONTENT:**

The different minerals observed were listed, further study on mineral content was done by point counting and in the electron microscope (SEM).

**GRAIN SIZE:**

The grain size were found by measuring several of the grains observed in the microscope, converting the measurements to millimetres (mm) and using the Wentworth scale (**Table 3.2**). Grain size was also observed and visually determined in the field during logging. The thin section grain size is on average 0.7 of actual grain size because it is very unlikely that the plane intersects the max grain dimensions of any sand grain.

**Table 3.2:** Grain size table based on grain size classes defined by Wentworth (1922).

| Millimeters (mm) | Micrometers (μm) | Phi (ϕ) | Wentworth size class | | Rock type |
|---|---|---|---|---|---|
| 4096 | | -12.0 | Boulder | | |
| 256 | | -8.0 | Cobble | Gravel | Conglomerate/ breccia |
| 64 | | -6.0 | Pebble | | |
| 4 | | -2.0 | Granule | | |
| 2.00 | | -1.0 | Very coarse sand | | |
| 1.00 | | 0.0 | Coarse sand | | |
| 1/2 0.50 | 500 | 1.0 | Medium sand | Sand | Sandstone |
| 1/4 0.25 | 250 | 2.0 | Fine sand | | |
| 1/8 0.125 | 125 | 3.0 | Very fine sand | | |
| 1/16 0.0625 | 63 | 4.0 | Coarse silt | | |
| 1/32 0.031 | 31 | 5.0 | Medium silt | | |
| 1/64 0.0156 | 15.6 | 6.0 | Fine silt | Silt | Siltstone |
| 1/128 0.0078 | 7.8 | 7.0 | Very fine silt | | |
| 1/256 0.0039 | 3.9 | 8.0 | | | |
| 0.00006 | 0.06 | 14.0 | Clay | Mud | Claystone |

**SORTING:**

Sorting was described based on the sorting chart by Longiaru (1987) (**Fig. 3.5**), which is based on the descriptive terminology from Folk (1966). Sorting describes the standard deviation in grain sizes in phi (ϕ) values.

Standard Deviation:

| | |
|---|---|
| < 0.35 ϕ | very well sorted |
| 0.35 – 0.50 ϕ | well sorted |
| 0.50 – 0.71 ϕ | moderately well sorted |
| 0.71 – 1.00 ϕ | moderately sorted |
| 1.00 – 2.00 ϕ | poorly sorted |
| 2.00 – 4.00 ϕ | very poorly sorted |

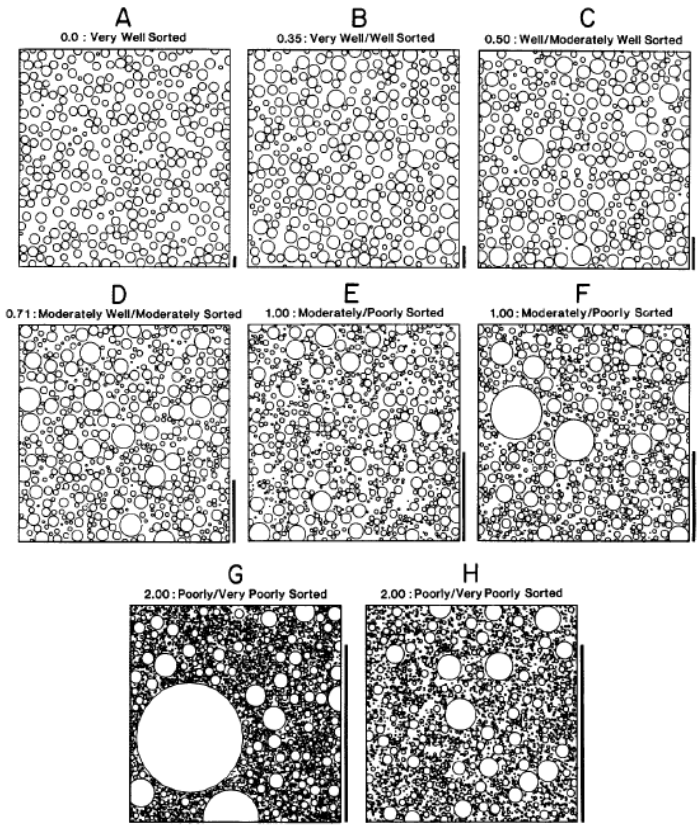


**Fig. 3.5:** Longiaru (1987) created this sorting chart which is based on the sorting terminology in Folk (1966). The number in front of the description represents the approximately standard deviation of the grain sizes in phi (ϕ).

**GRAIN ROUNDNESS:**

**Fig. 3.6** was used as reference for describing the roundness of grains. The figure is based on Powers' grain images (Powers, 1953).

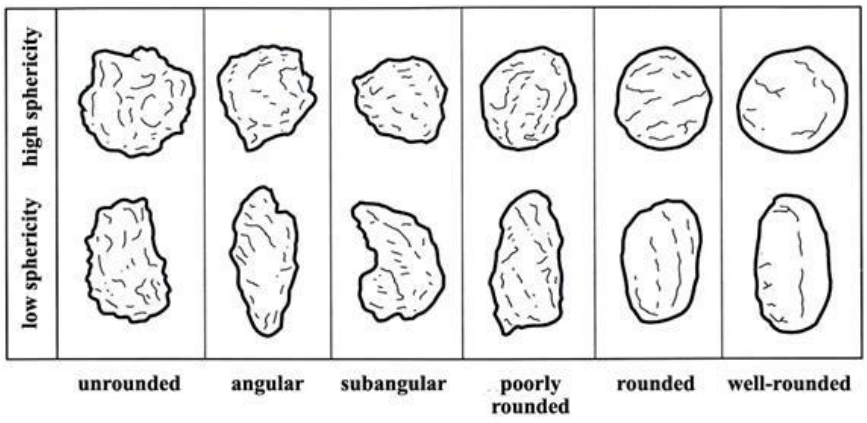


**Fig. 3.6:** The degree of rounding and sphericity determined by Powers (1953). This figure is redrawn from the classification images in Powers (1953)

**GRAIN CONTACT:**

Grain contact are described based on the classification in Taylor (1950) (**Fig. 3.7**)

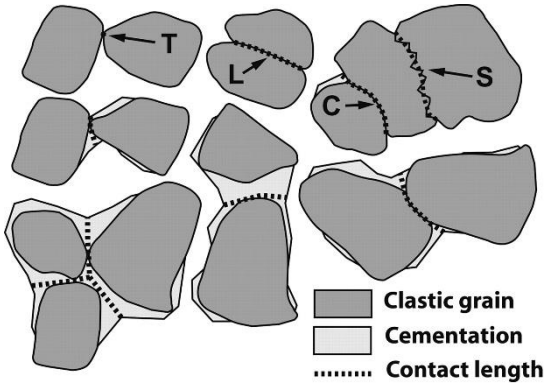


**Fig. 3.7:** An illustration of grain contacts based on the contact definition in Taylor (1950). T and L are point contacts, T is tangential contact and L is long contact. C is a concavo-convex contact and S is Sutured contact. The illustration is from (Storvoll and Bjørlykke, 2004)

### 3.2.2 MICROSCOPY LAB – POINT COUNTING

Point counting was conducted to find the proportion of minerals, cement and porosity. In this work 300 points were counted per thin section in 81 samples. **Fig. 3.8** shows the point-counter equipment used. The stage moves the thin section 300 times (**Fig. 3.9**), and the mineral, cement or pore space observed under the cross in the centre of the microscope is registered on the point counter. The stage was moved with a spacing of ~1.5 mm along the long axis and a spacing of ~2.5 mm along the short axis, 10 lines were counted and 30 points were counted per line for each thin section (**Fig. 3.9**). The thin sections were counted with a magnification of 100.

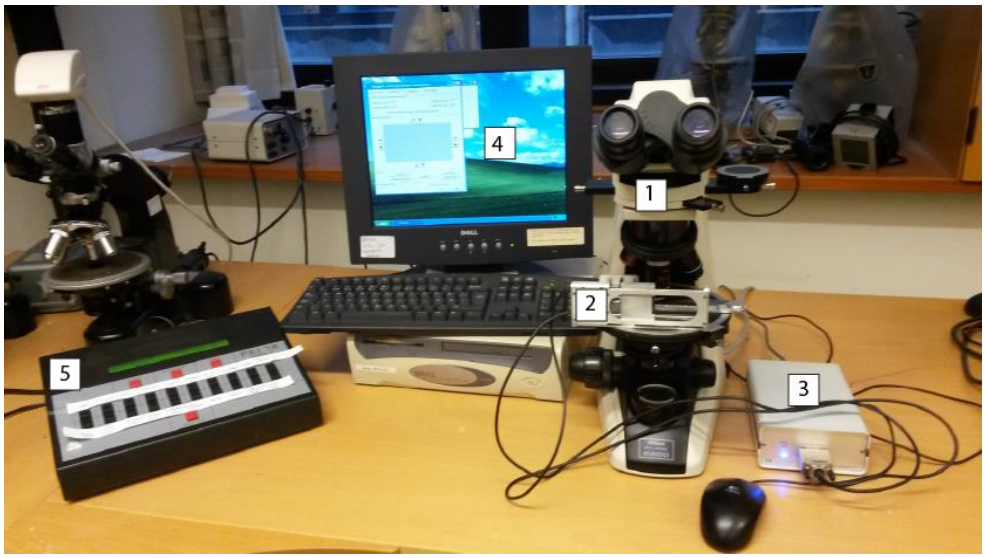


**Fig. 3.8:** Shows the point counting equipment in the Microscopy Lab at the University of Bergen. 1) Nikon EclipseE200POL, polarizing microscope 2) MicroStepper stage, Mk1.5 "wire-connected" 3) MicroStepper stage controller box 4) PETROG Lite software 5)PRIOR MODEL G point counter

The stepping stage is controlled by the PETROG Lite software and the composition is registered manually on the PRIOR MODEL G point counter.

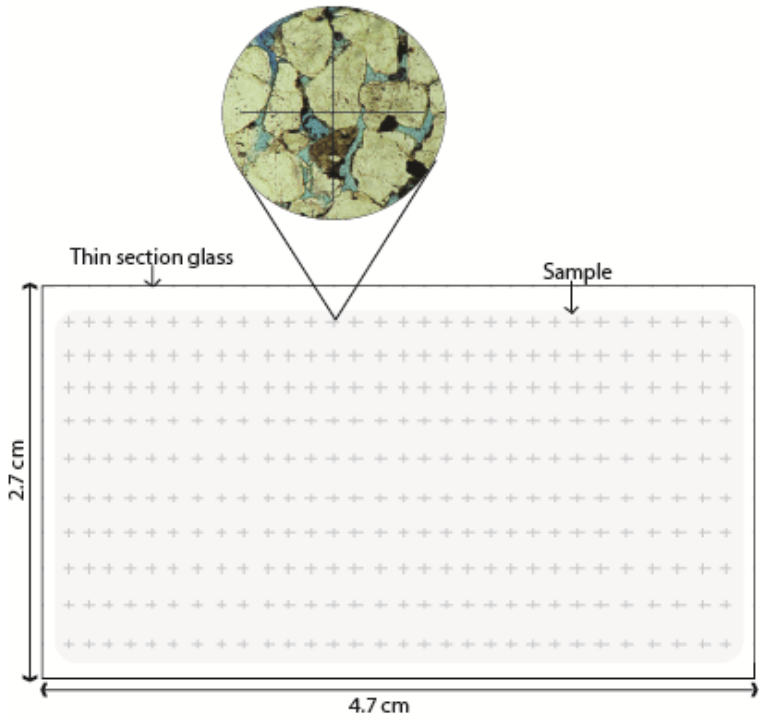


**Fig. 3.9:** The crosses represent the points that were counted. The shaded area represents the sample on the thin section glass. For each point the mineral in the centre was registered, for this example that would be the quartz grain underling the cross.

#### ERRORS CONNECTED TO POINT COUNTING

Point counting is based on visual observations in the microscope and there are several uncertainties connected with the result. In this study mineral grains with low abundance were registered once or twice if observed several times but not observed in the centre of the thin section, this could result in a slight overestimation of the grains with abundance of 1% or less.

According to Solomon (1963) there are three principal error sources tied to point counting;

1. *Operator errors*, with different operators the results will vary. Solomon (1963) considered this as the most insignificant of the three error sources.
2. *Counting errors*, errors in counting are dependent on the size of the grains, the area counted and the stepping length. Solomon (1963) concluded that the stepping length is the controlling factor for the variance in counting results and should at least half of the grain radius.
3. *Sampling errors*, these errors are connected with estimating the composition of a volume based on the composition of one section in the volume. Low degree of error is dependent on randomly distribution of grains, regular grain shape and a small variance of composition within the volume (Solomon, 1963).

### 3.2.3 LABORATORY FOR ELECTRON MICROSCOPY – (SEM)

Four thin sections from different facies associations and different stratigraphic members were selected for further analysis with SEM. The thin sections were polished and steamed with carbon before being inserted in the SEM. Several pictures were taken of the thin sections with different magnifications before the analysis; the reason for this was to make it easier to navigate the SEM. The purpose of analysis in SEM was to identify mineral grains, cement etc. which were hard to visually identify during point counting.

Both detection of backscattered electrons (AsB) and detection of secondary electrons (SE2) were used to get the chemical composition of different elements in the thin sections. The magnification varied between 64X on the lowest to 464X on the highest. The high voltages (EHT) used for these analyses were 15 KV, and the distance from the electron shooter varied mostly between 8 and 12 mm. Detection of SE2 was used when the AsB did not produce sharp images.

## 3.3 STATISTICAL METHODS

### 3.3.1 ANALYSIS OF MULTIVARIATE POPULATIONS – CLUSTER ANALYSIS

Cluster analysis was used to create a dendrogram showing the similarities between the different compositional factors, such as minerals, cement and porosity. The dendrogram was created using the average pair-group clustering method (Romesburg, 2004).

- First the Spearman's ($r_s$) correlation coefficient was calculated using PAST*
- "Closed" data cannot be used in this calculation (Nemec, 2011). Therefore input data was the number of grains counted, and not the compositional per cent calculated from the point counting data.
- A dendrogram was created using the average pair-group method for clustering and correlation as the similarity index.

* PAST is free software created by Øyvind Hammer, Natural History Museum at the University of Oslo. This software is developed for scientific data analysis, where univariate and multivariate statistics are some of the functions.

A zone of insignificant correlations was calculated using the "Fisher test for the significance of linear correlation" (Cohen et al., 2013). **Equation 2.1** was used to calculate this zone. The area is defined by positive and negative values of Pearson's correlation coefficient ($r_{xy)}$. The critical value (t) was found in Table 2 in Nemec (2011) with a degree of freedom (DF) of 80 and a level of significance (α) of 0.1.

(**Equation 2.1**) $$t = |r_{xy}|\sqrt{\frac{DF}{1-r_{xy}^2}}$$

# 4 SEDIMENTOLOGY

The sedimentology of the Cretaceous deposits of the Book Cliffs and Wasatch Plateau has been extensively described, analysed and interpreted in previous studies (e.g. Young, 1955; Balsley, 1980; Van Wagoner et al., 1990; Van Wagoner, 1995; Edwards et al., 2005; Pattison et al., 2007; Bhattacharya and MacEachern, 2009; Hampson, 2010; Olariu et al., 2010; Deveugle et al., 2011; Hampson et al., 2014). The purpose of this thesis is not to reinterpret the sedimentology of the area, but to investigate petrological and petrophysical properties of the deposits. The following chapter is a summary of the field observations from this study, seen in the light of previously published work.

## 4.1 FACIES AND FACIES ASSOCIATIONS

Seventeen sedimentary facies associations have been distinguished in the studied succession. They are described and interpreted in the present chapter, and are further analysed in terms of related depositional environment. The sedimentological logs are presented in chapter 5 and in **Fig. 1** in **Appendix II.**

### 4.1.1 FACIES ASSOCIATION A – SHELF TURBIDITES (ST)

**OBSERVATION:**

This facies association consists predominately of laminated mudstone/siltstone facies, but locally isolated very fine grained sandstone facies are observed (**Fig. 4.1 A**). The sedimentary structures observed in the sandstones generally represent facies within the Bouma sequence ($T_{bc}$). The sandstones commonly contains plane parallel-stratification (PPS) at the base ($T_b$) (**Fig. 4.1 C**), which grades into current-, wave- and combined flow-ripple cross-lamination (RCL) at the top ($T_c$). The ripple cross-lamination is often observed as supercritical climbing ripples (**Fig. 4.1 B**).

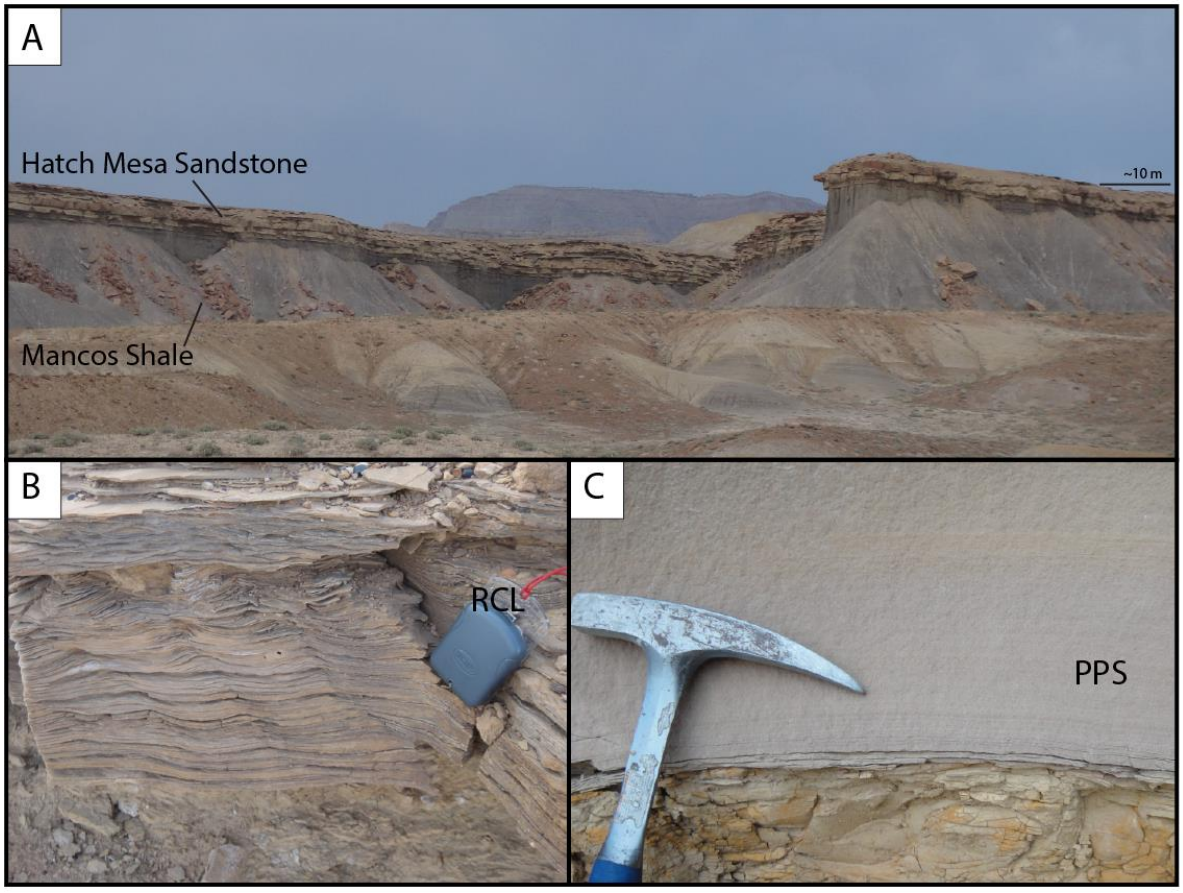


**Fig. 4.1:** Photos from submarine turbidites of the Prairie Canyon Mb. **A)** An overview photo of Hatch Mesa gravity flow deposited sandstones, isolated in Mancos Shale offshore muds. **B)** Supercritical climbing ripple cross-lamination (Tc) in the Mancos B sandstone unit. **C)** Plane parallel-stratified facies (Tb) in Hatch Mesa Sst.

**INTERPRETATION:**

This facies association has previously been interpreted as prodelta deposits, but a more recent interpretation based on detailed mapping suggests these deposits to be submarine channel and lobe deposits, deposited by gravity flows (Hampson, 2010). The isolated sandstone facies are further interpreted as turbidites deposited by hyperpycnal flows. The sediments bypassed the delta-front trough subaqueous channels and were deposited on the lower part of the delta slope, palaeoseaward of the clinoforms toe (Pattison, 2005; Pattison et al., 2007; Bhattacharya and MacEachern, 2009; Hampson, 2010; Li et al., 2011). The presence of wave and combined flow ripples suggests that the water depth was relatively shallow, above storm wave base and probably lay on a shallow marine, open shelf.

### 4.1.2 FACIES ASSOCIATION B – OFFSHORE MUD (OS)

**OBSERVATION:**

This facies association consists predominantly of grey silty claystone, and the only sedimentary structure observed is horizontal lamination.

**INTERPRETATION:**

This facies association is interpreted to be offshore shale deposits, which has been deposited from suspension in a quiet open marine environment (Young, 1955; Matheny and Picard, 1985; Hettinger and Kirschbaum, 2002). It represents the key facies association within the Mancos Shale Fm., and makes up a large part of the sections studied in this thesis.

### 4.1.3 FACIES ASSOCIATION C – DISTAL DELTA FRONT (DDF)

**OBSERVATION:**

This facies association consists of interbedded sandstone and siltstone layers (**Fig. 4.2**). The siltstones can be divided into two facies; highly bioturbated siltstones and laminated siltstones. The sandstone facies commonly consists of very fine sandstone layers with current and wave ripple cross-lamination (RCL). Locally very fine sandstone with plane-parallel stratification (PPS) and hummocky cross-stratification (HCS) can also be observed.


**Fig. 4.2:** Interbedded sandstone and siltstone interpreted as distal delta front deposits from the Upper Ferron member of the Mancos Shale Fm. in Ivie Creek along I-70. The blue line represents a flooding surface separating two parasequences from each other.

**INTERPRETATION:**

This facies association is interpreted to be distal delta front deposits (dDF) belonging to a river-dominated delta front depositional environment. The abundance of siltstone indicates a distal environment and the sandstone facies are episodically deposited by hyperpycnal flows (Enge et al., 2010; Olariu et al., 2010; Deveugle et al., 2011). Bhattacharya and MacEachern (2009) interpreted the local presence of HCS to represent influence by storm events and wave activity. They suggest a linkage between the river floods and storm events when generating these hyperpycnal flows.

### 4.1.4 FACIES ASSOCIATION D – PROXIMAL DELTA FRONT (PDF)

**OBSERVATION:**

This facies association is relatively similar to facies association **A**, but with a higher sandstone/siltstone ratio and it occurs in a different setting. The siltstone facies are mostly structureless or laminated ($T_d$). Organic rich siltstones are also observed. The siltstone facies are interbedded with the sandstone facies (**Fig. 4.3 A**). Often very fine to fine grained

sandstone facies constituting parts of a Bouma sequence ($T_{abc/abcd}$; massive, plane parallel-stratification (PPS) and ripple cross-lamination (RCL)) are observed (**Fig. 4.3 B**). These sequences commonly have an erosive base. Locally hummocky cross-stratification (HCS) is also occasionally observed (**Fig. 4.3 C**) in this facies association.

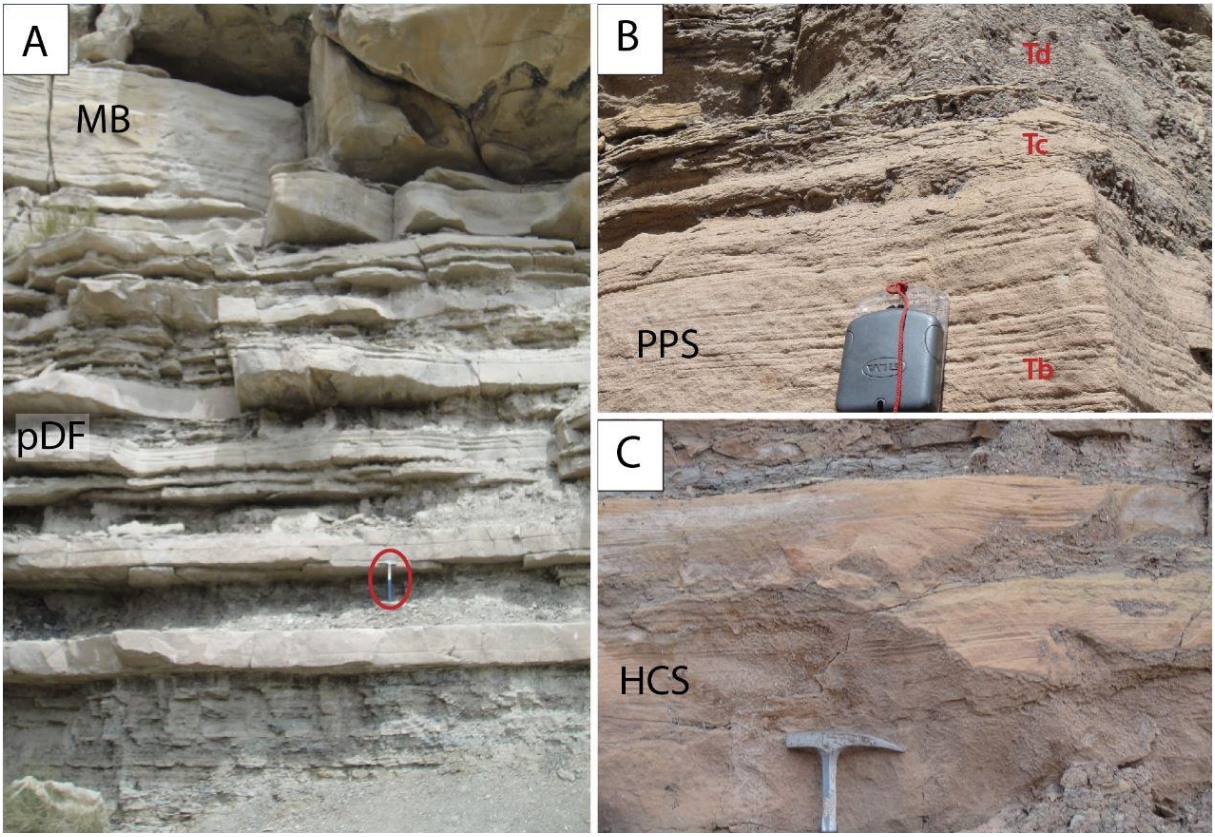


**Fig. 4.3:** Proximal delta-front deposits (pDF). **A)** pDF Sandstone interbedded with siltstone deposited by hyperpycnal flows, overlain by mouth bar deposits (MB) from the Panther Tongue Mb. in Gentile Wash, see geological hammer in red circle for scale. **B)** Part of a Bouma sequence observed in pDF deposits in Ferron Fm. Tb = Plane parallel-stratified (PPS) sandstone , Tc = Ripple cross-laminated sandstone and Td =laminated mudstone. **C)** Locally observed Hummocky cross-stratified (HCS) sandstone in Ferron Fm.

**INTERPRETATION:**

This facies association is interpreted as proximal delta-front deposits (pDF) associated with a river-dominated delta, with minor reworking by waves (Pattison, 2005; Olariu et al., 2010; Deveugle et al., 2011; Li et al., 2011). The sandstone beds are interpreted to have been deposited episodically by hyperpycnal flows (Bhattacharya and MacEachern, 2009; Enge et al., 2010; Deveugle et al., 2011). Deveugle et al. (2011) suggest that the presence of interbedded organic rich siltstone represents deposition close to a deltaic distributary mouth.

### 4.1.5 FACIES ASSOCIATION E – MOUTH BAR (MB)

**OBSERVATION:**

This facies association consist of amalgamated sandstone. Siltstone facies is absent in this facies association. Some parts of the sandstone have a massive appearance, but plane parallel stratification (PPS) and cross-stratification (mostly low angle, some trough) are also present. This facies is commonly observed overlying proximal delta-front deposits (**Fig. 4.3 A**), and is locally capped by transgressive lag deposits. These deposits generally have a low degree of bioturbation.

**INTERPRETATION:**

This facies association is interpreted as mouth bar deposits (MB), which were deposited on the delta-front, landward of the pDF deposits. Mouth bars form at the mouth of a distributary channel, where unidirectional currents run into a standing body of water. The unidirectional currents cause subaqueous dunes to migrate, resulting in mouth bar deposits on the delta-front. Palaeoseaward of these deposits, sands are deposited on the delta-front by hyperpycnal flows. The mouth bars are deposited in a river dominated depositional system (Enge et al., 2010; Deveugle et al., 2011).

### 4.1.6 FACIES ASSOCIATION F – DISTRIBUTARY CHANNEL FILL (DC)

**OBSERVATION:**

This facies association consist of amalgamated very fine to fine grained channelized sand-bodies (**Fig. 4.4**) with only minor occurrence of organic rich siltstone facies (**Fig. 4.4 B**). The sedimentary structures in the different sandstone facies varies between massive, low angle cross-stratification (LCS), plane parallel-stratification (PPS) and current ripple cross-lamination (RCL). The thickness of these deposits observed during the fieldwork for this thesis varies from meters to tens of metres. The largest observed channel body is in the Panther Tongue Mb. as is 22 m thick (**Fig. 4.4 C**).

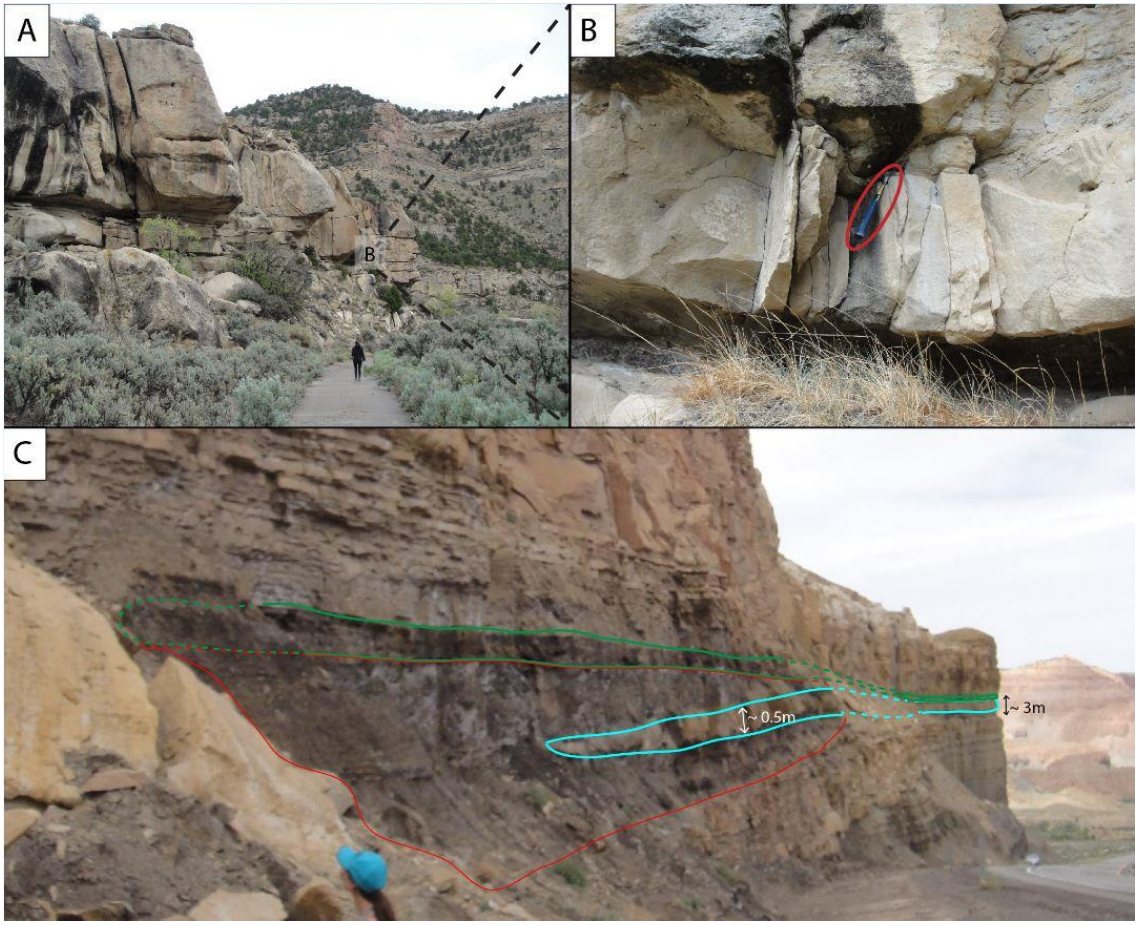


**Fig. 4.4:** Photos of distributary channel deposits in the Panther Tongue Mb. in Spring Canyon. **A)** An overview photo, this channel thins out to the sides ("B" in this photo represents the location of photo B). **B)** Close up of the distributary channel with an erosive base, see geological hammer in red circle for scale. **C)** The blue channelized body represents a distributary channel in the Ferron Sandstone, the thickness varies from decimetre scale were it pinches out towards the west (left in this photo) to meter scale in the cliffs (right in this photo). The siltstones observed within the red area in this photo are interpreted as lagoonal deposits (facies association **M**). The green unit represents continental coal swamp deposits (facies association **N**).

**INTERPRETATION:**

This facies association is interpreted as distributary channel fills, deposited on the delta top and cutting down in to the delta- front in a river dominated depositional environment (Olariu et al., 2010; Deveugle et al., 2011; Li et al., 2011). Distributary channels are the most distal feature of the fluvial feeding system and can be both subaerial and subaqueous. In outcrops these deposits are often observed on top of the delta-front deposits (MB and pDF) (Olariu and Bhattacharya, 2006).

### 4.1.7 FACIES ASSOCIATION G – TRANSGRESSIVE LAG (LAG)

**OBSERVATION:**

This facies association consists of amalgamated massive and homogeneous fine to coarse grained sandstone. The main facies has gone through intensive bioturbation which gives it a massive appearance (**Fig. 4.5**), but locally a facies with some laminated and cross-stratified structures can be observed. This facies association also contains oyster shells and shark teeth (Hwang and Heller, 2002). This facies association caps the top of several parasequences; both in the river dominated Panther Tongue Mb. and in the wave dominated Blackhawk Formation (Hampson 2010).

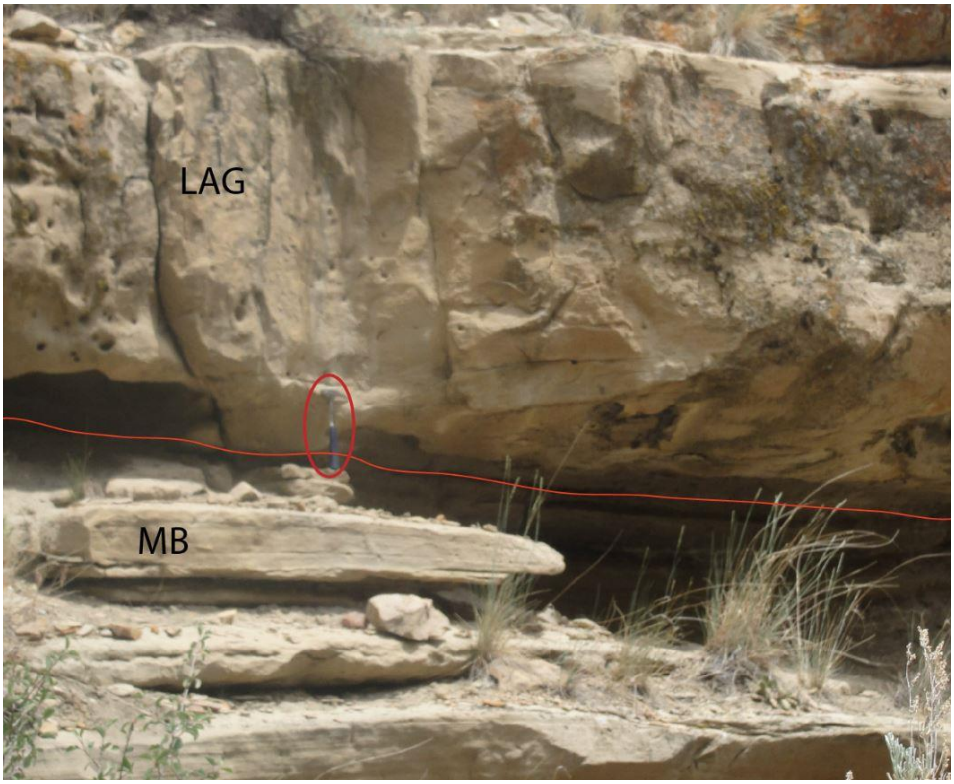


**Fig. 4.5:** Photo of transgressive lag deposits (LAG) in the Panther Tongue Member in Gentile Wash. The red line represents the erosive base of the transgressive lag. The sandstone underlying the red line represents (facies association **E**) mouth bar deposits (MB). See geological hammer in red circle for scale

**INTERPRETATION:**

This facies association is interpreted to be transgressive ravinement lag deposits. Transgressive lags are deposited by wave reworking of the delta front top during sea-level rise (Hwang and Heller, 2002; Olariu et al., 2010).

### 4.1.8 FACIES ASSOCIATION H – OFFSHORE TRANSITION ZONE (OTZ)

**OBSERVATION:**

This facies association consists of alternating very fine sandstone and siltstone (**Fig. 4.6**). The sedimentary structures observed in the sandstone facies are predominately hummocky (HCS) and wave ripple cross-lamination (RCL). A low degree of bioturbation is observed in these facies. The sand/silt ratio gradually increases upwards until it reaches facies association H.

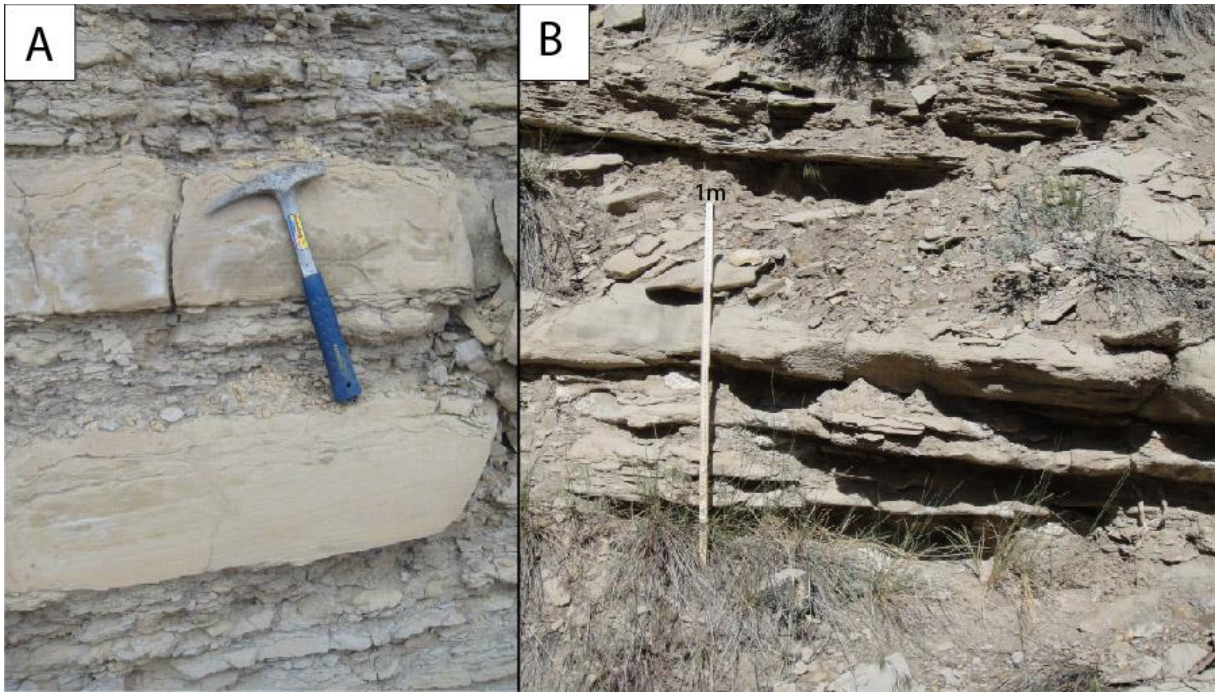


**Fig. 4.6:** Photos of offshore transition zone (OTz) deposits. **A)** OTz deposits in Ferron Fm. **B)** OTz deposits in Kenilworth Mb. of Blackhawk Fm. in Horse Canyon, the measuring stick used for scale is 1m long.

**INTERPRETATION:**

This facies association is interpreted as offshore transition zone deposits (OTz) in a wave/storm dominated shoreface depositional environment. Some authors have interpreted these deposits to be from the distal part of the lower shoreface (Taylor and Lovell, 1995; Li et al., 2011; Eide et al., 2014). The sandstone facies were deposited below fair weather wave base during storms and the siltstone facies were deposited during fair weather conditions (Machent et al., 2007)

### 4.1.9 FACIES ASSOCIATION I – LOWER SHOREFACE DEPOSITS (LSF)

**OBSERVATION:**

This facies association consists of amalgamated very fine to fine grained sandstone with some interbedded siltstone. The siltstone facies is only observed in the lower part where the sandstone beds are not amalgamated. The sedimentary structures observed in the sandstone facies are predominantly hummocky cross-stratification (HCS) and swaley cross-stratification (SCS), but wave ripple cross-lamination and plane parallel-stratification (PPS) can also be observed (**Fig. 4.7**). This facies usually has a low to moderate degree of bioturbation, locally this facies has been observed with intense bioturbation.

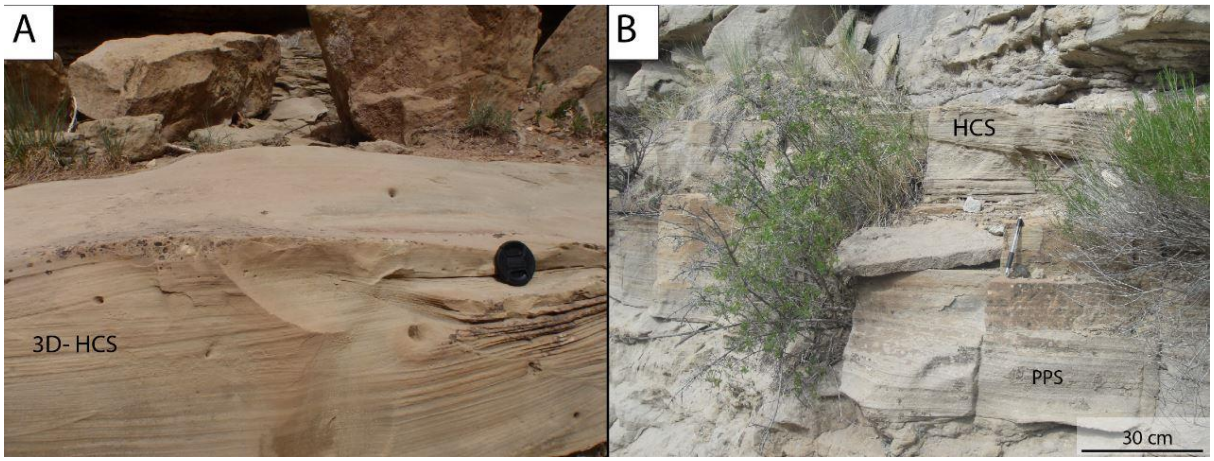


**Fig. 4.7:** Photos of lower shoreface (LSF) deposits. **A)** 3D Hummocky cross-stratification (HCS) in LSF deposits in Spring Canyon Mb. of the Blackhawk Fm. in Gentile Wash. **B)** HCS and PPS in LSF deposits in Kenilworth Mb. of the Blackhawk Fm. in Horse Canyon.

**INTERPRETATION:**

This facies has been interpreted as lower shoreface deposits (LSF) in a wave/storm dominated shoreface depositional environment (Clifton, 2006; Machent et al., 2007; Li et al., 2011; Hampson et al., 2014). HCS and SCS are formed below fair weather wave-base due to combined flow of oscillatory waves and a unidirectional current (Dumas et al., 2005). The PPS forms during strong oscillatory currents. When the HCS and SCS have very long wavelengths it can have a similar appearance to PPS and it can be hard to distinguish these sedimentary structures (Taylor and Lovell, 1995).

### 4.1.10 FACIES ASSOCIATION J – MIDDLE SHOREFACE DEPOSITS (MSF)

**OBSERVATION:**

This facies association consist of intensively bioturbated fine grained sandstones (**Fig. 4.8**). Locally within the facies association some weak low angle cross-stratification (LCS), SCS or HCS can be observed, but in most cases the bioturbation has removed all sedimentary structures. This facies association is located between LSF- and USF deposits, and is only present in some of the studied parasequences. Trace fossils observed in this facies are *Skolithos*, *Ophiomorpha*, *Thalassinoides* among others (MacEachern, 1992; Howell and Flint, 2003)

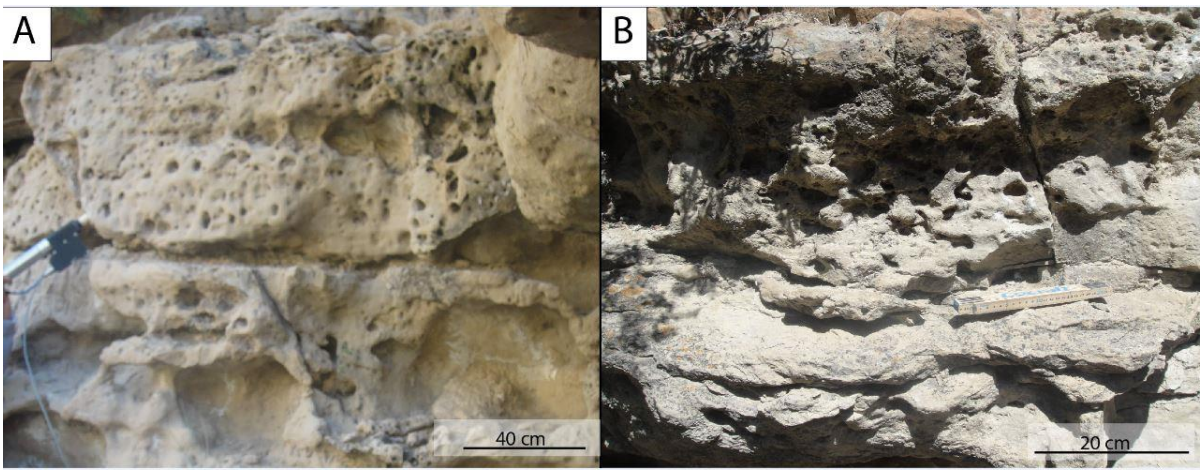


**Fig. 4.8:** Photos of middle shoreface (MSF) deposits. **A)** Intensively bioturbated MSF deposits in Spring Canyon Member of the Blackhawk Fm. in Gentile Wash. **B)** Intensively bioturbated MSF sandstone overlying LSF sandstone in Kenilworth Mb. of the Blackhawk Fm. in Horse Canyon.

**INTERPRETATION:**

This facies association is interpret as middle shoreface deposits (MSF) (Howell and Flint, 2003; Clifton, 2006). The trace fossils assembly observed in the middle shoreface represents a change in ichnofacies from the *Cruziana* ichnofacies of LSF to the *Skolithos* ichnofacies of MSF (MacEachern, 1992; Clifton, 2006).

### 4.1.11 FACIES ASSOCIATION K – UPPER SHOREFACE DEPOSITS (USF)

**OBSERVATION:**

This facies association consists of fine grained sandstone with trough cross-stratification (TCS) (**Fig. 4.9**), locally low angle cross-stratification (**Fig. 4.9 B**) can be observed. These deposits generally exhibit a low degree of bioturbation.

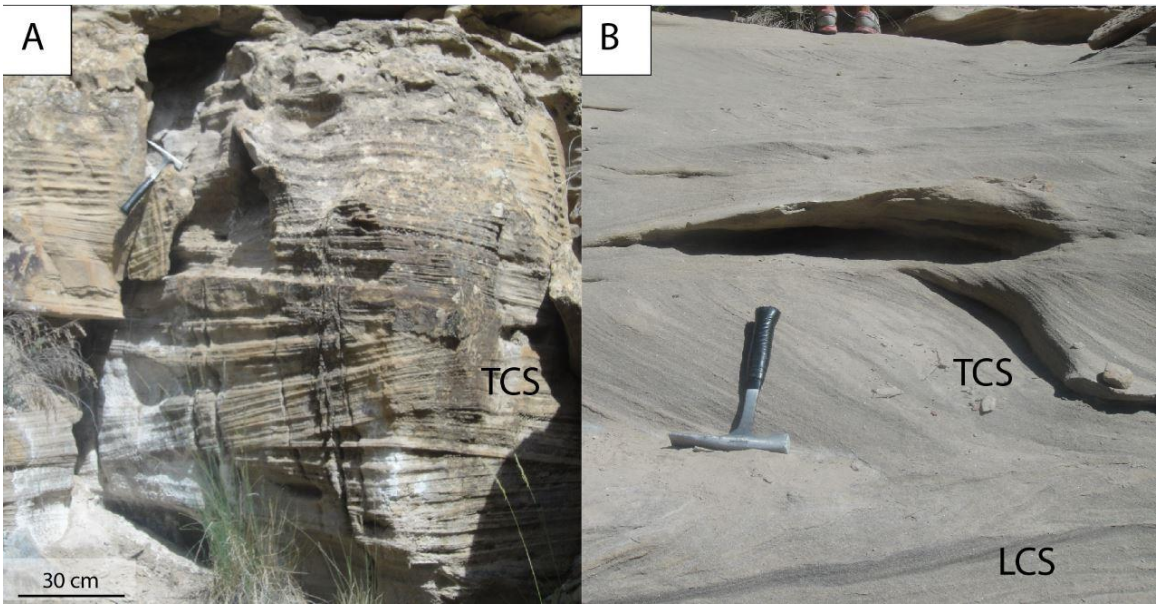


**Fig. 4.9:** Photos of upper shoreface (USF) deposits. **A)** USF deposits with through cross-stratification (TCS) in Kenilworth Mb., Blackhawk Fm. **B)** USF deposits with TCS and low angle cross-stratification (LCS) in Spring Canyon Mb., Blackhawk Fm.

**INTERPRETATION:**

These sandstones are interpreted as upper shoreface deposits (USF). This facies association is deposited in a wave/storm dominated shoreface depositional environment (Li et al., 2011; Eide et al., 2015). The sedimentary structures are formed during fair weather conditions as a

result of migration of dunes on nearshore bars and rip channels by longshore and offshore directed currents (Clifton, 2006; Hampson et al., 2011; Eide et al., 2015).

### 4.1.12 FACIES ASSOCIATION L – FORESHORE DEPOSITS (FS)

**OBSERVATION:**

This facies association predominantly consists of fine grained sandstone facies with plane parallel-stratification (PPS) (**Fig. 4.10 A**) and rootlets. The uppermost part of this facies is often observed as a white cap underlying a coal bed or an erosive boundary (**Fig. 4.10 B**).

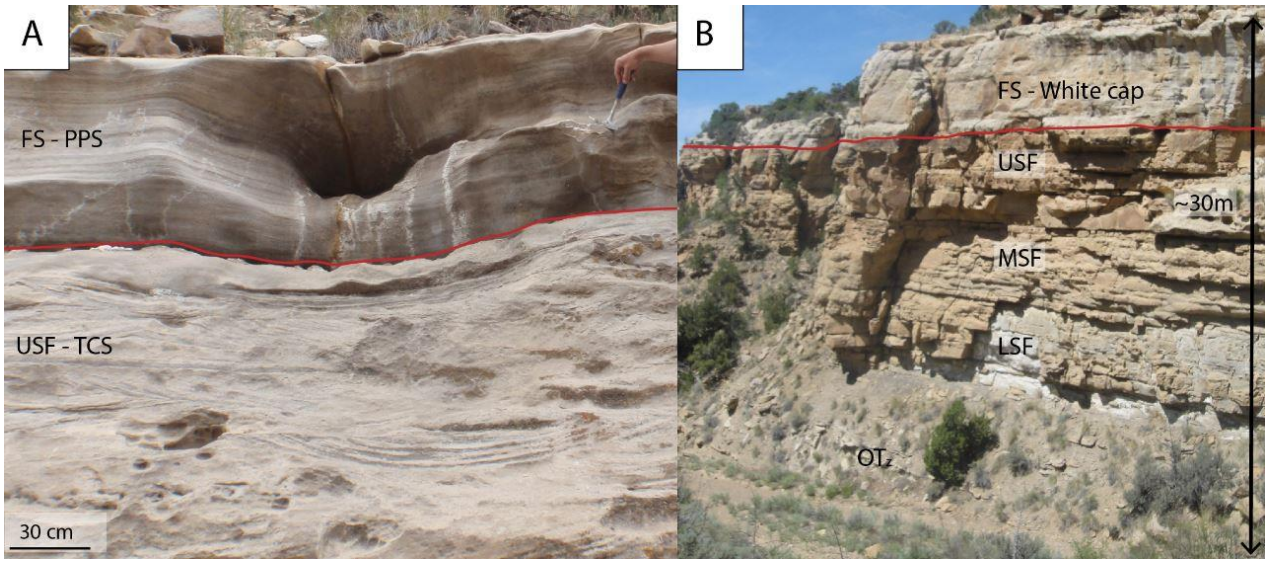


**Fig. 4.10: A)** Photo of plane-parallel stratified (PPS) foreshore (FS) sandstone overlying trough cross-stratified (TCS) upper shoreface (USF) sandstone in Spring Canyon Mb., Blackhawk Fm. in Gentile Wash. The red line separates the two facies associations. **B)** Photo from the Kenilworth Mb. of the Blackhawk Fm. in Horse Canyon. This photo shows FS as a white cap on top of the other shoreface deposits.

**INTERPRETATION:**

This facies is interpreted as foreshore deposits (FS) in a wave/storm dominated shoreface depositional environment (Clifton, 2006; Li et al., 2011). The plane parallel-stratification is formed by sheet floods and swash lamination due to breaking waves on the strandplain (Clifton, 2006; Hampson et al., 2011; Eide et al., 2015). The whitecap is formed by organic acids from the overlying coal, during early burial and diagenesis these acids have caused mineral leaching of the underlying FS deposits (Taylor et al., 2000; Taylor and Machent, 2010).

### 4.1.13 FACIES ASSOCIATION M – LAGOONAL DEPOSITS (CP/L)

**OBSERVATION:**

This facies association consists of laminated carbonaceous mudstone, rich in organic fragments. Laterally continuous coal beds can be observed (Eide et al., 2015). This facies association is observed with a distributary channel deposit of the Ferron Formation in the Ivie Creek location (**Fig. 4.4 C**).

**INTERPRETATION:**

This facies has been interpreted as coastal plain/lagoonal deposits (CP/L) because of the evidence of standing water, the sedimentary structures (laminated mud) indicating low energy and the accumulation of organic debris (Garrison Jr and Van den Bergh, 2006; Deveugle et al., 2011; Eide et al., 2015)

### 4.1.14 FACIES ASSOCIATION N – MIRE AND PEAT SWAMP COAL (C)

**OBSERVATION:**

Several lateral consistent coal beds and seams are observed in this study area. These coal beds are often observed overlying foreshore or distributary channel deposits (**Fig. 4.4 C**), or in-between meandering channel fill deposits (**Fig. 4.11 A**).

**INTERPRETATION:**

These deposits are interpreted as mire and coal swamp deposits (CS) on the coastal plain (Davies et al., 2005)

### 4.1.15 FACIES ASSOCIATION O – MEANDERING CHANNEL FILL (MC)

**OBSERVATION:**

This facies association consists of heterolithic deposits, fine to medium grained sandstones are interbedded with siltstones or coals (**Fig. 4.11 A**). These sandstone facies generally show a fining upwards trend. The sedimentary structures observed in the different facies are trough cross-stratification (TCS) (**Fig. 4.11 B**), current ripple cross-lamination and locally low angle cross-stratification. The deposits commonly have an erosive base, and show lateral accretion surfaces.

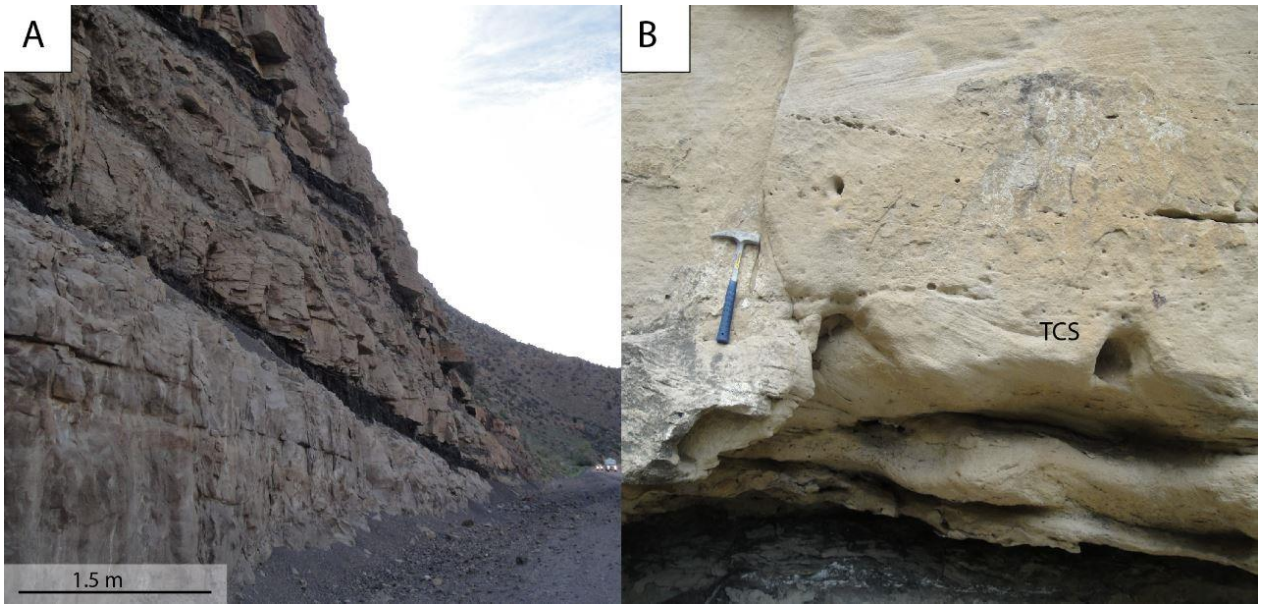


**Fig. 4.11: A)** Photo of coal seams in-between meandering channel-fill deposits in the Non-marine Blackhawk Fm., close to the Castlegate Mine. **B)** Photo of meandering channel-fill deposits with trough cross stratification (TCS) in the Non-marine Blackhawk Fm., in Joe's Valley.

**INTERPRETATION:**

This facies association has been interpreted to be fluvial channel fill deposits from sinuous meandering channels on the coastal plain (Hampson, 2010; Deveugle et al., 2011). The lateral accretion packages form as point bars in meandering channels (Allen, 1982). The siltstone facies are interpreted as abandonment plugs within channels that have avulsed (Hampson et al., 2011).

### 4.1.16 FACIES ASSOCIATION P–CREVASSE SPLAY, FLOODPLAIN (CS/F)

**OBSERVATION:**

This facies association consists of fine grained sheetlike sandstone beds interbedded with siltstone (**Fig. 4.12**). The sedimentary structures observed in the sandstone are current ripple cross-lamination and some plane parallel stratification. Rootlets and thin coal beds underlain by roots are common in this facies association. These deposits belong to the non-marine part of the Blackhawk Fm. and are observed adjacent to meandering river deposits.

**Fig. 4.12:** Photo showing crevasse splay sandstones interbedded with floodplain mudstone, from Non-marine Blackhawk Fm., in Joe's Valley. Note geological hammer in the red circle for scale.

**INTERPRETATION:**

This facies association is interpreted to have been deposited in a floodplain environment. The siltstone facies represents low energy floodplain deposits, while the sheetlike sandstone facies represents crevasse-splay deposits , Roots and in situ coal beds indicate subaerial exposure (Hampson, 2010; Hampson et al., 2013).

### 4.1.17 FACIES ASSOCIATION Q – BRAIDED CHANNEL BAR (BC)

**OBSERVATION:**

This facies association consists of generally 1-2 m thick vertically stacked sandstone beds. The beds have an occasionally coarsening upwards trend where grain size varies from fine-medium sand to coarse sand and the beds often contain an increasingly amount of pebble clasts towards the top (**Fig. 4.13 B**). The sedimentary structures observed are tabular and trough (TCS) cross-stratifications (**Fig. 4.13C**) and current ripple cross-laminations (RCL). The sandstone beds are often separated by relatively thin siltstone units (**Fig. 4.13A**).

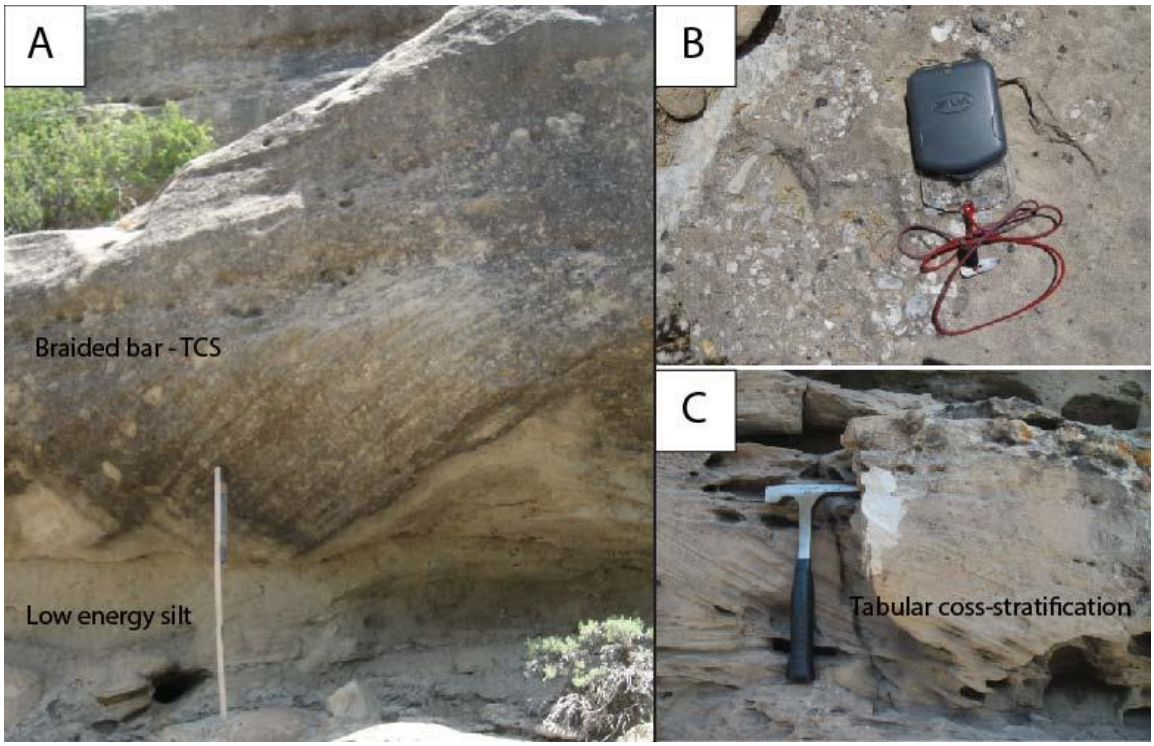


**Fig. 4.13: A)** Braided channel bar deposits on top of low energy siltstone deposits, in Castlegate sandstone in Joe's Valley, note 60 cm high measuring stick for scale. **B)** Pebble clasts observed at the top of a braided channel bar deposit, in Castlegate sandstone in Joe's Valley. **C)** Tabular cross-stratification in photo from Castlegate sandstone in Bear Canyon.

**INTERPRETATION:**

These deposits are interpreted to be braided bars, deposited under high aggradation rates in a fluvial depositional system (McLaurin and Steel, 2007; Hampson, 2010; Hampson et al., 2013). The siltstone facies represents deposition during low energy conditions. The

amalgamated sandstone facies is interpreted as thalweg-fill and mid-channel barforms deposited by braided rivers with low to intermediate sinuosity (McLaurin and Steel, 2007).

## 4.2 DEPOSITIONAL SYSTEMS

Deposits from several different environments can be observed in the Book Cliffs and Wasatch Plateau. The depositional systems during the Late Cretaceous varied from a palaeoseaward offshore and gravity flow depositional system, to wave- and river-dominated shallow marine shoreline systems. Palaeolandward coastal plain systems were present, these included meandering rivers, floodplains, coal swamps, also braided alluvial environments were present (Howell and Flint, 2003; Hampson, 2010).

### 4.2.1 OFFSHORE MUD AND SHELF TURBIDITES

The Mancos Shale represents the offshore deposits (facies association **B**) of Late Cretaceous in Utah. Deposition occured palaeoseaward of the transition line for sand and mud in the shallow water of the Western Interior Seaway (Young, 1955; Hintze, 2005, p.58). Isolated sandbodies can be observed locally within the Mancos Shale group, such as the Hatch Mesa Sandstone and Mancos B Sandstone of the Prairie Canyon Member. These sandbodies were deposited by gravitational flows in the offshore depositional environment (Pattison, 2005; Pattison et al., 2007; Hampson, 2010), see facies association **A** for detailed description.

### 4.2.2 WAVE-DOMINATED SHOREFACE SHALLOW MARINE SYSTEMS

Most of the shallow marine deposits observed in the Book Cliffs and Wasatch Plateau belong to the wave-dominated shoreface depositional system. The exceptions are the Panther Tongue Mb. of the Star Point Fm. and parts of the Ferron Sandstone Mb., which comprise river-dominated delta deposits (**Fig. 4.14**) (Howell and Flint, 2003; Li et al., 2011). Shallow marine sandstones were deposited into the Western Interior Seaway as the shoreline prograded eastward during Late Cretaceous. The progradational parasequences of this depositional system includes the facies associations **H-L (Fig. 4.14** and **Fig. 4.16)** (Howell and Flint, 2003).

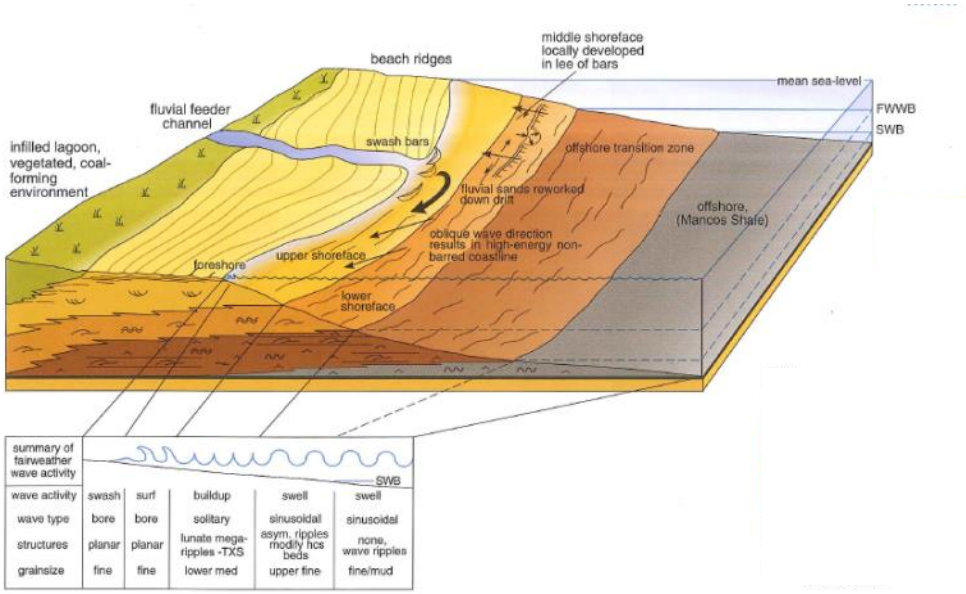


**Fig. 4.14:** Illustrates a progradational shoreline with the different facies associations in a wave- dominated depositional system. FWWB = fair weather wave base, SWB =s storm wave base. The figure is taken from Howell and Flint (2003).

### 4.2.3 RIVER-DOMINATED DELTAIC DEPOSITIONAL SYSTEM

Both during the deposition of parts of the Ferron Formation and the Panther Tongue Member of the Star Point Formation, river dominated delta lobes prograded into the Western Interior Seaway. Facies associations **C-G** are connected to this river dominated depositional system (**Fig. 4.15**) (Enge et al., 2010; Deveugle et al., 2011; Li et al., 2011). A conceptual model of this depositional system with lobe geometry and facies associations is shown in **Fig. 4.15.**

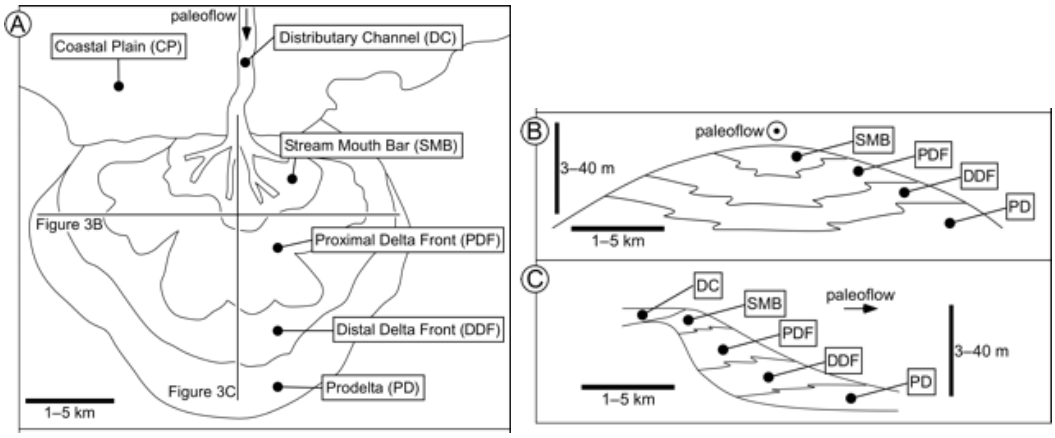


**Fig. 4.15:** A conceptual illustration of a river dominated deltaic system, and its belonging facies associations. **A)** A map view of the system. **B)** A cross-section along the axis of the shoreline (90° on the palaeoflow direction). **C)** A cross-section in the palaeoflow direction. Figure from Deveugle et al. (2011).

### 4.2.4 COASTAL PLAIN DEPOSITIONAL SYSTEM

This depositional system consists of the facies associations **M-P**. It is observed palaeolandward of the shoreline systems (**Fig. 4.16**) (Howell and Flint, 2003; Hampson, 2010). In this thesis this system was studied mostly in the non-marine Blackhawk Formation (facies associations **M-P**) and in in the Ferron Formation (facies association **M-O**).

### 4.2.5 ALLUVIAL PLAIN DEPOSITIONAL SYSTEM

In this study the alluvial plain depositional system comprises the braided river deposits (facies association **Q**). These alluvial plain deposits were predominantly from the Castlegate Mb. of the Price River Fm. and located in the NW part of the study area (**Fig. 1.1**) (Miall and Arush, 2001; McLaurin and Steel, 2007).


**Fig. 4.16:** A modern day analogue for the depositional systems belonging to the facies associations described above. The analogue is from Cabo Gracias a Dios in Nicaragua, satellite photo from google earth.

# 5 RESULTS

In this chapter results from each of the sampled stratigraphic units are presented illustrated with data from both outcrops and thin sections. The permeability data is also presented, showing variations by facies associations and stratigraphic units. In addition the petrographic data is presented together with the scanning electron microscope (SEM) results, showing the petrographic composition and properties.

The sampling locations (**Fig. 5.1**) and number of samples gathered in each of these locations is shown in **Table 5.1**.

**Table 5.1:** Table showing location of rock samples and which lithostratigraphic units the samples belong to. For a map of locations, see **Fig. 5.1**.

| **Location** | **Samples collected** | **Formations (Fm.)/ Members (Mb.)** | |
|---|---|---|---|
| *Ivie Creek, along Interstate 70* | 7 | Ferron Mb. | (Upper Member) |
| *Quitchupah Creek, West of State 10* | 4 | Emery Mb. | (Northern delta lobe) |
| *Huntington Creek* | 1 | Ferron Mb. | (Lower Member) |
| *Cottonwood Creek* | 1 | Star Point Fm. | (Storrs Mb.) |
| *Joe's Valley* | 4 | Blackhawk Fm. | (Non-Marine) |
| | 2 | Price River Fm. | (Castlegate Mb.) |
| | 1 | Star Point Fm. | (Storrs Mb.) |
| *Harmond Hills, North of Price* | 2 | Emery Mb. | (Southern delta lobe) |
| *Spring Canyon* | 3 | Star Point Fm. | (Panther Tongue Mb.) |
| *Gentile Wash* | 3 | Blackhawk Fm. | (Non-Marine) |
| | 9 | Blackhawk Fm. | (Spring Canyon Mb.) |
| | 1 | Star Point Fm. | (Storrs Mb.) |
| | 5 | Star Point Fm. | (Panther Tongue Mb.) |
| *Castle Gate Mine No 1, along U.S. 6* | 2 | Blackhawk Fm. | (Non-Marine) |
| *Bear Canyon, along U.S. 6* | 2 | Price River Fm. | (Castlegate Mb.) |
| *Solider Creek* | 1 | Blackhawk Fm. | (Non-Marine) |
| | 1 | Blackhawk Fm. | (Kenilworth Mb.) |
| *Sunnyside* | 1 | Blackhawk Fm. | (Kenilworth Mb.) |
| *Horse Canyon* | 14 | Blackhawk Fm. | (Kenilworth Mb.) |
| *Woodside Canyon* | 2 | Blackhawk Fm. | (Kenilworth Mb.) |
| | 1 | Prairie Canyon Mb. | (Woodside Sandstone) |
| *Gray Canyon* | 1 | Blackhawk Fm. | (Non-Marine) |
| | 10 | Blackhawk Fm. | (Grassy Mb.) |
| *Hatch Mesa* | 2 | Prairie Canyon Mb. | (Hatch Mesa) |
| *East of Hatch Mesa* | 1 | Prairie Canyon Mb. | (Mancos B) |

**Table 1** in **Appendix I** shows a more extensive table with location, formation and member, interpretation of facies association and GPS coordinates for each sample.

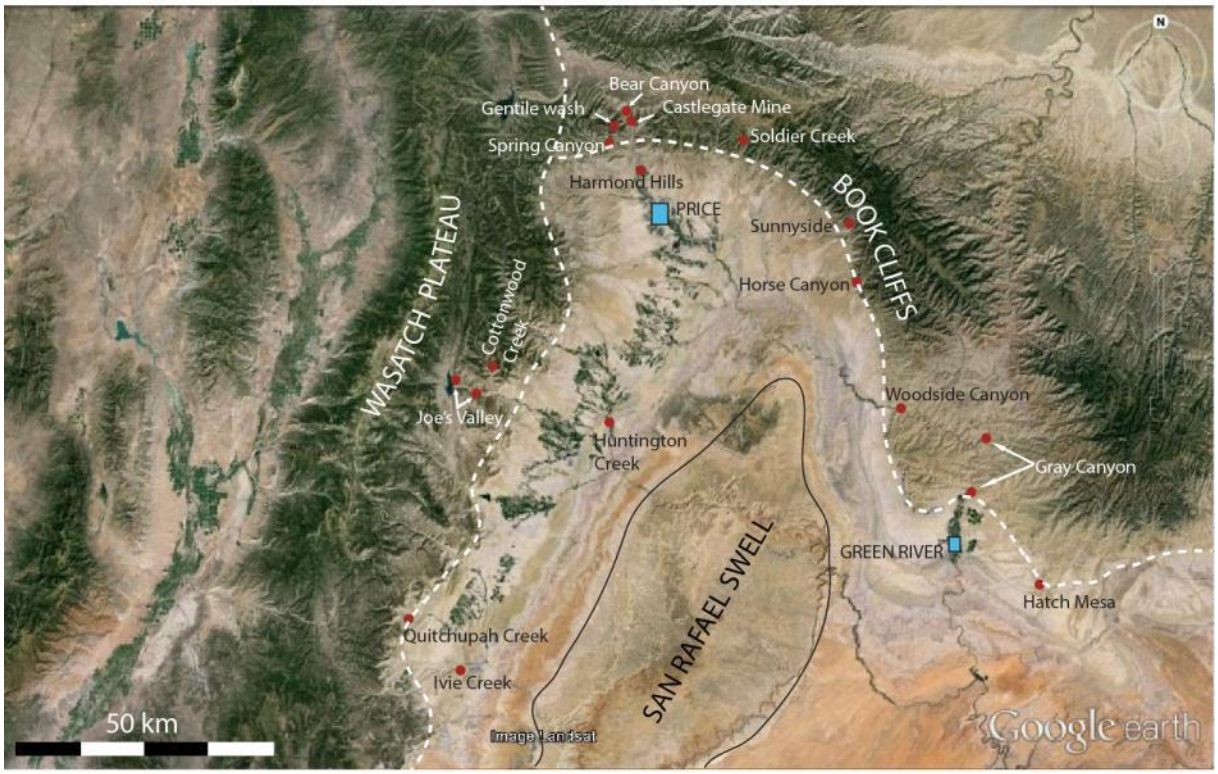


**Fig. 5.1:** Satellite photo of study area. The red dots indicate outcrop locations, blue boxes represent the towns of Price and Green River, and dashed lines represent the cliff edges of the Wasatch Plateau and Book Cliffs.

# 5.1 DESCRIPTION OF FORMATIONS AND MEMBERS

## 5.1.1 MANCOS SHALE FORMATION

### FERRON SANDSTONE MEMBER

The study of the Ferron Sandstone in this thesis focuses mostly on the Upper Ferron Member exposed in outcrops along Interstate 70 at the Ivie Creek locality (**Fig. 5.1**). One sample was collected from lower shoreface/offshore transition zone deposits of the Lower Ferron Member in the Huntington Creek location, but no further studies were performed on this sample, as it was out of scope for this thesis.

In the Upper Ferron Member the two lowermost parasequences (**Fig. 5.2**) from the north-eastward prograding Last Chance Delta system (Bhattacharya and MacEachern, 2009; Deveugle et al., 2011) were studied and logged (**Fig. 5.3**). The lower parasequence (Kf1) represents deposits from a river dominated deltaic depositional system, while the upper parasequence (Kf2) represents deposits from a wave dominated shoreline system. The facies associations found in this member are presented in **Table 5.2,** and their expression in outcrop and thin section is shown in **Fig. 5.2**. Sedimentological aspects of these facies associations are described in detail in Chapter 4.

The Ferron deposits exposed in Ivie Creek have been tilted by 2-5° towards the west after deposition, but they have not been subject to any major deformation, and facies architecture can therefore be studied without any structural reconstructions (Deveugle et al., 2011).

**Table 5.2:** Showing the facies associations observed in the two parasequences studied in Ivie Creek.

| Parasequence | Facies Associations | Abbreviation |
|---|---|---|
| Kf1 | C- Distal delta-front deposits | dDF |
| | D- Proximal delta-front deposits | pDF |
| | E- Mouth bar deposits | MB |
| | F- Distributary channel | DC |
| | M- Coastal plain/Lagoonal deposits | CP/L |
| | N- Coal swamp deposits | C |
| Kf2 | H- Offshore transition zone deposits | OTz |
| | I- Lower shoreface deposits | LSF |
| | L- Foreshore deposits | FS |
| | N- Coal swamp deposits | C |
| | O- Meandering channel fill | MC |

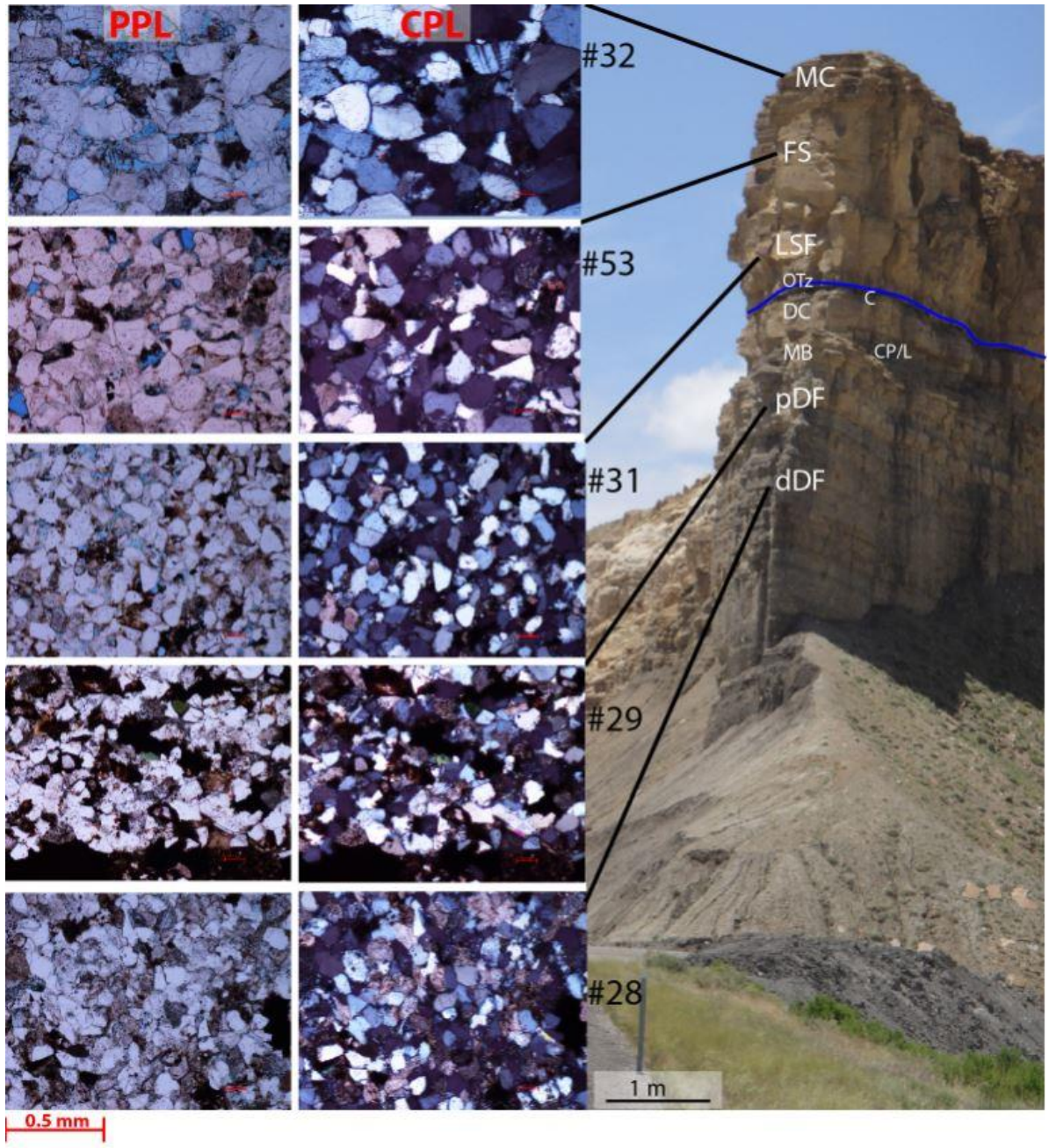


**Fig. 5.2:** Thin sections correlated to beds in the outcrop studied along I-70 at the Ivie Creek locality. Both parasequences (Kf1 and Kf2) are shown in the picture. The blue line represents the flooding surface separating the two parasequences. Abbreviations for the different facies associations are shown on the outcrop and explained in **Table 5.2**. This section was logged 150 m further up the road (**Fig. 5.3)**. The black lines indicate which facies association the thin section photos correspond to, and the red scale is representative for all the thin section photos. PPL represents plane-polarised light, CPL represents cross-polarised light and # represent the sample number. The thin section photos show clear differences between the wave-dominated and river-dominated environments. The river-dominated deposits exhibit a smaller grain size and are more cemented (both carbonate and iron-oxide) and are less porous than the wave dominated deposits. Note also the difference in roundness and sorting of the grains. The thin sections from the river-dominated parts of the delta show moderate sorting and angular grains (**Table 3** in **Appendix I**), while the wave-dominated thin sections show more sub-angular to sub-rounded grains which are moderately-well sorted.

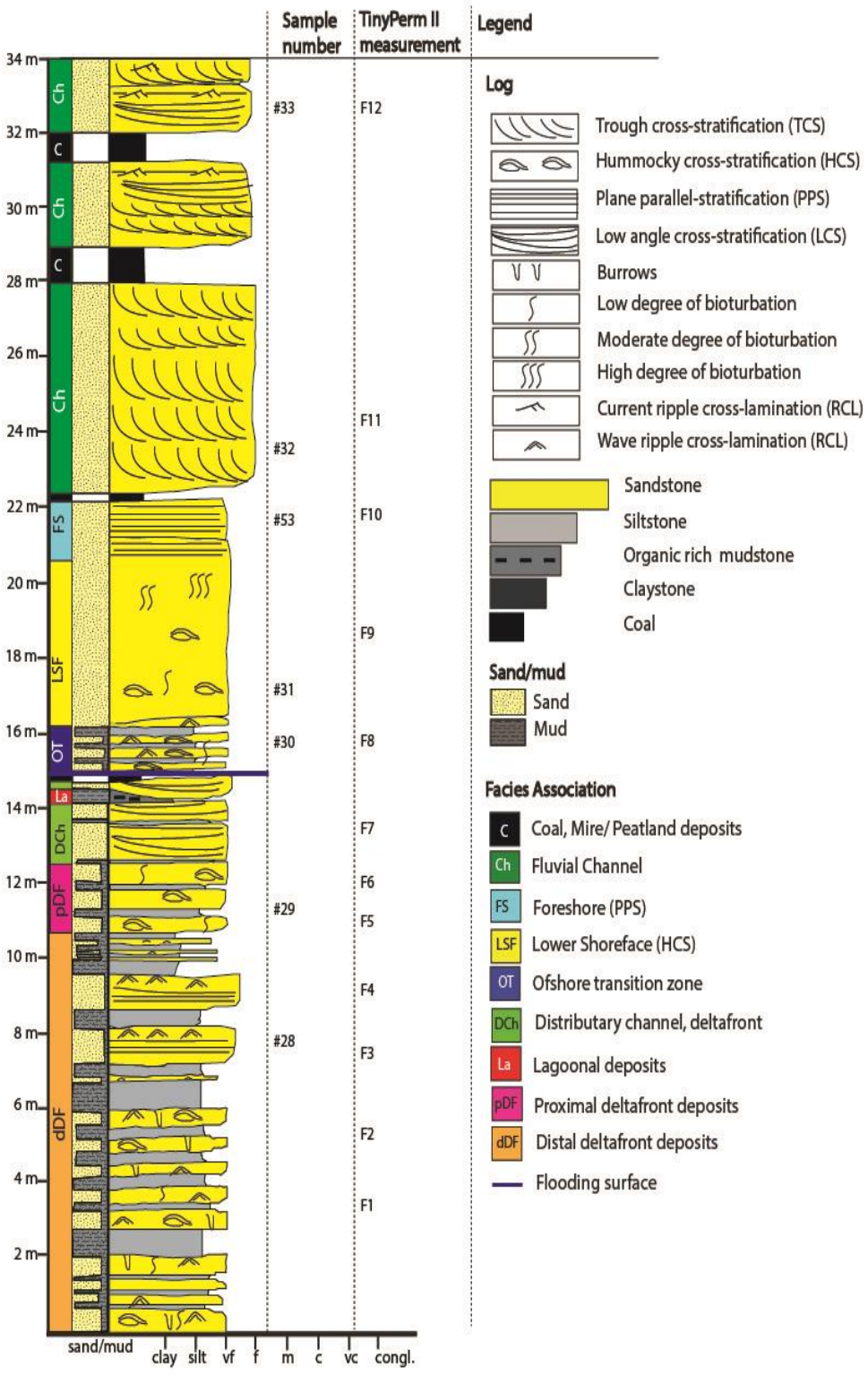


**Fig. 5.3:** Log 1 from the outcrop exposed along I-70 in the Ivie Creek location. The log also shows the collected samples and permeability measurements.

### EMERY SANDSTONE MEMBER

The studied parasequences of the Emery Sandstone have an upward coarsening trend, and consist predominantly of hummocky cross-stratified sandstone with a high degree of bioturbation. These deposits are interpreted as lower shoreface deposits (Edwards et al., 2005).

The lower shoreface deposits of the Emery Mb. exhibit alternating hummocky cross-stratified (HCS) and intensely bioturbated sandstone beds (**Fig. 5.4** and **Fig. 5.5**). In this study three samples from the HSC beds and three samples from the bioturbated beds were collected.

The Emery Mb. was studied in two locations. These locations represent the two different delta lobes prograding into the Western Interior Seaway (described in more detail in chapter 2). The outcrops in the Quitchupah Creek location represent deposits of the southern Emery Delta, while deposits of the northern Emery Delta are exposed in outcrops around Price.

In this thesis four samples and several permeability measurements were taken, and one parasequence was logged (**Fig. 5.6**) within the southern Emery Delta at the Quitchupah Creek location. Two samples and measurements were taken from the northern Emery Delta deposits in the Harmond Hills location (**Fig. 5.4**) just north of the town Price.

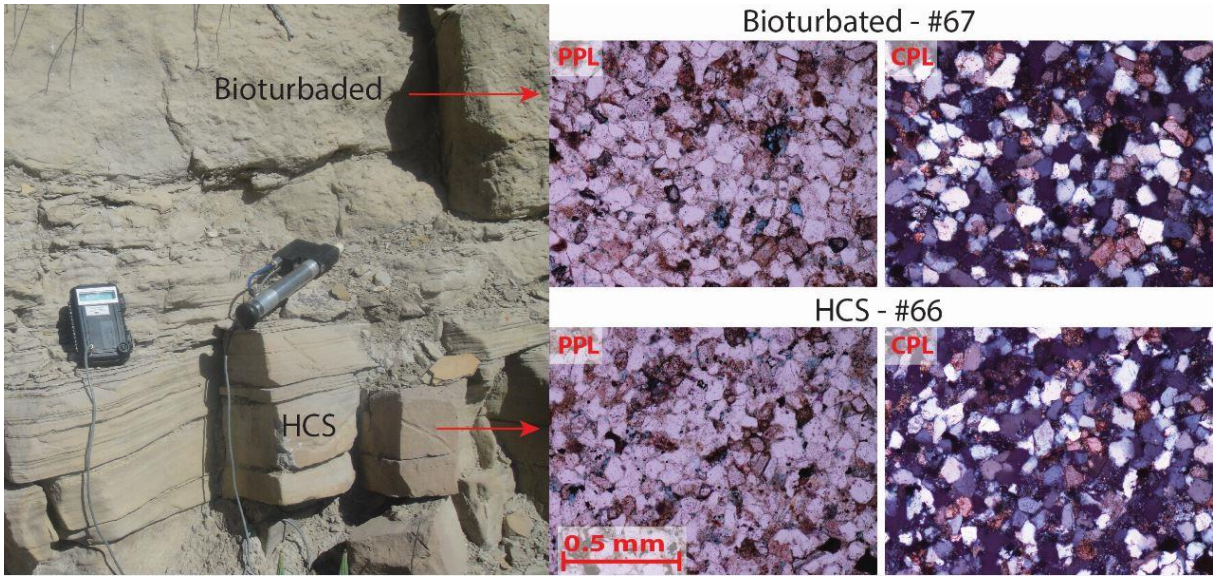


**Fig. 5.4:** Outcrop and thin section photos from the samples collected from the northern Emery Delta in the Harmond Hills location. The composition of the bioturbated and hummocky cross-stratified sample is relatively similar. These samples are in general less porous and show a smaller grain size and a poorer sorting than the samples from the southern Emery Delta (**Fig. 5.5**).

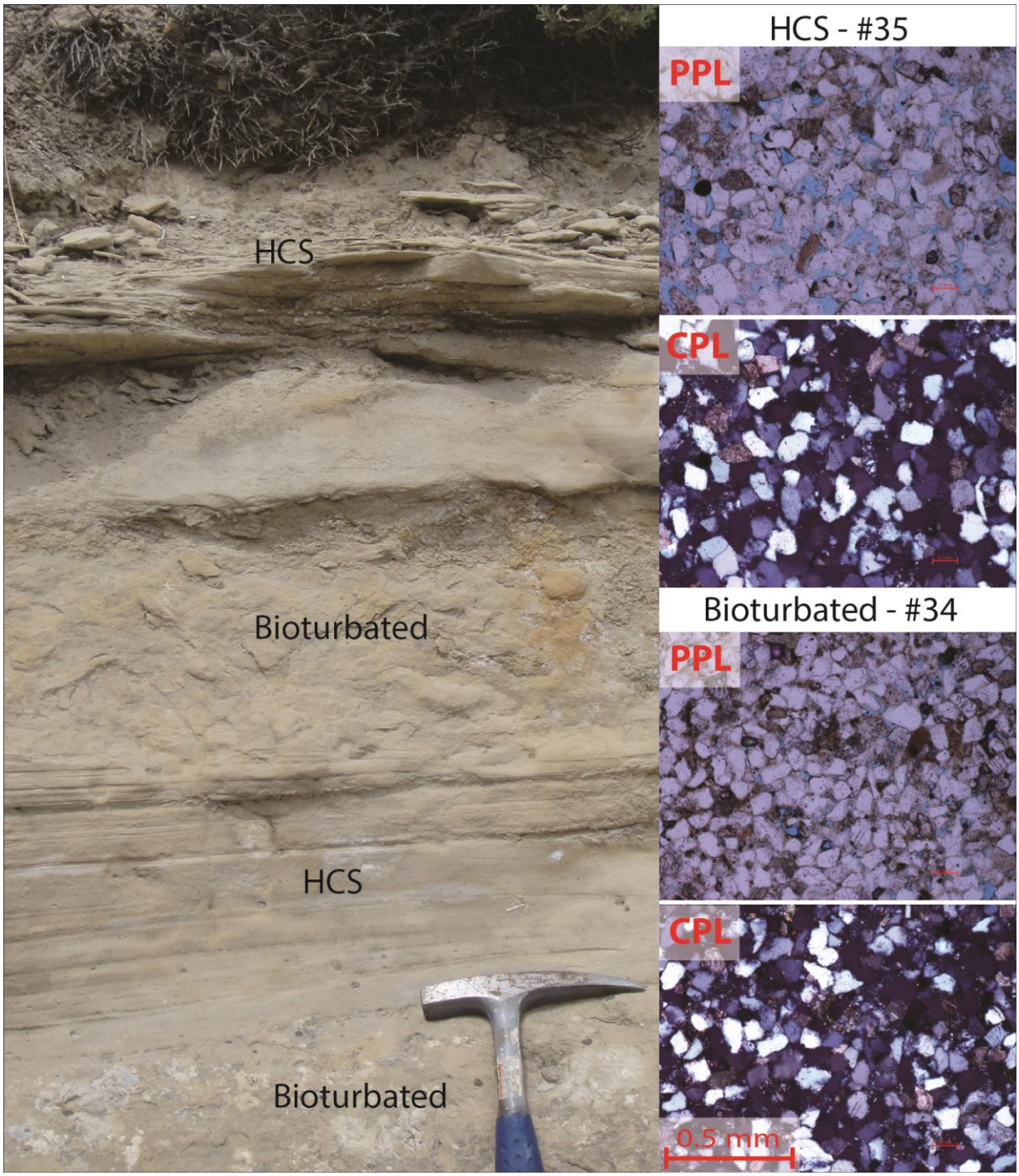


**Fig. 5.5:** Photos from the southern Emery Delta deposits. The outcrop photo shows how the sedimentary structures in the lower shoreface deposits alternates between intense bioturbation and HCS. The HCS samples in this location are more porous and less cemented than the bioturbated samples. The same trend is not observed in the samples form the northern delta lobe (**Fig. 5.4**).

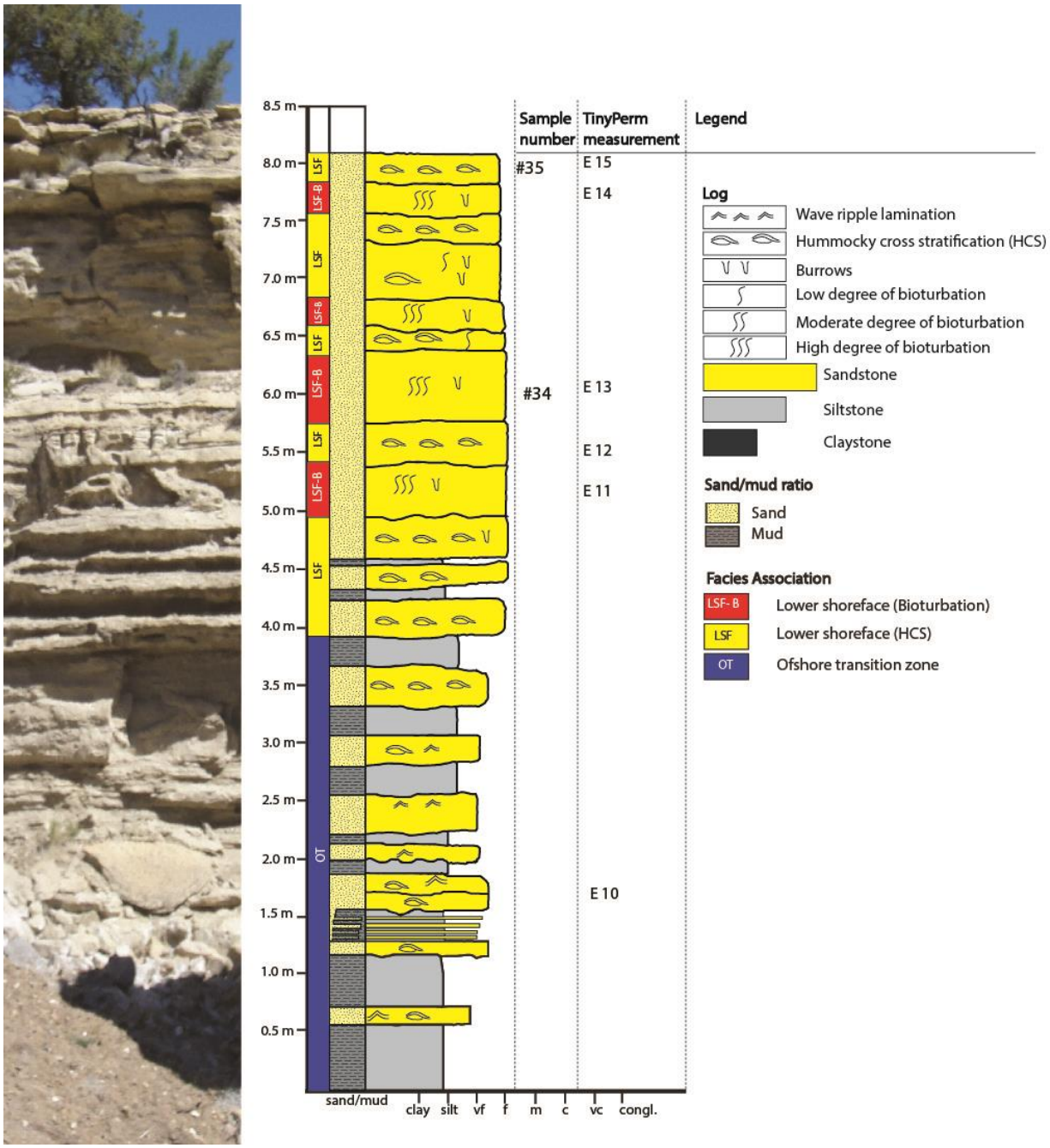


**Fig. 5.6:** Log 2 from one of the exposed parasequences of the southern Emery Delta. The log illustrates the alternation in sedimentary structures within the lower shoreface. The location of samples and permeability measurements within this parasequence are indicated on the side of the log. The outcrop photo shows the logged section.

**PRAIRIE CANYON MB.**

Four samples were collected from the Prairie Canyon Mb. An overview of these four samples, locations and facies associations are presented in **Table 5.3.**

**Table 5.3:** Information on the samples collected within the Prairie Canyon Mb.

| # | Sandstone unit | Facies Associations | Location |
|---|---|---|---|
| **22** | Woodside Sandstone | Subaqueous channel | *Woodside Canyon* |
| **25** | Mancos B | Hyperpycnal turbidites | *East of Hatch Mesa* |
| **26** | Hatch Mesa Sandstone | Hyperpycnal turbidites | *Hatch Mesa* |
| **27** | Hatch Mesa Sandstone | Hyperpycnal turbidites | *Hatch Mesa* |

The Woodside Sandstone sample (#22) consists of ~67% silt-grains, and the sand-grains in this sample consist of quartz and carbonate. This sample also has a relatively high abundance of opaque materials. The opaque materials in these deposits consist primarily of organic fragments. This is shown in further detail in the scanning electron microscope (SEM) results in section 5.3.1.

Pattison (2005) characterises the hyperpycnal turbidites in the Prairie Canyon Mb. as shelf turbidites, this interpretation is used in this study.

The Mancos B sample has a higher proportion of organic fragments than the Hatch Mesa samples (**Fig. 5.7**). Large amounts of organic fragments could also be observed in the field, especially at bed boundaries and partings.

The Mancos B and the Woodside Sandstone samples contain a greater proportion of organic fragments than any of the other samples acquired in this study.

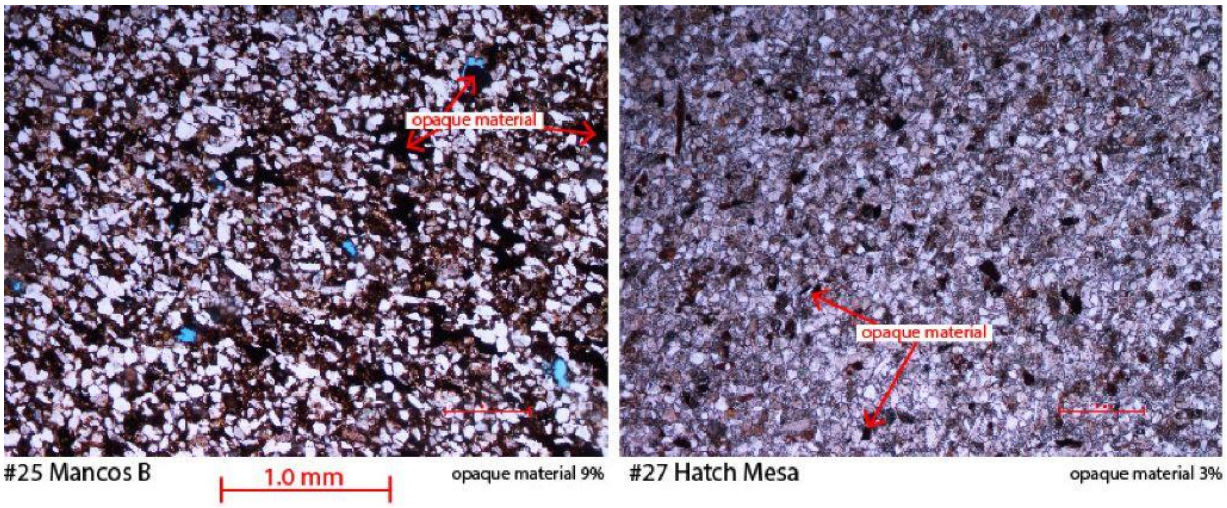


**Fig. 5.7:** Thin section photos of the hyperpycnal turbidite samples with the highest (#25) and lowest (#27) opaque material content. The opaque material is completely black in the microscope and SEM results show that the majority of these opaque materials are most likely organic fragments (section 5.3.1).

### 5.1.2 STAR POINT FORMATION

In this study samples and measurements were taken from both the Panther Tongue Mb. and the Storrs Mb. of the Star Point Fm. The facies associations observed in these members are displayed in **Table 5.4.**

**Table 5.4:** The different facies associations observed within the Star Point Fm.

| Member | Facies Associations | Abbreviation |
|---|---|---|
| Panther Tongue | C- Distal delta-front deposits | dDF |
| | D- Proximal delta-front deposits | pDF |
| | E- Mouth bar deposits | MB |
| | F- Distributary channel | DC |
| | G- Transgressive lag | LAG |
| Storrs | H- Offshore transition zone deposits | OTz |
| | I- Lower shoreface deposits | LSF |
| | K- Upper shoreface deposits | USF |

#### PANTHER TONGUE MEMBER

The Panther Tongue deposits were studied in two locations: Spring Canyon and Gentile Wash. A total of 8 samples were collected and 17 permeability measurements were taken.

Proximal delta-front deposits were studied in both locations, while distributary channel deposits were only studied in the Spring Canyon location (**Fig. 5.8**). Mouth bar and transgressive lag deposits were studied in Gentile Wash (**Fig. 5.9**)

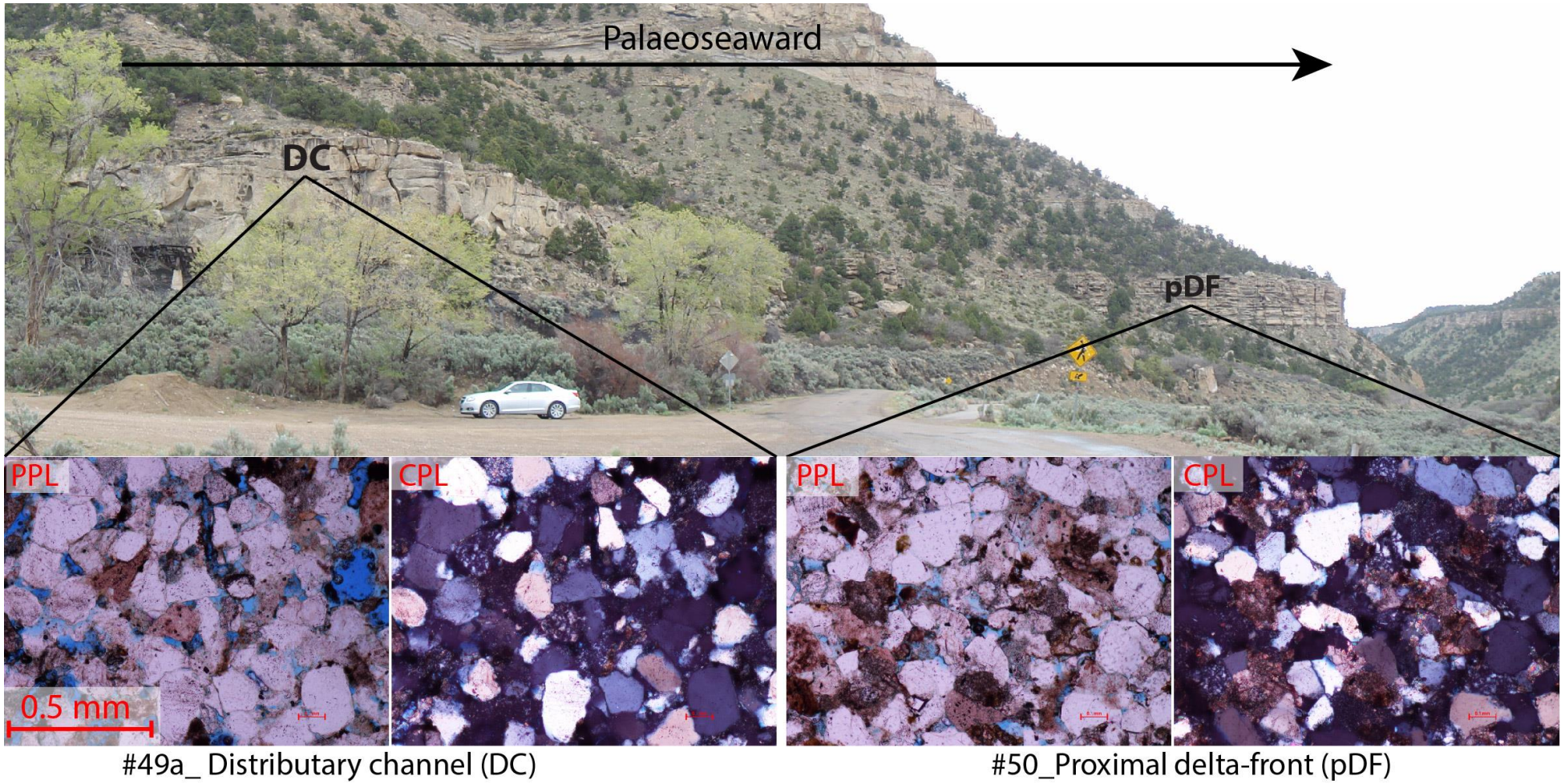


**Fig. 5.8:** Outcrop and thin section photos from Panther Tongue in Spring Canyon. The composition is relatively similar in the distributary channel and proximal delta front deposits, but porosity decreases towards more distal environments, as demonstrated in the thin section photos. Also more opaque material (organic fragments) is found in the distributary channel deposits, but this cannot be seen in these photos

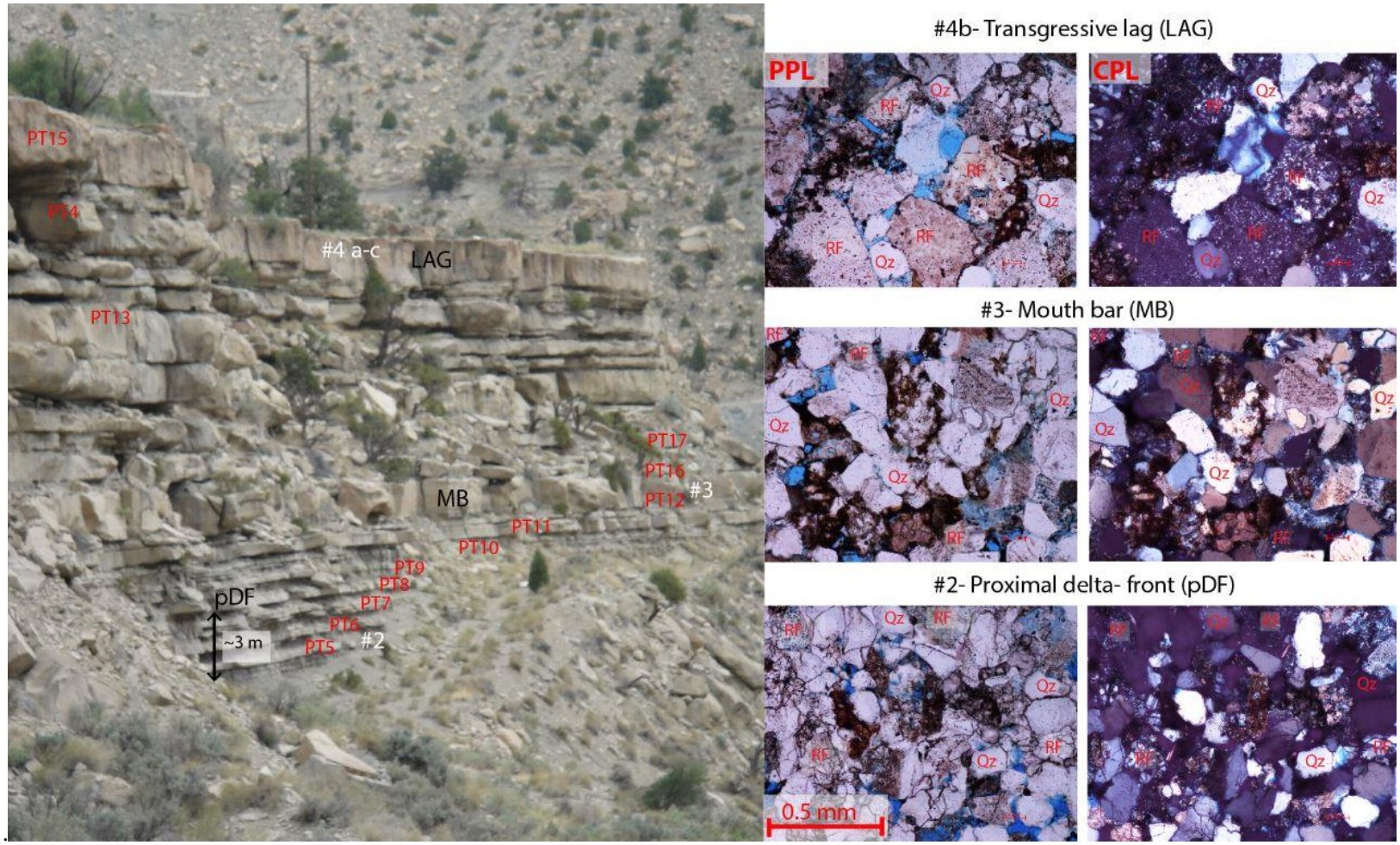


**Fig. 5.9:** The outcrop photo shows the locations of rock samples (white) and permeability measurements (red letters) within the Panther Tongue Mb. in the Gentile Wash location. Permeability measurement PT13-15 and #4a-c were taken from the same beds as shown in this photo, but the location was 100 m further up the trail in Gentile Wash. The Panther Tongue contains a higher proportion of rock fragments than the other studied members and formations in this area. Within the Panther Tongue Mb. the transgressive lag deposits contain the highest proportion of rock fragments, as shown in these thin section photos.

**STORRS MEMBER:**

In this member three samples were collected from three different facies associations in three different locations (**Table 5.5** and **Fig. 5.10**). In addition five permeability measurements were taken. This member was deposited in a wave dominated depositional environment (Edwards et al., 2005), sedimentary structured observed in this study are hummocky cross-stratification in the OTz and LSF deposits. In the USF deposit observed in Joe's Valley sigmoidal cross-stratification was observed.

**Table 5.5:** The three samples collected from the Storrs Mb. are listed in this table with corresponding facies association, location and permeability measurements.

| # | Facies Associations | Location | GPS |
|---|---|---|---|
| **44** | USF | *Joe's Valley* | N 39°16'56.592" W 111°13'58.284" |
| **38** | LSF | *Cottonwood Creek* | N 39°19'05.915" W 111°11'22.690" |
| **5** | OTz | *Gentile Wash* | N 39°42'51.390" W 110°52'26.000" |

There is some extensional faulting within Joe's Valley which juxtaposes shallow marine Storrs Mb against the the non-marine Blackhawk Fm (c.f. geological map by Hintze, 2005). Care was taken to sample the shallow marine portion. Hammer and chisel could not be used on this outcrop without damaging the sedimentary structures. Therefore the upper shoreface sample and the surface for the corresponding permeability measurement had been subjected to more weathering and were not as fresh as the other samples.

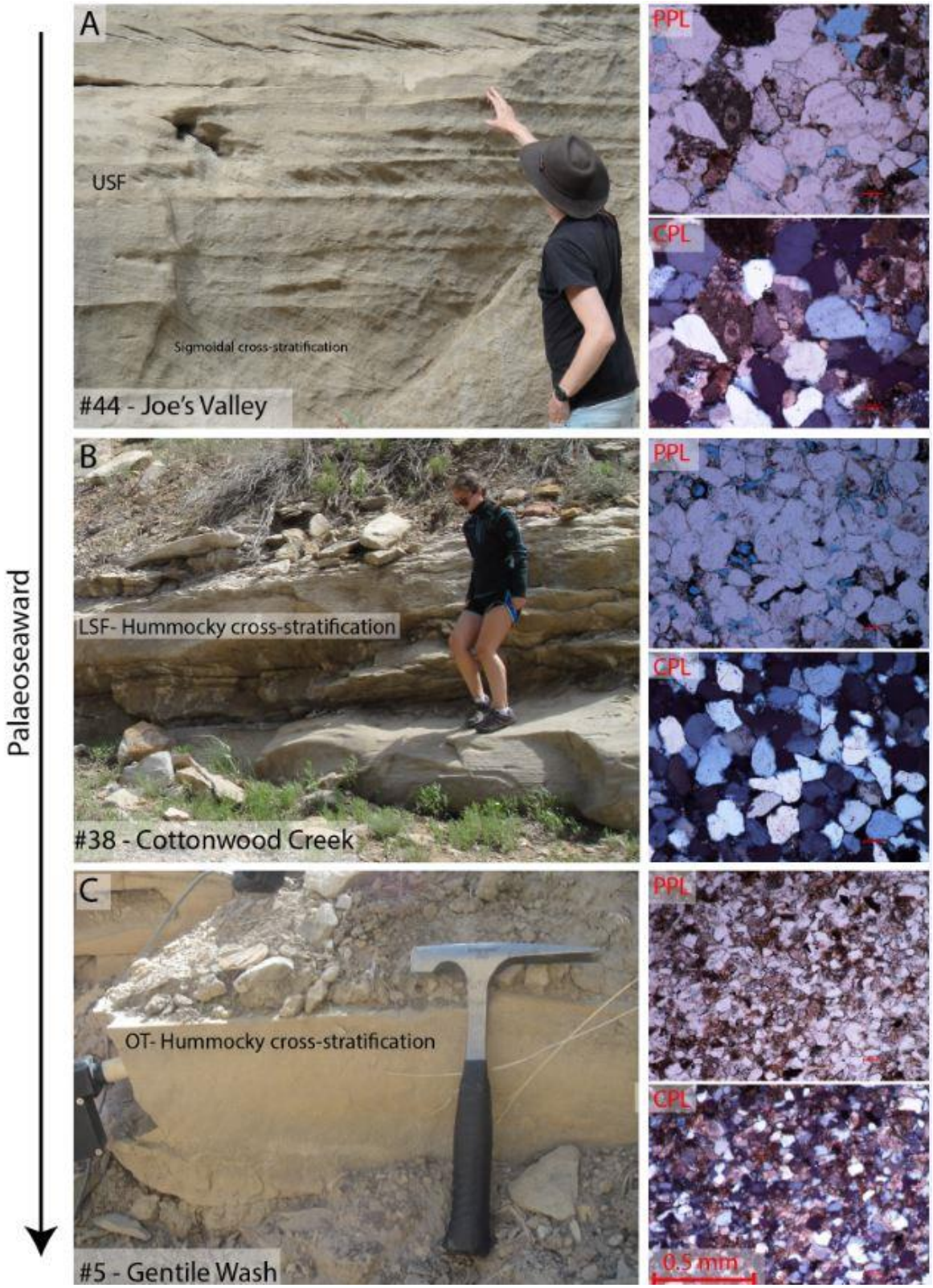


**Fig. 5.10:** Outcrop and thin section photos from the three samples collected within the Storrs Mb. The lower shoreface sandstone (#38) is one of the most compositionally mature sandstones collected in this study. The total carbonate content is much higher in the more weathered USF sandstone and in the more distal deposited OTz sandstone. These photos also show a decrease in grain size in the palaeoseaward direction.

### 5.1.3 BLACKHAWK FORMATION

In this formation the non-marine and three of the shallow marine members (Spring Canyon Mb., Kenilworth Mb. and Grassy Mb.) were studied. **Table 5.6** gives an overview of the facies associations observed within these members.

**Table 5.6:** The different facies associations observed and studied within the Blackhawk Fm.

| Member | Facies Associations | Abbreviation |
|---|---|---|
| Non-marine part of Blackhawk Fm. | N- Coal | C |
| | O- Meandering channel fill | MC |
| | Q- Braided channel bar | BC |
| | P- Crevasse splay/ Floodplain | CS/F |
| Shallow marine members of the Blackhawk Fm. | H- Offshore transition zone deposits | OTz |
| | I- Lower shoreface deposits | LSF |
| | J- Middle shoreface | MSF |
| | K- Upper shoreface deposits | USF |
| | L- Foreshore | FS |
| | G- Transgressive lag | LAG |

#### NON-MARINE BLACKHAWK FM.

The non-marine part of the Blackhawk Fm. was studied in outcrops along Straight Canyon close to Joe's Valley in the Wasatch Plateau and in several outcrops along the Book Cliffs (Table 5.1 and **Fig. 5.1)**. A total of 11 samples were collected. Nine of these samples were collected from meandering channel fill deposits. The two remaining sandstone samples were from braided channel bar and crevasse splay deposits; these were collected in the non-marine part of the Blackhawk Fm. close to Joe's Valley (**Fig. 5.11 A**).

The samples from Straight Canyon show a higher total carbonate amount in the crevasse-splay deposits than in the meandering channel fill deposits (except sample #54), and the lowest amount is found in the braided river deposit (**Fig. 5.11 B-E**). Sample #54 has the highest amount of carbonate grains and carbonate-cement of all studied samples, it is almost completely cemented. The carbonate cement is most likely siderite (iron-carbonate) due to the relative high relief observed in the microscope (**Fig. 5.11 E**).

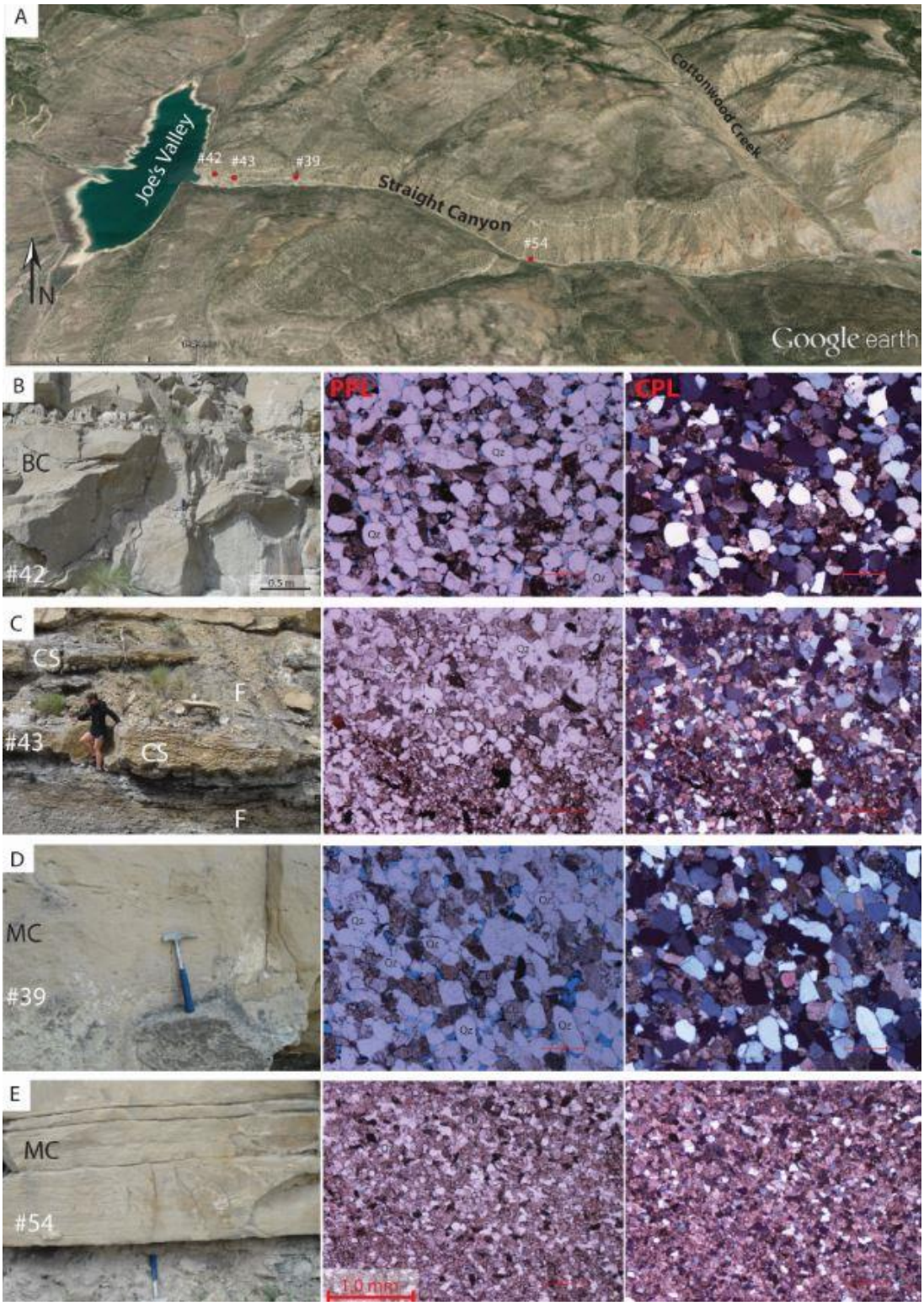


**Fig. 5.11:** Photos and location of the four samples collected in Straight Canyon close to Joe's Valley. Abbreviations: BC, Braided channel bar; CS, Crevasse-splay; F, Floodplain; MC, Meandering channel fill. The braided bar deposits (**B**) contain less carbonate cement than meandering channel fill (**D & E**) and crevasse-splay deposits (**C**). The crevasse-splay sample contains the second highest amount of carbonate cement of all the samples collected from the non-marine part of the Blackhawk Fm. The only sample with higher amount of carbonate and carbonate cement is sample #54 (**E**).

Excluding sample #54, the meandering channel fill samples collected do not show any major variations in composition, but the sample collected at the highest stratigraphic level equivalent to the Grassy Mb. (#64) shows a lower amount of carbonate than most of the other samples. Only one (# 15) of the samples collected in the lower part of the stratigraphy showed a similar low abundance of carbonate, this sample also showed the highest content of opaque material (most likely organic fragments) (**Fig. 5.12**).

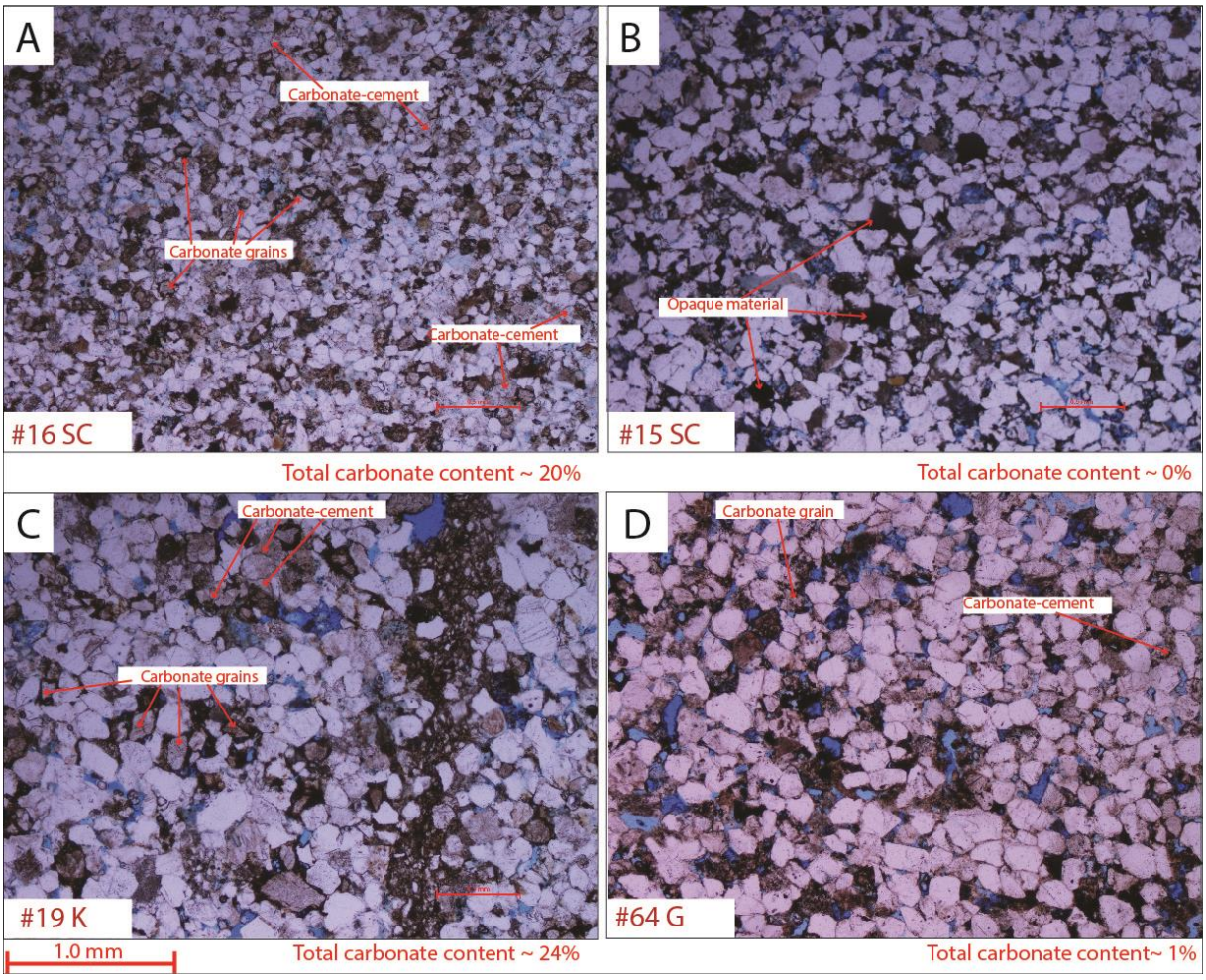


**Fig. 5.12:** Thin section photos (PPL) of four meandering channel fill samples collected at different locations in the Book Cliffs. These samples were collected from the non-marine part of the Blackhawk Fm. at stratigraphic levels equivalent to Spring Canyon Mb. (SC), Kenilworth Mb. (K) and Grassy Mb. (G). The uppermost stratigraphic sample (#64) and the sample (#15) containing the highest proportion of opaque material (organic fragments) are the ones with the lowest amount of carbonate grains and carbonate-cement. These are the only meandering channel fill samples with a total carbonate content of less than 10 %.

**SPRING CANYON MB.**

The Spring Canyon Mb. is the lowermost stratigraphic member of the Blackhawk Fm. This member is well exposed in the Gentile Wash location. A total of 9 samples were collected, and several permeability measurements were taken at this location, see log in **Fig. 1** in **Appendix II** for location for sampling and permeability measurements in this location.

The composition of the Spring Canyon Mb. is relatively similar to the composition of Kenilworth Mb. and Grassy Mb., but some variations are observed in the cement content (**Fig. 5.13**). The Spring Canyon Mb. generally contains more carbonate-cement and less quartz-cement than the stratigraphically overlying members.

**KENILWORTH MB.**

Samples from the Kenilworth Mb. were collected in several locations along the Book Cliffs from Soldier Creek to Gray Canyon. The samples were collected from the fourth parasequence (K4), see section 2.3.3 for a more detailed description. This was the only member of the Blackhawk Fm. where a sample from transgressive lag deposits was collected (#24). This transgressive lag capped the top of the fourth parasequence (K4) and was most likely deposited during the sea-level rise between K4 and K5 (Pattison, 1995).

A total of 19 samples were collected within the Kenilworth Mb. In Horse Canyon several samples and permeability measurements were taken from each facies association within one parasequence. The composition within this parasequence was generally similar, but the type of cement and porosity was found to vary with the different facies associations (**Fig. 5.14**).

A log through the Kenilworth K4 parasequence was acquired in Horse Canyon. The log shows the position of sampling and permeability measurements at this location (**Fig. 5.15**)

**GRASSY MB.**

The Grassy Mb. of the Blackhawk Fm. was studied in the Gray Canyon location. In this location one parasequence was logged and several samples and permeability measurements were taken (**Fig. 5.16**). The facies associations studied in this member are the same as the ones studied in Spring Canyon Mb and Kenilworth Mb.

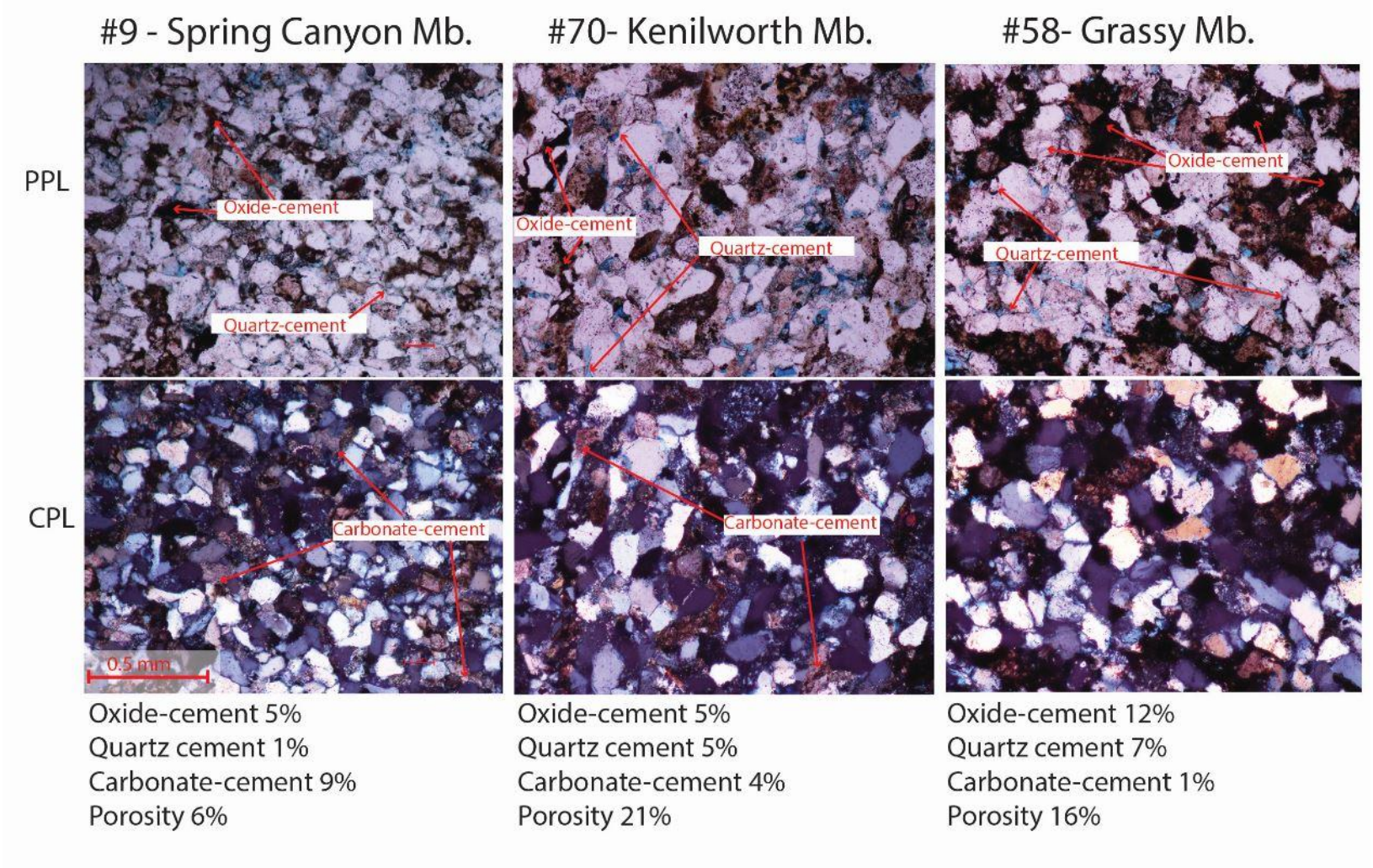


**Fig. 5.13:** Cement and porosity variation within LSF samples from three different shallow marine members of the Blackhawk Fm. This figure shows an increase in oxide- and quartz-cement and a decrease in carbonate cement when moving stratigraphically upwards, from Spring Canyon Mb. to Grassy Mb.

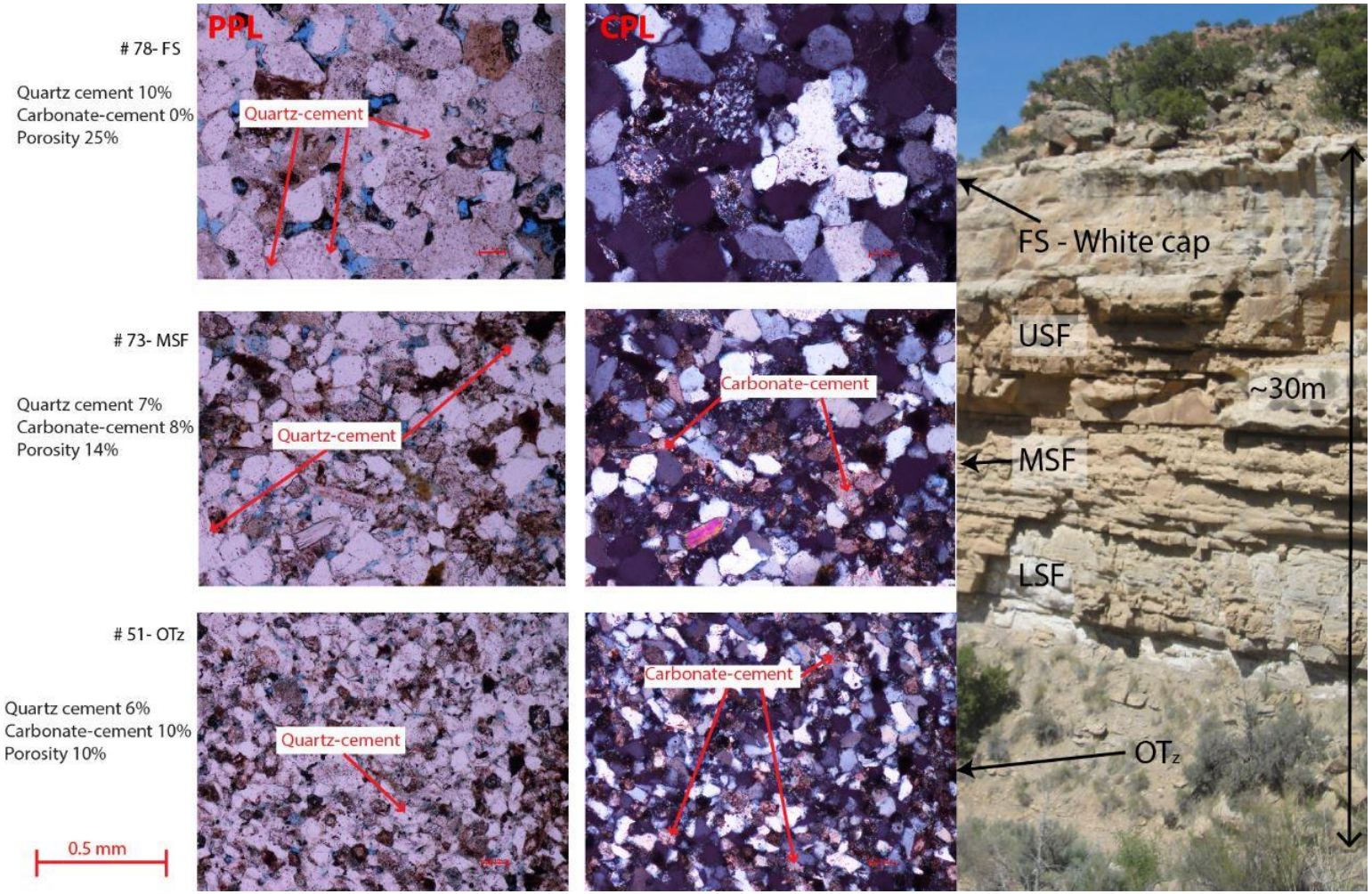


**Fig. 5.14:** Shows an outcrop photo of the studied parasequence in Horse Canyon, and thin section photos from three representative samples. The thin sections show a trend where quartz-cement and porosity decrease and the carbonate-cement increase when moving palaeoseaward from FS to OTz. The greatest change in composition in these examples is between the FS and MSF sample.

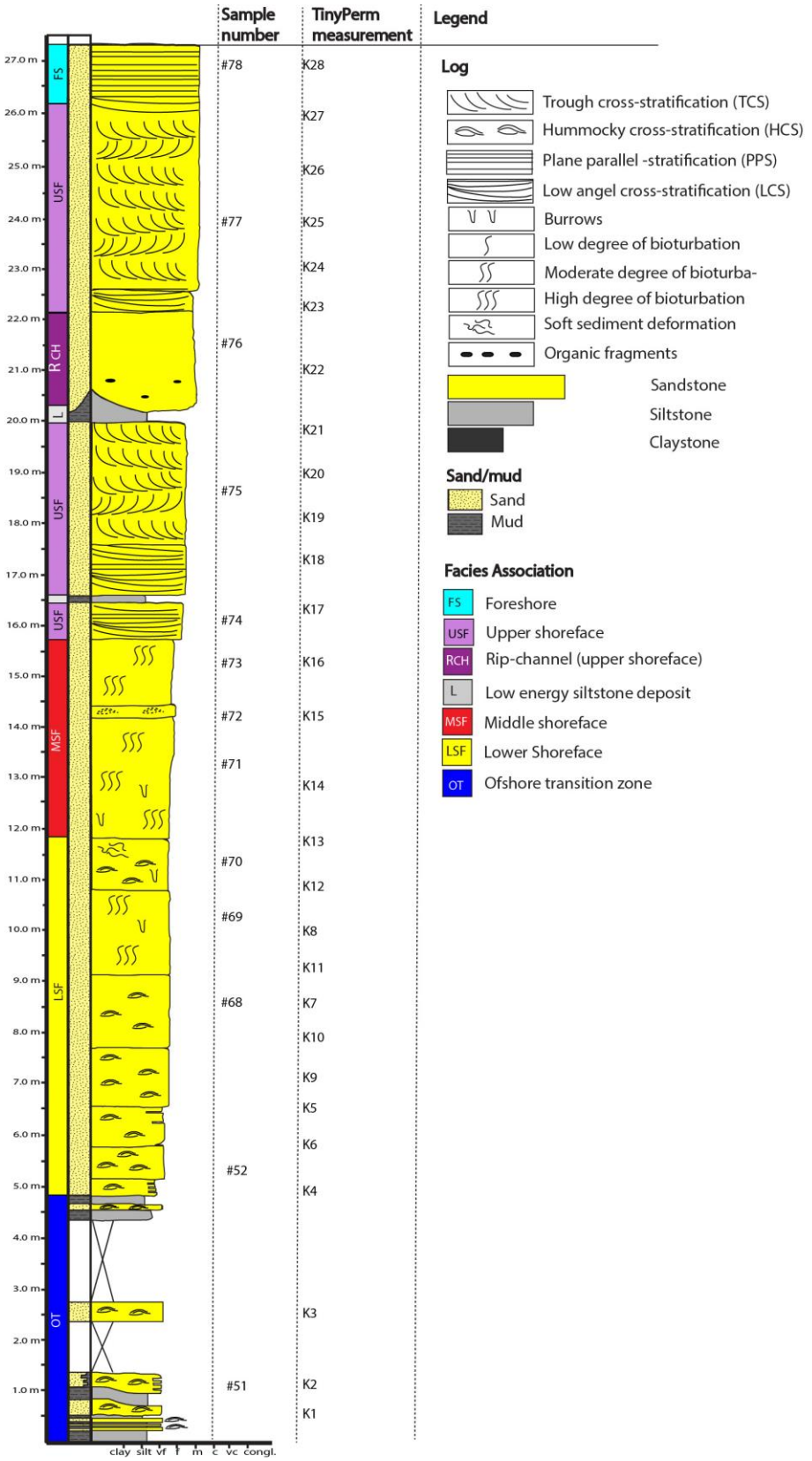


**Fig. 5.15:** Log 3 of K4 from Horse Canyon. The log represents all the typical facies associations in a prograding shoreline in a wave-dominated depositional environment. The locations of rock samples and permeability measurements within this parasequence are indicated in the log.

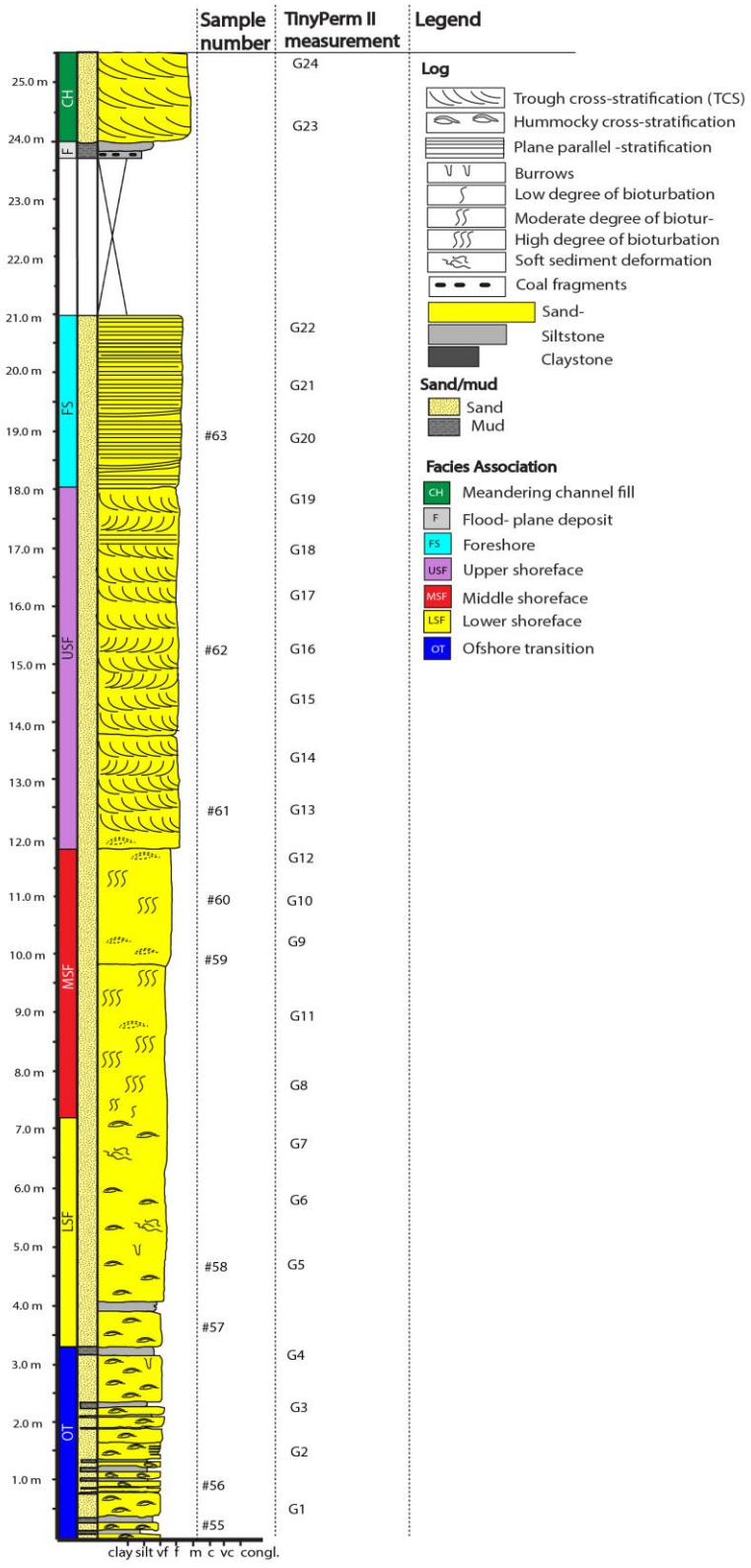


**Fig. 5.16:** Log 4 from Grassy Mb. in Gray Canyon. The different facies associations related to a prograding shoreline in a wave-dominated depositional environment are presented in this log. Also the locations of sampling and permeability measurement within this parasequence are indicated in the log.

### 5.1.4 PRICE RIVER FORMATION

#### CASTLEGATE SANDSTONE MB.

The Castlegate sandstone was studied in two locations: Bear Canyon and Joe's Valley. A total of four samples were collected, 19 permeability measurements were taken and one log was made (**Fig. 5.17**).

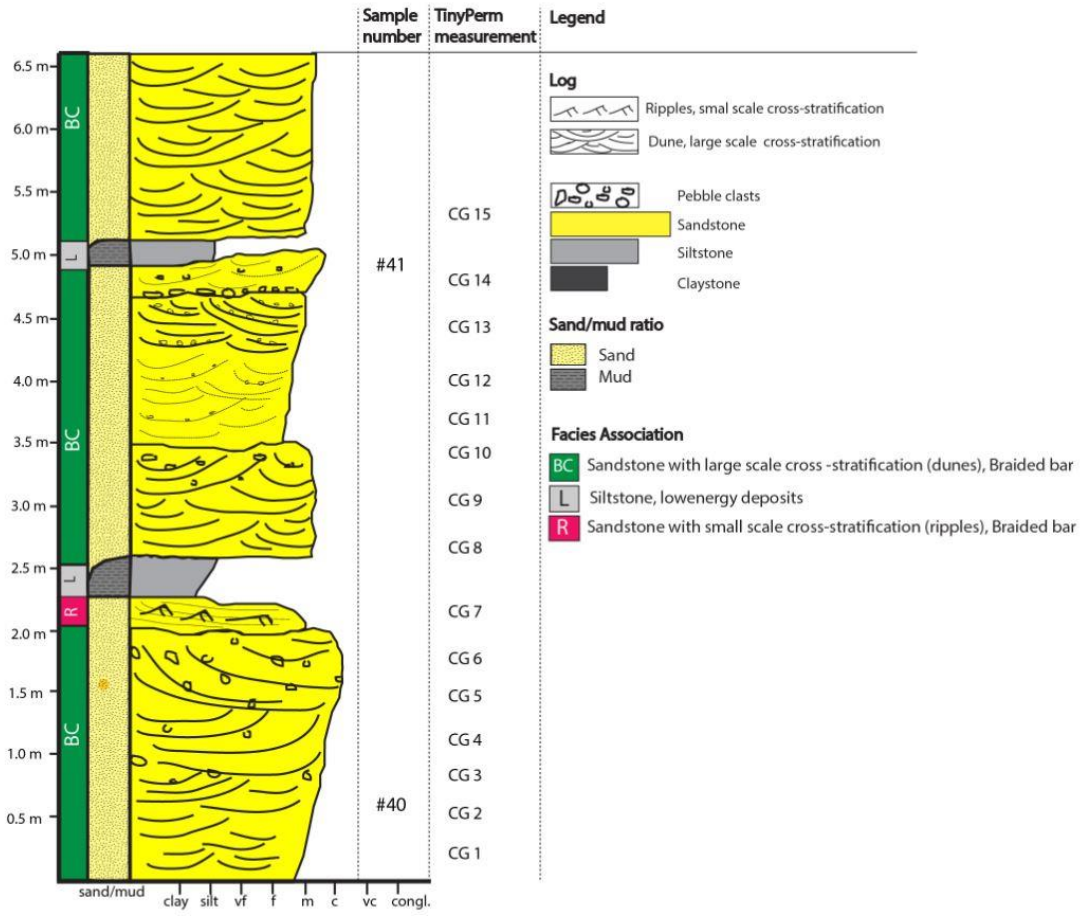


**Fig. 5.17:** Log 5 from Castlegate Sandstone in Joe's Valley. It shows vertically stacked braided bars. The locations of sampling and permeability measurements in Joe's Valley are indicated in the log.

The samples collected from this member contain a lower amount of carbonate grains and carbonate-cement than most of the samples from the other formations (**Fig. 5.18**).

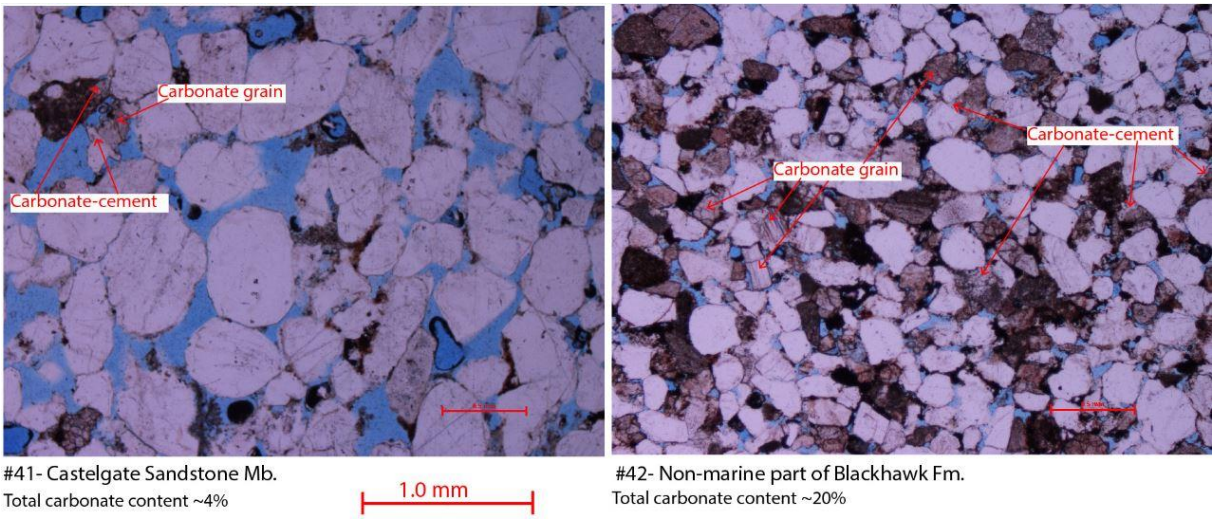


**Fig. 5.18:** Samples from braided bar deposits collected in Joe's Valley. Note the difference in carbonate content between the samples from the Castlegate Mb. and the Blackhawk Fm. The four samples collected from the Castlegate Mb. all contain a low amount of carbonates.

## 5.2 PERMEABILITY DATA

Numerous permeability measurements were taken within the different stratigraphic members. All these measurements are presented in **Table 2** in **Appendix I**. The average permeability is also presented as order of magnitude (**Table 5.7**).

Of the 194 sandstone surfaces measured in this study 192 measurements have an order of magnitude between 10 and 10 000 mD. The first exception is the least permeable measurement (NM-BH 3) taken in the non-marine part of the Blackhawk Fm., this measurement was taken in the same location as sample #54 (**Fig. 5.11**), which was almost completely cemented by carbonate cement (most likely siderite). The permeability registered form this location had an average permeability of 8 mD. The Second exception was measurement 8 (CG8) within the Castlegate Sandstone Mb. in Joe's Valley this measurement showed the highest permeability with an average of 11 467 mD. Other measurements within this member came close to a permeability with an order of magnitude of 10 000 mD.

The permeability measurements show trends both within facies and formations. **Table 5.7** shows the average permeability varying with facies associations and formations. The permeability trends are most visible when focusing on the order of magnitude of the average and not just on the exact number.

The three shallow marine members of the Blackhawk Fm. and the wave-dominated part of Ferron Mb. all show a facies dependent trend with the permeability decreasing basinward. Another facies dependent trend is that permeability is lower in meandering channel fill deposits than in braided channel bar deposits. Meandering channel deposits which are stratigraphic equivalent to Spring Canyon Mb. contain a relatively high content of carbonate-cement, and have relatively low permeability.

**Table 5.7:** Presenting the average permeability within the different facies associations and formations. This table is color-coded with the order of magnitude.

| Facies association | | Mancos Shale Fm. | | Star Point Fm. | | Blackhawk Fm. | | | | Price River Fm. |
|---|---|---|---|---|---|---|---|---|---|---|
| | | Ferron Mb. | Emery Mb. | Storrs Mb. | Panther Tongue Mb. | Non-marine | Spring Canyon Mb. | Kenilworth Mb. | Grassy Mb. | Castlegate Mb. |
| Coastal plain | BC | - | - | - | - | 2399 | - | - | - | 3674 |
| | MC | 488 | - | - | - | 273 | 123 | - | 1092 | - |
| Wave-dominated shoreline | FS | 441 | - | - | - | - | 456 | 781 | 1060 | - |
| | USF | - | - | 128 | - | - | 428 | 493 | 1336 | - |
| | MSF | - | - | - | - | - | 405 | 202 | 209 | - |
| | LSF | 49 | 547 | 178 | - | - | 91 | 236 | 161 | - |
| | OTz | 42 | 125 | 146 | - | - | 67 | 103 | 107 | - |
| River-dominated shoreline | LAG | - | - | - | 424 | - | - | - | - | - |
| | DCh | 28 | - | - | 710 | - | - | - | - | - |
| | MB | - | - | - | 158 | - | - | - | - | - |
| | pDF | 175 | - | - | 344 | - | - | - | - | - |
| | dDF | 48 | - | - | - | - | - | - | - | - |

→ Palaeoseaward direction | 10-100 mD | 100-1 000 mD | 100-1 000 mD

Within the Blackhawk Fm. the permeability seems to increase upwards in the stratigraphy. The Grassy Mb. is generally the most permeable, and the Spring Canyon Mb. is generally the least permeable, while the Kenilworth Mb. plots in the middle of these two (**Fig. 5.19)**. This trend is especially visible for the USF measurements, but also for the OTz and MC measurements. The "non-marine" permeability measurements were measured in the Joe's Valley and Castlegate Mine location, and are stratigraphically equivalent to Spring Canyon Mb. and Aberdeen Mb. No permeability measurements were made in meandering channel deposits stratigraphically corresponding to the Kenilworth Mb.

Only small variations in permeability were found within the Star Point Fm., and all of the measurements have the same order of magnitude.

A plot showing porosity plotted against permeability was made for the Blackhawk Fm. (**Fig. 5.19)**. For this plot only permeability measurements taken in the same location as rock samples were used (**Table 5.8**)

**Table 5.8:** Porosity and permeability data from where samples and measurements were taken from the same location within the Blackhawk Fm. This data is used as input in **Fig.5.19**.

**A**

| Permeability measurement | # | Spring Canyon Mb. Facies association | Permeability mD | Porosity % |
|---|---|---|---|---|
| SC42 | 15 | MC | 151 | 19.3 |
| SC30 | 13 | FS | 547 | 23.7 |
| SC27 | 12 | USF | 607 | 26.3 |
| SC17 | 10 | LSF | 65 | 14.3 |
| SC10 | 9 | LSF | 44 | 5.7 |

**B**

| Permeability measurement | # | Kenilworth Mb. Facies association | Permeability mD | Porosity % |
|---|---|---|---|---|
| K28 | 78 | FS | 781 | 25 |
| K25 | 77 | USF | 574 | 22.3 |
| K16 | 73 | MSF | 244 | 20.3 |
| K15 | 72 | MSF | 132 | 15.3 |
| K7 | 68 | LSF | 217 | 20.7 |
| K2 | 51 | OT | 59 | 9.7 |

**C**

| Permeability measurement | # | Grassy Mb. Facies association | Permeability mD | Porosity % |
|---|---|---|---|---|
| G20 | 63 | FS | 1049 | 20.7 |
| G16 | 62 | USF | 1468 | 26.3 |
| G13 | 61 | USF | 978 | 19 |
| G10 | 60 | MSF | 318 | 18 |
| G5 | 58 | LSF | 144 | 16.3 |

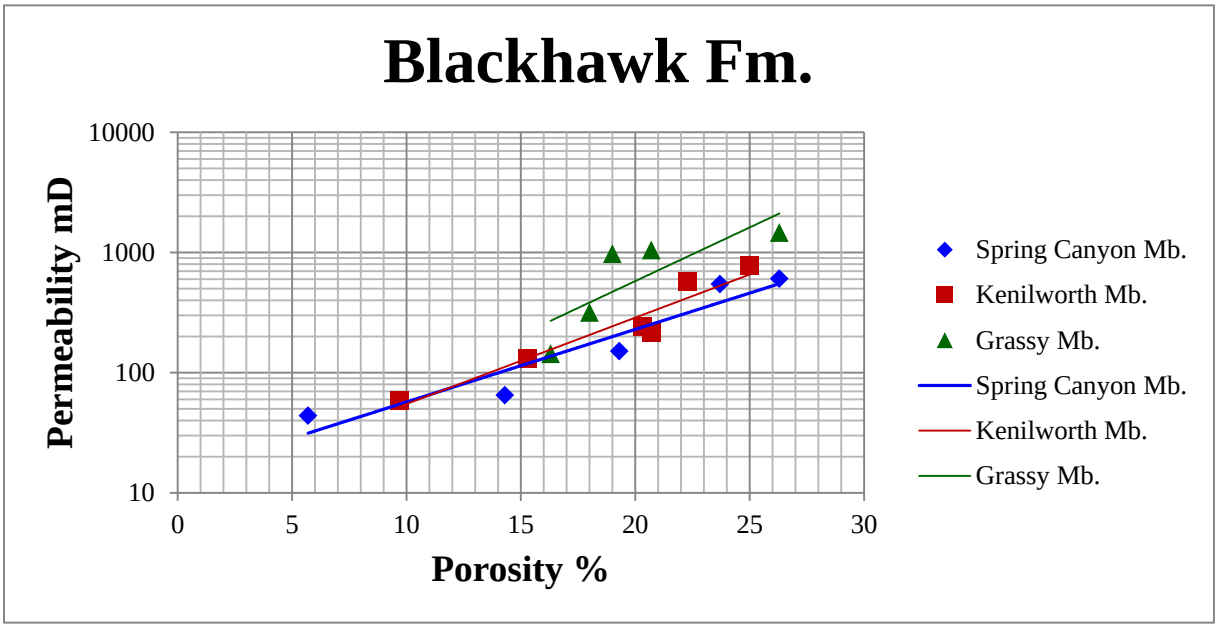


**Fig. 5.19:** Porosity versus permeability plot from three members within the Blackhawk Fm. The exponential trends in this diagram show and increase in permeability when moving upwards in the stratigraphy. The porosity is relatively similar for these three members, with exception of the LSF samples from the Spring Canyon Mb. and the OTz sample from Kenilworth Mb. These are the only samples with permeability less than 100 mD and porosity less than 15%. The Grassy Mb. is the only member which has permeability measurements higher than 1000 mD.

## 5.3 PETROGRAPHIC DATA

All the thin sections were described during microscope studies and almost the entire spectrum of grain properties were observed. The grain size varied from silt in the subaqueous channel and some of the shelf turbidites and offshore transition zone deposits to medium sand in the braided bar deposits. The most common grain size was very fine and fine sand. The grain sorting varied between poor to very well sorted, but was predominantly moderate to moderately well sorted. The grain shape was predominantly sub-rounded and sub-angular with varying degree of sphericity, but also some rounded and angular grains could be observed. Primarily point and concave-convex (formed by pressure solution) contacts were observed between the grains. Locally some sutured contacts were observed, but these were rare. The description for each of the 81 samples is presented in **Table 3** in **Appendix I**.

The detrital grain classes used in the point counting were quartz, feldspar, rock fragments, carbonate, muscovite, biotite and heavy minerals. The feldspars were not separated in to plagioclase and K-feldspars (such as microcline). The heavy minerals were also not separated. The reason for these two groups not being separated into several minerals is due to theirs overall low abundance (<4%). The heavy minerals observed in these samples are apatite, zircon, tourmaline and rutile. The carbonate grains were also not divided into specific minerals; this is because different carbonate minerals are visually hard to distinguish from each other without specific staining

During point counting alteration products, cement and porosity were also recorded in addition to the detrital grains. The different cement types that were registered were quartz-, oxide- and carbonate-cement .

In addition to the above three further classes were also registered; opaque material, unknown minerals and silt-grains. The opaque material is completely black in thin sections and the SEM was used to find the composition of these minerals and fragments. The group registered as silt-grains consisted of very small grains making up local matrix or mud-clasts. The grains were too small to distinguish visually, but the composition appeared to contain a high proportion of mica grains. It is also likely that some clay minerals are present in this group.

The average composition of the different facies associations and the different stratigraphic units are presented in **Table 5.9** and **Table 5.10**, while the raw data from the point counting is presented in **Table 4** in **Appendix I. Appendix III** includes thin section photos of all the samples collected in this study.

**Table 5.9:** The average composition for the different facies associations

| Facies Association | Qz | Fsp | RF | Ms | Cb | HM | AP | Bt | Op | Hem-cement | Qz-cement | Cb-cement | Silt | ϕ | UM |
|---|---|---|---|---|---|---|---|---|---|---|---|---|---|---|---|
| Braided channel bar | 43% | 0% | 6% | 0% | 5% | 1% | 1% | 0% | 2% | 2% | 13% | 2% | 1% | 25% | 0% |
| Meandering channel fill | 42% | 1% | 3% | 0% | 7% | 1% | 3% | 0% | 3% | 3% | 6% | 12% | 3% | 15% | 1% |
| Crevasse-splay | 42% | 0% | 6% | 0% | 20% | 0% | 1% | 0% | 2% | 3% | 2% | 12% | 8% | 1% | 1% |
| | | | | | | | | | | | | | | | |
| Foreshore | 47% | 1% | 6% | 1% | 0% | 0% | 7% | 0% | 4% | 2% | 8% | 0% | 0% | 21% | 1% |
| Upper shoreface | 38% | 0% | 8% | 0% | 5% | 0% | 7% | 0% | 2% | 2% | 8% | 4% | 0% | 23% | 1% |
| Middle shoreface | 39% | 1% | 6% | 1% | 6% | 1% | 5% | 0% | 4% | 3% | 8% | 6% | 2% | 16% | 2% |
| Lower shoreface | 45% | 1% | 6% | 1% | 7% | 1% | 4% | 0% | 4% | 4% | 5% | 6% | 1% | 15% | 2% |
| Offshore transition zone | 44% | 1% | 4% | 1% | 8% | 2% | 4% | 0% | 3% | 4% | 2% | 14% | 1% | 8% | 3% |
| | | | | | | | | | | | | | | | |
| Subaqueous channel fill | 7% | 0% | 0% | 0% | 4% | 0% | 0% | 0% | 16% | 3% | 0% | 1% | 67% | 1% | 1% |
| Shelf turbidite lobe | 33% | 1% | 5% | 3% | 15% | 1% | 4% | 1% | 6% | 9% | 1% | 11% | 2% | 6% | 3% |
| | | | | | | | | | | | | | | | |
| Transgressive Lag | 32% | 3% | 24% | 1% | 4% | 1% | 4% | 0% | 1% | 2% | 1% | 11% | 1% | 14% | 1% |
| Distributary channel fill | 32% | 0% | 11% | 0% | 4% | 0% | 2% | 0% | 6% | 6% | 11% | 7% | 1% | 17% | 2% |
| Mouth bar | 43% | 1% | 9% | 0% | 5% | 0% | 2% | 0% | 0% | 8% | 6% | 20% | 0% | 6% | 0% |
| Proximal delta-front | 41% | 1% | 9% | 1% | 5% | 0% | 3% | 0% | 3% | 6% | 5% | 15% | 1% | 9% | 1% |
| Distal delta-front | 46% | 1% | 3% | 1% | 14% | 1% | 6% | 1% | 4% | 6% | 2% | 5% | 2% | 7% | 1% |

***Abbreviations:*** *Qz-quartz; Fsp-feldspar; RF: rock fragments; Ms-muscovite; Cb-carbonate; HM-heavy minerals; AP-alteration products; Bt-biotite; Op-opaque material; Hem-hematite; ϕ-porosity; UM-unknown mineral*

**Table 5.10:** The average composition for the different stratigraphic units

| Stratigraphic unit | Qz | Fsp | RF | Ms | Cb | HM | AP | Bt | Op | Hem-cement | Qz-cement | Cb-cement | Silt | ϕ | UM |
|---|---|---|---|---|---|---|---|---|---|---|---|---|---|---|---|
| Castlegate Mb. (CG) | 43% | 0% | 7% | 0% | 2% | 1% | 0% | 0% | 1% | 2% | 15% | 1% | 1% | 27% | 0% |
| Non-marine Blackhawk Fm. | 41% | 0% | 3% | 0% | 10% | 1% | 2% | 0% | 3% | 3% | 6% | 13% | 3% | 13% | 1% |
| Grassy Mb. (G) | 42% | 0% | 7% | 0% | 2% | 0% | 5% | 0% | 4% | 4% | 10% | 2% | 1% | 18% | 2% |
| Kenilworth Mb. (K) | 38% | 1% | 6% | 1% | 7% | 1% | 5% | 0% | 4% | 5% | 7% | 8% | 1% | 16% | 2% |
| Spring Canyon Mb. (SC) | 46% | 1% | 7% | 1% | 6% | 1% | 7% | 0% | 2% | 2% | 2% | 7% | 2% | 12% | 2% |
| Prairie Canyon Mb.(PC) | 27% | 1% | 4% | 2% | 12% | 1% | 3% | 1% | 9% | 7% | 1% | 9% | 18% | 5% | 2% |
| Storrs. (St) | 44% | 0% | 2% | 0% | 8% | 1% | 2% | 0% | 2% | 1% | 5% | 17% | 0% | 16% | 1% |
| Panther Tongue Mb. (PT) | 35% | 1% | 16% | 1% | 4% | 1% | 3% | 0% | 2% | 4% | 6% | 12% | 1% | 14% | 1% |
| Emery Mb. (E ) | 48% | 1% | 5% | 0% | 7% | 2% | 2% | 0% | 5% | 2% | 3% | 7% | 2% | 15% | 2% |
| Ferron Mb.: Non-marine (Kf2) | 51% | 1% | 5% | 1% | 5% | 1% | 6% | 0% | 4% | 1% | 3% | 2% | 3% | 16% | 1% |
| Ferron Mb.: (Kf2) | 51% | 1% | 5% | 1% | 8% | 1% | 4% | 0% | 4% | 4% | 2% | 3% | 1% | 16% | 1% |
| Ferron Mb.: (Kf1) | 43% | 1% | 4% | 1% | 10% | 1% | 6% | 1% | 8% | 9% | 1% | 8% | 3% | 4% | 2% |

***Abbreviations:*** *Qz-quartz; Fsp-feldspar; RF: rock fragments; Ms-muscovite; Cb-carbonate; HM-heavy minerals; AP-alteration products; Bt-biotite; Op-opaque material; Hem-hematite; ϕ-porosity; UM-unknown mineral*

### 5.3.1 ELECTRON MICROSCOPE - SEM DATA

The SEM was used to identify minerals that were hard to distinguish visually, and to determine the accuracy of the point counting results. In the following sections some of these results will be presented. Four representative thin sections were analysed in SEM (**Table 5.11**)

**Table 5.11:** Presents the representative thin sections analysed in the electron microscope and the corresponding facies association, formation, member and number of compositional analysis done within the thin section.

| # Sample | Facies Association | Formation | Member | Number of compositional analyses |
|---|---|---|---|---|
| **36** | Lower shoreface | Mancos Shale | Emery | 78 |
| **40** | Braided bar | Price River | Castlegate | 47 |
| **62** | Upper Shoreface | Blackhawk | Grassy | 43 |
| **71** | Middle shoreface | Blackhawk | Kenilworth | 56 |

The following sections will include some examples from the thin section analysis of these samples. These examples show results that were present in all of the four samples which were analysed; the raw data from the SEM analysis is represented in **Appendix III**.

#### FELDSPAR

Certain feldspars can be hard to distinguish from quartz, and since the samples in this study were not stained for feldspar it is likely to assume some underestimation of the feldspar content. The feldspar registered in this thesis show characteristic twinning; both polysynthetic (characteristic for plagioclase) and "tartan" (characteristic for microcline). Orthoclase is typically very hard to distinguish from quartz in thin section, and SEM results show an example of a feldspar grain visually registered as quartz (**Fig. 5.20**). Based on SEM results it is likely to assume that the underestimation of detrital feldspar grains is less than 5%, since the highest case of underestimation observed in SEM was approximately 2-3% for the LSF deposits in sample 36. The lowest case of underestimation found in SEM was for the braided river deposits in sample 40, where no detrital feldspar grains were recognised neither visually nor in the SEM. It is therefore assumed that the samples do not contain detrital feldspar if no visual grains are observed during the point counting.

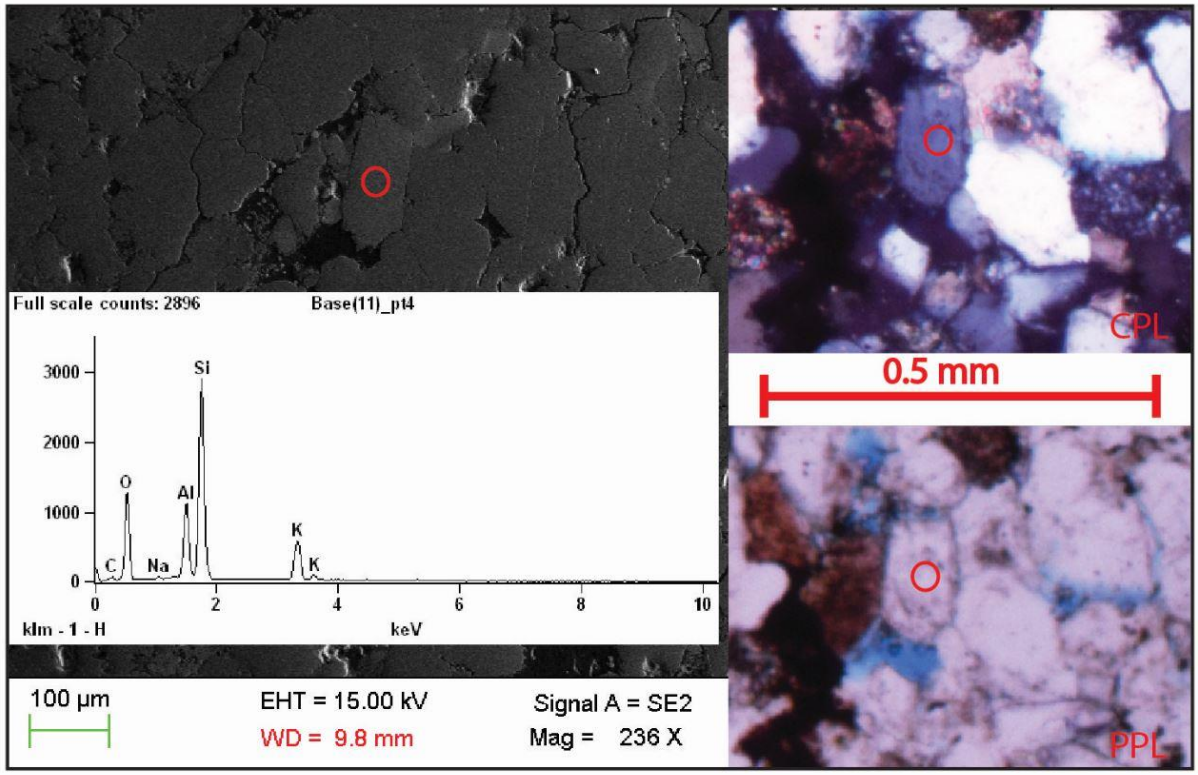


**Fig. 5.20:** This figure shows the SEM result of one feldspar grain that could be visually classified as quartz. This grain is most likely a kali-feldspar which has the composition $KAlSi_3O_8$. The red circle represents the area for SEM-analysis. This thin section analysis is from sample 71, see **Table 5.11**.

### ALTERATION PRODUCTS

Several of the detrital feldspar grains have been dissolved and other minerals have crystallised in their place. The feldspars are typically replaced by muscovite or chlorite (**Fig. 5.21**). These types of cases have in this study been registered as "alteration product" even if some residual feldspar can be recognised.

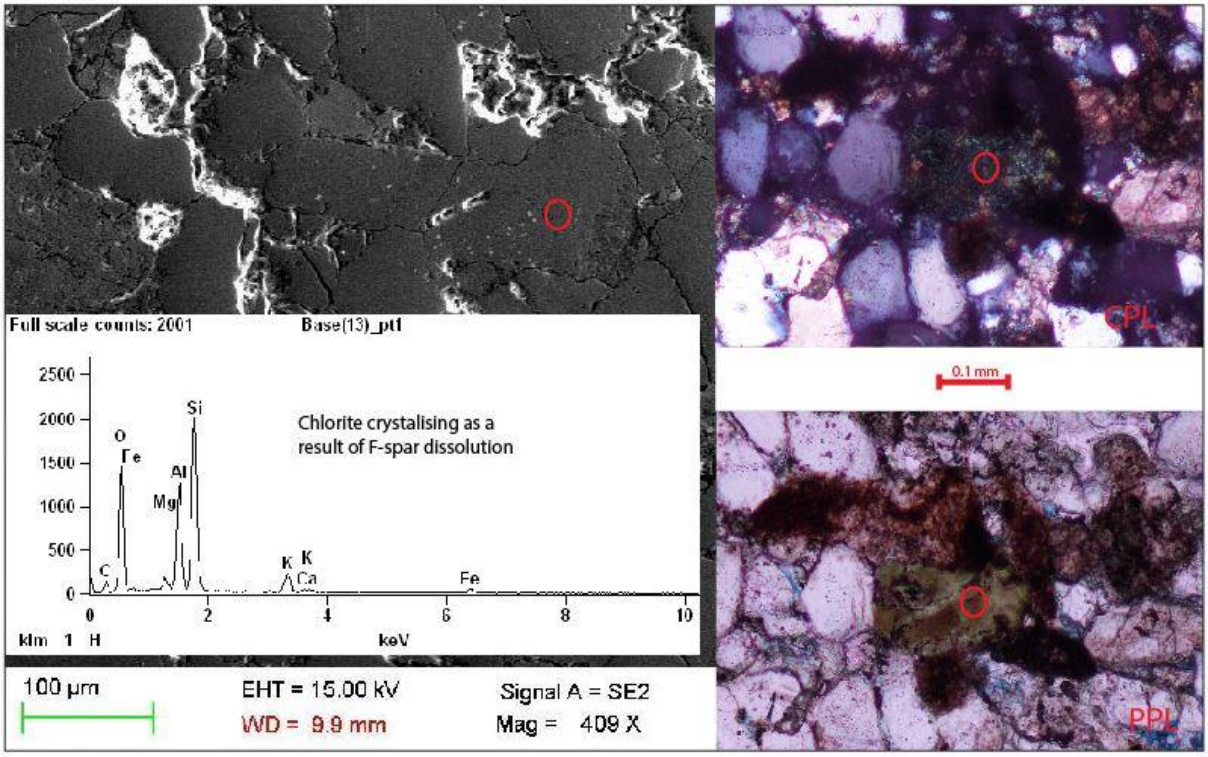


**Fig. 5.21:** Chlorite which crystallised in a space where feldspar has been dissolved. This has visually been interpreted as a chlorite grain and an alteration product. In the SEM results the Potassium (K) content could indicate some residual feldspar ($KAlSi_3O_8$) in this grain. The Fe, Mg and Al content is typical for chlorite, which has the chemical formula $(Mg,Fe,Al)_3(SiAl)_4O_{10}(OH)_2 \cdot (Mg,Fe,Al)_3(OH)_6$. This thin section analysis is from sample 71, see **Table 5.11**.

### OXIDE-CEMENT

SEM results from all the four thin sections show that visually interpreted oxide-cement consists of the iron-oxide Hematite (**Fig. 5.22**)

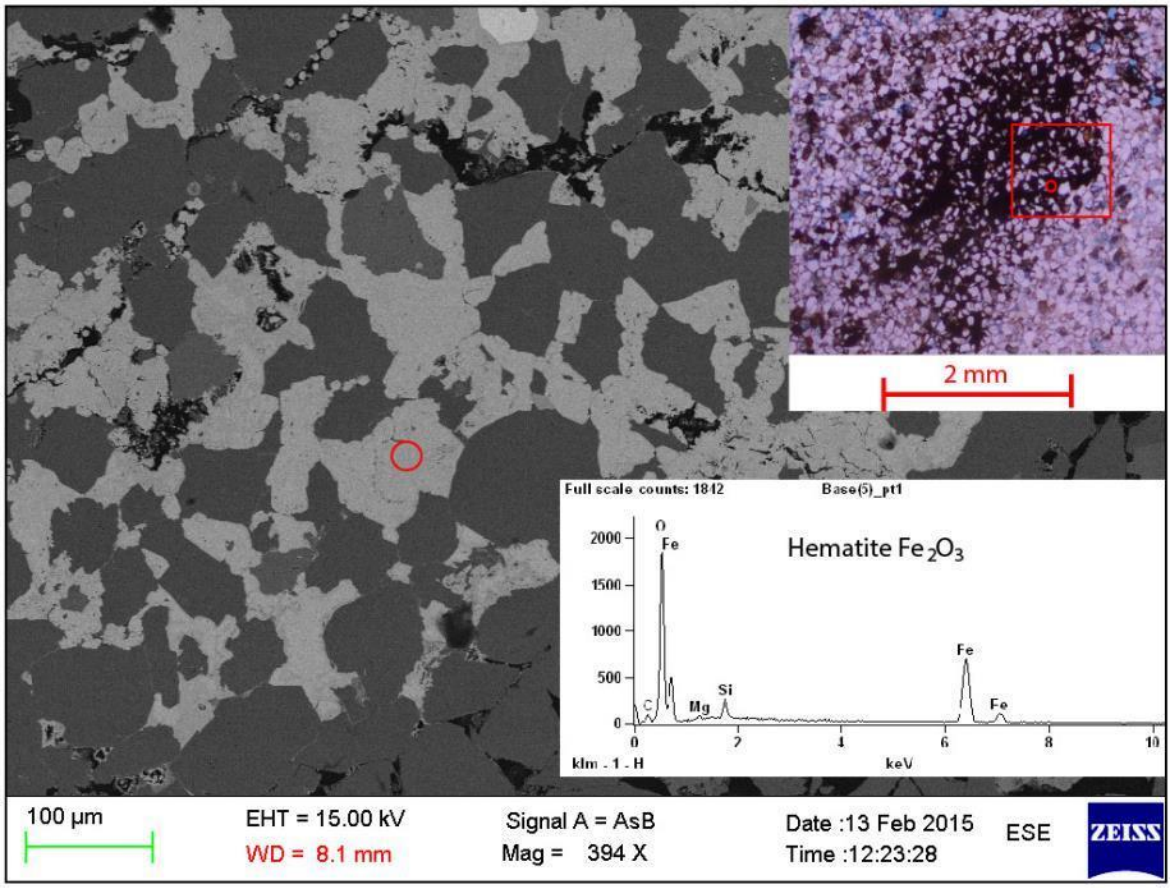


**Fig. 5.22:** SEM analysis was done on this highly cemented area of the thin section. This cemented area is not representative for the entire thin section. The areas left and right of the cemented area are much more representative for the majority of the thin section. Nevertheless this figure illustrates the typical Hematite composition observed in the oxide cement for all the four samples. This thin section analysis is from sample 36, see **Table 5.11**.

### OPAQUE MATERIAL

Opaque minerals and fragments observed in the thin sections were registered as opaque material. SEM analysis was used to define the composition of these minerals and fragments. The opaque fragments are interpreted to be organic and consist predominantly of a matrix of carbon, and often include some iron oxides and heavy minerals (pyrite, apatite etc.) (**Fig. 5.23**), but some fragments consisting purely of carbon were found.

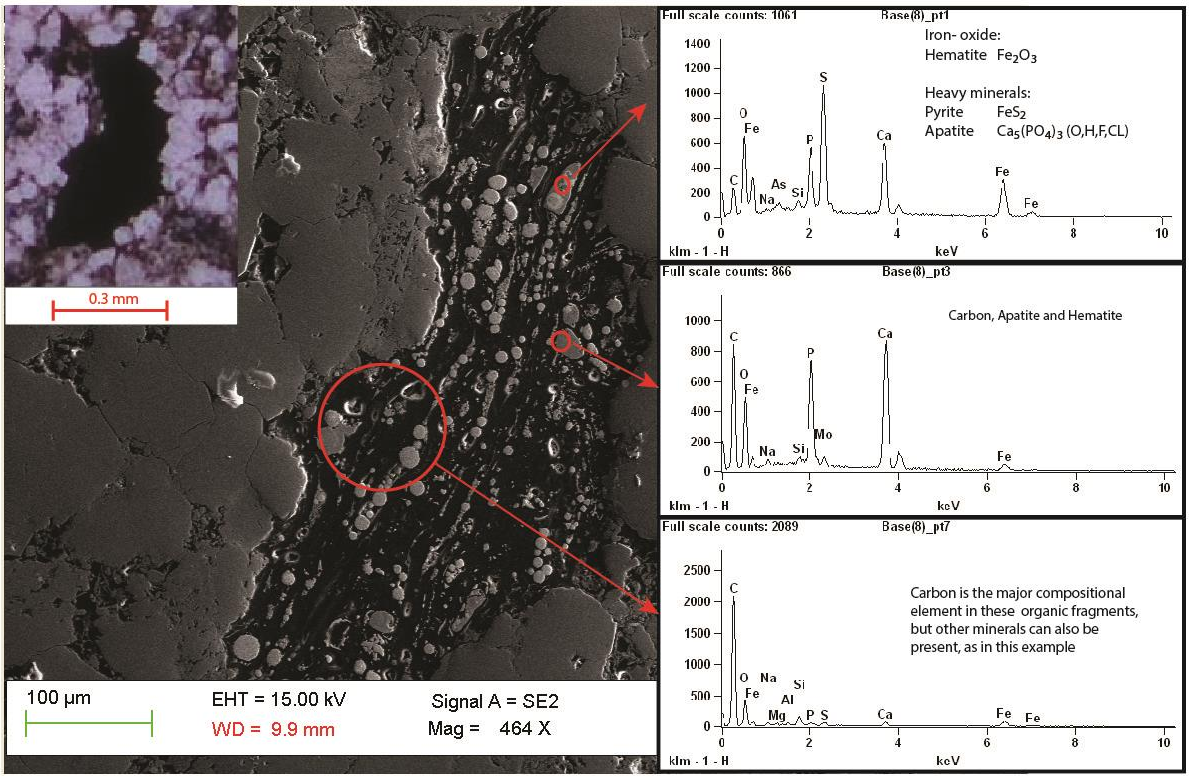


**Fig. 5.23:** Shows the SEM analysis of an organic fragment. The black area represents the carbon content of the organic fragment, while the grey dots represent different minerals. Hematite is the most abundant mineral, but apatite is also commonly found within these fragments. Pyrite can also occur in these fragments. This thin section analysis is from sample 71, see **Table 5.11**.

The opaque minerals analysed in SEM represent different mineral compositions. Iron-oxide such as Hematite is the most common composition of the opaque minerals, but also minerals such as rutile occurs.

### ROCK FRAGMENTS

SEM results show that the rock fragments consist predominantly of quartz (**Fig. 5.24**). Visually the rock fragments look like several small quartz grains which together compose a larger grain. These fragments can sometimes resemble alteration products since the quartz grains are so small and alteration products often are observed as numerous small crystals. The rock fragments can however easily be separated from the alteration products because of their grain shape. Rock fragments are grains in point or concave-convex contact with other mineral-grains, while the alteration products fill the space where feldspars have been dissolved, and do not necessarily form as one large grain.

In this study the rock fragments consist predominantly of poly- and microcrystaline quartz, these rock fragment are stable rock fragments derived from sandstones and chert. The mirocrystaline rock fragments are typical chert-fragments and were observed in large amounts within the Panther Tongue Mb. (**Fig. 5.9**)

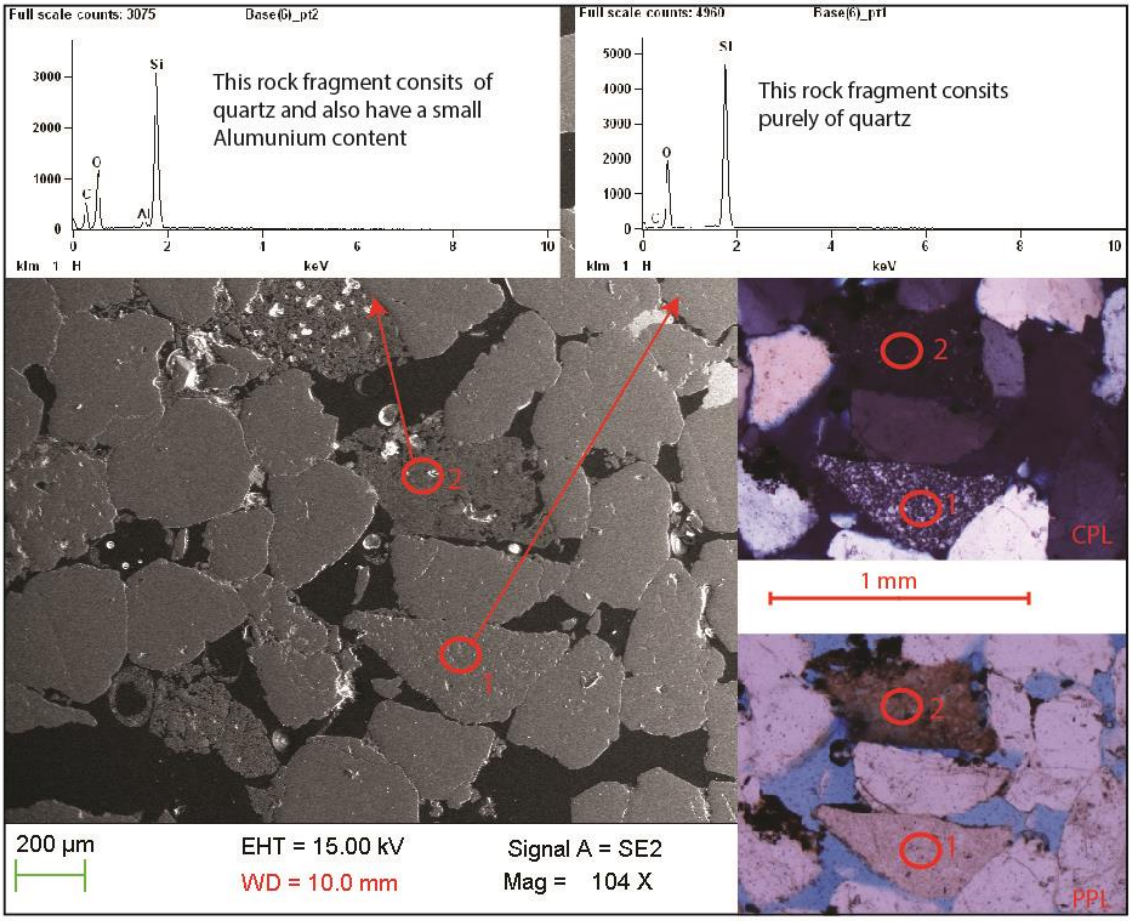


**Fig. 5.24:** Composition for two rock fragments (chert) measured using SEM. The rock fragments consist predominantly of quartz ($SiO_2$), but the rock fragments with a red/brown colour in PPL often contain a small abundance of aluminium and carbon in addition to the quartz. This thin section analysis is from sample 40, see **Table 5.11**.

## UNKNOWN MINERALS

During point counting some minerals were very hard to identify and were therefore registered as unknown minerals. These typically had a red-brown colour in plane polarised light (PPL) and were completely extinct in cross polarised light (CPL). SEM analysis on these minerals showed different minerals. Apatite was common, also mica (**Fig. 5.25**) and in some cases iron-oxides. Because the composition varied among the different grains analysed in the SEM this unknown mineral group was not studied for trends. The abundance of this group within each sample is shown in the raw-data table (**Table 4** in **Appendix I**). The average content of these unknown minerals is 1.7 % and the majority (90%) of the samples have a content of 3% or less.

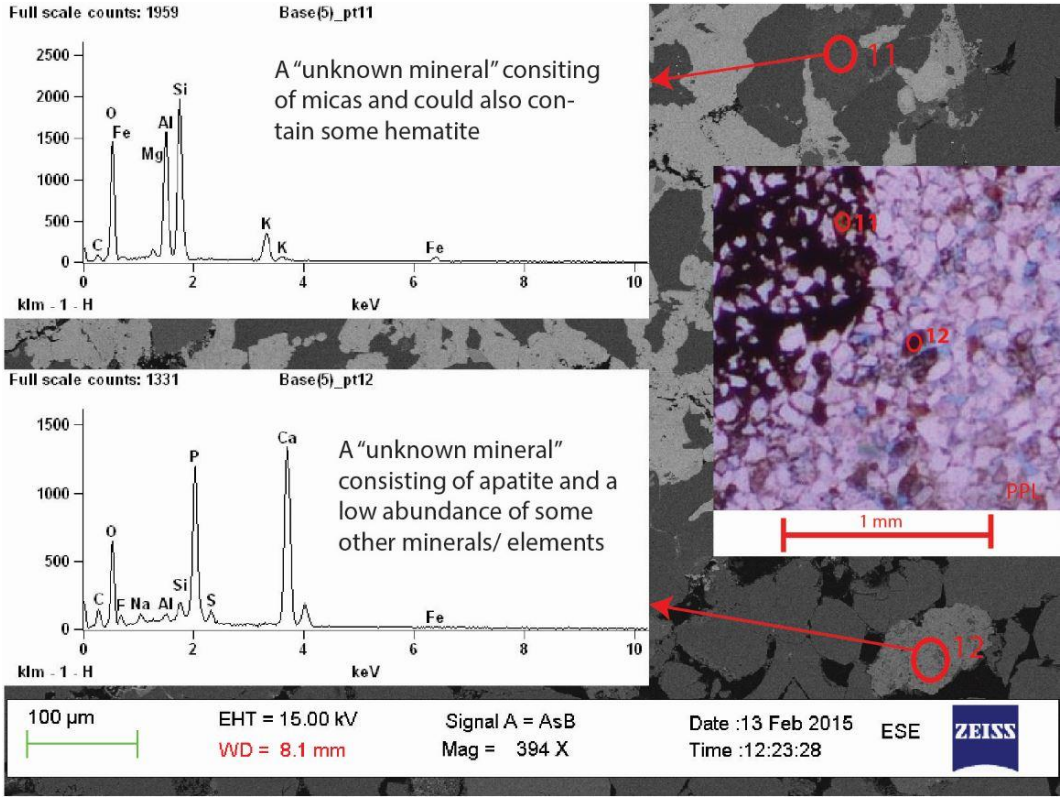


**Fig. 5.25:** The SEM analysis results for two grains which would be registered as "unknown mineral". The first analysis in this example (marked with "11") shows a content of micas (most likely biotite), and there could also be some iron-oxides in this grain or surrounding the grain. Apatite has the chemical formula $Ca_5(PO_4)_3(O,H,F,Cl)$, hematite is $Fe_2O_3$, and dark mica (biotite) has the chemical formula $K(Mg,Fe)_3AlSi_3O_{10}(OH)_2$. This thin section analysis is from sample 36, see **Table 5.11**.

### CORRELATION OF POINT COUNTING INTERPRETATIONS AND SEM RESULTS

There is a low discrepancy between visually interpreted grains during point counting and the SEM results. The visually interpreted oxide-cement is shown to contain iron-oxides such as Hematite, and the opaque fragments consist predominantly of carbon and are therefore being interpreted as organic fragments. Opaque fragments and minerals were registered together during point-counting. Oxide-cement could in some cases look completely opaque, but often a weak touch of dark brown/red colour could be observed.

The discrepancies that were present (underestimation of feldspar and variety of composition within the unknown minerals) have generally too low abundance to be of any significance to the overall trend.

The low discrepancies indicate a sufficient precision in the point counting results for the interpretation of major trends analysed in the following chapter.

# 6 ANALYSIS OF RESULTS

The point count dataset includes data from 80 samples, this chapter presents an analysis of those data to address the following issues: (1) the correlation between the different compositional classes (subchapter 6.1), (2) describing how the content varies by facies associations (3) how the composition varies by stratigraphic units (subchapter 6.2) and (3) determining if the geographic position within the basin has an impact on the mineralogy (subchapter 6.3). Only the compositional classes with an average content above 4% has been analysed, as the smaller classes were too variable and showed no consistent trends without more specialist separation and analysis which is beyond the scope of the current study.

All the raw data for the following analysis are presented in **Table 2-4** in **Appendix II**.

## 6.1 CLUSTER ANALYSIS

Cluster analysis of the point counting data was used to the see which compositional classes (mineral grains, cement, porosity etc.) that correlate best. **Table 6.1** shows the data from which the dendrogram (**Fig. 6.1**) is created.

**Table 6.1:** Spearman's correlation coefficient ($r_s$) for the compositional classes with an average content higher than 4%. Calculated by the use of the statistical software PAST.

| | **Quartz** | **Rock fragments** | **Carbonate grains** | **Alteration product** | **Quartz-cement** | **Carbonate-cement** | **Oxide-cement** | **Opaque material** | **Porosity** |
|---|---|---|---|---|---|---|---|---|---|
| **Quartz** | 1.00 | -0.22 | -0.11 | -0.02 | -0.22 | -0.27 | -0.19 | 0.00 | 0.07 |
| **Rock fragments** | -0.22 | 1.00 | -0.43 | 0.19 | 0.27 | -0.27 | 0.00 | -0.15 | 0.20 |
| **Carbonate grains** | -0.11 | -0.43 | 1.00 | -0.09 | -0.48 | 0.54 | 0.03 | 0.05 | -0.51 |
| **Alteration product** | -0.02 | 0.19 | -0.09 | 1.00 | -0.08 | -0.15 | -0.01 | 0.00 | -0.05 |
| **Quartz-cement** | -0.22 | 0.27 | -0.48 | -0.08 | 1.00 | -0.43 | -0.05 | 0.10 | 0.57 |
| **Carbonate-cement** | -0.27 | -0.27 | 0.54 | -0.15 | -0.43 | 1.00 | 0.07 | -0.11 | -0.67 |
| **Oxide-cement** | -0.19 | 0.00 | 0.03 | -0.01 | -0.05 | 0.07 | 1.00 | 0.16 | -0.32 |
| **Opaque material** | 0.00 | -0.15 | 0.05 | 0.00 | 0.10 | -0.11 | 0.16 | 1.00 | -0.20 |
| **Porosity** | 0.07 | 0.20 | -0.51 | -0.05 | 0.57 | -0.67 | -0.32 | -0.20 | 1.00 |

The belt of insignificant correlation on the dendrogram (**Fig. 6.1**) is calculated from Equation 6.1, which is obtained from the formula of the Fisher test (subchapter 3.3).

Equation 6.1: $r = \sqrt{\frac{t^2}{(n-2+t^2)}}$

The value of t is read from Table 2 in (Nemec, 2011), for α = 0.10 and DF = n-2. In this analysis n=81 and t= 1.293. Equation 6.1 then gives us the critical value r = 0.1439

The compositional classes which correlate the best are quartz-cement with porosity and carbonate grains with carbonate-cement. These correlations form the base of the two major "families" in this cluster analysis. Rock fragments have a weaker, but still significant correlation to the quartz-cement/porosity group. The weakest positive correlation that still gives a correlation value >0.144 is the link between oxide-cement and opaque material. This group is insignificantly linked to the carbonate group. Alteration products and quartz grains show an insignificant link to the "quartz-cement, porosity and rock fragment group".

The first major "family" consisting of carbonate (grains and cement), oxide-cement and opaque material show a weak but significant negative correlation with the second major "family", which consist of quartz-cement, porosity, rock fragments and alteration products. The correlation coefficient ($r_s$) between only the carbonate group (grains and cement) and the quartz-cement and porosity group gives a negative value of -0.52.

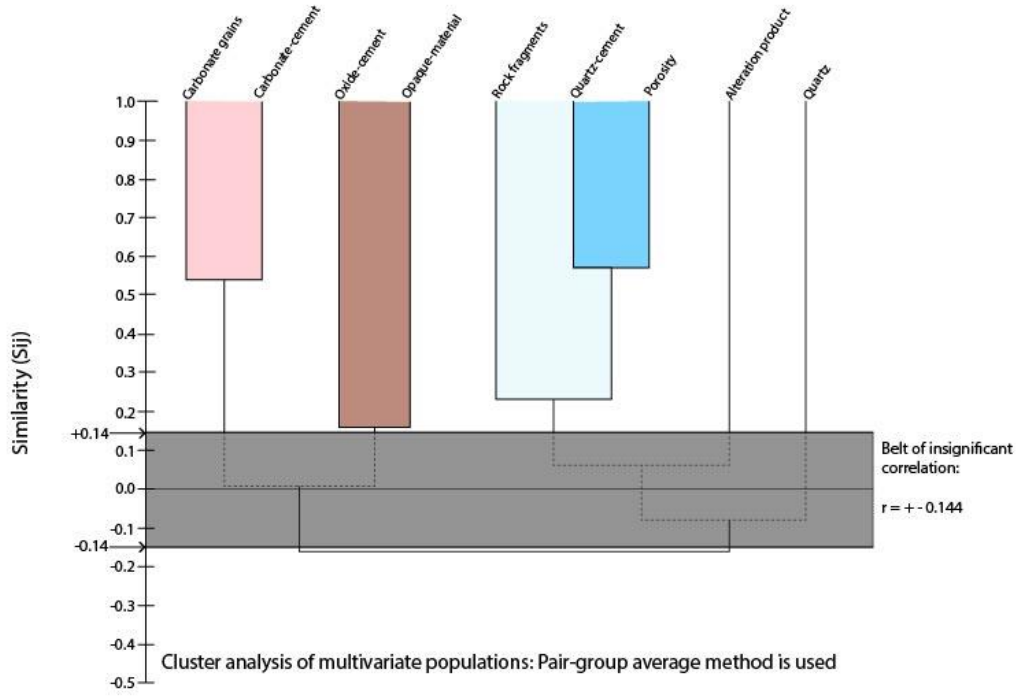


**Fig. 6.1:** Dendrogram showing clustering of the compositional classes based on Spearrman's correlation coefficient. Positive values show a positive correlation between the compositional classes, if the content of one variable increases the other will also increase. Negative values show a negative correlation between the compositional classes. A value of 1 equals perfect positive correlation, 0 equals no correlation and -1 equals perfect negative correlation. The compositional classes which correlate the best are quartz-cement with porosity (blue) and carbonate grains with carbonate-cement (pink). Rock fragments have a weaker, but still significant correlation to the quartz-cement/porosity group (light blue). The weakest positive correlation that still gives a correlation value >0.144 is the link between oxide-cement and opaque material (brown). The first major "family" consisting of the pink and brown group show a weak but significant negative correlation with the second major "family", which consist of the blue group and alteration products.

The relationships found during the cluster analysis will be discussed in detail in the following sections, and possible mechanisms will be examined in chapter 7.

## 6.2 ANALYSIS BY FACIES ASSOCIATIONS AND STRATIGRAPHIC POSITION

The point counting results were analysed both in regards to the facies associations (depositional environment) and stratigraphic units. **Fig. 6.2** shows an overview of some of the major trends found in this study. The trends in the diagrams show how the content of different minerals, type of cement and porosity varies with the facies associations and the stratigraphic units sampled in this study. These diagrams show the average content and are not normalised, for diagrams showing normalised data with all the compositional classes see **Fig. 2**. in **Appendix II.**

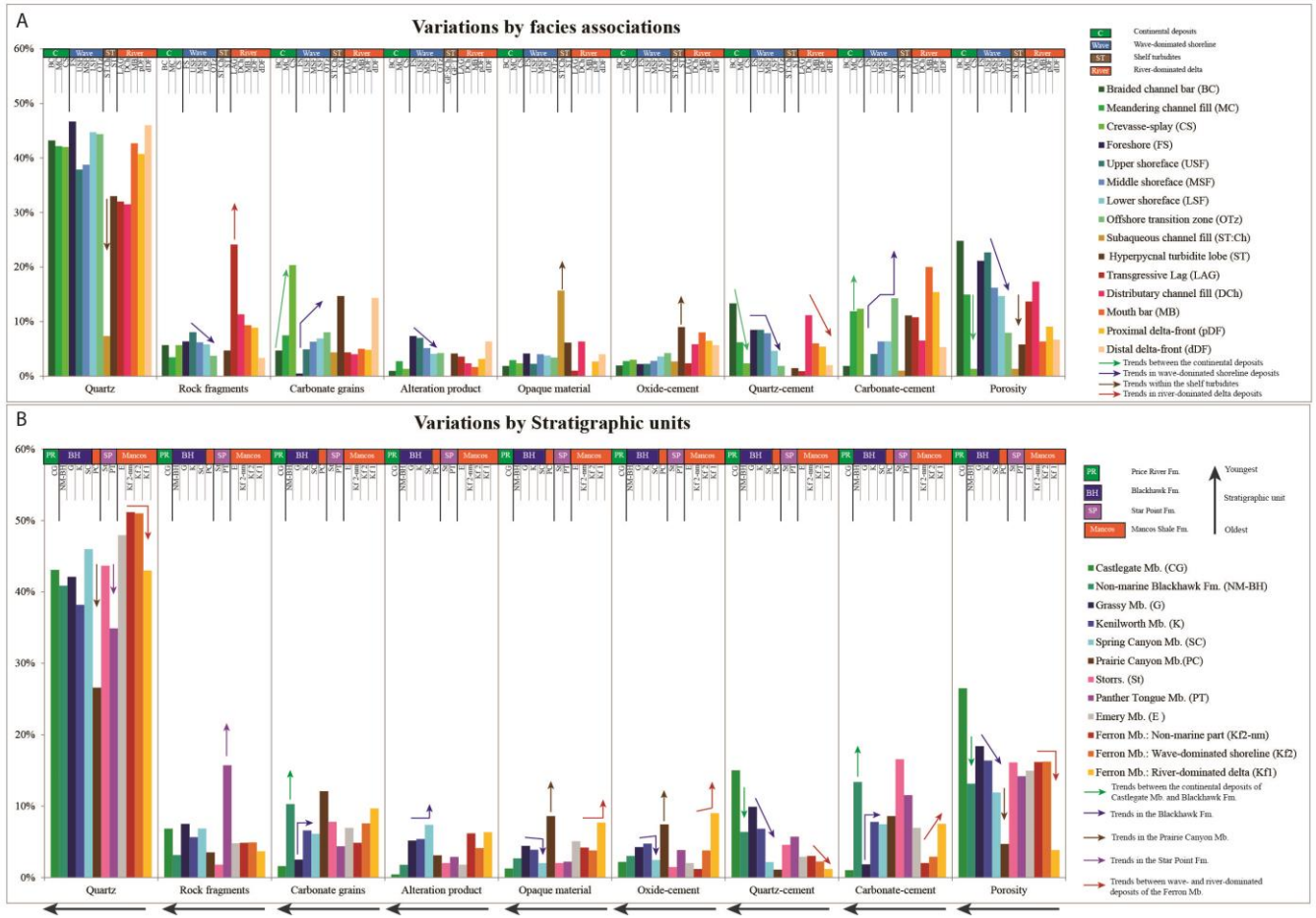


**Fig. 6.2:** These diagrams show an overview of the average composition by facies associations (**A**) and by stratigraphic unit (**B**). These diagrams are not normalised to 100 %, but show the average content within the compositional classes containing on average >4%. For diagrams containing all the different compositional classes see **Fig. 2** in **Appendix II**. **A)** The arrows represent major trends within different depositional environments and are explained in further detail in section 6.2.1 **B)** The arrows represent major trends within different stratigraphic members and are explained in further detail in section 6.2.2.

### 6.2.1 ANALYSIS OF RESULTS BY FACIES ASSOCIATIONS

When analysing results by facies associations several trends are observed. The trends are presented as variations in the palaeoseaward direction within the marine depositional environments, and as variations between braided bar, meandering channel fill and crevasse-splay deposits in the coastal plain environment.

Similar trends can be observed within the compositional classes which have a significant positive correlation (**Fig. 6.1**), these classes are therefore presented together in the following sections.

#### QUARTZ-CEMENT AND POROSITY

The strongest positive correlation found in the cluster analyses (**Fig. 6.1**) was between quartz-cement and porosity. These compositional factors show the same trends for the continental and wave-dominated shoreline environments (**Fig. 6.3** and **Fig. 6.4**), but not for the river-dominated delta environment (**Fig. 6.4**).

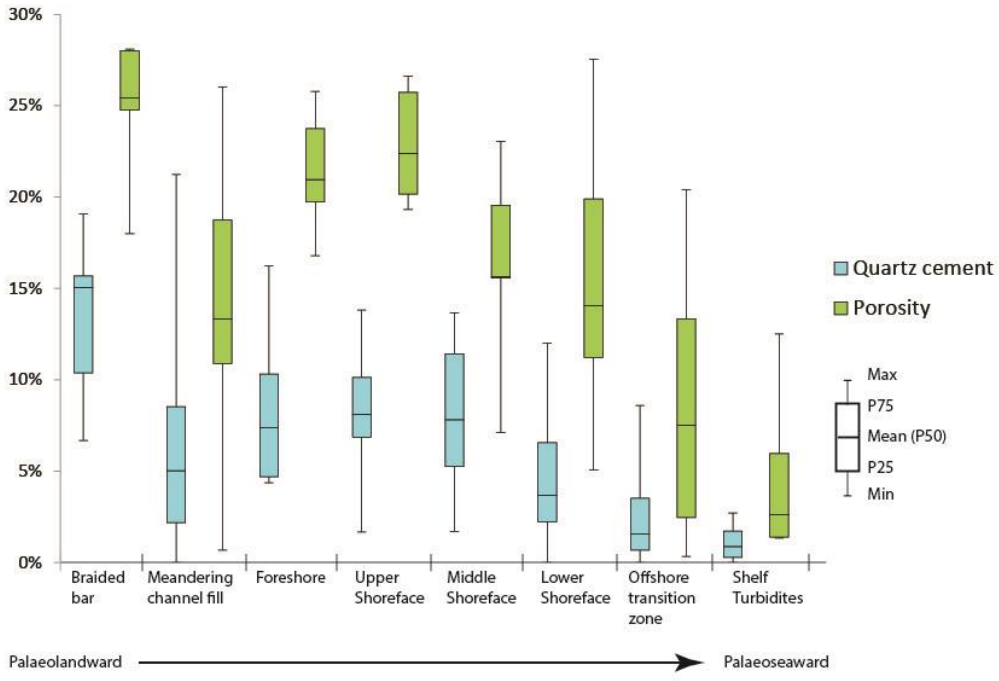


**Fig. 6.3:** This Box and Whisker plot indicates a facies dependent trend in the quartz-cement and porosity content. The porosity and quartz cement decrease by facies associations in a palaeoseaward direction. Within the continental samples the braided bars are generally more porous and contain more quartz-cement than the meandering river deposits. The FS and USF deposits have a relatively similar content, while the content decreases gradually when moving towards the shelf turbidite deposits.

The general trend observed within both quartz-cement and porosity is a decrease in content in the palaeoseaward direction within the depositional environments. Braided channel bars show the highest proportion of quartz cement and porosity, while the lowest proportion of these classes are found in the crevasse-splay, subaqueous channel and self turbidite deposits (**Fig. 6.4**).

The common factor for the deposits with a lower quartz-cement and porosity content was a high carbonate content and vice versa. The Spearman's correlation coefficients show negative correlations between the quartz-cement/porosity group and the carbonate (grains and cement) group. The average correlation is -0.52 (calculated from the values in **Table 6.1**).

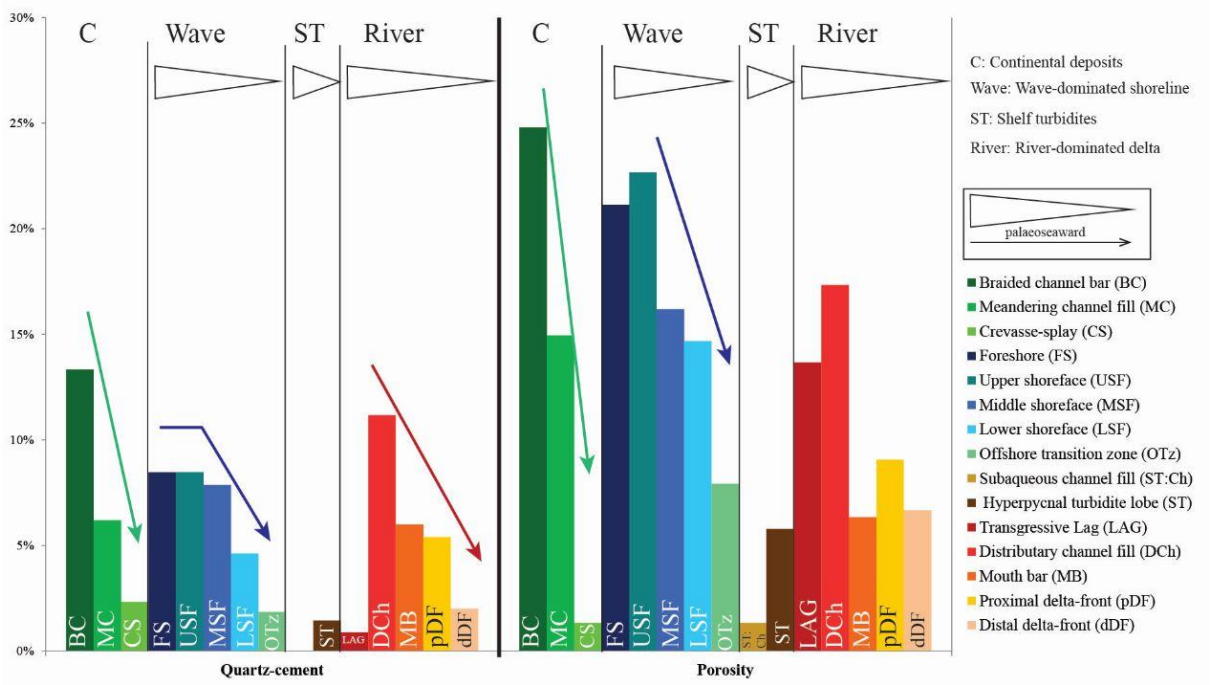


**Fig. 6.4:** Histogram of the average quartz-cement and porosity content within different facies associations. These diagrams show a clear decrease in both quartz-cement and porosity when moving palaeoseaward in the marine environments. They also show a difference in the continental deposits. The braided bar deposits are more porous and contain more quartz-cement than the meandering channel fill. Within the coastal plain environment the crevasse-splay deposits show the lowest amount of quartz-cement and porosity.

Note that these trends are consistent with the permeability (**Table 5.7**), which also decreases in the palaeoseaward direction and is highest for the braided bar deposits.

### CARBONATE GRAINS AND CARBONATE CEMENT

The group which shows the second highest correlation is the carbonate and carbonate-cement group (**Fig. 6.1**). Both carbonate and carbonate-cement show similar facies dependent trends (**Fig. 6.5**). These trends are generally reversed compared to the trends in the section above (**Fig. 6.4**).

There is an overall increase in content when moving palaeoseaward within the wave-dominated environment (**Fig. 6.5**). The lowest content is clearly seen in the foreshore deposits. The content increases radically from foreshore to upper shoreface deposits followed by a more gradual palaeoseaward increase. The carbonate cement content is also clearly highest within the offshore transition zone in this environment.

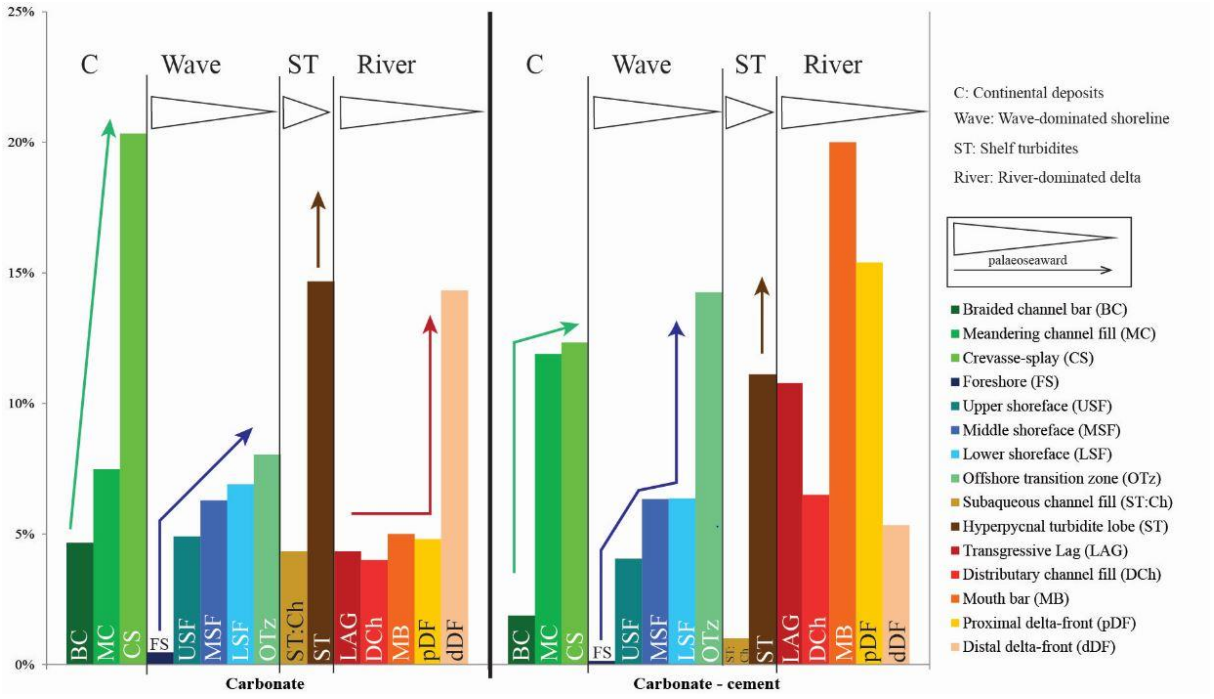


**Fig. 6.5:** Histogram of the average carbonate (detrital carbonate grains) and carbonate-cement content within different facies associations. The carbonate and carbonate-cement content is increasing palaeoseaward in the wave dominated depositional environment, with a sharp increase between FS and USF. In the coastal plain environment the content increases between the braided and meandering river systems. Within the river-dominated delta deposits there is no clear trend controlled by facies associations.

Within the river-dominated environment the carbonate grain content is very similar for most of the deposits except for the distal delta-front sample. This trend is not considered as a significant trend since only one sample was collected from distal delta-front deposits and since the same trend is not recognised in the carbonate-cement content.

The carbonate and carbonate-cement content within the coastal plain depositional environment is lowest for the braided bar deposits and highest for the meandering and crevasse-splay deposits in (**Fig. 6.5**). This trend between different facies could also represent a trend between formations. Most of the braided bar samples (4/5) are from the Castlegate Sandstone, while most of the meandering channel fill samples (10/12) are from the non-marine part of the Blackhawk Fm., this is examined further in section 6.2.2.

### OXIDE-CEMENT AND OPAQUE MATERIAL

The oxide-cement and opaque material content have a positive correlation of $r_s$=016 (**Table 6.1**), but do not show many similar trends within the different facies associations. The two most striking similarities are (1) the relatively high content of oxide cement and opaque material within the sub-aqueous channels and shelf turbidites and (2) the relatively low proportion within the transgressive lag deposits (**Fig. 6.6**).

Otherwise the opaque materials show very few facies dependent trends. The oxide-cement (iron oxide) on the other hand shows a small increase in the palaeoseaward direction for the wave-dominated deposits, and a higher content for the meandering river systems than for the braided (**Fig. 6.6**).

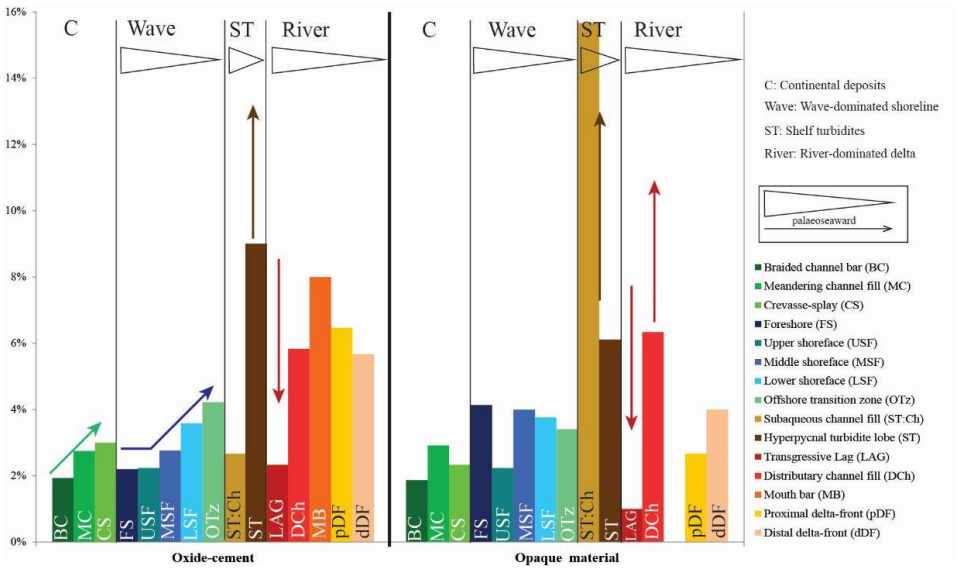


**Fig. 6.6:** This histogram shows how the average content of oxide–cement and opaque material varies with the facies associations. The oxide-cement shows an increasing trend when moving palaeoseaward in the wave-dominated environment. The content of oxide cement is also slightly lower of the meandering channel fill and crevasse-splay deposits than the braided bars. The opaque minerals and fragments do not show any clear facies dependent trend, but the content is significantly higher for the sub-aqueous channel and self turbidites.

The trend for the oxide cement is similar to the trends found in carbonate and carbonate cement content. The cluster analysis also indicates a slightly positive correlation between the oxide cement and the positive carbonate group, but this plots in the belt of insignificant correlations (**Fig. 6.1**).

The content of oxide cement is also generally larger for the river dominated deposits than the wave-dominated (**Fig. 5.2** and **Fig. 6.6**). This trend is also found in the rock fragments (**Fig. 6.7**).

### ALTERATION PRODUCTS AND ROCK FRAGMENTS

The rock fragments show a weak correlation to the quartz-cement/porosity group, and the alteration products are only insignificantly linked to these other classes (**Fig. 6.1**). Not many trends are recognised within the alteration products and the rock fragments, but a general decrease in the palaeoseaward direction can be recognised.

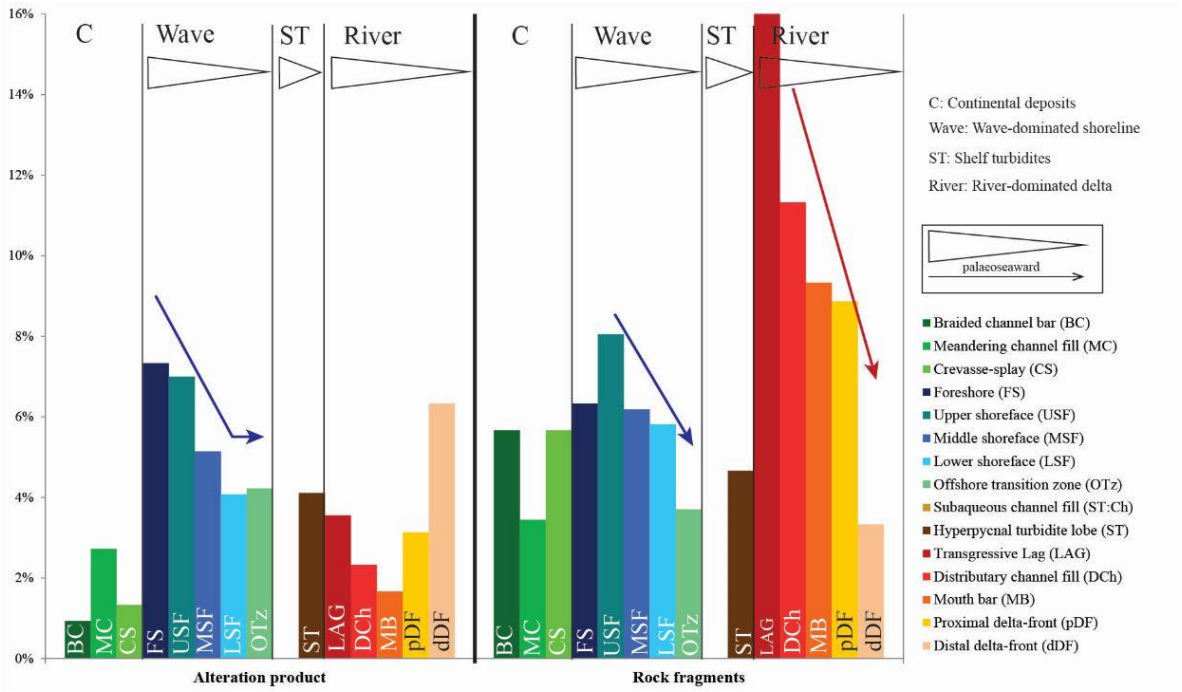


**Fig. 6.7:** This histogram shows how the average content of altered grains (feldspar altered to mica or chlorite) and rock fragments (mostly chert) varies with the facies associations. The alteration is decreasing palaeoseaward in the wave-dominated environment. No trend is observed in the other depositional environments. The rock fragment content is the main trend in the river-dominated environment, and the content decrease palaeoseaward.

The proportion of rock fragments is generally higher for the river-dominated environment, but this trend could be more dependent on the formation than depositional environment since

most of the river-dominated samples (8/10) are from the Panther Tongue Mb. This is examined further in section 6.2.2.

### 6.2.2 ANALYSIS OF RESULTS BY STRATIGRAPHIC UNITS

In the following sections each stratigraphic unit is presented with trends characteristic for or within the formation. In **Fig. 6.2** some of the major formation controlled trends are presented, these trends will be further explained within each formation.

#### MANCOS SHALE FORMATION

This formation includes a very thick succession of offshore shale with several major sandstone members (Ferron, Emery) and a minor sandstone (Manco's B). In the overall formation no clear stratigraphic dependent trend was found, but within the two sandstone members some trends are recognised.

In the Ferron Mb. trends mark a difference between the different depositional environments. The Ferron Mb. of the Last Chance delta can be divided into the two parasequence sets Kf1 and Kf2. Parasequence set Kf1 represents deposition during a river-dominated deltaic environment, while Kf2 was deposited during a wave-dominated shoreline environment (Deveugle et al., 2011). **Fig. 6.8** shows some clear trends between these two different environments. The deltaic deposits are less porous and contain a lower amount of quartz grains, while the opaque material and carbonate cement content is higher. These trends can also be demonstrated in **Fig. 5.2** in section 5.1.1.

Within the Emery Mb. the northern and southern delta lobe show some difference in composition (**Fig. 6.8**). The southern deposits are on average more porous and less cemented, and carbonate cement is the dominant cement within this member. The southern deposits also contain less opaque material, quartz grains, carbonate grains and rock fragments. There is also a clear difference in grain size between these two delta deposits (**Fig. 5.4** and **Fig. 5.5**), where the northern delta has a smaller grain size than the southern delta, this could be the controlling factor for the difference in composition and porosity.

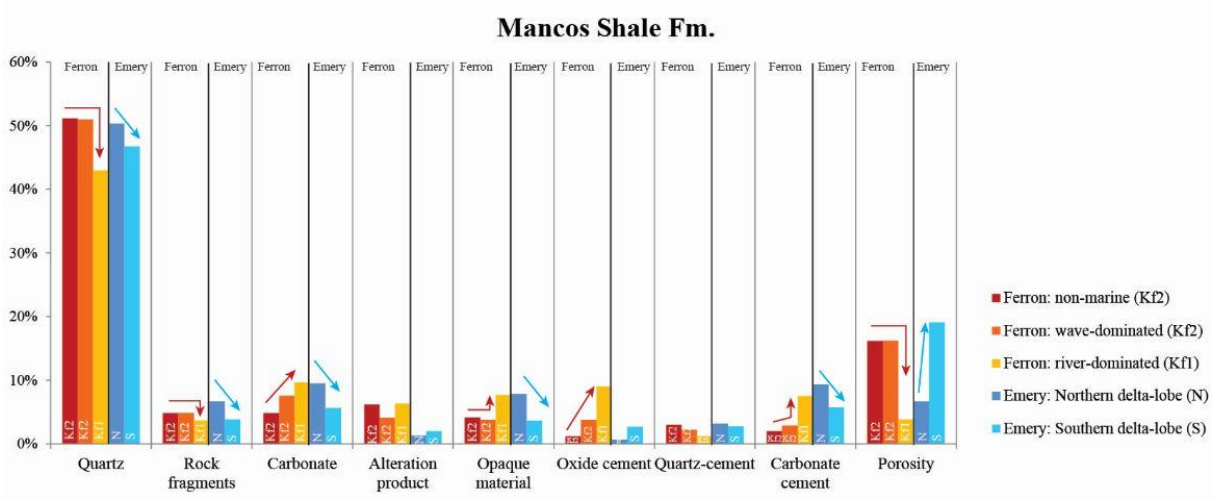


**Fig. 6.8:** Histogram showing the average composition within the Mancos Shale Fm. No clear connection can be observed between the Ferron Mb. and Emery Mb. Within the Ferron Mb. the trends observed (red arrows) indicate differences between depositional environments. The river-dominated samples are on average more cemented and less porous than the wave-dominated samples. The composition within Kf2 is relatively similar for the shallow marine and non-marine deposits. In the Emery Fm. the deposits from the northern delta-lobe differs some from the southern delta-lobe deposits.

The changes within the Ferron Mb. seem to be controlled by the depositional environments, while the changes in the Emery Mb. seem to be controlled by the difference in grain size, where the northern deposits were sampled in a more distal part of the lower shoreface than the southern deposits (**Fig. 6.8**).

### STAR POINT FORMATION

The trends within this formation show a significant difference in quartz and rock fragment content. The Panther Tongue Mb. shows the strongest stratigraphic trend with its high proportion rock fragments and a low proportion quartz grains. The Storrs Mb. has on the other hand a high proportion quartz grains and a low proportion rock fragments (**Fig. 6.9** and **Fig. 6.10**). The rock fragments are, as mentioned in section 5.3.1 stable fragments, consisting of polycrystalline quartz grains and chert fragments (microcrystalline quartz). These chert fragments are stable grains, thus the high content of rock fragment in the Panther Tongue Mb. does not indicate less compositional maturity, but a change in source area, suggesting that the member was derived from a chert-rich provenance area.

The feldspar content is generally very low, as mentioned in section 5.3.1. As well as being illustrated in **Fig. 6.9** and **Fig. 6.10**.

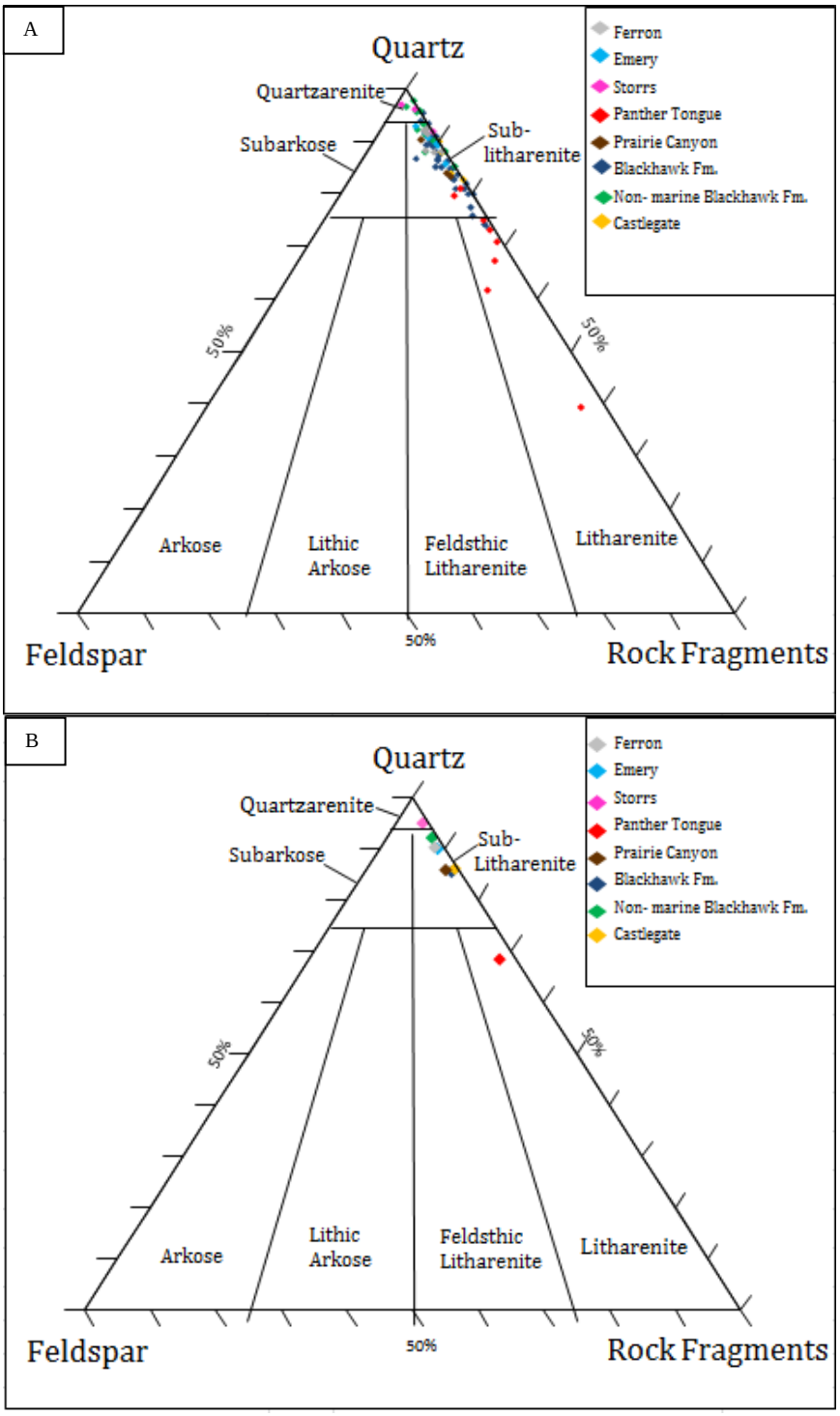


**Fig. 6.9: A)** A triangular plot including all the samples except sample #22 (Woodside sandstone, because it had a mud content of ~67%). **B)** A triangular plot with the average from each member or formation. The clear trend from these diagrams is the Panther Tongue is more chert-rich than the other samples. Both of these diagrams show clearly that the Panther Tongue Mb. differs from all the studied stratigraphic units. The Storrs Mb. plots on average highest in these diagrams, but does not deviate from the other members in as much as the Panther Tongue does. It needs to be emphasized that the rock fragments are stable, and consist predominantly of quartz. If these fragments had been registered as quartz grains instead all the samples would plot as quartzarenite.

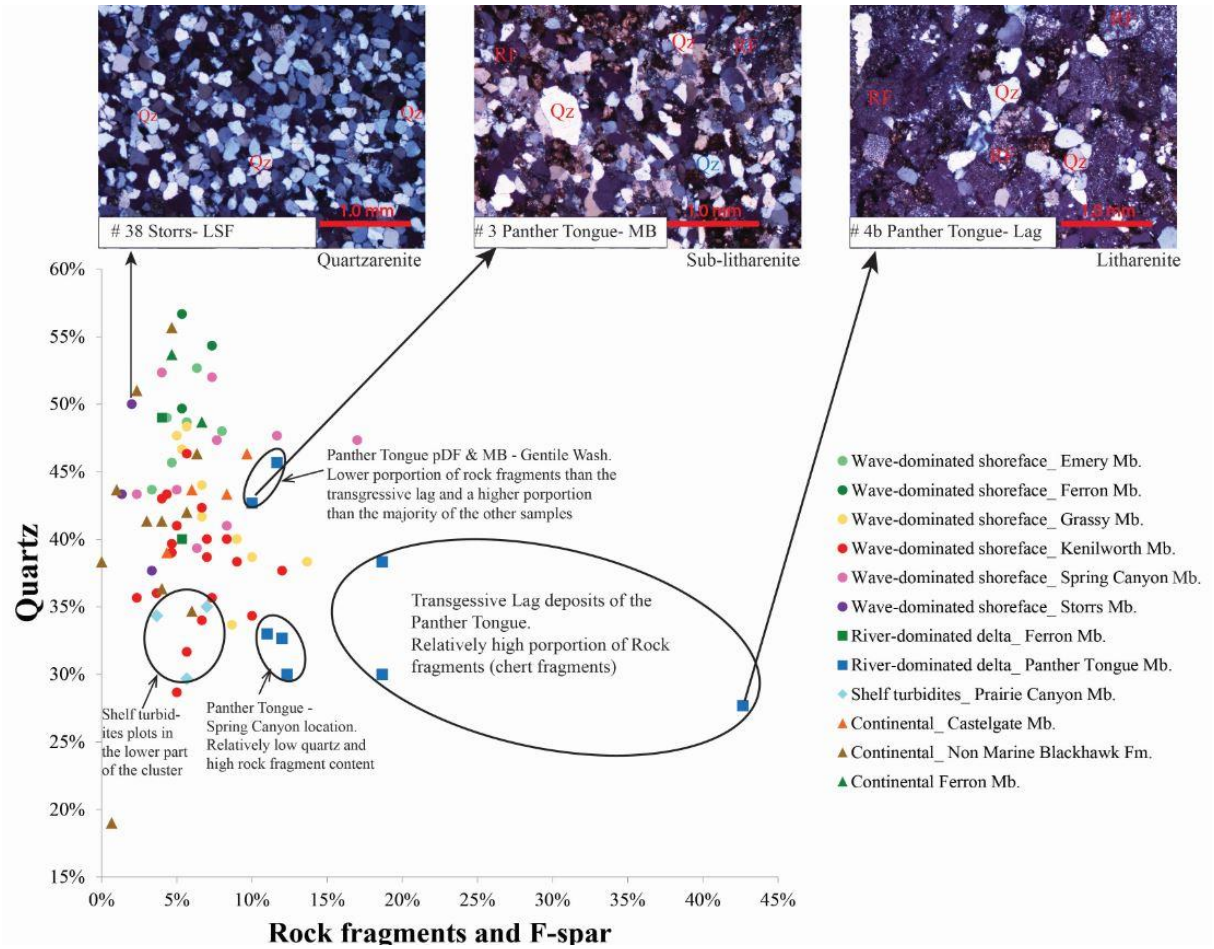


**Fig. 6.10:** This figure shows detrital quartz (Qz) plotted against rock fragments (RF) and feldspar (Fsp). Also in this plot the Panther Tongue Mb. is clearly distinguished from the others with a higher proportion rock fragments (chert-grains). The Storrs Mb. in comparison contains a relatively small amount of RF. This diagram shows that the transgressive lag deposits contain the highest proportion of rock fragments. The thin-section photos show how the sandstone composition changes from chert-poor in the Storrs Mb. (# 38) to chert-rich in the Panther Tongue (# 4b). Abbreviations: LSF, Lower shoreface; MB, Mouth bar; Lag, Transgressive lag.

## BLACKHAWK FORMATION

The different shallow marine members of the Blackhawk Fm. do not show any clear trends in the quartz, feldspar and rock fragment content. The majority plots within the sub-litharenite sandstone classification (**Fig. 6.11** and **Fig. 6.12**).

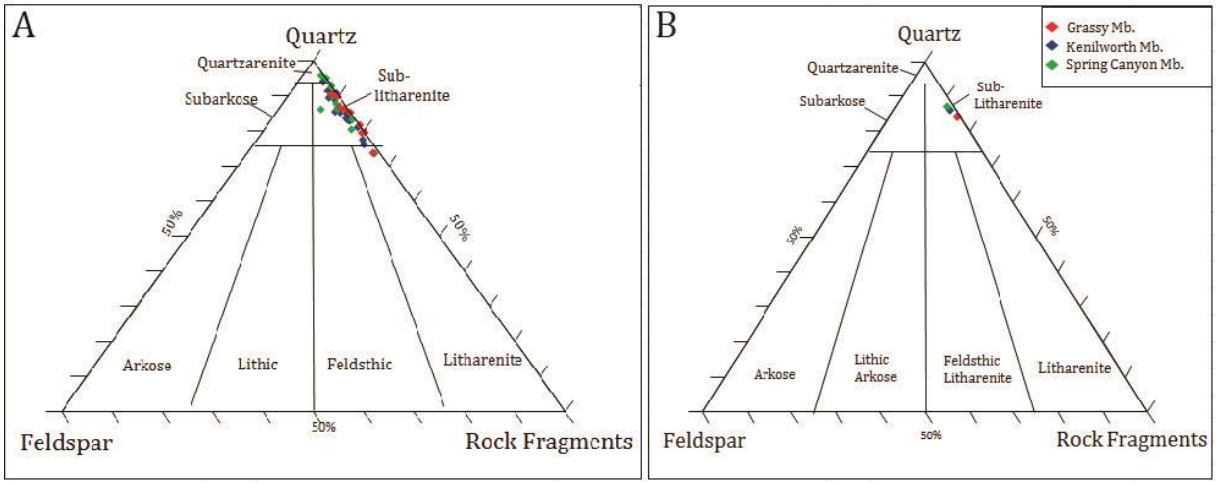


**Fig. 6.11:** Triangular diagrams for the shallow marine samples of the Blackhawk Fm. **A)** All the samples are represented. **B)** The average is presented. These diagrams show that the quartz, feldspar and rock fragment content is relatively similar, and they show no trend within this formation.

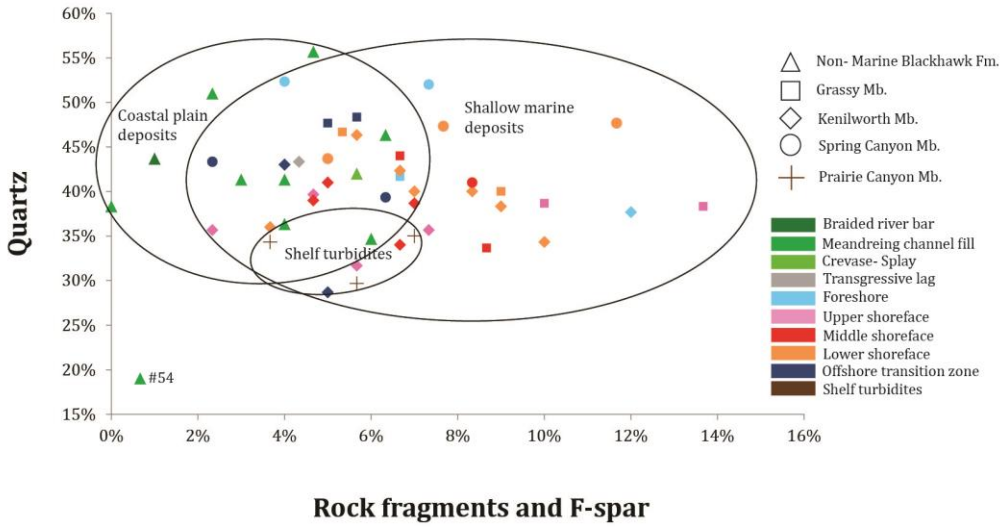


**Fig. 6.12:** The quartz, feldspar and rock fragment content do not show any clear trends within the Blackhawk Fm. The circles mark the range of continental deposits, shallow marine shoreface deposits (FS, USF, MSF, LSF & OTz) and the shelf turbidites of the Prairie Mb (Mancos Shale Fm.). More than 50 % of these samples plot within the area where at least two of these circles overlap. Within this overlapping area all the members and all of the depositional environments (except braided bar) are plotted. The two marine circles overlap completely, and the continental and the marine deposits overlap quite well when sample #54 is excluded. # 54 deviates from the other non-marine meandering channel fill deposits, as demonstrated in **Fig. 5.11**.

However, some stratigraphically controlled petrographic trends are found within the Blackhawk Fm. (**Fig. 6.13**). These are reflected in the cement content rather than the detrital grain content (**Fig. 5.13**).

The most prominent trend within the Blackhawk Fm. is the change in quartz-cement with stratigraphic member (**Fig. 6.13**), but also the carbonate (grains and cement) and porosity content show some trends. The carbonate content is generally very low for the FS and USF deposits and very high for the OTz deposits, therefor the trends observed within the MSF and LSF gives the most accurate picture on how the carbonate content varies with the stratigraphic units.

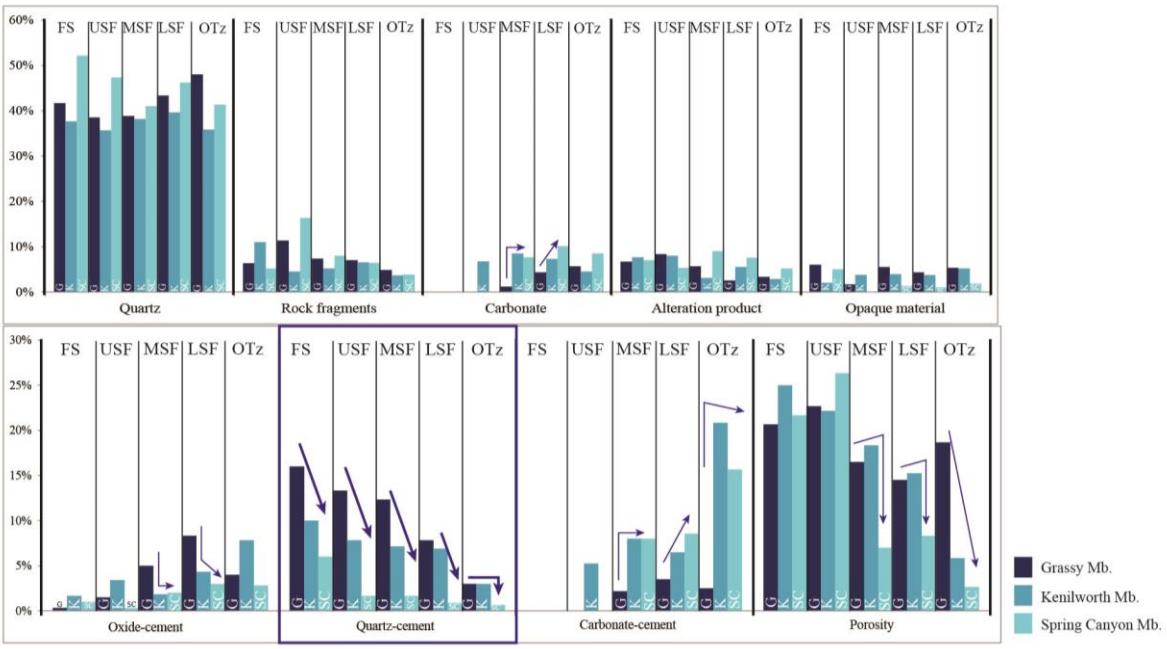


**Fig. 6.13:** This figure shows the average petrographic composition for the mineral grains (upper diagram), as wells as cement and porosity (lower diagram). The abundance of quartz-cement is highest in the Grassy Mb. and decreases stratigraphically downwards through the Kenilworth Mb. and Spring Canyon Mb. This trend is present within all of the different facies association. The carbonate-cement and carbonate grain classes show an opposite trend of the quartz-cement. The carbonate content is generally highest for the statigraphically lowest member (Spring Canyon Mb.) and decreases upwards in the stratigraphy. The carbonate trends are most visible for the MSF and LSF deposits. Note the general absence of carbonate in the FS and USF deposits.

## PRICE RIVER FORMATION - CASTLEGATE MEMBER

The most prominent trends for the Castlegate Mb. compared with other formations is the low carbonate content (**Fig. 5.18**) and high porosity and permeability (**Table 5.7**). The Castlegate sandstone also has higher quartz-cement content. In **Fig. 6.14** the average compositions of the braided bar samples in the Castlegate Mb. are compared with the braided bar samples from the Blackhawk Fm. The Castlegate Mb. is generally more porous and quartz-cemented than the Blackhawk Fm., which has higher total carbonate content.

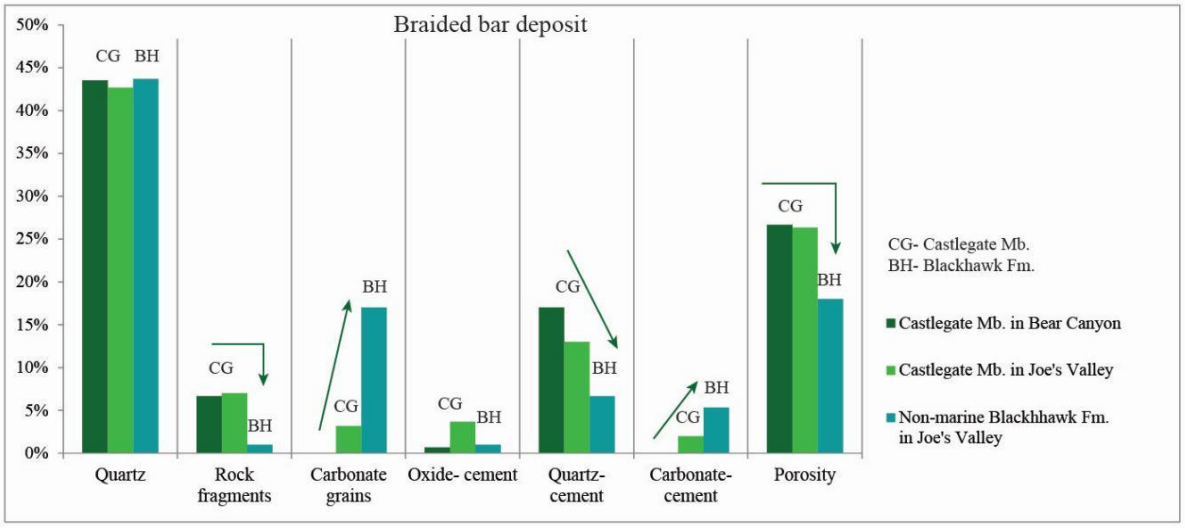


**Fig. 6.14:** Histogram from the braided bar deposits. The histogram shows average composition from each location where braided bar were sampled. Minerals with maximum amount less than 5% is not presented in this histogram. The average content for the Castlegate samples are relatively similar for the two locations. There is a prominent difference between the samples from the Castlegate Mb. and the Blackhawk Fm. especially in the total carbonate, quartz-cement and porosity content.

## 6.3 LATERAL VARIATION WITHIN A MEMBER

### 6.3.1 KENILWORTH MB.

The Kenilworth Mb. was sampled in several locations (**Table 6.2**), and the purpose was to see if the mineralogy changed laterally within a single formation.

**Table 6.2:** Locations for sampling within the Kenilworth Mb.

| Location | Number of samples collected | Facies associations |
|---|---|---|
| *Soldier Creek* | 2 | MC & MSF |
| *Sunnyside* | 1 | LSF |
| *Horse Canyon* | 14 | FS,USF,MSF,LSF & OTz |
| *Woodside Canyon* | 2 | LAG & LSF |
| *Gray Canyon* | 1 | OTz |

These samples do not indicate any prominent variation with geographic location. The only weak trend observed is within the rock fragment content (**Fig. 6.15**). In **Fig. 6.15** only the average from MSF and LSF samples are presented, this is because these two facies associations are relatively similar in content.

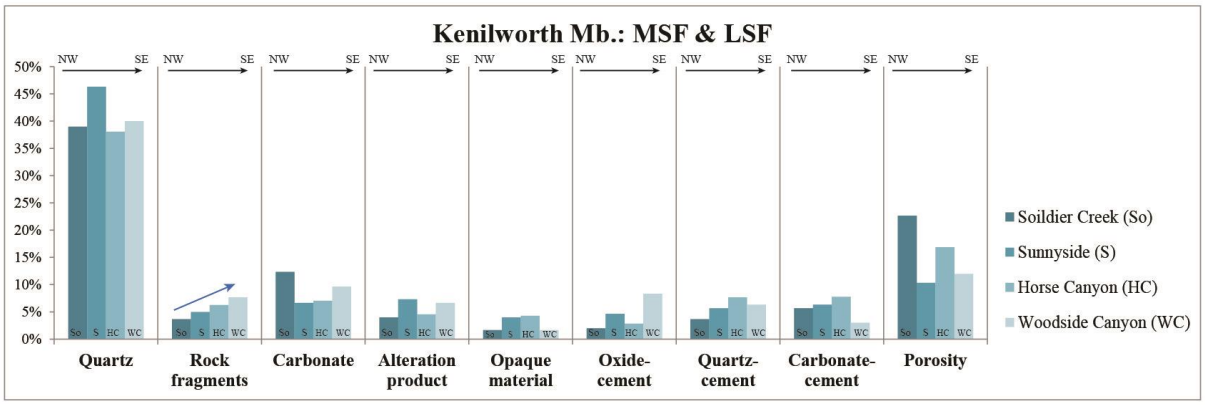


**Fig. 6.15:** Histogram showing the average content of the MSF and LSF samples collected at the different locations within the Book Cliffs. The only trend observed is an increase in rock fragments in the SE-direction.

# 7 DISCUSSION

The purpose of this thesis is to investigate how the petrographic content and petrophysical properties (permeability and porosity) vary with, and hence are dependent on depositional environment (**Fig. 7.1**) and stratigraphic position (**Fig. 7.2**). The results suggest that there are systematic differences by facies association and by unit, these are discussed further below. However, no lateral trends within single units were found within the studied parts of the succession suggesting that the long-shore drift was the dominant sediment transport mechanism and was very efficient at moving sediment over great distances. In this chapter, the mechanisms and processes responsible for the observed variations will be discussed. Hypotheses which explain the observed provenance changes will also be proposed and discussed.

## 7.1 TRENDS CONTROLLED BY FACIES ASSOCIATIONS

Most of the compositional classes indicate some facies dependent trends (**Fig. 6.2** and **Fig. 7.1**). The most prominent trends are: (1) the total carbonate content increases palaeoseaward, and is also high within the meandering river deposits (**Fig. 6.5** and **Fig. 7.1**). (2) The proportion of quartz-cement and petrophysical properties decrease palaeoseaward, and are highest within the braided river deposits (**Fig. 6.4** and **Fig. 7.1**). These trends are described further in the following sections.

### 7.1.1 PETROGRAPHIC AND PETROPHYSICAL TRENDS

#### CARBONATE CONTENT

The total carbonate content in the foreshore deposits is very low (**Fig. 5.14**), while both palaeolandward meandering channel fill deposits and the palaeoseaward deposits contain considerably more carbonates (**Fig. 6.5**). It is therefore likely to assume that processes acting in the foreshore zone result in a lower amount of carbonate grains and cement. Taylor et al. (2004) suggest that organic acids produced from the overlying coal seams initiated early diagenetic leaching/dissolving of detrital carbonate grains in the foreshore. This resulted in removal of reddish iron carbonate-cement present elsewhere in the deposits, which forms the prominent white-caps often found below coal beds. Meteoric fluids will later remobilize the dissolved carbonate seawards, and initiated precipitation in more distal facies associations.

Another explanation for the low carbonate proportion within the foreshore could be due to grain crushing, dissolution and redistribution of carbonates by waves during high energy conditions.

Within the wave-dominated environment the offshore transition zone sandstones are found to contain the highest proportion of carbonate-cement (**Fig. 6.5**). The same trend was observed by Machent et al. (2007). They suggested that the calcite-cement in the offshore transition zone is derived from oxidation of organic matter, sulphate reduction and from marine waters.

The cluster analysis preformed in this study shows a high correlation between the detrital carbonate grains and the carbonate-cement (**Fig. 6.1**). Taylor et al. (2004) described a similar connection and proposed that the detrital carbonate grains in the shoreface sandstones formed nucleation sites for the precipitation of carbonate-cement which was leached from higher up the profile. The results from Taylor et al. (2004) and Machent et al. (2007) agree with the results in this study, which show: (1) a clear connection between carbonate grains and cement, (2) very low total carbonate content in the foreshore deposits and an increase palaeoseaward, and (3) the highest carbonate-cement content in the finer grained offshore transition zone deposits.

High carbonate content in the meandering fluvial deposits is postulated to have a somewhat different origin. Siderite is commonly precipitated in organic rich environments as early nodules which in extreme cases will coalesce (e.g sample #54 from meandering channel fill deposits which is almost completely siderite-cemented). This relationship is also found by Rossi et al. (2001), who found the siderite-cement to be most abundant in facies with a high content of organic material. In these facies microbial organic degradation and iron reduction lead to supersaturated, reducing and non-sulphitic pore water, resulting in suboxic conditions and siderite precipitation (Curtis and Coleman, 1986; Rossi et al., 2001; El-ghali et al., 2006). These conditions are common in the meandering channel deposits of the lower coastal plain which is rich in organic material (peat) and also typically anoxoic just below the surface.

#### QUARTZ-CEMENT CONTENT

Concave-convex grain contacts are commonly observed within the quartz-cemented sandstones in this study. These contacts are formed due to pressure solution (chemical

compaction) between the grains (Boggs, 2011). McBride (1989) proposes three likely sources for quartz cementation in un-metamorphosed sandstones: (1) pressure solution at the contact of detrital quartz grains, (2) alteration of detrital feldspar and (3) possible carbonate replacement of silicate minerals at quartz-grain margins. In this study the alteration products show similar trend by facies associations as the quartz-cement (**Fig. 6.2 A**), which could indicate the alteration of feldspar grains together with pressure solution contacts as possible sources for the quartz-cement.

### QUARTZ-CEMENT VERSUS CARBONATE-CEMENT

Within the coastal plain and wave-dominated environments the quartz-cement shows an inverse relationship with carbonate- and oxide cements (**Fig. 7.1**). The cluster analysis also shows negative correlations between the quartz-cement and the carbonate/oxide-cement content (**Fig. 6.1**). An explanation for this negative correlation could be that quartz-cement forms at deeper burial depths than the two other types of cement. The presence of earlier diagenetic cement (e.g. carbonate- and oxide-cement) prevents the formation of quartz-cement (Heald and Larese, 1974). The Spearman's correlation coefficients for the quartz-cement show a much stronger negative correlation with the carbonate-cement than with the oxide-cement. It is likely that the carbonate-cement (calcite, dolomite and siderite) content has the strongest effect on preventing quartz cementation. Heald and Larese (1974) describe the effect of carbonate and hematite coating on quartz cementation. They state that both carbonate and hematite coating may prevent quartz-cementation, but emphasize that the hematite coating is relatively ineffective. Rossi et al. (2001) studied facies-related diagenesis and siderite cementation in sandstones; their results show that the siderite-cement precipitates before quartz-cement during diagenesis, which will restrict the quartz cementation.

Several studies have investigated quartz cementation during burial (e.g. Oelkers et al., 1996; Walderhaug, 1996; Bjørkum and Nadeau, 1998; Bjørkum et al., 2001). These articles state that quartz cementation starts around 90 °C and ~2.5 km burial depth, and becomes very high around 120 °C and ~3.5 km burial depth. Calcite cementation is more important during shallow burial. Calcite-cement can be precipitated from meteoric water near the surface at temperature between 15- 40 °C, or from supersaturated pore water around 50-70 °C at approximately 1.5 km depth (Saigal and Bjørlykke, 1987). These studies indicate that carbonate cementation occurs before quartz cementation during sandstone diagenesis.

## POROSITY AND PERMEABILITY

Both the porosity and permeability show the same facies association dependent trends as quartz-cement, and also an inverse trend with the carbonate content (**Fig. 6.2** and **Table 5.7**). This decrease in porosity and permeability in the palaeoseaward direction (**Fig. 7.1**) is controlled by a combination of the decrease in grain size and increase in carbonate cement.

The least porous and permeable sample in this study is also the sample with the highest amount of carbonate-cement and no quartz-cement. This sample (#54) was collected from the non-marine part of the Blackhawk Fm. The carbonate-cement is most likely siderite cement due to the relatively high optical relief observed in the thin section. The siderite-cement formation has most likely prevented quartz cementation during burial. Rossi et al. (2001) interpreted the siderite-cement in comparable deposits in the Middle Jurassic Khatatba Formation. They found the siderite-cement to have been formed through multiphase precipitation with three main phases: precipitation near the sediment surface, during shallow burial and during deeper burial. These three phases were separated by dissolution events. The siderite-cement prevented quartz cementation, and created secondary porosity later when it was dissolved. Their study showed fluvial channel fill to be more porous and permeable than crevasse-splay deposits. This is also observed within this study with the exception of sample #54. For this sample the siderite-cement had most likely not been dissolved and no secondary porosity has been created.

Quartz-cement is often described in the literature (Oelkers et al., 1996; Walderhaug, 1996; Bjørkum and Nadeau, 1998; Bjørkum et al., 2001; Bjørlykke and Jahren, 2010) as a controlling factor on porosity. The porosity generally decreases as the amount of quartz-cement increases. The quartz-cement content is proportional with chemical compaction and increases with depth and temperature. As mentioned above, quartz cementation starts at 90 °C (~2.5 km depth) and increases rapidly from 120°C (~3.5 km depth), assuming a typical geothermal gradient of ~35°/km. At temperatures between 180-200 °C (~5.5 km depth) most of the porosity has been replaced by quartz-cement (Oelkers et al., 1996; Walderhaug, 1996; Bjørkum and Nadeau, 1998; Bjørkum et al., 2001; Bjørlykke, 2010; Bjørlykke and Jahren, 2010).

In this study however, the carbonate-cement appears to be the controlling factor for porosity and permeability. Samples with high porosity have a high proportion of quartz-cement and a low proportion of carbonate-cement. This can be explained by the relatively shallow burial depth of the Cretaceous sediments in Utah. Nuccio and Condon (1996) and Nuccio and Roberts (2003) created burial and thermal history curves for the area, showing that the sedimentary rocks around Green River (SE in this study area) were buried at approximately 2.5 km and achieved a maximum temperature of ~105 °C. These curves also show low variations in burial close to the study area. This depth is too shallow for quartz-cement to significantly influence the petrophysical properties.Therefore any intervals with good reservoir qualities (high porosity and permeability) must be associated with a low content of carbonate-cement. With deeper burial the quartz-cement would probably have shown a stronger negative influence on these intervals.

### 7.1.2 TRENDS WITHIN DEPOSITIONAL ENVIRONMENTS

#### COASTAL PLAIN ENVIRONMENT

The three different facies associations in this environment (braided bar, meandering channel fill and crevasse-splay) show clear facies association dependent trends within the total carbonate and quartz-cement content and within the petrophysical properties. The braided bar facies association shows a higher content of quartz-cement, porosity and permeability than the more carbonate cemented meandering channel fill and crevasse-splay deposits (**Fig. 6.4** and **Fig. 7.1**). Rossi et al. (2001) explained the earliest precipitation of siderite-cement to happen in suboxic tropical coastal swamp areas. Since coastal swamp areas are low-lying areas associated with meandering channels and low-gradient floodplain environments it is likely to assume that this first phase of siderite cementation would not occur in the braided bar deposits, thus permitting quartz cementation during burial.

Another explanation for the lower content of carbonate-cement and higher content of quartz-cement in the braided bar deposits could be that they predominantly represent younger sediments from the Castlegate Mb., which has a different primary mineralogical composition. The meandering channel deposits are from the Ferron Mb. and the non-marine Blackhawk Fm. This is further discussed in section 7.2.3.

### WAVE-DOMINATED SHALLOW MARINE ENVIRONMENT

Within the wave-dominated environment, several trends are observed. These trends are indicating increase or decrease of some of the classes in the palaeoseaward direction (**Fig. 6.2**). Some of the major compositional trends are discussed in section 7.1.1. The grain size shows a palaeoseaward decrease through the facies associations. Smaller grains require less energy to be transported by currents (e.g. Hjulström, 1935), and smaller grains are therefore transported further seaward than large grains. During microscope description carbonate grains were generally observed to have a smaller grain size compared to e.g. quartz grains, while rock fragments had a relatively large grain size. As the result in **Fig. 6.5** and **Fig. 6.7** show, the proportion of carbonate grains increases in the seaward direction, while the rock fragment content decreases. The porosity and permeability also decreases in the palaeoseaward direction (**Table 5.7**, **Fig. 6.2** and **Fig. 7.1**). This decrease is probably caused by a reduction in pore-space due to a decrease in grain size and increase in carbonate-cement.

### RIVER-DOMINATED SHALLOW MARINE ENVIRONMENT

Within the Ferron Mb. some trends can be found between the wave-dominated and the river dominated depositional environment. Firstly the river-dominated deposits have a poorer grain sorting, containing more angular grains and generally having a smaller grain size than the wave-dominated deposits (**Fig. 5.2**). The river-dominated deposits have a higher content of carbonate grains and cement, opaque material and oxide-cement, and also a lower content of quartz grains and a lower porosity (**Fig. 6.8**). The trends between the river- and wave-dominated deposits could be a product of the difference in shoreline energy. In the wave-dominated environment strong longshore currents and high energy waves rework the sediments. The high energy waves cause crushing and dissolution of carbonate and organic fragments, in addition to grain sorting and winnowing of the fine grained material.

The rock fragment content is generally higher for the river-dominated deposits than for the wave-dominated deposits (**Fig. 6.7**). This is most likely due to properties of the studied stratigraphic unit rather than change in depositional environment, since most of the river-dominated samples (8/10) were collected from the Panther Tongue Mb. This trend is examined further in section 7.2.2. The rock fragment content also shows a decrease towards more palaeoseaward facies associations within the Panther Tongue Mb. This facies

association dependent trend could be a result of distally decreasing grain size. Since the rock fragments in this study generally show a larger grain size than the other grains the content are decreasing by downsystem decrease in flow energy.

### SHELF TURBIDITES

The subaqueous channel fill and lobes of shelf turbidites show some facies association dependent trends; they are generally less porous and have a higher proportion of opaque material and oxide-cement than any of the other deposits (**Fig. 6.6** and **Fig. 7.1**).

The SEM results indicate that the opaque materials predominantly consist of organic fragments. These organic fragments have most likely been deposited as organic debris transported seawards by hyperpycnal currents during frequent river flood events.

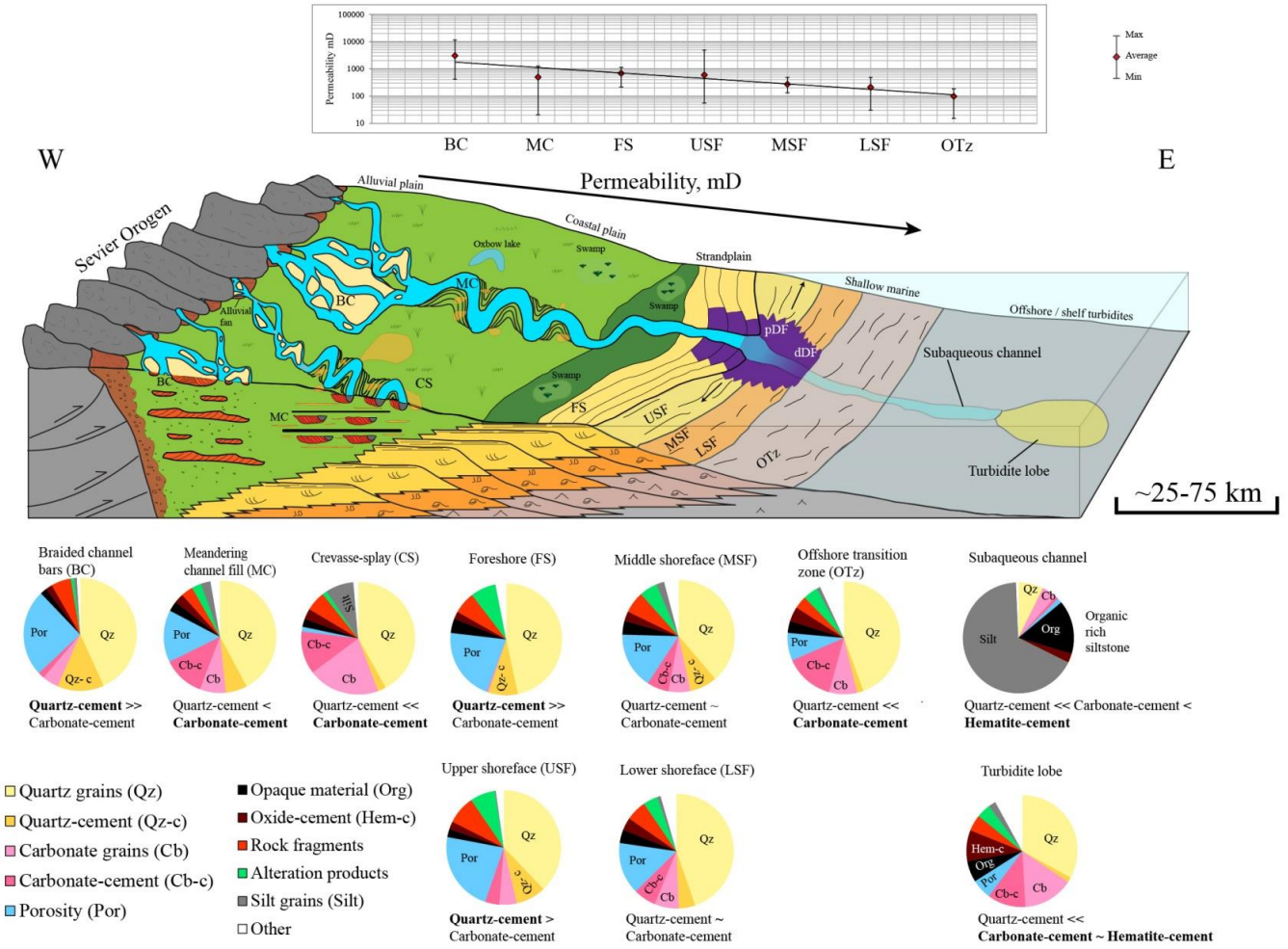


**Fig. 7.1:** Generalized sketch showing how the petrographic content and the petrophysical properties vary with the different facies association. The circle-plots show the average content within the different facies association. Vertical scale is exaggerated and not to scale. The purple area represents the wave-dominated delta-front.

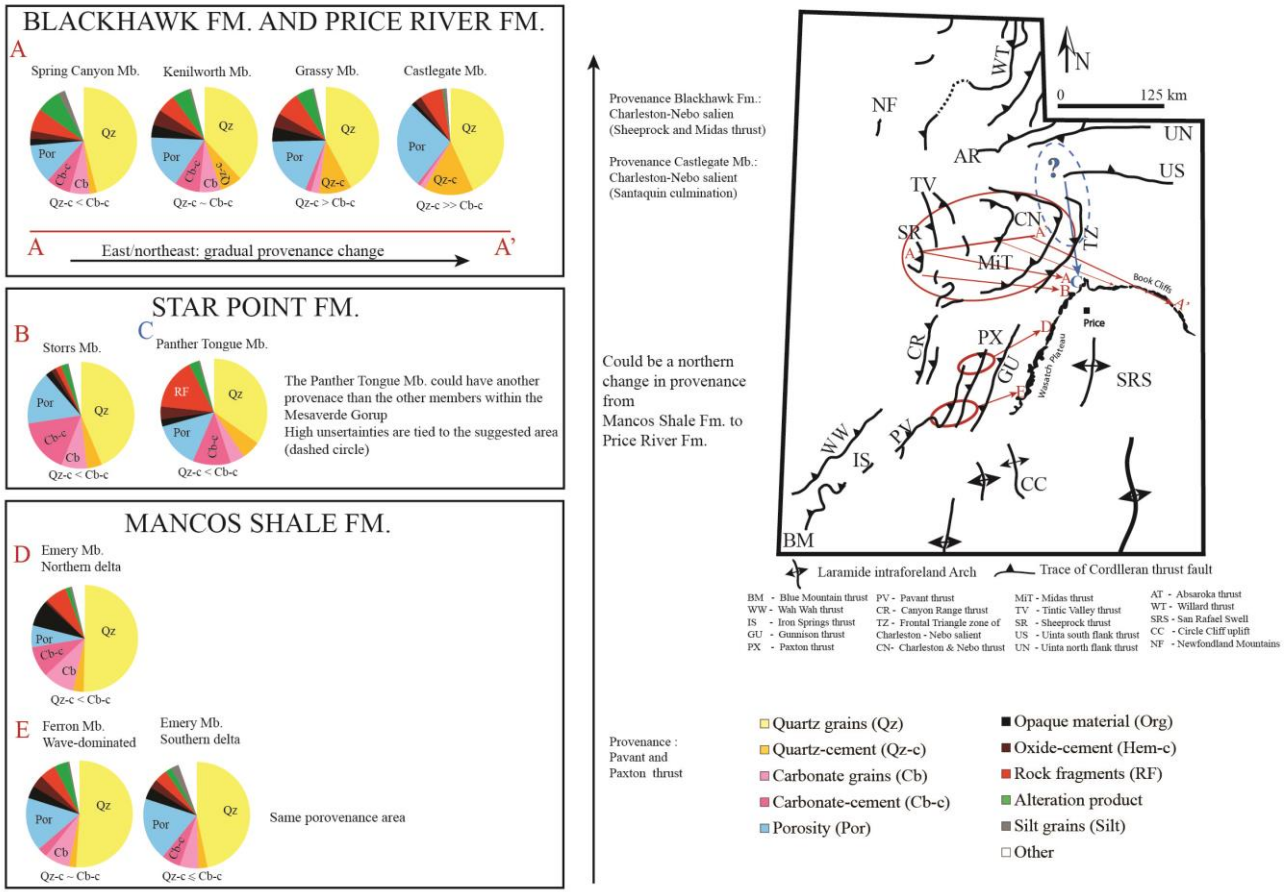


**Fig. 7.2:** The provenance could have changed from the Pavant and Paxton thrust sheets during deposition of the Ferron and Emery members to the Charleston-Nebo salient during deposition of the Star Point, Blackhawk and Price River formations. The circle diagrams represent the average composition within each stratigraphic unit. The arrows represent the approximate sediment transport direction from provenance area to deposition. During the deposition of the Panther Tongue Mb. the sediment transport changed from W-E to N-S (blue arrow). At this time the W-E trending rivers did not reach the shoreline due to partial infilling of newly created small topographic basins, while the N-S trending rivers supplied the shoreline with great amount of sediments causing the progradation of a river-dominated wax lake delta. At the end of the Panther Tongue Mb. progradation the N-S sediment supply declined and the W-E trending river had then filled the small topographic basins and reached the shoreline once again.

## 7.2 TRENDS CONTROLLED BY STRATIGRAPHIC UNITS

### 7.2.1 MANCOS SHALE FM.

In the Emery Mb. the total carbonate, quartz and opaque material content is higher in the northern delta lobe (**Fig. 6.8**). These trends are probably a result of smaller grain size within the northern delta deposits, which could also explain why the southern delta deposits show higher porosity. Finer grain sizes pack tighter together and form smaller pores, thus decreasing the primary porosity and permeability during early burial (mechanical compaction) (Boggs, 2011). The decrease in grain size is most likely a function of the hydrodynamic energy and not of the provenance. The waves will sort the sediments and the samples from the northern lobe are simply more distal than the samples from the southern lobe.

Palaeogeographic reconstructions from Edwards et al. (2005) show the northern delta being sourced from rivers eroding the northern part of the Pavant and Paxton thrusts, while the southern delta is fed by a drainage system located further south (draining the southern part of the Pavant and Paxton thrusts) (**Fig. 2.8** and **Fig. 7.2**). These reconstructions also show the same drainage area and system for the Last Chance Delta of the Ferron Mb. and the southern delta of the Emery Mb. The wave-dominated part of the Ferron Mb., the Last Chance Delta, is relative similar in composition to the southern lobe of the Emery Mb. (**Fig. 6.8** and **Fig. 7.2**). Literature on the Pavant and Paxton thrust sheets do not indicate any difference in lithology or grain size between the northern and southern part (e.g DeCelles et al., 1995; DeCelles, 2004; DeCelles and Coogan, 2006).

### 7.2.2 STAR POINT FM.: PANTHER TONGUE MB.

The Panther Tongue Mb. shows one of the clearest stratigraphic trends in this study. This member is distinguishable from all the other members in the study due to lower quartz- and higher rock fragment (chert) content, see section 6.2.2 (**Fig. 6.9** and **Fig. 6.10**). In addition to the sharp trend in mineralogy this member deviates from the other studied units with respect to shoreline style and sediment transport direction. The change between wave- dominated (Emery Mb. and Storrs Mb.) and river-dominated (Panther Tongue Mb.) shorelines is most likely not due to a change in the wave influence, but probably a result of a change in sediment supply and progradation rate into the basin. River-dominated deltas consist of multiple terminal distributary channels causing a more rapid progradation into the basin (Olariu and

Bhattacharya, 2006). The rate of sediment supply exceeds the rate of wave redistribution, thus giving the Panther Tongue Mb. a river-dominated shoreline.

Palaeogeographic reconstructions and palaeocurrent measurements (Newman and Chan, 1991; Edwards et al., 2005; Olariu et al., 2010; Hampson et al., 2011) show a change in transport direction from eastward to southward during the deposition of the Panther Tongue Mb (**Fig. 7.2**).

The results from this study cannot explain why the sediment supply increased and the change in sediment transport direction occurred, but do indicate a clear change in provenance causing more chert fragments to be transported to the study area and deposited. Some speculative hypotheses attempting to explain the increase in sediment supply could be: (1) a sudden increase in topography of the source area which caused extensive erosion and sediment supply. (2) Unconsolidated sediments dammed in smaller topographic basins (such as piggyback basins) were suddenly released by sudden change in sediment routing, possibly created by thrust movement. These are just hypotheses, and there are numerous potential reasons for the increase in sediment supply.

Olariu et al. (2010) summarised three different hypotheses trying to explain the change in sediment transport direction; (1) change in transport direction as a result of the partial infilling of newly created small topographic basins due to rapid and episodic uplift in the orogeny (Balsley (1980) cited in Olariu et al. (2010)), (2) damping of waves influence on the shoreline by a short-lived eastward-lying structural high. (3) The shoreline was protected by a spit which was later eroded. A more extensive description of these hypotheses is presented in chapter 2.

Only the first of these hypotheses could explain the mineralogical difference. In this hypothesis the N-S trending rivers depositing the Panther Tongue Mb. could have eroded a different area than the W-E trending Storrs rivers which were infilling newly created small topographic basins (**Fig. 7.2**). The Panther Tongue rivers transported a higher proportion of chert fragments to the shoreline, but this hypothesis do not clarify the increase in sediment supply. The two latter theories seems less likely since neither of these hypotheses can explain the difference in mineralogy nor the increase in sediment supply. So basically none of these three hypotheses can explain the increase in sediment supply alone. However, the increase

could be explained if the sediment release within the northern source area was caused by the same tectonic events which created the small topographic basins in the hypothesis by Balsley (1980).

### 7.2.3 BLACKHAWK FM. AND CASTLEGATE MB.

Within the Blackhawk Fm. the detrital mineral grains show few stratigraphic variations (**Fig. 6.11** and **Fig. 6.12**). However, the total carbonate and quartz-cement content in addition to porosity and permeability show some clear trends between the stratigraphic units (**Table 5.7** and **Fig. 6.13**). The total carbonate content decrease upwards in the stratigraphy, while the quartz-cement, porosity and permeability increase.

The same trends are observed between the Castlegate Mb. and the non-marine Blackhawk Fm. (**Fig. 5.18** and **Fig. 6.14**). The Castlegate Mb. has the lowest carbonate content and the highest porosity and permeability of all the studied members.

The provenance area of the Blackhawk Fm. is interpreted to be the Charleston-Nebo salient and predominantly the western Midas and Sheeprock thrust sheets (**Fig. 7.2**). This provenance consists of Precambrian–Cambrian quartzites, Palaeozoic-Mesozoic carbonates and Palaeozoic cherts, quartzites and sandstones (e.g. Mitra, 1997; Constenius et al., 2003; Horton et al., 2004). The provenance for the Castlegate Fm. is interpreted to be the Pennsylvanian and Permian quartzites and sandstones of the Oquirrh Group located in the roof sheet of the Santaquin culmination within the Charleston- Nebo salient (Horton et al., 2004). Horton et al. (2004) propose an abrupt tectonically driven shift in provenance between the Blackhawk and Price River formations.

In the stratigraphic column of central Utah created by Hintze et al. (2000) the most carbonate rich stratigraphic succession spans the interval from Cambrian to Mississippian age, while the Proterozoic, Pennsylvanian, Permian and Mesozoic succession comprise predominantly clastic rocks with only minor carbonate units (**Fig. 7.3**). It is likely that the most carbonate rich succession have supplied sediments to the more carbonate rich, older members within the Blackhawk Fm., but further examination is required in order to pin-point the source of the Late Cretaceous sedimentary rocks to specific stratigraphic successions within the provenance area.

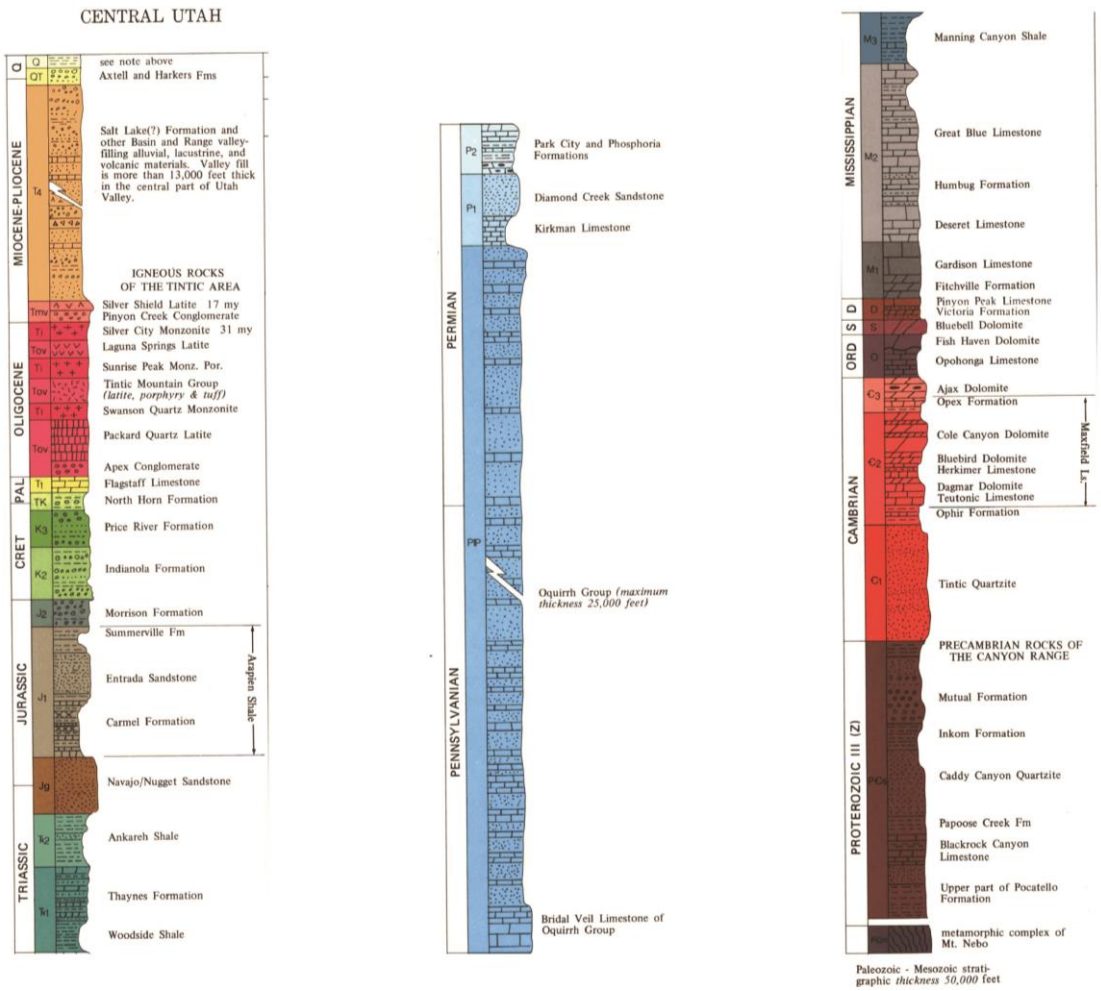


**Fig. 7.3:** Stratigraphic column of central Utah by Hintze et al. (2000). The Oquirrh Group, which is interpreted to be the source of the Castlegate Mb. (Horton et al., 2004), is represented by the darkest shade of blue in the middle column. The most carbonate rich part of the stratigraphy is of Upper Cambrian to Mississippian age, and it is likely that some of this succession has been exposed in the provenance area during the deposition of the more carbonate rich members in the lower part of the Mesaverde group (e.g. Storrs Mb. and Spring Canyon Mb.).

The following, speculative hypotheses may explain the gradual change in total carbonate and quartz-cement content through the Mesaverde Group: (1) a gradual change in provenance area from the Sheeprock and Midas thrust sheets towards the Santaquin culmination within the Charleston-Nebo salient (**Fig. 7.2**). The provenance lithology changed gradually from older Proterozoic (Sheeprock thust sheet) and Palaeozoic (Midas thrust sheet) rock to younger Pennsylvanian and Permian rocks (Santaquin culmination). The gradual change in petrography within the Mesaverde group is caused by this gradual change in exposed lithology as the provenance area moves eastwards. (2) Progressive erosion within the provenance area causing depletion of carbonate rich rocks. This hypothesis indicates a higher proportion of exposed carbonate rocks during the deposition of the oldest members. As the

carbonate rocks are progressively eroded, a larger proportion of the underlying clastic rocks are exposed. In this case, older carbonate rich rocks (Cambrian-Mississippian) have most likely been thrusted on top of the younger Oquirrh Group (Pennsylvanian-Permian). This resulted in erosion of the older rocks prior to the younger, which is opposite of a typical unroofing trend. (3) A combination of the first two hypotheses could also be possible. In the Blackhawk Fm. a progressive erosion within the provenance could have happened, while the change between the Blackhawk Fm. and Price River Fm. could indicate a shift in provenance from the western part of the Charleston-Nebo salient (Sheeprock and Midas thrust sheets) to the Oquirrh Group within the Santaquin culmination.

These three hypotheses are equally possible based on the available data. More knowledge on the petrology and chemistry of the provenance is required in order to better understand this gradual change in petrology.

## 7.3 LATERAL CHANGE WITHIN THE KENILWORTH MB.

The study of the lateral variation within the fourth parasequence in the Kenilworth Mb. (K4) shows that the composition is relatively similar within the same facies associations and members. There are some variations in composition between the different samples, but they are not significant and do not show any clear decrease or increase laterally. The only exception is the rock fragment content which shows a slightly increase in the SE direction (**Fig. 6.15**). These observations could indicate that the source area has been relatively stable through deposition of the Kenilworth Mb., and that the efficient long-shore drift was the dominant sediment transport mechanism in the shallow marine deposits. The variations in composition within one member are thus mainly controlled by facies associations, and not lateral position in the basin.

North et al. (2005) preformed a study on the geochemical correlation in deltaic succession of the Kenilworth Mb. where they looked at trace element abundance. They found the general chemistry to be consistent within the Kenilworth Mb. For their geochemical correlation they assumed a lateral consistency within the member, which is supported in the current study. They did however, noticed a decrease in the Zr/Y ratio in the basinward (SE) direction, which they suggested could be connected to the grain size distribution within the member,

since the parasequence (K3) showing the strongest trend had the largest lateral variation in grain size.

## 7.4 SUMMARY

The following summary presents the main facies association (**Fig. 7.1**) and stratigraphic trends (**Fig. 7.2**) found in this study. In addition, speculative hypotheses will be proposed regarding the provenance.

### 7.4.1 FACIES ASSOCIATION CONTROLS

Several compositional classes show clear facies association controlled trends; the clearest trends are within the total carbonate-, quartz-cement- and petrophysical content (**Fig. 7.1**).

The total carbonate content is most likely controlled by the energy and compositional conditions present within the depositional environment. In high energy zones such as the foreshore and braided river environments, carbonates are often lacking from the deposits. In the foreshore zone waves can crush and dissolve the existing carbonates. There is also more chance of anoxic conditions in low energy settings, which favours siderite (iron-carbonate) formation. Another important factor for the low carbonate content in the foreshore deposits is the presence of overlying coal layers. This caused leaching of carbonated from the foreshore and sometimes also the upper shoreface by organic acids during early diagenesis and a remobilisation further down in the shoreface environment (Taylor et al., 2004). Within the wave-dominated environment, the offshore transition zone deposits are relatively rich in carbonate-cement (**Fig. 7.1**). This carbonate-cement is derived from oxidation of organic matter, sulphate reduction and from marine waters (Machent et al., 2007).

Another facies dependent trend observed in this study is in the organic material and iron-oxide cement content, which is highest for the shelf turbidites (Prairie Canyon) (**Fig. 7.1**). The high proportion of organic material is most likely a result of organic debris transported seawards during river flood events.

The quartz-cement, porosity and permeability show facies and stratigraphic dependent trends which are reverse of the carbonate trends (**Fig. 7.1**). The cluster analysis correspondingly shows a strong negative correlation between the carbonate-cement and the quartz-

cement/porosity. These trends could be an effect of carbonate cementation during early diagenesis preventing quartz cementation and filling of the pores (Heald and Larese, 1974; Rossi et al., 2001). The increase in carbonate-cement results in a decrease in primary porosity and permeability. In several previous studies (e.g. Oelkers et al., 1996; Bjørkum and Nadeau, 1998; Bjørkum et al., 2001; Bjørlykke and Jahren, 2010) quartz-cement is described as the most negative factor for porosity and permeability. This is not applicable in the studied deposits since quartz cementation first start to increase rapidly when the rock is buried at ~3.5 km and has reached a temperature of ~120 °C (e.g. Bjørkum and Nadeau, 1998). The sedimentary rocks in this study have not been buried deeper than ~2.5 km and have reached higher temperatures than ~105 °C (Nuccio and Condon, 1996; Nuccio and Roberts, 2003).

### 7.4.2 STRATIGRAPHIC CONTROLS

During the deposition of the Late Cretaceous sediments in Utah the material was derived from the Sevier Orogen and deposited in the Western Interior Seaway (Stokes, 1986). It is likely that the provenance area may have changed within the Sevier Orogen and that different thrust sheets were the source for different members of the Late Cretaceous stratigraphy (**Fig. 7.2**).

#### MANCOS SHALE FM.

Based upon the palaeogeographic reconstructions by Edwards et al. (2005), the provenance area of the sandstone members of the Mancos Shale Fm. can be located within the Pavant and Paxton thrust sheets (**Fig. 7.2**). These palaeogeographic maps indicate provenance in the southern part of these thrust sheets for the Ferron Mb. and the southern Emery delta lobe, and provenance in the northern part for the northern Emery delta lobe. The stability in provenance between the Ferron Mb. and Emery Mb. is supported by relatively similar petrographic content for the two members. The deposits in the northern Emery lobe are finer grained, less porous and have a slightly larger total carbonate content than the southern Emery lobe. The latter is probably not caused by changes in lithology or grain size within the Pavant or Paxton thrust sheets, but because the samples from the northern outcrops were collected from a more distal part of the lower shoreface deposits than the southern samples.

### PANTHER TONGUE MB.

The overlying Panther Tongue Mb. is best exposed in outcrops northeast of the Pavant and Paxton thrust sheets. Furthermore, palaeocurrent measurements indicate that the Panther Tongue Mb. had a southward sediment transport contrary to the eastwards transport in the over- and underlying members (Edwards et al., 2005; Olariu et al., 2010; Hampson et al., 2011). This could indicate that the provenance of the Panther Tongue was located north/northeast of the provenance areas of the other members (**Fig. 7.2**). In addition the Panther Tongue Mb. is distinct from the surrounding stratigraphic units by consisting of river-dominated shallow marine deposits rather than wave-dominated, and by containing a significantly higher proportion rock fragments (chert fragments). The change in shoreline style was most likely due to the sediments being supplied faster than the waves were able to rework them.

Balsley (1980) cited in Olariu et al. (2010) had a hypothesis of the switch in transport direction being a result of the partial infilling of newly created small topographic basins due to rapid and episodic uplift in the orogeny. The rivers transporting sediments from the west towards the east had to infill these small topographic basins before reaching the seaway, thus slowing down the eastward progradation and causing southward progradation to dominate the shoreline. This hypothesis by Balsley (1980) could explain the progradation of the Panther Tongue Mb. if the episodic uplift of the orogeny caused release of accumulated sediments in the north simultaneously as creating the small topographic basins in the west. The large proportion of sediments released was then transported towards the south, causing rapid progradation into the basin and building of a river dominated delta, similar to the modern day Wax Lake Delta (Wellner et al., 2005). More studies are needed on the subject in order to confirm or dismiss this speculative hypothesis.

### BLACKHAWK FM. AND CASTLEGATE MB.

The provenance of the Late Cretaceous rocks has often been interpreted to be from the south-central part of the Sevier Orogeny in Utah, consisting of the Canyon Range, Pavant, Paxton and Gunnison thrust sheets (e.g. DeCelles et al., 1995; Willis, 1999; DeCelles, 2004; DeCelles and Coogan, 2006). However, other studies suggest that the Mesaverde group (Star Point Fm., Blackhawk Fm. and Castelgate Mb.) were sourced from the more proximal Charleston-Nebo

salient in the north-central Sevier thrusts systems, including the Sheeprock, Midas thrusts (e.g. Mitra, 1997; Constenius et al., 2003; Horton et al., 2004). One possibility is that the provenance moved from the south-central part of Utah during the deposition of the Ferron and Emery members to the north-central part of Utah during deposition of the Star Point, Blackhawk and Price River formations.

Horton et al. (2004) imply an abrupt change in provenance between the Blackhawk Fm. and Castlegate Mb. within the Charleston Nebo-salient. However, the results from this study indicate that this change could have occurred gradually, since there is a gradual change in total carbonate- and quartz-cement content upwards within the shallow marine members of the Mesaverde Group. Several speculative hypotheses can be proposed to explain this gradual change; (1) a gradual change in provenance area (**Fig. 7.2**). (2) Progressive erosion within the provenance area. (3) A combination of change in provenance area and progressive erosion within one area. These hypotheses are explained further in section 7.2.3.

Based on the available data it is not possible to fully explain the stratigraphic changes observed in this study. Further work is required to confirm or dismiss these hypotheses.

## 7.5 FURTHER WORK

The following section will present some suggestions for further work that might resolve some of the issues raised in this study.

### 7.5.1 STUDIES ON THE COLLECTED SAMPLES

#### LOSS-ON-IGNITION TEST

In order to ascertain if the opaque materials represent organic fragments and to determine the amount of organic material in the samples a detailed SEM analysis or a loss-on-ignition test could be performed. This will also give an indication of the source rock potential to the shelf turbidites.

#### HEAVY MINERAL DATING

The types of observed heavy minerals in this study, and the abundance of them (**Table 4** in **Appendix I**) are consistent with most of the collected samples and predominantly the same as found in the Kenilworth Mb. by North et al. (2005). Detrital thermochronology methods can be used to date the heavy minerals. This is a common method used to provide information on provenance and thermal history.

Detrital zircons are found in nearly all of the facies associations and members, and the ages of these zircons can be determined through uranium-lead (U-Pb) dating. Argon-argon ($^{40}$A-$^{39}$A) can be used to date the white micas, and the apatite minerals can be dated through uranium-thorium/helium (U-Th/He) thermochronology (Boggs, 2011).

A problem with dating these heavy minerals can occur because the provenance area consists of sedimentary rocks, which is indicated both by the degree of rounding observed in the zircons and by literature on the provenance area (e.g. DeCelles et al., 1995; Mitra, 1997; Constenius et al., 2003; DeCelles, 2004; Horton et al., 2004; DeCelles and Coogan, 2006). The zircons have most likely been eroded and deposited several times, so the age of these minerals can vary within one member and will not be the same as the sedimentary rocks of the provenance area.

#### ANALYSIS OF FLUID INCLUSIONS

Fluid inclusion analysis of the thin sections can provide more details on the thermal and burial history of the samples (Boggs, 2011).

### 7.5.2 FURTHER FIELD STUDY

#### IN THE STUDY AREA

More samples can be collected within the braided river deposits of the Blackhawk Fm. and in the shallow marine deposits of the Castlegate Mb. in order to see if the change in petrography is gradual or abrupt. Samples from the Aberdeen, Sunnyside and Desert members could also be collected and studied to fully investigate this change in petrographic content

#### IN THE PROVENANCE AREA

Detailed studies of the petrography and chemistry within the study area can be used to tie the different members from this study to a specific thrust sheet and stratigraphic successions within the Sevier Orogen, and thus clarify the provenance evolution during the Late Cretaceous times.

# 8 CONCLUSIONS

The purpose of this study was to determine the main controlling factors of the petrographic content and the pertrophysical properties within Turonian to Campanian sandstones, deposited in the Western Interior Seaway in east-central Utah. The mineralogy and porosity were registered using traditional point counting and through scanning electron microscope, while the permeability was measured in the field using a portable permeameter. The results of the in-field measurements and analyses of thin sections produced the following conclusions:

- The results show that facies association is the dominant parameter controlling the petrographic content. The strongest trends are found in the total carbonate and quartz-cement content and also in porosity and permeability. In addition the alteration products, opaque materials and oxide-cement show some facies association dependent trends.
- The total amount of carbonate increases in the palaeoseaward direction within deposits from the wave-dominated environment. The total carbonate content is very low to absent in foreshore deposits, and increases too relatively high (~22%) in the offshore transition zone deposits.
- Carbonate grains and cement are dissolved and remobilised from the proximal foreshore to the distal environments. This removal can occasionally be observed also in the upper shoreface deposits. The dissolution of carbonate grains is most likely due to leaching by organic acids which originates from the overlying coal beds. Another possible explanation can be reworking, crushing and removal of the carbonate grains by waves in the high energy conditions present in the foreshore zone.
- Cluster analysis shows a high positive correlation between the carbonate grains and carbonate-cement, which indicates that the amount of carbonate-cement formed in these samples is related to the amount carbonate grains deposited. This implies that part of the carbonate-cement is sourced from the detrital carbonate grains.
- The quartz-cement content shows inverse trends compared to the carbonate-cement content, and decreases palaeoseawards. The cluster analysis also indicates a strong negative correlation between these compositional classes. The proportion of quartz cement is highly connected to the carbonate-cement content which is probably a result

of carbonate cement forming at shallower burial depths than quartz-cement. The presence of early diagenetic carbonate-cement inhibited formation of quartz-cement.

- The carbonate-cement seems to have the main compositional control on the reservoir quality. This is most likely a consequence of the shallow burial depth (~2.5 km) and the low maximum temperature (~105 °C) of the sandstones. With deeper burial the quartz-cement would probably have shown a greater proportion and thus a stronger negative influence on the reservoir quality in the sandstone samples.
- The clearest stratigraphic control is found in the Panther Tongue Mb. of the Star Point Fm. This member has a greater proportion of rock fragments than the other studied members. The rock fragments consist mainly of microcrystalline quartz, which indicates a chert rich source area. Based on these results it is likely to assume a change in provenance during the deposition of the Panther Tongue Mb.
- The total carbonate content does not only show facies association dependent trends, but also some variation with the different stratigraphic units. The content shows a gradual decrease upwards in the stratigraphy; from the Storrs Mb. of Star Point Fm. to the Castlegate Mb. in the Price River Fm. This could be caused by a gradual change in provenance, either through unroofing within the source area or by a gradual eastward movement of the sediment source.
- The low variation between the wave-dominated Ferron and southern Emery deposits can indicate a relatively stable provenance area during the deposition of these two sandstone members of the Mancos Shale Fm.
- The results from this study do not show any clear compositional variations with respect to the lateral position in the basin. This can indicate an effective reworking of shoreline sediments by wave activity, and a lateral homogeneity of the sediment source area, in general agreement with the regional geology.

# 9 REFERENCES

Adams, M. M., and Bhattacharya, J. P., 2005, No change in fluvial style across a sequence boundary, Cretaceous Blackhawk and Castlegate Formations of central Utah, USA: Journal of Sedimentary Research, v. 75, no. 6, p. 1038-1051.

Allen, J. R. L., 1982, Sedimentary structures, their character and physical basis, Elsevier.

Armstrong, R. L., 1968, Sevier orogenic belt in Nevada and Utah: Geological Society of America Bulletin, v. 79, no. 4, p. 429-458.

Balsley, J., 1980, Cretaceous wave-dominated delta systems: Book Cliffs, east-central Utah: AAPG Continuing Education Course, Field Guide, v. 163.

Bhattacharya, J. P., 2011, Practical problems in the application of the sequence stratigraphic method and key surfaces: integrating observations from ancient fluvial–deltaic wedges with Quaternary and modelling studies: Sedimentology, v. 58, no. 1, p. 120-169.

Bhattacharya, J. P., and Giosan, L., 2003, Wave-influenced deltas: Geomorphological implications for facies reconstruction: Sedimentology, v. 50, no. 1, p. 187-210.

Bhattacharya, J. P., and MacEachern, J. A., 2009, Hyperpycnal rivers and prodeltaic shelves in the Cretaceous seaway of North America: Journal of Sedimentary Research, v. 79, no. 4, p. 184-209.

Bjørkum, P., and Nadeau, P., 1998, Temperature controlled porosity/permeability reduction, fluid migration, and petroleum exploration in sedimentary basins: APPEA Journal, v. 38, no. Part 1, p. 452-464.

Bjørkum, P., Walderhaug, O., and Nadeau, P., 2001, Thermally driven porosity reduction: impact on basin subsidence: Geological Society, London, Special Publications, v. 188, no. 1, p. 385-392.

Bjørlykke, K., 2010, Compaction of sedimentary rocks including shales, sandstones and carbonates, Petroleum Geoscience, Springer, p. 329-337.

Bjørlykke, K., and Jahren, J., 2010, Sandstones and sandstone reservoirs, Petroleum Geoscience, Springer, p. 113-140.

Blakey, R. C., 2011, Palaeogeographic maps, URL: http://jan.ucc.nau.edu/~rcb7/globaltext2.html, [Accessed: 13.04.2015].

Blakey, R. C., and Ranney, W., 2008, Ancient landscapes of the Colorado Plateau, Grand Canyon Assn.

Boggs, S., 2011, Principles of sedimentology and stratigraphy, Prentice Hall New Jersey.

Clifton, H. E., 2006, A reexamination of facies models for clastic shorelines: Special publication-SEPM, v. 84, p. 293.

Cohen, J., Cohen, P., West, S. G., and Aiken, L. S., 2013, Applied multiple regression/correlation analysis for the behavioral sciences, Routledge.

Constenius, K. N., Esser, R. P., and Layer, P. W., Extensional collapse of the Charleston-Nebo salient and its relationship to space-time variations in Cordilleran orogenic belt tectonism and continental stratigraphy2003, Rocky Mountain Section (SEPM).

Cotter, E., 1975, Late Cretaceous sedimentation in a low-energy coastal zone: the Ferron Sandstone of Utah: Journal of Sedimentary Research, v. 45, no. 3.

Cross, T. A., and Pilger Jr., R. H., 1978, Tectonic controls of late Cretaceous sedimentation, western interior, USA: Nature, v. 274.

Curtis, C., and Coleman, M., 1986, Controls on the precipitation of early diagenetic calcite, dolomite and siderite concretions in complex depositional sequences: Special publication-SEMP.

Davies, R., Diessel, C., Howell, J., Flint, S., and Boyd, R., 2005, Vertical and lateral variation in the petrography of the Upper Cretaceous Sunnyside coal of eastern Utah, USA—implications for the recognition of high-resolution accommodation changes in paralic coal seams: International Journal of Coal Geology, v. 61, no. 1, p. 13-33.

DeCelles, P. G., 2004, Late Jurassic to eocene evolution of the Cordilleran thrust belt and foreland basin system, western USA: American Journal of Science, v. 304, no. 2, p. 105-168.

DeCelles, P. G., and Coogan, J. C., 2006, Regional structure and kinematic history of the Sevier fold-and-thrust belt, central Utah: Geological Society of America Bulletin, v. 118, no. 7-8, p. 841-864.

DeCelles, P. G., Lawton, T. F., and Mitra, G., 1995, Thrust timing, growth of structural culminations, and synorogenic sedimentation in the type Sevier orogenic belt, western United States: Geology, v. 23, no. 8, p. 699-702.

Deveugle, P. E., Jackson, M. D., Hampson, G. J., Farrell, M. E., Sprague, A. R., Stewart, J., and Calvert, C. S., 2011, Characterization of stratigraphic architecture and its impact on fluid flow in a fluvial-dominated deltaic reservoir analog: Upper Cretaceous Ferron Sandstone Member, Utah: AAPG bulletin, v. 95, no. 5, p. 693-727.

Edwards, C. M., Howell, J. A., and Flint, S. S., 2005, Depositional and stratigraphic architecture of the Santonian Emery Sandstone of the Mancos Shale: implications for late Cretaceous evolution of the Western Interior Foreland Basin of central Utah, USA: Journal of Sedimentary Research, v. 75, no. 2, p. 280-299.

Eide, C. H., Howell, J. A., and Buckley, S., 2014, Distribution of discontinuous mudstone beds within wave-dominated shallow-marine deposits: Star Point Sandstone and Blackhawk Formation, Eastern Utah: AAPG Bulletin, v. 98, no. 7, p. 1401-1429.

Eide, C. H., Howell, J. A., and Buckley, S. J., 2015, Sedimentology and reservoir properties of tabular and erosive offshore transition deposits in wave-dominated, shallow-marine strata: Book Cliffs, USA: Petroleum Geoscience, p. 2014-2015.

El-ghali, M., Tajori, K., Mansurbeg, H., Ogle, N., and Kalin, R., 2006, Origin and timing of siderite cementation in Upper Ordovician glaciogenic sandstones from the Murzuq basin, SW Libya: Marine and petroleum geology, v. 23, no. 4, p. 459-471.

Enge, H. D., Howell, J. A., and Buckley, S. J., 2010, The geometry and internal architecture of stream mouth bars in the Panther Tongue and the Ferron Sandstone Members, Utah, USA: Journal of Sedimentary Research, v. 80, no. 11, p. 1018-1031.

Filomena, C., Hornung, J., and Stollhofen, H., 2014, Assessing accuracy of gas-driven permeability measurements: a comparative study of diverse Hassler-cell and probe permeameter devices: Solid Earth, v. 5, no. 1, p. 1-11.

Folk, R. L., 1966, A review of grain-size parameters: Sedimentology, v. 6, no. 2, p. 73-93.

Fossen, H., Schultz, R. A., and Torabi, A., 2011, Conditions and implications for compaction band formation in the Navajo Sandstone, Utah: Journal of Structural Geology, v. 33, no. 10, p. 1477-1490.

Fouch, T., Lawton, T., Nichols, D., Cashion, W., and Cobban, W., Patterns and timing of synorogenic sedimentation in Upper Cretaceous rocks of central and northeast Utah1983, Rocky Mountain Section (SEPM).

Garrison Jr, J. R., and Van den Bergh, T. C. V., 2004, High-resolution depositional sequence stratigraphy of the upper Ferron Sandstone Last Chance Delta: an application of coal-zone stratigraphy: Regional to wellbore analog for fluvial-deltaic reservoir modeling: The Ferron Sandstone of Utah: AAPG Studies in Geology, v. 50, p. 125-192.

Garrison Jr, J. R., and Van den Bergh, T. V. C., 2006, Effects of Sedimentation Rate, Rate of Relative Rise in Sea Level, and Duration of Sea-Level Cycle on the Filling of Incised Valleys: Examples of Filled and overfilled Incised Valleys From the Upper Ferron Sandstone, Last Chance Delta, East-Central Utah: Special publication-SEMP.

Hampson, G. J., 2010, Sediment dispersal and quantitative stratigraphic architecture across an ancient shelf: Sedimentology, v. 57, no. 1, p. 96-141.

Hampson, G. J., Burgess, P. M., and Howell, J. A., 2001, Shoreface tongue geometry constrains history of relative sea-level fall: examples from Late Cretaceous strata in the Book Cliffs area, Utah: Terra Nova, v. 13, no. 3, p. 188-196.

Hampson, G. J., Duller, R. A., Petter, A. L., Robinson, R. A., and Allen, P. A., 2014, Mass-Balance Constraints On Stratigraphic Interpretation of Linked Alluvial–Coastal–Shelfal Deposits From Source To Sink: Example From Cretaceous Western Interior Basin, Utah and Colorado, USA: Journal of Sedimentary Research, v. 84, no. 11, p. 935-960.

Hampson, G. J., Gani, M. R., Sharman, K. E., Irfan, N., and Bracken, B., 2011, Along-strike and down-dip variations in shallow-marine sequence stratigraphic architecture: Upper Cretaceous Star Point Sandstone, Wasatch Plateau, Central Utah, USA: Journal of Sedimentary Research, v. 81, no. 3, p. 159-184.

Hampson, G. J., and Howell, J. A., 2005, Sedimentologic and geomorphic characterization of ancient wave-dominated deltaic shorelines: Upper Cretaceous Blackhawk Formation, Book Cliffs, Utah, USA: Society of Sedimentary Geology (SEPM).

Hampson, G. J., Jewell, T. O., Irfan, N., Gani, M. R., and Bracken, B., 2013, Modest change in fluvial style with varying accommodation in regressive alluvial-to-coastal-plain wedge: Upper

Cretaceous Blackhawk Formation, Wasatch Plateau, central Utah, USA: Journal of Sedimentary Research, v. 83, no. 2, p. 145-169.

Heald, M., and Larese, R., 1974, Influence of coatings on quartz cementation: Journal of Sedimentary Research, v. 44, no. 4.

Hettinger, R. D., and Kirschbaum, M. A., 2002, Stratigraphy of the Upper Cretaceous Mancos Shale (upper part) and Mesaverde Group in the southern part of the Uinta and Piceance basins, Utah and Colorado.

Hintze, L. F., 2005, Utah's spectacular geology: how it came to be, Department of Geology, Brigham Young University.

Hintze, L. F., Willis, G. C., Laes, D. Y., Sprinkel, D. A., and Brown, K. D., 2000, Digital geologic map of Utah, Utah Geological Survey, Utah Department of Natural Resources.

Hjulström, F., 1935, Studies of the morphological activity of rivers as illustrated by the River Fyris: Inaugural Dissertation, Almqvist & Wiksells.

Holgate, N. E., Hampson, G. J., Jackson, C. A., and Petersen, S. A., 2014, Constraining uncertainty in interpretation of seismically imaged clinoforms in deltaic reservoirs, Troll field, Norwegian North Sea: Insights from forward seismic models of outcrop analogs: AAPG Bulletin, no. 20,140,710.

Horton, B. K., Constenius, K. N., and DeCelles, P. G., 2004, Tectonic control on coarse-grained foreland-basin sequences: An example from the Cordilleran foreland basin, Utah: Geology, v. 32, no. 7, p. 637-640.

Howell, J. A., and Flint, S. S., 2003, Part 3 Siliciclastics case study: The Book Cliffs, *in* Coe, A. L., ed., The sedimentary record of sea-level change, Cambridge University Press, p. 135-208.

Hwang, I. G., and Heller, P. L., 2002, Anatomy of a transgressive lag: Panther Tongue Sandstone, Star Point Formation, central Utah: Sedimentology, v. 49, no. 5, p. 977-999.

Joeckel, R. M., Ludvigson, G. A., Witzke, B. J., Kvale, E. P., P.L, P., Brenner, R. L., Thomas, S. G., and Howard, L. M., 2005, Palaeogeography and fluvial to estuarine architecture of the Dakota Formation (Cretaceous, Albian), eastern Nebraska, USA: Fluvial Sedimentology VII, International, Association of Sedimentologists Special Publication, v. 35, p. 453-480.

Kalkreuth, W., and Leckie, D. A., 1989, Sedimentological and petrographical characteristics of Cretaceous strandplain coals: a model for coal accumulation from the North American Western Interior Seaway: International Journal of Coal Geology, v. 12, no. 1, p. 381-424.

Kamola, D. L., and Huntoon, J. E., 1995, Repetitive stratal patterns in a foreland basin sandstone and their possible tectonic significance: Geology, v. 23, no. 2, p. 177-180.

Kamola, D. L., and Van Wagoner, J. C., 1995, Stratigraphy and facies architecture of parasequences with examples from the Spring Canyon Member, Blackhawk Formation, Utah.

Kauffman, E. G., 1984, Paleobiogeography and evolutionary response dynamic in the Cretaceous Western Interior Seaway of North America: Jurassic-Cretaceous Biochronology and

Paleogeography of North America: Geological Association of Canada, Special Paper, v. 27, p. 273-306.

Kellogg, H. E., 1977, Geology and petroleum of the Mancos B formation Douglas Creek Arch area Colorado and Utah: Rocky Mountain Association of Geologists, AAPG.

Klausen, T. G., 2010, Sedimentology and seuence stratigraphy of the late cretaceous lowe Ferron Sandstone: Application of 3-D geocellular modelling to the drunkards wash CBM-field in central Utha, USA: Master Thesis, University of Bergen.

Knudsen, T. A., 2008, Application of 3D, Geocellular modelling to understand the large scale stratigraphic architecture and stacking patterns in the Cretaceous Central Utah, USA: Master Thesis, University of Bergen.

Li, W., Bhattacharya, J. P., Zhu, Y., Garza, D., and Blankenship, E., 2011, Evaluating delta asymmetry using three-dimensional facies architecture and ichnological analysis, Ferron 'Notom Delta', Capital Reef, Utah, USA: Sedimentology, v. 58, no. 2, p. 478-507.

Longiaru, S., 1987, Visual Comparators for Estimating the Degree of Sorting from Plane and Thin Section: Journal of Sedimentary Research, v. 57, no. 4.

Lynds, R., and Hajek, E., 2006, Conceptual model for predicting mudstone dimensions in sandy braided-river reservoirs: AAPG bulletin, v. 90, no. 8, p. 1273-1288.

MacEachern, J. A., 1992, Ichnological aspects of Cretaceous shoreface successions and shoreface variability in the Western Interior Seaway of North America: Core workshop notes, SEMP.

Machent, P. G., Taylor, K. G., Macquaker, J. H. S., and Marshall, J. D., 2007, Patterns of early post-depositional and burial cementation in distal shallow-marine sandstones: Upper Cretaceous Kenilworth Member, Book Cliffs, Utah, USA: Sedimentary Geology, v. 198, no. 1–2, p. 125-145.

Matheny, J., and Picard, M., 1985, Sedimentology and depositional environments of the Emery Sandstone Member of the Mancos Shale: Emery and Sevier Counties, Utah: The Mountain Geologist, v. 22, p. 94-109.

McBride, E. F., 1989, Quartz cement in sandstones: a review: Earth-Science Reviews, v. 26, no. 1, p. 69-112.

McLaurin, B. T., and Steel, R. J., 2007, Architecture and origin of an amalgamated fluvial sheet sand, lower Castlegate Formation, Book Cliffs, Utah: Sedimentary Geology, v. 197, no. 3–4, p. 291-311.

Miall, A. D., 1993, The architecture of fluvial-deltaic sequences in the Upper Mesaverde Group (Upper Cretaceous), Book Cliffs, Utah: Geological Society, London, Special Publications, v. 75, no. 1, p. 305-332.

Miall, A. D., and Arush, M., 2001, The Castlegate Sandstone of the Book Cliffs, Utah: sequence stratigraphy, paleogeography, and tectonic controls: Journal of Sedimentary Research, v. 71, no. 4, p. 537-548.

Mitra, G., 1997, Evolution of salients in a fold-and-thrust belt: the effects of sedimentary basin geometry, strain distribution and critical taper, Evolution of Geological Structures in Micro-to Macro-scales, Springer, p. 59-90.

Morris, W., Posamentier, H., Loomis, K., Bhattacharya, J., Kupecz, J., Wu, C., Lopez-Blanco, M., Thompson, P., Spear, D., and Landis, C., Cretaceous Panther Tongue sandstone outcrop case study II: evolution of delta type within a forced regression, *in* Proceedings American Association of Petroleum Geologists annual convention, Houston, USA1995, Volume 5.

Muto, T., Steel, R. J., and Swenson, J. B., 2007, Autostratigraphy: a framework norm for genetic stratigraphy: Journal of Sedimentary Research, v. 77, no. 1, p. 2-12.

Nemec, W., 2011, Geostatistics: Course GEOV301 Lecture Notes: Bergen, University of Bergen, p. 62-86.

Newman, K. F., and Chan, M. A., 1991, Depositional facies and sequences in the Upper Cretaceous Panther Tongue Member of the Star Point Formation, Wasatch Plateau, Utah.

North, C. P., Hole, M. J., and Jones, D. G., 2005, Geochemical correlation in deltaic successions: A reality check: Geological Society of America Bulletin, v. 117, no. 5-6, p. 620-632.

Nuccio, V. F., and Condon, S. M., 1996, Burial and thermal history of the Paradox Basin, Utah and Colorado, and petroleum potential of the Middle Pennsylvanian Paradox Formation: U.S. Geol. Surv. Bull., 2000-O.

Nuccio, V. F., and Roberts, L. N., 2003, Thermal maturity and oil and gas generation history of petroleum systems in the Uinta-Piceance Province, Utah and Colorado: Petroleum Systems and Geologic Assessment of Oil and Gas in the Uinta–Piceance Province, Utah and Colorado: United States Geological Survey, Digital Data Series DDS-69-B.

O'Byrne, C. J., and Flint, S., 1993, High-resolution sequence stratigraphy of Cretaceous shallow marine sandstones, Book Cliffs outcrop, Utah, USA-application to reservoir modelling: First Break, v. 11, no. 10.

O'Byrne, C. J., and Flint, S., 1995, Sequence, parasequence, and intraparasequence architecture of the Grassy Member, Blackhawk Formation, Book Cliffs, Utah, USA.

Oelkers, E. H., Bjørkum, P., and Murphy, W. M., 1996, A petrographic and computational investigation of quartz cementation and porosity reduction in North Sea sandstones: American Journal of Science, v. 296, no. 4, p. 420-452.

Olariu, C., and Bhattacharya, J. P., 2006, Terminal distributary channels and delta front architecture of river-dominated delta systems: Journal of Sedimentary Research, v. 76, no. 2, p. 212-233.

Olariu, C., Steel, R. J., and Petter, A. L., 2010, Delta-front hyperpycnal bed geometry and implications for reservoir modeling: Cretaceous Panther Tongue delta, Book Cliffs, Utah: AAPG bulletin, v. 94, no. 6, p. 819-845.

Pattison, S. A. J., 1995, Sequence stratigraphic significance of sharp-based lowstand shoreface deposits, Kenilworth Member, Book Cliffs, Utah: AAPG bulletin, v. 79, no. 3, p. 444-462.

Pattison, S. A. J., 2005, Isolated highstand shelf sandstone body of turbiditic origin, lower Kenilworth Member, Cretaceous Western Interior, Book Cliffs, Utah, USA: Sedimentary Geology, v. 177, no. 1–2, p. 131-144.

Pattison, S. A. J., Ainsworth, B. R., and Hoffman, T. A., 2007, Evidence of across-shelf transport of fine-grained sediments: turbidite-filled shelf channels in the Campanian Aberdeen Member, Book Cliffs, Utah, USA: Sedimentology, v. 54, no. 5, p. 1033-1064.

Posamentier, H. W., Morris, W. R., Bhattacharya, J. P., Kupecz, J. A., Loomis, K. B., Lopez-Blanco, M., Wu, C., Kendall, B. A., Landis, C. R., and Spear, D. B., Cretaceous Panther Tongue sandstone outcrop case study I: regional sequence stratigraphic analysis, *in* Proceedings American Association of Petroleum Geologists annual convention, Houston, USA1995, Volume 5.

Powers, M. C., 1953, A new roundness scale for sedimentary particles: Journal of Sedimentary Research, v. 23, no. 2.

Romesburg, C., 2004, Cluster analysis for researchers, Lulu Press.

Rossi, C., Marfil, R., Ramseyer, K., and Permanyer, A., 2001, Facies-related diagenesis and multiphase siderite cementation and dissolution in the reservoir sandstones of the Khatatba Formation, Egypt's Western Desert: Journal of Sedimentary Research, v. 71, no. 3, p. 459-472.

Saigal, G., and Bjørlykke, K., 1987, Carbonate cements in clastic reservoir rocks from offshore Norway—relationships between isotopic composition, textural development and burial depth: Geological Society, London, Special Publications, v. 36, no. 1, p. 313-324.

Solomon, M., 1963, Counting and sampling errors in modal analysis by point counter: Journal of Petrology, v. 4, no. 3, p. 367-382.

Spieker, E. M., 1931, The Wasatch Plateau Coal Field, Utah, US Government Printing Office.

Spieker, E. M., and Reeside, J. B., 1925, Cretaceous and tertiary formations of the Wasatch Plateau, Utah: Geological Society of America Bulletin, v. 36, no. 3, p. 435-454.

Stikes, M. W., 2007, Fluvial Facies and Architecture of the Poison Strip Sandstone Lower Cretaceous Cedar Mountain Formation, Grand County, Utah, Utah Geological Survey, v. 2.

Stokes, W. L., 1986, Geology of Utah, Utah Museum of Natural History Salt Lake City.

Storvoll, V., and Bjørlykke, K., 2004, Sonic velocity and grain contact properties in reservoir sandstones: Petroleum Geoscience, v. 10, no. 3, p. 215-226.

Swift, D. J., Hudelson, P. M., Brenner, R. L., and Thompson, P., 1987, Shelf construction in a foreland basin: storm beds, shelf sandbodies, and shelf-slope depositional sequences in the Upper Cretaceous Mesaverde Group, Book Cliffs, Utah: Sedimentology, v. 34, no. 3, p. 423-457.

Taylor, D. R., and Lovell, R. W., 1995, High-frequency sequence stratigraphy and paleogeography of the Kenilworth member, Blackhawk Formation, Book Cliffs, Utah, USA.

Taylor, J. M., 1950, Pore-space reduction in sandstones: AAPG Bulletin, v. 34, no. 4, p. 701-716.

Taylor, K. G., Gawthorpe, R. L., Curtis, C. D., Marshall, J. D., and Awwiller, D. N., 2000, Carbonate cementation in a sequence-stratigraphic framework: Upper Cretaceous sandstones, Book Cliffs, Utah-Colorado: Journal of Sedimentary Research, v. 70, no. 2, p. 360-372.

Taylor, K. G., Gawthorpe, R. L., and Fannon-Howell, S., 2004, Basin-scale diagenetic alteration of shoreface sandstones in the Upper Cretaceous Spring Canyon and Aberdeen Members, Blackhawk Formation, Book Cliffs, Utah: Sedimentary Geology, v. 172, no. 1–2, p. 99-115.

Taylor, K. G., Gawthorpe, R. L., and Van Wagoner, J. C., 1995, Stratigraphic control on laterally persistent cementation, Book Cliffs, Utah: Journal of the Geological Society, v. 152, no. 2, p. 225-228.

Taylor, K. G., and Machent, P. G., 2010, Systematic sequence-scale controls on carbonate cementation in a siliciclastic sedimentary basin: Examples from Upper Cretaceous shallow marine deposits of Utah and Coloradao, USA: Marine and Petroleum Geology, v. 27, no. 7, p. 1297-1310.

Van Wagoner, J. C., 1995, Sequence stratigraphy and marine to nonmarine facies architecture of foreland basin strata, Book Cliffs, Utah, USA: The American Association of Petroleum Geologists, AAPG.

Van Wagoner, J. C., Mitchum, R. M., Campion, K. M., and Rahmanian, V. D., 1990, Siliciclastic sequence stratigraphy in well logs, cores, and outcrops: Tulsa, OK (USA); American Association of Petroleum Geologists.

Walderhaug, O., 1996, Kinetic modeling of quartz cementation and porosity loss in deeply buried sandstone reservoirs: AAPG bulletin, v. 80, no. 5, p. 731-745.

Wellner, R., Beaubouef, R., Van Wagoner, J., Roberts, H., and Sun, T., 2005, Jet-plume depositional bodies—the primary building blocks of Wax Lake delta: Gulf Coast Association of Geological Societies Transactions, AAPG, v. 55, p. 867-909.

Wentworth, C. K., 1922, A scale of grade and class terms for clastic sediments: The Journal of Geology, p. 377-392.

Willis, G. C., 1999, The Utah thrust system-an overview: Geology of Northern Utah and Vicinity, AAPG, p. 1-10.

Yoshida, S., Miall, A. D., and Willis, A., 1998, Sequence stratigraphy and marine to nonmarine facies architecture of foreland basin strata, Book Cliffs, Utah, USA: discussion: AAPG bulletin, v. 82, no. 8, p. 1596-1606.

Yoshida, S., Willis, A., and Miall, A. D., 1996, Tectonic control of nested sequence architecture in the Castlegate Sandstone (Upper Cretaceous), Book Cliffs, Utah: Journal of Sedimentary Research, v. 66, no. 4.

Young, R. G., 1955, Sedimentary facies and intertonguing in the Upper Cretaceous of the Book Cliffs, Utah-Colorado: Geological Society of America Bulletin, v. 66, no. 2, p. 177-202.

# APPENDIX I

## TABLES

**Table 1:** Samples and location, the abbreviations under facies association are explained in chapter 4.

| # | Location | Formation (Fm.) | Member (Mb.) | Facies association | GPS Coordinates |
|---|---|---|---|---|---|
| **1** | Huntington Creek | Mancos Shale Fm. | Lower Ferron Mb. | OTz/LSF | N 39°13'18.260" W 110°55'42.480" |
| **2** | Gentile Wash | Star Point Fm. | Panther Tongue Mb. | pDF | N 39°42'43.700" W 110°52'07.060" |
| **3** | Gentile Wash | Star Point Fm. | Panther Tongue Mb. | MB | N 39°42'43.700" W 110°52'07.060" |
| **4 a,b and c** | Gentile Wash | Star Point Fm. | Panther Tongue Mb. | LAG | N 39°42'44.160" W 110°52'21.710" |
| **5** | Gentile Wash | Star Point Fm. | Storrs Mb. | OTz | N 39°42'51.390" W 110°52'26.000" |
| **6** | Gentile Wash | Blackhawk Fm. | Spring Canyon Mb. | LSF | N 39°42'57.180" W 110°52'32.170" |
| **7** | Gentile Wash | Blackhawk Fm. | Spring Canyon Mb. | OTz | N 39°42'58.340" W 110°52'34.110" |
| **8** | Gentile Wash | Blackhawk Fm. | Spring Canyon Mb. | OTz | N 39°42'58.340" W 110°52'34.110" |
| **9** | Gentile Wash | Blackhawk Fm. | Spring Canyon Mb. | LSF | N 39°43'01.110" W 110°52'34.910" |
| **10** | Gentile Wash | Blackhawk Fm. | Spring Canyon Mb. | LSF | N 39°43'01.110" W 110°52'34.910" |
| **11** | Gentile Wash | Blackhawk Fm. | Spring Canyon Mb. | MSF | N 39°43'01.680" W 110°52'36.130" |
| **12** | Gentile Wash | Blackhawk Fm. | Spring Canyon Mb. | USF | N 39°43'04.900" W 110°52'37.530" |
| **13** | Gentile Wash | Blackhawk Fm. | Spring Canyon Mb. | FS | N 39°43'05.650" W 110°52'38.850" |
| **14** | Gentile Wash | Blackhawk Fm. | Spring Canyon Mb. | FS with rootlets | N 39°43'05.650" W 110°52'38.850" |
| **15** | Gentile Wash | Blackhawk Fm. | Non-marine part (Spring Canyon) | MC | N 39°43'05.650" W 110°52'38.850" |
| **16** | Gentile Wash | Blackhawk Fm. | Non-marine part (Spring Canyon) | MC | N 39°43'05.650" W 110°52'38.850" |
| **17** | Gentile Wash | Blackhawk Fm. | Non-marine part (Spring Canyon) | MC | N 39°43'05.650" W 110°52'38.850" |
| **18** | Solider Creek | Blackhawk Fm. | Kenilworth Mb. | MSF | N 39°41'52.920" W 110°36'53.580" |
| **19** | Solider Creek | Blackhawk Fm. | Non-marine part (Kenilworth) | MC | N 39°42'00.980" W 110°36'39.790" |
| **20** | Sunnyside | Blackhawk Fm. | Kenilworth Mb. | LSF | N 39°33'31.730" W 110°22'45.030" |
| **21** | Horse Canyon | Blackhawk Fm. | Kenilworth Mb. | LSF | N 39°27'28.570" W 110°21'36.430" |
| **22** | Woodside Canyon | Blackhawk Fm. | Prairie Canyon Mb.: Woodside sst. | ST: Subaqueous channel | N 39°15'21.530" W 110°18'48.530" |
| **23** | Woodside Canyon | Blackhawk Fm. | Kenilworth Mb. | LSF | N 39°14'57.580" W 110°15'55.580" |
| **24** | Woodside Canyon | Blackhawk Fm. | Kenilworth Mb. | LAG | N 39°14'57.580" W 110°15'55.580" |
| **25** | East of Hatch Mesa | Blackhawk Fm. | Prairie Canyon Mb.: Mancos B | ST: hyperpycnal turbidites | - |
| **26** | Hatch Mesa | Blackhawk Fm. | Prairie Canyon Mb.: Hatch Mesa | ST: hyperpycnal turbidites | N 38°56'32.620" W 109°57'35.080" |

| # | Location | Formation (Fm.) | Member (Mb.) | Facies association | GPS Coordinates |
|---|---|---|---|---|---|
| **27** | Hatch Mesa | Blackhawk Fm. | Prairie Canyon Mb.: Hatch Mesa | ST: hyperpycnal turbidites | N 38°56'32.620" W 109°57'35.080" |
| **28** | Ivie Creek by I-70 | Mancos Shale Fm. | Upper Ferron Mb. | dDF | N 38°48'19.690" W 111°15'46.390" |
| **29** | Ivie Creek by I-70 | Mancos Shale Fm. | Upper Ferron Mb. | pDF | N 38°48'19.017" W 111°15'47.626" |
| **30** | Ivie Creek by I-70 | Mancos Shale Fm. | Upper Ferron Mb. | OTz | N 38°48'17.713" W 111°15'51.059" |
| **31** | Ivie Creek by I-70 | Mancos Shale Fm. | Upper Ferron Mb. | LSF | N 38°48'14.115" W 111°15'53.009" |
| **32** | Ivie Creek by I-70 | Mancos Shale Fm. | Upper Ferron Mb. | MC | N 38°48'09.281" W 111°15'56.772" |
| **33** | Ivie Creek by I-70 | Mancos Shale Fm. | Upper Ferron Mb. | MC | N 38°48'00.000" W 111°16'09.901" |
| **34** | Quitchupah Creek | Mancos Shale Fm. | Emery Mb.: southern delta lobe | LSF (Bioturbated) | N 38°53'36.728" W 111°23'10.265" |
| **35** | Quitchupah Creek | Mancos Shale Fm. | Emery Mb.: southern delta lobe | LSF (HCS) | N 38°53'36.728" W 111°23'10.265" |
| **36** | Quitchupah Creek | Mancos Shale Fm. | Emery Mb.: southern delta lobe | LSF (HCS) | N 38°51'36.552" W 111°21'34.684" |
| **37** | Quitchupah Creek | Mancos Shale Fm. | Emery Mb.: southern delta lobe | LSF (Bioturbaded) | N 38°51'36.552" W 111°21'34.684" |
| **38** | Cottonwood Creek | Star Point Fm. | Storrs Mb. | LSF (HCS) | N 39°19'05.915" W 111°11'22.690" |
| **39** | Joe's Valley | Blackhawk Fm. | Non- marine part | MC | N 39°17'21.518" W 111°15'21.094" |
| **40** | Joe's Valley | Price River Fm. | Lower Castlegate Mb. | BC | N 39°18'00.066" W 111°16'16.355" |
| **41** | Joe's Valley | Price River Fm. | Lower Castlegate Mb. | BC | N 39°18'00.066" W 111°16'15.833" |
| **42** | Joe's Valley | Blackhawk Fm. | Non-marine part | BC | N 39°17'21.340" W 111°16'05.480" |
| **43** | Joe's Valley | Blackhawk Fm. | Non-marine part | CS | N 39°17'18.716" W 111°15'54.575" |
| **44** | Joe's Valley | Star Point Fm. | Storrs Mb. | USF | N 39°16'56.592" W 111°13'58.284" |
| **45** | Bear Canyon | Price River Fm. | Lower Castlegate Mb. | BC | N 39°45'04.628" W 110°53'12.545" |
| **46** | Bear Canyon | Price River Fm. | Lower Castlegate Mb. | BC | N 39°45'04.628" W 110°53'12.545" |
| **47** | Castelgate Mine no1 | Blackhawk Fm. | Non-marine part (Aberdeen) | MC | N 39°44'43.117" W 110°52'54.197" |
| **48** | Castelgate Mine no1 | Blackhawk Fm. | Non-marine part (Aberdeen) | MC | N 39°43'56.609" W 110°52'17.173" |
| **49 a** | Spring Canyon | Star Point | Panther Tongue Mb. | DCh | N 39°42'00.113" W 110°55'12.460' |
| **49 b** | Spring Canyon | Star Point | Panther Tongue Mb. | DCh | N 39°42'00.840" W 110°55'17.102" |
| **50** | Spring Canyon | Star Point | Panther Tongue Mb. | pDF | N 39°41'53.878" W 110°55'02.216" |
| **51** | Horse Canyon | Blackhawk | Kenilworth Mb. | OTz | N 39°27'28.570" W 110°21'36.430" |
| **52** | Horse Canyon | Blackhawk | Kenilworth Mb. | LSF | N 39°27'28.570" W 110°21'36.430" |

| # | Location | Formation (Fm.) | Member (Mb.) | Facies association | GPS Coordinates |
|---|---|---|---|---|---|
| **53** | Ivie Creek by I-70 | Mancos Shale Fm. | Upper Ferron Mb. | FS | N 38°48'09.281" W 111°15'56.772" |
| **54** | Joe's Valley | Blackhawk Fm. | Non-marine part | MC | N 39°16'29.346" W 111°13'15.520" |
| **55** | Gray Canyon | Blackhawk Fm. | Grassy Mb. | OTz | N 39°11'40.845" W 110°04'31.088" |
| **56** | Gray Canyon | Blackhawk Fm. | Grassy Mb. | OTz | N 39°11'40.845" W 110°04'31.088" |
| **57** | Gray Canyon | Blackhawk Fm. | Grassy Mb. | LSF | N 39°11'40.845" W 110°04'31.088" |
| **58** | Gray Canyon | Blackhawk Fm. | Grassy Mb. | LSF | N 39°11'40.845" W 110°04'31.088" |
| **59** | Gray Canyon | Blackhawk Fm. | Grassy Mb. | MSF | N 39°11'40.845" W 110°04'31.088" |
| **60** | Gray Canyon | Blackhawk Fm. | Grassy Mb. | MSF | N 39°11'40.845" W 110°04'31.088" |
| **61** | Gray Canyon | Blackhawk Fm. | Grassy Mb. | USF | N 39°11'40.845" W 110°04'31.088" |
| **62** | Gray Canyon | Blackhawk Fm. | Grassy Mb. | USF | N 39°11'40.845" W 110°04'31.088" |
| **63** | Gray Canyon | Blackhawk Fm. | Grassy Mb. | FS | N 39°11'40.845" W 110°04'31.088" |
| **64** | Gray Canyon | Blackhawk Fm. | Non-marine part (Grassy) | MC | N 39°11'40.845" W 110°04'31.088" |
| **65** | Gray Canyon | Blackhawk Fm. | Kenilworth Mb. | OT | N 39°06'10.068" W 110°06'34.019" |
| **66** | Harmond Hills | Mancos Shale Fm. | Emery Mb.: northern delta lobe | LSF (HCS) | N 39°39'04.414" W 110°51'13.618" |
| **67** | Harmond Hills | Mancos Shale Fm. | Emery Mb.: northern delta lobe | LSF (Bioturbaded) | N 39°39'04.414" W 110°51'13.618" |
| **68** | Horse Canyon | Blackhawk Fm. | Kenilworth Mb. | LSF | N 39°27'28.570" W 110°21'36.430" |
| **69** | Horse Canyon | Blackhawk Fm. | Kenilworth Mb. | LSF | N 39°27'28.570" W 110°21'36.430" |
| **70** | Horse Canyon | Blackhawk Fm. | Kenilworth Mb. | LSF | N 39°27'28.570" W 110°21'36.430" |
| **71** | Horse Canyon | Blackhawk Fm. | Kenilworth Mb. | MSF | N 39°27'29.440" W 110°21'36.050" |
| **72** | Horse Canyon | Blackhawk Fm. | Kenilworth Mb. | MSF | N 39°27'29.440" W 110°21'36.050" |
| **73** | Horse Canyon | Blackhawk Fm. | Kenilworth Mb. | MSF | N 39°27'29.440" W 110°21'36.050" |
| **74** | Horse Canyon | Blackhawk Fm. | Kenilworth Mb. | USF | N 39°27'30.520" W 110°21'35.000" |
| **75** | Horse Canyon | Blackhawk Fm. | Kenilworth Mb. | USF | N 39°27'30.520" W 110°21'35.000" |
| **76** | Horse Canyon | Blackhawk Fm. | Kenilworth Mb. | USF- Rip channel | N 39°27'30.520" W 110°21'35.000" |
| **77** | Horse Canyon | Blackhawk Fm. | Kenilworth Mb. | USF | N 39°27'32.206" W 110°21'32.130" |
| **78** | Horse Canyon | Blackhawk Fm. | Kenilworth Mb. | FS | N 39°27'32.206" W 110°21'32.130" |

**Table 2:** Permeability measurements from each member

## FERRON MB.

| Measurement | Location | Facies association | Min | Max | Average | Order of magnitude |
|---|---|---|---|---|---|---|
| F1 | *Ivie Creek* | Distal delta-front | 23 | 54 | 36 | **10-100 mD** |
| F2 | *Ivie Creek* | Distal delta-front | 20 | 123 | 46 | **10-100 mD** |
| F3 | *Ivie Creek* | Distal delta-front | 20 | 53 | 35 | **10-100 mD** |
| F4 | *Ivie Creek* | Distal delta-front | 56 | 90 | 76 | **10-100 mD** |
| F5 | *Ivie Creek* | Proximal delta-front | 90 | 167 | 128 | **100-1 000 mD** |
| F6 | *Ivie Creek* | Proximal delta-front | 149 | 301 | 221 | **100-1 000 mD** |
| F7 | *Ivie Creek* | Distributary channel | 22 | 43 | 28 | **10-100 mD** |
| F8 | *Ivie Creek* | OTz | 25 | 93 | 42 | **10-100 mD** |
| F9 | *Ivie Creek* | LSF | 22 | 116 | 49 | **10-100 mD** |
| F10 | *Ivie Creek* | FS | 410 | 458 | 441 | **100-1 000 mD** |
| F11 | *Ivie Creek* | MC | 527 | 1448 | 905 | **100-1 000 mD** |
| F12 | *Ivie Creek* | MC | 54 | 116 | 71 | **10-100 mD** |

## EMERY MB.

| Measurement | Location | Facies association | Min | Max | Average | Order of magnitude |
|---|---|---|---|---|---|---|
| E1 | *Quitchupah Creek* | LSF (Bioturbaded) | 234 | 377 | 301 | **100-1 000 mD** |
| E2 | *Quitchupah Creek* | LSF(HCS) | 227 | 421 | 305 | **100-1 000 mD** |
| E3 | *Quitchupah Creek* | LSF(HCS) | 215 | 318 | 247 | **100-1 000 mD** |
| E4 | *Quitchupah Creek* | LSF (Bioturbaded) | 950 | 1094 | 1015 | **1 000-10 000 mD** |
| E5 | *Quitchupah Creek* | LSF(HCS) | 197 | 337 | 259 | **100-1 000 mD** |
| E6 | *Quitchupah Creek* | LSF (Bioturbaded) | 141 | 590 | 221 | **100-1 000 mD** |
| E7 | *Quitchupah Creek* | LSF(HCS) | 527 | 738 | 648 | **100-1 000 mD** |
| E8 | *Quitchupah Creek* | LSF(HCS) | 301 | 458 | 384 | **100-1 000 mD** |
| E9 | *Quitchupah Creek* | LSF (Bioturbaded) | 292 | 309 | 298 | **100-1 000 mD** |
| E10 | *Quitchupah Creek* | OTz | 107 | 167 | 125 | **100-1 000 mD** |
| E11 | *Quitchupah Creek* | LSF (Bioturbaded) | 64 | 850 | 192 | **100-1 000 mD** |
| E12 | *Quitchupah Creek* | LSF(HCS) | 153 | 187 | 173 | **100-1 000 mD** |
| E13 | *Quitchupah Creek* | LSF (Bioturbaded) | 158 | 197 | 182 | **100-1 000 mD** |
| E14 | *Quitchupah Creek* | LSF (Bioturbaded) | 574 | 899 | 672 | **100-1 000 mD** |
| E15 | *Quitchupah Creek* | LSF(HCS) | 590 | 698 | 636 | **100-1 000 mD** |
| E16 | *Quitchupah Creek* | LSF(HCS) | 318 | 387 | 353 | **100-1 000 mD** |
| E17 | *Quitchupah Creek* | LSF (Bioturbaded) | 1369 | 1762 | 1517 | **1 000-10 000 mD** |
| E18 | *Quitchupah Creek* | LSF(HCS) | 240 | 624 | 410 | **100-1 000 mD** |
| E19 | *Quitchupah Creek* | LSF (Bioturbaded) | 607 | 826 | 711 | **100-1 000 mD** |
| E20 | *Quitchupah Creek* | LSF(HCS) | 234 | 346 | 282 | **100-1 000 mD** |
| E21 | *Quitchupah Creek* | LSF (Bioturbaded) | 40 | 50 | 43 | **10-100 mD** |
| E22 | *Quitchupah Creek* | LSF(HCS) | 458 | 874 | 692 | **100-1 000 mD** |
| E23 | *Quitchupah Creek* | LSF (Bioturbaded) | 924 | 1063 | 1015 | **1 000-10 000 mD** |
| E24 | *Harmond Hills* | LSF(HCS) | 1258 | 1713 | 1489 | **1 000-10 000 mD** |
| E25 | *Harmond Hills* | LSF (Bioturbaded) | 498 | 3976 | 1181 | **1 000-10 000 mD** |

# STORRS MB.

| Measurement | Location | Facies association | Min | Max | Average | Order of magnitude |
|---|---|---|---|---|---|---|
| S1 | *Cottonwood Canyon* | LSF | 153 | 203 | 178 | **100-1 000 mD** |
| S2 | *Joe's Canyon* | USF | 76 | 209 | 128 | **100-1 000 mD** |
| S3 | *Gentile Wash* | OTz | 56 | 221 | 112 | **100-1 000 mD** |
| S4 | *Gentile Wash* | OTz | 116 | 284 | 187 | **100-1 000 mD** |
| S5 | *Gentile Wash* | OTz | 74 | 284 | 141 | **100-1 000 mD** |

# PANTHER TONGUE MB.

| Measurement | Location | Facies association | Min | Max | Average | Order of magnitude |
|---|---|---|---|---|---|---|
| PT1 | *Spring Canyon* | Proximal deltafront | 133 | 162 | 146 | **100-1 000 mD** |
| PT2 | *Spring Canyon* | Proximal deltafront | 1575 | 3177 | 2145 | **1 000-10 000 mD** |
| PT3 | *Spring Canyon* | Distributary Channel | 292 | 542 | 415 | **100-1 000 mD** |
| PT4 | *Spring Canyon* | Distributary Channel | 899 | 1190 | 1005 | **1 000-10 000 mD** |
| PT5 | *Gentile Wash* | Proximal deltafront | 113 | 277 | 151 | **100-1 000 mD** |
| PT6 | *Gentile Wash* | Proximal deltafront | 21 | 107 | 57 | **10-100 mD** |
| PT7 | *Gentile Wash* | Proximal deltafront | 46 | 56 | 50 | **10-100 mD** |
| PT8 | *Gentile Wash* | Proximal deltafront | 23 | 145 | 57 | **10-100 mD** |
| PT9 | *Gentile Wash* | Proximal deltafront | 53 | 141 | 88 | **10-100 mD** |
| PT10 | *Gentile Wash* | Proximal deltafront | 50 | 61 | 57 | **10-100 mD** |
| PT11 | *Gentile Wash* | Mouth bar | 63 | 88 | 73 | **10-100 mD** |
| PT12 | *Gentile Wash* | Mouth bar | 247 | 277 | 266 | **100-1 000 mD** |
| PT13 | *Gentile Wash* | Mouth bar | 158 | 356 | 232 | **100-1 000 mD** |
| PT14 | *Gentile Wash* | Mouth bar | 41 | 70 | 55 | **10-100 mD** |
| PT15 | *Gentile Wash* | Transgressive lag | 247 | 718 | 424 | **100-1 000 mD** |
| PT16 | *Gentile Wash* | Mouth bar | 46 | 158 | 86 | **10-100 mD** |
| PT17 | *Gentile Wash* | Mouth bar | 162 | 337 | 235 | **100-1 000 mD** |

# SPRING CANYON MB.

| Measurement | Location | Facies association | Min | Max | Average | Order of magnitude |
|---|---|---|---|---|---|---|
| SC1 | *Gentile Wash* | OTz | 16 | 53 | 31 | **10-100 mD** |
| SC2 | *Gentile Wash* | OTz | 39 | 64 | 51 | **10-100 mD** |
| SC3 | *Gentile Wash* | OTz | 63 | 123 | 94 | **10-100 mD** |
| SC4 | *Gentile Wash* | OTz | 32 | 110 | 64 | **10-100 mD** |
| SC5 | *Gentile Wash* | OTz | 27 | 32 | 29 | **10-100 mD** |
| SC6 | *Gentile Wash* | OTz | 64 | 141 | 100 | **100-1 000 mD** |
| SC7 | *Gentile Wash* | OTz | 107 | 187 | 138 | **100-1 000 mD** |
| SC8 | *Gentile Wash* | OTz | 25 | 34 | 30 | **10-100 mD** |
| SC9 | *Gentile Wash* | LSF | 38 | 187 | 76 | **10-100 mD** |
| SC10 | *Gentile Wash* | LSF | 16 | 110 | 44 | **10-100 mD** |
| SC11 | *Gentile Wash* | LSF | 72 | 126 | 96 | **10-100 mD** |
| SC12 | *Gentile Wash* | LSF | 57 | 116 | 84 | **10-100 mD** |
| SC13 | *Gentile Wash* | LSF | 19 | 42 | 31 | **10-100 mD** |
| SC14 | *Gentile Wash* | OTz | 29 | 137 | 64 | **10-100 mD** |
| SC15 | *Gentile Wash* | OTz | 85 | 182 | 120 | **100-1 000 mD** |
| SC16 | *Gentile Wash* | OTz | 10 | 20 | 15 | **10-100 mD** |
| SC17 | *Gentile Wash* | LSF | 57 | 83 | 65 | **10-100 mD** |
| SC18 | *Gentile Wash* | LSF | 182 | 277 | 238 | **100-1 000 mD** |
| SC19 | *Gentile Wash* | MSF | 277 | 759 | 489 | **100-1 000 mD** |
| SC20 | *Gentile Wash* | MSF | 240 | 679 | 458 | **100-1 000 mD** |
| SC21 | *Gentile Wash* | MSF | 346 | 826 | 494 | **100-1 000 mD** |
| SC22 | *Gentile Wash* | MSF | 227 | 485 | 309 | **100-1 000 mD** |
| SC23 | *Gentile Wash* | MSF | 182 | 698 | 421 | **100-1 000 mD** |
| SC24 | *Gentile Wash* | MSF | 80 | 1063 | 257 | **100-1 000 mD** |
| SC25 | *Gentile Wash* | USF | 309 | 513 | 398 | **100-1 000 mD** |
| SC26 | *Gentile Wash* | USF | 158 | 192 | 172 | **100-1 000 mD** |
| SC27 | *Gentile Wash* | USF | 558 | 718 | 607 | **100-1 000 mD** |
| SC28 | *Gentile Wash* | USF | 527 | 679 | 595 | **100-1 000 mD** |
| SC29 | *Gentile Wash* | USF | 158 | 698 | 370 | **100-1 000 mD** |
| SC30 | *Gentile Wash* | FS | 377 | 1063 | 547 | **100-1 000 mD** |
| SC31 | *Gentile Wash* | FS | 781 | 1971 | 1135 | **1 000-10 000 mD** |
| SC32 | *Gentile Wash* | FS | 410 | 759 | 563 | **100-1 000 mD** |
| SC33 | *Gentile Wash* | FS | 113 | 642 | 260 | **100-1 000 mD** |
| SC34 | *Gentile Wash* | FS | 177 | 327 | 243 | **100-1 000 mD** |
| SC35 | *Gentile Wash* | FS | 215 | 433 | 324 | **100-1 000 mD** |
| SC36 | *Gentile Wash* | FS | 337 | 458 | 395 | **100-1 000 mD** |
| SC37 | *Gentile Wash* | FS | 149 | 261 | 215 | **100-1 000 mD** |
| SC38 | *Gentile Wash* | FS | 318 | 607 | 450 | **100-1 000 mD** |
| SC39 | *Gentile Wash* | FS | 377 | 590 | 458 | **100-1 000 mD** |
| SC40 | *Gentile Wash* | FS | 269 | 624 | 429 | **100-1 000 mD** |
| SC41 | *Gentile Wash* | MC | 83 | 167 | 124 | **100-1 000 mD** |
| SC42 | *Gentile Wash* | MC | 130 | 187 | 151 | **100-1 000 mD** |
| SC43 | *Gentile Wash* | MC | 113 | 209 | 164 | **100-1 000 mD** |

| | | | | | | |
|---|---|---|---|---|---|---|
| SC44 | *Gentile Wash* | MC | 57 | 76 | 66 | **10-100 mD** |
| SC45 | *Gentile Wash* | MC | 63 | 80 | 71 | **10-100 mD** |
| SC46 | *Gentile Wash* | MC | 149 | 410 | 256 | **100-1 000 mD** |
| SC47 | *Gentile Wash* | MC | 18 | 130 | 53 | **10-100 mD** |
| SC48 | *Gentile Wash* | MC | 90 | 209 | 131 | **100-1 000 mD** |
| SC49 | *Gentile Wash* | MC | 61 | 123 | 91 | **10-100 mD** |

# KENILWORTH MB.

| Measurement | Location | Facies association | Min | Max | Average | Order of magnitude |
|---|---|---|---|---|---|---|
| K1 | *Horse Canyon* | Otz | 123 | 137 | 130 | **100-1 000 mD** |
| K2 | *Horse Canyon* | OTz | 45 | 72 | 59 | **10-100 mD** |
| K3 | *Horse Canyon* | OTz | 113 | 126 | 119 | **100-1 000 mD** |
| K4 | *Horse Canyon* | LSF | 346 | 471 | 401 | **100-1 000 mD** |
| K5 | *Horse Canyon* | LSF | 133 | 234 | 173 | **100-1 000 mD** |
| K6 | *Horse Canyon* | LSF | 398 | 527 | 454 | **100-1 000 mD** |
| K7 | *Horse Canyon* | LSF | 177 | 240 | 217 | **100-1 000 mD** |
| K8 | *Horse Canyon* | LSF | 68 | 70 | 69 | **10-100 mD** |
| K9 | *Horse Canyon* | LSF | 68 | 113 | 93 | **10-100 mD** |
| K10 | *Horse Canyon* | LSF | 410 | 485 | 454 | **100-1 000 mD** |
| K11 | *Horse Canyon* | LSF | 284 | 421 | 330 | **100-1 000 mD** |
| K12 | *Horse Canyon* | LSF | 46 | 76 | 61 | **10-100 mD** |
| K13 | *Horse Canyon* | LSF | 70 | 149 | 104 | **100-1 000 mD** |
| K14 | *Horse Canyon* | MSF | 149 | 377 | 230 | **100-1 000 mD** |
| K15 | *Horse Canyon* | MSF | 107 | 149 | 132 | **100-1 000 mD** |
| K16 | *Horse Canyon* | MSF | 234 | 254 | 244 | **100-1 000 mD** |
| K17 | *Horse Canyon* | USF | 80 | 261 | 141 | **100-1 000 mD** |
| K18 | *Horse Canyon* | USF | 42 | 74 | 56 | **10-100 mD** |
| K19 | *Horse Canyon* | USF | 177 | 301 | 227 | **100-1 000 mD** |
| K20 | *Horse Canyon* | USF | 377 | 558 | 480 | **100-1 000 mD** |
| K21 | *Horse Canyon* | USF | 119 | 421 | 199 | **100-1 000 mD** |
| K22 | *Horse Canyon* | Rip-channel | 513 | 1331 | 731 | **100-1 000 mD** |
| K23 | *Horse Canyon* | USF | 607 | 679 | 642 | **100-1 000 mD** |
| K24 | *Horse Canyon* | USF | 309 | 660 | 494 | **100-1 000 mD** |
| K25 | *Horse Canyon* | USF | 542 | 607 | 574 | **100-1 000 mD** |
| K26 | *Horse Canyon* | USF | 1094 | 1762 | 1369 | **1 000-10 000 mD** |
| K27 | *Horse Canyon* | USF | 660 | 826 | 745 | **100-1 000 mD** |
| K28 | *Horse Canyon* | FS | 698 | 899 | 781 | **100-1 000 mD** |

# GRASSY MB.

| Measurement | Location | Facies association | Min | Max | Average | Order of magnitude |
|---|---|---|---|---|---|---|
| G1 | *Gray Canyon* | OTz | 80 | 247 | 127 | **100-1 000 mD** |
| G2 | *Gray Canyon* | OTz | 95 | 221 | 148 | **100-1 000 mD** |
| G3 | *Gray Canyon* | OTz | 66 | 240 | 136 | **100-1 000 mD** |
| G4 | *Gray Canyon* | OTz | 11 | 27 | 18 | **10-100 mD** |
| G5 | *Gray Canyon* | LSF | 95 | 182 | 144 | **100-1 000 mD** |
| G6 | *Gray Canyon* | LSF | 172 | 387 | 234 | **100-1 000 mD** |
| G7 | *Gray Canyon* | LSF | 57 | 153 | 107 | **100-1 000 mD** |
| G8 | *Gray Canyon* | MSF | 85 | 172 | 131 | **100-1 000 mD** |
| G9 | *Gray Canyon* | MSF (HCS) | 145 | 162 | 153 | **100-1 000 mD** |
| G10 | *Gray Canyon* | MSF | 247 | 410 | 318 | **100-1 000 mD** |
| G11 | *Gray Canyon* | MSF | 101 | 318 | 169 | **100-1 000 mD** |
| G12 | *Gray Canyon* | MSF | 153 | 356 | 273 | **100-1 000 mD** |
| G13 | *Gray Canyon* | USF | 803 | 1408 | 978 | **100-1 000 mD** |
| G14 | *Gray Canyon* | USF | 398 | 433 | 413 | **100-1 000 mD** |
| G15 | *Gray Canyon* | USF | 4089 | 6406 | 4873 | **1 000-10 000 mD** |
| G16 | *Gray Canyon* | USF | 1224 | 1812 | 1468 | **1 000-10 000 mD** |
| G17 | *Gray Canyon* | USF | 421 | 527 | 454 | **100-1 000 mD** |
| G18 | *Gray Canyon* | USF | 366 | 1258 | 781 | **100-1 000 mD** |
| G19 | *Gray Canyon* | USF | 366 | 410 | 384 | **100-1 000 mD** |
| G20 | *Gray Canyon* | FS | 826 | 1531 | 1049 | **1 000-10 000 mD** |
| G21 | *Gray Canyon* | FS | 924 | 1094 | 1005 | **1 000-10 000 mD** |
| G22 | *Gray Canyon* | FS | 1005 | 1224 | 1125 | **1 000-10 000 mD** |
| G23 | *Gray Canyon* | MC | 1063 | 1408 | 1198 | **1 000-10 000 mD** |
| G24 | *Gray Canyon* | MC | 850 | 1224 | 987 | **100-1 000 mD** |

# NON-MARINE PART OF BLACKHAWK FM.

| Measurement | Location | Facies association | Min | Max | Average | Order of magnitude |
|---|---|---|---|---|---|---|
| NM-BH 1 | *Joe's Valley* | MC | 803 | 1812 | 1267 | **1 000-10 000 mD** |
| NM-BH 2 | *Joe's Valley* | MC | 64 | 74 | 68 | **10-100 mD** |
| NM-BH 3 | *Joe's Valley* | MC | 8 | 9 | 8 | **1-10 mD** |
| NM-BH 4 | *Joe's Valley* | MC | 116 | 277 | 184 | **100-1 000 mD** |
| NM-BH 5 | *Joe's Valley* | MC | 21 | 56 | 32 | **10-100 mD** |
| NM-BH 6 | *Joe's Valley* | MC | 387 | 542 | 454 | **100-1 000 mD** |
| NM-BH 7 | *Joe's Valley* | MC | 18 | 61 | 23 | **10-100 mD** |
| NM-BH 8 | *Joe's Valley* | MC | 14 | 39 | 21 | **10-100 mD** |
| NM-BH 9 | *Joe's Valley* | MC | 133 | 177 | 149 | **100-1 000 mD** |
| NM-BH 10 | *Joe's Valley* | MC | 950 | 1094 | 1034 | **1 000-10 000 mD** |
| NM-BH 11 | *Joe's Valley* | BC | 1917 | 2920 | 2399 | **1 000-10 000 mD** |
| NM-BH 12 | *Castlegate Mine* | MC | 133 | 182 | 155 | **100-1 000 mD** |
| NM-BH 13 | *Castlegate Mine* | MC | 104 | 141 | 117 | **100-1 000 mD** |
| NM-BH 14 | *Castlegate Mine* | MC | 158 | 234 | 183 | **100-1 000 mD** |
| NM-BH 15 | *Castlegate Mine* | MC | 63 | 240 | 127 | **100-1 000 mD** |

# CASTLEGATE MB.

| Measurement | Location | Facies association | Min | Max | Average | Order of magnitude |
|---|---|---|---|---|---|---|
| CG1 | *Joe's Valley* | BC | 5414 | 8019 | 6497 | **1 000-10 000 mD** |
| CG2 | *Joe's Valley* | BC | 5118 | 8019 | 6840 | **1 000-10 000 mD** |
| CG3 | *Joe's Valley* | BC | 2085 | 2468 | 2247 | **1 000-10 000 mD** |
| CG4 | *Joe's Valley* | BC | 3759 | 7581 | 5023 | **1 000-10 000 mD** |
| CG5 | *Joe's Valley* | BC | 1331 | 1666 | 1531 | **1 000-10 000 mD** |
| CG6 | *Joe's Valley* | BC | 5118 | 6057 | 5568 | **1 000-10 000 mD** |
| CG7 | *Joe's Valley* | BC | 2333 | 3003 | 2610 | **1 000-10 000 mD** |
| CG8 | *Joe's Valley* | BC | 8481 | 13666 | 11467 | **10 000- 100 000 mD** |
| CG9 | *Joe's Valley* | BC | 3360 | 6229 | 4705 | **1 000-10 000 mD** |
| CG10 | *Joe's Valley* | BC | 1489 | 1971 | 1635 | **1 000-10 000 mD** |
| CG11 | *Joe's Valley* | BC | 1713 | 2399 | 2009 | **1 000-10 000 mD** |
| CG12 | *Joe's Valley* | BC | 2085 | 2538 | 2333 | **1 000-10 000 mD** |
| CG13 | *Joe's Valley* | BC | 1448 | 1531 | 1489 | **1 000-10 000 mD** |
| CG14 | *Joe's Valley* | BC | 7371 | 12562 | 9668 | **1 000-10 000 mD** |
| CG15 | *Joe's Valley* | BC | 1620 | 2028 | 1829 | **1 000-10 000 mD** |
| CG16 | *Bear Canyon* | BC | 1190 | 3003 | 2028 | **1 000-10 000 mD** |
| CG17 | *Bear Canyon* | BC | 421 | 421 | 421 | **100-1 000 mD** |
| CG18 | *Bear Canyon* | BC | 1224 | 1369 | 1294 | **1 000-10 000 mD** |
| CG19 | *Bear Canyon* | BC | 446 | 978 | 618 | **100-1 000 mD** |

**Table 3**: Microscope descriptions, the abbreviations under facies association is explained in chapter 4.

| # | Member | Facies association | Grain size | Grain sorting | Grain roundness | Grain contact |
|---|---|---|---|---|---|---|
| **1** | Ferron | OTz/LSF | silt | Moderately sorted | Angular and sub-angular, with moderate to high sphericity. Some sub-rounded and rounded quartz grains, carbonate grains are more angular | Concave-convex contact & point contact, (some sutured contacts, but very few) |
| **2** | Panther Tongue | pDF | fine sand | Moderately sorted | Angular and sub-angular, with moderate to high sphericity. (Some sub-rounded and rounded quartz grains) | Concave-convex contact & point contact |
| **3** | Panther Tongue | MB | fine sand | Poorly sorted | Angular and sub-angular, with moderate to high sphericity. (Some sub-rounded and rounded quartz grains, carbonate grains are more angular) | Concave-convex contact & point contact |
| **4a** | Panther Tongue | LAG | fine sand | Moderately sorted | Angular and sub-angular, with moderate to high sphericity. | Concave-convex contact & sutured contact |
| **4b** | Panther Tongue | LAG | fine sand | Poorly sorted | Angular and sub-angular, with moderate to high sphericity. Some sub-rounded and rounded quartz grains, carbonate grains are more angular | Point contact, also some concave-convex contact can be observed. |
| **4c** | Panther Tongue | LAG | fine sand | Poorly sorted | Angular and sub-angular, with moderate to high sphericity. Some sub-rounded and rounded quartz grains, carbonate grains are more angular | Point contact, also some concave-convex contact can be observed. |
| **5** | Storrs | OTz | silt | Moderately well sorted | Angular and sub-angular, with moderate to high sphericity. (Some sub-rounded and rounded quartz grains, carbonate grains are more angular) | Concave-convex contact & point contact |
| **6** | Spring Canyon | LSF | very fine sand | Moderately well sorted | Sub-angular with moderate sphericity. (Some grains are more sub-rounded with both high and low sphericity.) | Concave-convex contact & point contact |

| # | Member | Facies association | Grain size | Grain sorting | Grain roundness | Grain contact |
|---|---|---|---|---|---|---|
| **7** | Spring Canyon | OTz | silt | Moderately well sorted | Angular and sub-angular, with moderate to high sphericity. (Some sub-rounded and rounded quartz grains, carbonate grains are more angular) | Concave-convex contact & point contact |
| **8** | Spring Canyon | OTz | silt | Moderately sorted | Angular and sub-angular, with moderate to high sphericity. Some sub-rounded and rounded quartz grains, carbonate grains are more angular | Point contact & concave-convex contact |
| **9** | Spring Canyon | LSF | very fine sand | Well sorted | Angular and sub-angular, with moderate to high sphericity. (Some sub-rounded and rounded quartz grains, carbonate grains are more angular) | Point contact & concave-convex contact |
| **10** | Spring Canyon | LSF | very fine sand | Well sorted | Sub-angular and sub-rounded with low to high sphericity | Concave-convex contact & point contact |
| **11** | Spring Canyon | MSF | very fine sand | Moderately well sorted | Sub-angular with moderate sphericity. (Some grains are more sub-rounded with both high and low sphericity.) | Concave-convex contact & point contact |
| **12** | Spring Canyon | USF | fine sand | Poorly sorted | Angular and sub-angular, with moderate to high sphericity. (Some sub-rounded and rounded quartz grains, carbonate grains are more angular) | Concave-convex contact & point contact |
| **13** | Spring Canyon | FS | fine sand | Well sorted | Sub-angular and sub-rounded with low to high sphericity | Point contact & concave-convex contact |
| **14** | Spring Canyon | FS with rootlets | fine sand | Very well sorted | Rounded and sub-rounded with both low and high sphericity. | Point contact, also some concave-convex contact can be observed. |
| **15** | Non marine Blackhawk Fm. (Spring Canyon) | MC | fine sand | Moderately well sorted | Sub-angular and sub-rounded with low to high sphericity | Point contact & concave-convex contact |

| # | Member | Facies association | Grain size | Grain sorting | Grain roundness | Grain contact |
|---|---|---|---|---|---|---|
| **16** | Non marine Blackhawk Fm. (Spring Canyon) | MC | fine sand | Moderately well sorted | Sub-angular with moderate sphericity. (Some grains are more sub-rounded with both high and low sphericity.) | Concave-convex contact & point contact |
| **17** | Non marine Blackhawk Fm. (Spring Canyon) | MC | fine sand | Moderately well sorted | Sub-angular and sub-rounded with low to high sphericity | Point contact & concave-convex contact |
| **18** | Kenilworth | MSF | very fine sand | Moderately well sorted | Sub-angular and sub-rounded with low to high sphericity | Concave-convex contact & point contact |
| **19** | Non marine Blackhawk Fm. (Kenilworth) | MC | fine sand | Moderately Sorted | Sub-angular and sub-rounded with low to high sphericity | Concave-convex contact & point contact |
| **20** | Kenilworth | LSF | very fine sand | Moderately Sorted | Sub-angular and sub-rounded with low to high sphericity | Concave-convex contact & point contact |
| **21** | Kenilworth | LSF | fine sand | Moderately well sorted | Sub-angular and sub-rounded with low to high sphericity, some quartz grains are more rounded | Concave-convex contact & point contact |
| **22** | Woodside sandstone | ST | silt | Poorly sorted | Sub-rounded with high sphericity. Some grains are sub-angular and some are rounded | Point contact & concave-convex contact |
| **23** | Kenilworth | LSF | very fine sand | Moderately Sorted | Sub-angular with moderate sphericity. Some grains are angular and sub-rounded with both high and low sphericity. | Point contact & concave-convex contact |
| **24** | Kenilworth | LAG | fine sand | Moderately Sorted | Sub-angular with moderate sphericity. Some grains are angular and sub-rounded with both high and low sphericity. | Point contact & concave-convex contact |

| # | Member | Facies association | Grain size | Grain sorting | Grain roundness | Grain contact |
|---|---|---|---|---|---|---|
| **25** | Mancos B | ST | silt | Moderately well sorted | Angular and sub-angular, with moderate to high sphericity | Point contact & concave-convex contact |
| **26** | Hatch Mesa | ST | very fine sand | Moderately Sorted | Angular and sub-angular with moderate sphericity. Some quartz grains are sub-rounded with both high and low sphericity. | Point contact, also some concave-convex contact can be observed. |
| **27** | Hatch Mesa | ST | silt | Moderately Sorted | Angular and sub-angular with moderate sphericity. Some quartz grains are sub-rounded with both high and low sphericity. | Point contact, also some concave-convex contact can be observed. |
| **28** | Ferron | dDF | very fine sand | Moderately Sorted | Angular and sub-angular, with moderate to high sphericity. Some sub-rounded and rounded quartz grains, carbonate grains are more angular | Point contact & concave-convex contact |
| **29** | Ferron | pDF | very fine sand | Moderately sorted | Angular and sub-angular, with moderate to high sphericity. Some sub-rounded and rounded quartz grains, carbonate grains are more angular | Point contact & concave-convex contact |
| **30** | Ferron | OTz | silt | Moderately well sorted | Sub-angular and sub-rounded with low to high sphericity, some quartz grains are more rounded | Concave-convex contact and Point contact |
| **31** | Ferron | LSF | very fine sand | Moderately well sorted | Sub-angular and sub-rounded with low to high sphericity, some quartz grains are more rounded | Concave-convex contact and Point contact |
| **32** | Ferron | MC | fine sand | Moderately well sorted | Sub-angular and sub-rounded with low to high sphericity, some quartz grains are more rounded | Point contact & concave-convex contact |
| **33** | Ferron | MC | fine sand | Moderately sorted | Sub-angular with moderate sphericity. Some grains are angular and sub-rounded with both high and low sphericity. | Point contact & concave-convex contact |
| **34** | Emery | LSF (Bio) | fine sand | Well sorted | Sub-angular and sub-rounded with low to high sphericity | Point contact & concave-convex contact |
| **35** | Emery | LSF (HCS) | fine sand | Well sorted | Sub-angular and sub-rounded with low to high sphericity | Point contact, also some concave-convex contact can be observed. |

| # | Member | Facies association | Grain size | Grain sorting | Grain roundness | Grain contact |
|---|---|---|---|---|---|---|
| **36** | Emery | LSF (HCS) | fine sand | Well sorted | Sub-angular and sub-rounded with low to high sphericity | Point contact & concave-convex contact |
| **37** | Emery | LSF (Bio) | fine sand | Moderately well sorted | Sub-angular and sub-rounded with low to high sphericity | Point contact & concave-convex contact |
| **38** | Storrs | LSF (HCS) | very fine sand | Very well Sorted | Sub-angular and sub-rounded with low to high sphericity | Point contact & concave-convex contact |
| **39** | Non marine | MC | medium sand | Moderately well sorted | Rounded and sub-rounded with both low and high sphericity. | Point contact |
| **40** | Castlegate | BC | medium sand | Very well sorted | Rounded and sub-rounded with both low and high sphericity. | Point contact |
| **41** | Castlegate | BC | medium sand | Very well sorted | Rounded and sub-rounded with both low and high sphericity. | Point contact |
| **42** | Non marine | BC | fine sand | Well sorted | Sub-rounded and some are rounded with both low and high sphericity. | Point contact |
| **43** | Non marine | CS | fine sand | Moderately sorted | Sub-angular and sub-rounded, with low to high phericity. | Concave-convex contact & point contact can be observed |
| **44** | Storrs | USF | medium sand | Moderately well sorted | Sub-rounded with high sphericity. Some grains are more sub-angular and some are more rounded | Point contact, also some concave-convex contact can be observed. |
| **45** | Castlegate | BC | fine sand | Very well sorted | Rounded and sub-rounded with both low and high sphericity. | Point contact, also some concave-convex contact can be observed. |
| **46** | Castlegate | BC | fine sand | Very well sorted | Rounded and sub-rounded with both low and high sphericity. | Point contact, also some concave-convex contact can be observed. |
| **47** | Non marine | MC | fine sand | Well sorted | Sub-angular and sub-rounded with low to high sphericity | Point contact, also some concave-convex contact can be observed. |
| **48** | Non marine | MC | fine sand | Well sorted | Sub-angular and sub-rounded with low to high sphericity, some quartz grains are more rounded | Point contact & concave-convex contact |

| # | Member | Facies association | Grain size | Grain sorting | Grain roundness | Grain contact |
|---|---|---|---|---|---|---|
| **49 a** | Panther Tongue | DCh | fine sand | Moderately Sorted | Sub-angular and sub-rounded with low to high sphericity | Point contact, also some concave-convex contact can be observed. |
| **49 b** | Panther Tongue | DCh | fine sand | Moderately sorted | Sub-angular and sub-rounded with low to high sphericity | Point contact, also some concave-convex contact can be observed. |
| **50** | Panther Tongue | pDF | fine sand | Moderately sorted | Sub-angular and sub-rounded with low to high sphericity | Point contact & concave-convex contact |
| **51** | Kenilworth | OTz | very fine sand | Moderately sorted | Angular and sub-angular, with moderate to high sphericity. Some sub rounded and rounded quartz grains, carbonate grains are more angular | Point contact, also some concave-convex contact can be observed. |
| **52** | Kenilworth | LSF | fine sand | Moderately sorted | Sub-angular with moderate sphericity. Some grains are angular or sub-rounded with both high and low sphericity. | Point contact, also some concave-convex contact can be observed. |
| **53** | Ferron | FS | fine sand | Moderately sorted | Sub-angular with moderate sphericity. Some grains are angular or sub-rounded with both high and low sphericity. | Point contact & concave-convex contact |
| **54** | Non marine Blackhawk Fm. | MC | very fine sand | Moderately sorted | Sub-angular and sub-rounded with low to high sphericity, some quartz grains are more rounded | Point contact |
| **55** | Grassy | OTz | fine sand | Moderately well sorted | Sub-angular and sub-rounded with low to high sphericity, some quartz grains are more rounded | Point contact & concave-convex contact |
| **56** | Grassy | OTz | fine sand | Moderately well sorted | Angular and sub-angular, with moderate to high sphericity. (Some sub-rounded and rounded quartz grains) | Point contact & concave-convex contact |
| **57** | Grassy | LSF | fine sand | Moderately sorted | Sub-angular with moderate sphericity. (Some grains are more sub-rounded with both high and low sphericity.) | Point contact & concave-convex contact |
| **58** | Grassy | LSF | fine sand | Moderately sorted | Sub-angular with moderate sphericity. (Some grains are more sub-rounded with both high and low sphericity.) | Point contact & concave-convex contact |

| # | Member | Facies association | Grain size | Grain sorting | Grain roundness | Grain contact |
|---|---|---|---|---|---|---|
| **59** | Grassy | MSF | fine sand | Moderately Sorted | Sub-angular and sub-rounded | Point contact & concave-convex contact |
| **60** | Grassy | MSF | fine sand | Moderately well sorted | Sub-angular with moderate sphericity. (Some grains are more sub-rounded with both high and low sphericity.) | Point contact & concave-convex contact |
| **61** | Grassy | USF | fine sand | Moderately well sorted | Sub-angular with moderate sphericity. (Some grains are more sub-rounded with both high and low sphericity.) | Point contact & concave-convex contact |
| **62** | Grassy | USF | fine sand | Moderately well sorted | Sub-angular with moderate sphericity. (Some grains are more sub-rounded with both high and low sphericity.) | Point contact & concave-convex contact |
| **63** | Grassy | FS | fine sand | Very well sorted | Sub-angular and sub-rounded with low to high sphericity | Point contact & concave-convex contact |
| **64** | Grassy | MC | fine sand | Well sorted | Sub-angular and sub-rounded with low to high sphericity | Point contact & concave-convex contact |
| **65** | Kenilworth | OTz | very fine sand | Moderately sorted | Angular and sub-angular | Point contact & concave-convex contact |
| **66** | Emery | LSF (HCS) | very fine sand | Moderately well sorted | Sub-angular and sub-rounded | Concave- convex contact & point contact |
| **67** | Emery | LSF (Bio) | very fine sand | Moderately well sorted | Sub-angular and sub-rounded | Point contact & concave-convex contact |
| **68** | Kenilworth | LSF | fine sand | Moderately sorted | Sub-angular with moderate sphericity. (Some grains are more sub-rounded with both high and low sphericity.) | Point contact & concave-convex contact |
| **69** | Kenilworth | LSF | fine sand | Moderately sorted | Sub-angular with moderate sphericity. (Some grains are more sub-rounded with both high and low sphericity.) | Point contact & concave-convex contact |

| # | Member | Facies association | Grain size | Grain sorting | Grain roundness | Grain contact |
|---|---|---|---|---|---|---|
| **70** | Kenilworth | LSF | fine sand | Moderately sorted | Angular and sub-angular, with moderate to high sphericity (some sub-rounded and rounded quartz grains). | Concave- convex contact & point contact |
| **71** | Kenilworth | MSF | fine sand | Moderately well sorted | Sub-angular with moderate sphericity. (Some grains are more sub-rounded with both high and low sphericity.) | Point contact & concave-convex contact |
| **72** | Kenilworth | MSF | fine sand | Moderately well sorted | Sub-angular with moderate sphericity. (Some grains are more sub-rounded with both high and low sphericity.) | Point contact & concave-convex contact |
| **73** | Kenilworth | MSF | fine sand | Moderately sorted | Angular and sub-angular, with moderate to high sphericity (some sub-rounded and rounded quartz grains). | Concave-convex contact and point contact |
| **74** | Kenilworth | USF | fine sand | Moderately sorted | Angular and sub-angular, with moderate to high sphericity (some sub-rounded and rounded quartz grains). | Point contact & concave-convex contact |
| **75** | Kenilworth | USF | fine sand | Moderately well sorted | Sub-angular and sub-rounded | Point contact & concave-convex contact |
| **76** | Kenilworth | USF- Rip channel | fine sand | Moderately well sorted | Sub-angular and sub-rounded | Point contact, also some concave-convex contact can be observed. |
| **77** | Kenilworth | USF | fine sand | Well sorted | Sub-rounded and rounded, with both low and high sphericity (some grains are more sub-angular with lower sphericity) | Point contact, also some concave-convex contact can be observed. |
| **78** | Kenilworth | FS | fine sand | Well sorted | sub-rounded and rounded, with both low and high sphericity (some grains are more sub-angular with lower sphericity) | Point contact, also some concave-convex contact can be observed. |

**Table4:** Raw data from point counting**,** the abbreviations in facies association is explained in chapter 4.

| # | Member | Facies association | Quartz | F-spar | Rock fragments | Carbonate -grains | Muscovite | Biotite | Heavy minerals | Heavy minerals | Quartz-cement | Carbonate-cement | Oxide-cement | Alteration products | Silt-grains | Opaque material | Unknown minerals | Porosity |
|---|---|---|---|---|---|---|---|---|---|---|---|---|---|---|---|---|---|---|
| **1** | Ferron | OTz/LSF | 56.7% | 0.7% | 4.7% | 9.3% | 2.3% | 0.0% | 2.7% | Zircon, Tourmaline | 2.7% | 13.7% | 1.0% | 5.3% | 0.0% | 0.0% | 0.7% | 0.3% |
| **2** | Panther Tongue | pDF | 45.7% | 1.7% | 10.0% | 4.3% | 0.3% | 0.0% | 0.7% | Zircon | 3.0% | 11.7% | 2.3% | 3.0% | 0.0% | 0.0% | 0.0% | 17.3% |
| **3** | Panther Tongue | MB | 42.7% | 0.7% | 9.3% | 5.0% | 0.3% | 0.0% | 0.0% | Zircon, | 6.0% | 20.0% | 8.0% | 1.7% | 0.0% | 0.0% | 0.0% | 6.3% |
| **4a** | Panther Tongue | LAG | 29.1% | 3.2% | 14.9% | 5.2% | 2.6% | 0.6% | 1.6% | Zircon, Tourmaline, Apatite | 0.6% | 15.9% | 1.0% | 6.9% | 0.0% | 2.9% | 5.2% | 10.4% |
| **4b** | Panther Tongue | LAG | 27.7% | 2.7% | 40.0% | 2.0% | 0.0% | 0.0% | 0.7% | Zircon | 2.0% | 7.0% | 2.3% | 1.3% | 0.0% | 0.0% | 0.0% | 14.3% |
| **4c** | Panther Tongue | LAG | 38.3% | 1.7% | 17.0% | 5.7% | 1.7% | 0.0% | 1.0% | Zircon | 0.0% | 9.0% | 3.7% | 2.3% | 2.7% | 0.0% | 1.0% | 16.0% |
| **5** | Storrs | OTz | 43.3% | 1.0% | 0.3% | 10.3% | 1.0% | 0.7% | 2.7% | Zircon, Tourmaline | 0.0% | 26.7% | 2.7% | 2.7% | 0.0% | 2.3% | 3.0% | 3.3% |
| **6** | Spring Canyon | LSF | 47.3% | 3.0% | 4.7% | 10.0% | 2.0% | 0.0% | 3.7% | Zircon, Tourmaline | 0.0% | 10.3% | 2.0% | 5.3% | 3.0% | 1.0% | 2.7% | 5.0% |
| **7** | Spring Canyon | OTz | 39.3% | 1.0% | 5.3% | 4.3% | 3.3% | 0.7% | 2.3% | Zircon, Tourmaline | 0.7% | 16.3% | 4.0% | 8.0% | 3.3% | 2.3% | 4.3% | 4.7% |
| **8** | Spring Canyon | OTz | 43.3% | 0.0% | 2.3% | 12.7% | 2.3% | 0.0% | 1.3% | Zircon, Tourmaline | 0.7% | 18.3% | 4.7% | 7.3% | 1.7% | 1.3% | 3.3% | 0.7% |
| **9** | Spring Canyon | LSF | 43.7% | 0.7% | 4.3% | 15.3% | 1.0% | 0.0% | 1.3% | Zircon, Tourmaline | 1.0% | 9.3% | 5.0% | 7.0% | 0.3% | 1.7% | 3.7% | 5.7% |
| **10** | Spring Canyon | LSF | 47.7% | 1.3% | 10.3% | 5.0% | 0.7% | 0.0% | 0.0% |  | 1.7% | 6.0% | 2.0% | 10.3% | 0.0% | 0.3% | 0.3% | 14.3% |
| **11** | Spring Canyon | MSF | 41.0% | 0.3% | 8.0% | 7.7% | 0.7% | 0.0% | 1.7% | Zircon, Tourmaline, Apatite | 1.7% | 8.0% | 2.0% | 9.0% | 10.0% | 1.3% | 1.7% | 7.0% |
| **12** | Spring Canyon | USF | 47.3% | 0.7% | 16.3% | 0.0% | 1.3% | 0.0% | 0.3% | Zircon | 1.7% | 0.0% | 0.3% | 5.3% | 0.0% | 0.0% | 0.3% | 26.3% |
| **13** | Spring Canyon | FS | 52.0% | 1.0% | 6.3% | 0.0% | 0.7% | 0.0% | 0.3% | Zircon | 4.7% | 0.0% | 1.0% | 8.7% | 0.0% | 1.3% | 0.3% | 23.7% |
| **14** | Spring Canyon | FS with rootlets | 52.3% | 0.0% | 4.0% | 0.0% | 0.7% | 0.0% | 0.7% | Zircon, Tourmaline | 7.3% | 0.0% | 1.0% | 5.3% | 0.0% | 8.7% | 0.3% | 19.7% |
| **15** | Non-marine Blackhawk Fm. (Spring Canyon) | MC | 51.0% | 0.3% | 2.0% | 0.0% | 0.3% | 0.0% | 0.7% | Zircon, Tourmaline | 3.3% | 0.0% | 2.0% | 1.0% | 13.7% | 5.7% | 0.7% | 19.3% |
| **16** | Non-marine Blackhawk Fm. (Spring Canyon) | MC | 41.3% | 0.7% | 3.3% | 10.3% | 1.3% | 0.0% | 1.3% | Zircon, Tourmaline, Apatite | 2.0% | 9.7% | 2.0% | 3.7% | 5.7% | 3.3% | 1.7% | 13.7% |

| # | Member | Facies association | Quartz | F-spar | Rock fragments | Carbonate -grains | Muscovite | Biotite | Heavy minerals | Heavy minerals | Quartz-cement | Carbonate-cement | Oxide-cement | Alteration products | Silt-grains | Opaque material | Unknown minerals | Porosity |
|---|---|---|---|---|---|---|---|---|---|---|---|---|---|---|---|---|---|---|
| **17** | Non-marine Blackhawk Fm. (Spring Canyon) | MC | 55.7% | 1.3% | 3.3% | 7.7% | 0.3% | 0.0% | 1.3% | Zircon, Tourmaline | 2.3% | 9.0% | 1.7% | 1.7% | 2.3% | 0.0% | 0.0% | 13.3% |
| **18** | Kenilworth | MSF | 39.0% | 1.0% | 3.7% | 12.3% | 0.0% | 0.0% | 0.3% | Tourmaline | 3.7% | 5.7% | 2.0% | 4.0% | 2.3% | 1.7% | 1.7% | 22.7% |
| **19** | Non marine Blackhawk Fm. (Kenilworth) | MC | 41.3% | 0.3% | 2.7% | 12.0% | 0.0% | 0.0% | 0.3% | Tourmaline | 5.3% | 12.0% | 4.7% | 2.0% | 6.7% | 0.7% | 0.3% | 11.7% |
| **20** | Kenilworth | LSF | 46.3% | 0.7% | 5.0% | 6.7% | 0.3% | 0.0% | 0.3% | Apatite | 5.7% | 6.3% | 4.7% | 7.3% | 2.0% | 4.0% | 0.3% | 10.3% |
| **21** | Kenilworth | LSF | 36.0% | 0.3% | 3.3% | 13.0% | 0.0% | 0.0% | 0.0% | | 7.7% | 8.3% | 0.0% | 6.7% | 0.7% | 5.3% | 2.3% | 16.3% |
| **22** | Woodside sandstone | ST | 7.3% | 0.0% | 0.0% | 4.3% | 0.0% | 0.0% | 0.0% | | 0.0% | 1.0% | 2.7% | 0.0% | 67.0% | 15.7% | 0.3% | 1.3% |
| **23** | Kenilworth | LSF | 40.0% | 0.7% | 7.7% | 9.7% | 1.7% | 0.0% | 1.0% | Zircon, Tourmaline, Apatite | 6.3% | 3.0% | 8.3% | 6.7% | 0.7% | 1.7% | 0.7% | 12.0% |
| **24** | Kenilworth | LAG | 43.3% | 0.0% | 4.3% | 3.7% | 0.7% | 0.0% | 0.7% | Zircon, Tourmaline | 5.0% | 7.7% | 21.0% | 2.3% | 0.0% | 4.3% | 1.3% | 5.7% |
| **25** | Mancos B | ST | 34.3% | 1.0% | 2.7% | 10.7% | 4.7% | 1.3% | 0.7% | Tourmaline, Apatite | 1.3% | 2.3% | 18.0% | 1.3% | 5.3% | 9.3% | 3.3% | 3.7% |
| **26** | Hatch Mesa | ST | 35.0% | 0.7% | 6.3% | 14.3% | 1.3% | 0.3% | 0.7% | Zircon, Apatite | 2.7% | 4.0% | 7.7% | 7.0% | 0.7% | 5.7% | 1.3% | 12.3% |
| **27** | Hatch Mesa | ST | 29.7% | 0.7% | 5.0% | 19.0% | 1.7% | 0.3% | 1.3% | Zircon, Tourmaline, Apatite | 0.3% | 27.0% | 1.3% | 4.0% | 0.3% | 3.3% | 4.7% | 1.3% |
| **28** | Ferron | dDF | 46.0% | 0.7% | 3.3% | 14.3% | 1.0% | 0.7% | 1.0% | Zircon, Tourmaline, Apatite | 2.0% | 5.3% | 5.7% | 6.3% | 2.3% | 4.0% | 0.7% | 6.7% |
| **29** | Ferron | pDF | 40.0% | 1.3% | 4.0% | 5.0% | 1.3% | 1.3% | 1.0% | Tourmaline, Apatite | 0.3% | 9.7% | 12.3% | 6.3% | 2.7% | 11.3% | 2.3% | 1.0% |
| **30** | Ferron | OTz | 49.0% | 0.3% | 3.7% | 15.3% | 0.3% | 0.0% | 1.0% | Zircon, Tourmaline | 0.7% | 6.7% | 2.0% | 2.3% | 1.0% | 3.7% | 0.7% | 13.3% |
| **31** | Ferron | LSF | 54.3% | 0.3% | 7.0% | 5.0% | 0.0% | 0.0% | 0.3% | Tourmaline | 1.7% | 1.3% | 2.3% | 1.7% | 0.7% | 5.0% | 1.7% | 18.7% |

| # | Member | Facies association | Quartz | F-spar | Rock fragments | Carbonate -grains | Muscovite | Biotite | Heavy minerals | Heavy minerals | Quartz-cement | Carbonate-cement | Oxide-cement | Alteration products | Silt-grains | Opaque material | Unknown minerals | Porosity |
|---|---|---|---|---|---|---|---|---|---|---|---|---|---|---|---|---|---|---|
| **32** | Ferron | MC | 48.7% | 1.0% | 5.7% | 2.7% | 0.3% | 0.0% | 1.0% | Apatite | 5.0% | 1.0% | 2.0% | 5.0% | 0.0% | 2.7% | 0.3% | 24.7% |
| **33** | Ferron | MC | 53.7% | 0.7% | 4.0% | 7.0% | 2.3% | 0.3% | 1.0% | Zircon, Tourmaline | 1.0% | 3.0% | 0.3% | 7.3% | 5.0% | 5.7% | 1.0% | 7.7% |
| **34** | Emery | LSF (Bio) | 48.7% | 0.3% | 5.3% | 6.0% | 0.0% | 0.3% | 2.0% | Zircon, Tourmaline | 2.7% | 6.0% | 1.0% | 1.7% | 5.3% | 5.0% | 2.0% | 13.7% |
| **35** | Emery | LSF (HCS) | 49.0% | 0.7% | 3.7% | 5.0% | 0.7% | 0.0% | 2.0% | Zircon, Tourmaline | 2.3% | 2.3% | 0.7% | 2.3% | 1.3% | 1.0% | 2.0% | 27.0% |
| **36** | Emery | LSF (HCS) | 45.7% | 0.7% | 4.0% | 6.3% | 1.3% | 0.0% | 1.3% | Zircon, Tourmaline & Apatite | 4.0% | 2.0% | 5.0% | 0.7% | 0.7% | 2.7% | 2.0% | 23.7% |
| **37** | Emery | LSF (Bio) | 43.7% | 1.0% | 2.3% | 5.3% | 0.3% | 0.7% | 2.3% | Zircon, Tourmaline | 2.0% | 12.7% | 4.0% | 3.3% | 2.0% | 6.0% | 2.3% | 12.0% |
| **38** | Storrs | LSF (HCS) | 50.0% | 0.3% | 1.7% | 1.3% | 0.3% | 0.0% | 1.0% | Zircon, Tourmaline | 6.7% | 6.3% | 1.3% | 3.0% | 0.0% | 2.3% | 1.0% | 24.7% |
| **39** | Non-marine Blackhawk Fm. | MC | 38.3% | 0.0% | 1.7% | 14.7% | 0.0% | 0.0% | 0.0% | | 8.3% | 16.0% | 0.0% | 2.0% | 0.0% | 1.0% | 0.0% | 18.0% |
| **40** | Castlegate | BC | 39.0% | 0.0% | 4.3% | 2.7% | 0.0% | 0.0% | 0.7% | Tourmaline | 15.7% | 0.0% | 6.3% | 0.0% | 3.3% | 0.0% | 0.0% | 28.0% |
| **41** | Castlegate | BC | 46.3% | 0.0% | 9.7% | 3.7% | 0.0% | 0.0% | 0.0% | | 10.3% | 4.0% | 1.0% | 0.0% | 0.0% | 0.0% | 0.3% | 24.7% |
| **42** | Non-marine Blackhawk Fm. | BC | 43.7% | 0.0% | 1.0% | 17.0% | 0.0% | 0.0% | 0.0% | | 6.7% | 5.3% | 1.0% | 3.0% | 0.0% | 4.3% | 0.0% | 18.0% |
| **43** | Non-marine Blackhawk Fm. | CS | 42.0% | 0.0% | 5.7% | 20.3% | 0.0% | 0.0% | 0.3% | Tourmaline | 2.3% | 12.3% | 3.0% | 1.3% | 8.0% | 2.3% | 1.0% | 1.3% |
| **44** | Storrs | USF | 37.7% | 0.0% | 3.3% | 11.7% | 0.0% | 0.0% | 0.3% | Tourmaline | 7.0% | 16.7% | 0.3% | 0.3% | 1.0% | 1.3% | 0.0% | 20.3% |
| **45** | Castlegate | BC | 43.7% | 0.3% | 5.7% | 0.0% | 0.0% | 0.0% | 1.3% | Zircon, Tourmaline | 15.0% | 0.0% | 1.3% | 0.7% | 0.7% | 3.0% | 0.3% | 28.0% |
| **46** | Castlegate | BC | 43.3% | 0.7% | 7.7% | 0.0% | 0.0% | 0.0% | 0.7% | Tourmaline | 19.0% | 0.0% | 0.0% | 1.0% | 0.0% | 2.0% | 0.3% | 25.3% |
| **47** | Non-marine Blackhawk Fm. | MC | 36.3% | 0.3% | 3.7% | 1.0% | 0.0% | 0.0% | 0.3% | Tourmaline | 8.7% | 26.7% | 5.3% | 0.7% | 0.0% | 3.7% | 0.3% | 13.0% |
| **48** | Non-marine Blackhawk Fm. | MC | 46.3% | 1.7% | 4.7% | 2.0% | 0.0% | 0.0% | 1.0% | Zircon, Tourmaline | 10.3% | 8.0% | 11.0% | 1.3% | 0.3% | 2.7% | 0.7% | 10.0% |
| **49a** | Panther Tongue | DCh | 30.0% | 0.3% | 12.0% | 2.7% | 0.3% | 0.0% | 0.0% | | 12.0% | 1.7% | 7.0% | 2.7% | 0.3% | 6.0% | 2.0% | 23.0% |

| # | Member | Facies association | Quartz | F-spar | Rock fragments | Carbonate -grains | Muscovite | Biotite | Heavy minerals | Heavy minerals | Quartz-cement | Carbonate-cement | Oxide-cement | Alteration products | Silt-grains | Opaque material | Unknown minerals | Porosity |
|---|---|---|---|---|---|---|---|---|---|---|---|---|---|---|---|---|---|---|
| **49b** | Panther Tongue | DCh | 33.0% | 0.3% | 10.7% | 5.3% | 0.3% | 0.0% | 0.3% | Tourmaline | 10.3% | 11.3% | 4.7% | 2.0% | 1.3% | 6.7% | 2.0% | 11.7% |
| **50** | Panther Tongue | pDF | 32.7% | 0.3% | 11.7% | 4.7% | 0.3% | 0.0% | 0.3% | Tourmaline | 11.7% | 15.7% | 1.7% | 3.0% | 0.0% | 2.0% | 1.7% | 14.3% |
| **51** | Kenilworth | OTz | 43.0% | 0.7% | 3.3% | 5.3% | 1.3% | 0.0% | 0.7% | Tourmaline | 6.0% | 10.0% | 2.3% | 2.3% | 3.7% | 7.0% | 4.7% | 9.7% |
| **52** | Kenilworth | LSF | 40.0% | 1.0% | 6.0% | 4.7% | 0.7% | 0.0% | 0.7% | Tourmaline, Apatite | 8.3% | 9.3% | 4.3% | 6.0% | 0.0% | 3.3% | 3.0% | 12.7% |
| **53** | Ferron | FS | 49.7% | 1.3% | 4.0% | 2.3% | 1.3% | 0.0% | 1.0% | Tourmaline, Apatite | 4.3% | 0.7% | 7.0% | 8.3% | 0.0% | 2.7% | 0.7% | 16.7% |
| **54** | Non marine | MC | 19.0% | 0.3% | 0.3% | 26.7% | 0.7% | 0.0% | 0.3% | Tourmaline | 0.0% | 48.0% | 0.0% | 0.0% | 0.0% | 2.7% | 1.3% | 0.7% |
| **55** | Grassy | OTz | 47.7% | 0.7% | 4.3% | 6.3% | 0.3% | 0.0% | 1.3% | Zircon, Tourmaline | 2.3% | 2.0% | 4.0% | 3.0% | 0.0% | 6.0% | 2.0% | 20.0% |
| **56** | Grassy | OTz | 48.3% | 0.3% | 5.3% | 5.0% | 0.3% | 0.3% | 1.0% | Zircon, Tourmaline | 3.7% | 3.0% | 4.0% | 3.7% | 0.0% | 4.7% | 3.0% | 17.3% |
| **57** | Grassy | LSF | 46.7% | 0.3% | 5.0% | 4.3% | 0.0% | 0.0% | 0.7% | Tourmaline, Apatite | 8.3% | 5.7% | 4.7% | 3.7% | 0.0% | 5.0% | 3.0% | 12.7% |
| **58** | Grassy | LSF | 40.0% | 0.0% | 9.0% | 4.3% | 0.3% | 0.0% | 0.0% | | 7.3% | 1.3% | 12.0% | 1.3% | 1.0% | 3.7% | 3.3% | 16.3% |
| **59** | Grassy | MSF | 33.7% | 0.0% | 8.7% | 2.3% | 0.3% | 0.0% | 0.3% | Tourmaline | 11.3% | 4.3% | 7.0% | 7.0% | 1.7% | 4.7% | 3.7% | 15.0% |
| **60** | Grassy | MSF | 44.0% | 0.7% | 6.0% | 0.0% | 0.7% | 0.0% | 0.3% | Tourmaline | 13.3% | 0.0% | 3.0% | 4.3% | 1.0% | 6.3% | 2.3% | 18.0% |
| **61** | Grassy | USF | 38.3% | 0.7% | 13.0% | 0.0% | 0.0% | 0.0% | 0.7% | Zircon, Tourmaline | 13.0% | 0.0% | 2.0% | 9.3% | 0.7% | 1.7% | 1.7% | 19.0% |
| **62** | Grassy | USF | 38.7% | 0.3% | 9.7% | 0.0% | 0.3% | 0.0% | 0.0% | | 13.7% | 0.0% | 1.0% | 7.3% | 0.0% | 1.7% | 1.0% | 26.3% |
| **63** | Grassy | FS | 41.7% | 0.3% | 6.3% | 0.0% | 0.3% | 0.0% | 0.0% | | 16.0% | 0.0% | 0.3% | 6.7% | 0.3% | 6.0% | 1.3% | 20.7% |
| **64** | Non-marine Blackhawk Fm. (Grassy) | MC | 34.7% | 0.0% | 6.0% | 1.3% | 0.0% | 0.0% | 1.3% | Zircon, Tourmaline | 20.7% | 0.0% | 2.3% | 2.7% | 0.0% | 3.0% | 2.7% | 25.3% |
| **65** | Kenilworth | OT | 28.7% | 1.0% | 4.0% | 3.7% | 1.3% | 0.3% | 0.7% | Tourmaline, Apatite | 0.0% | 31.7% | 13.3% | 3.3% | 0.0% | 3.3% | 6.7% | 2.0% |
| **66** | Emery | LSF (HCS) | 52.7% | 0.3% | 6.0% | 9.7% | 0.0% | 0.0% | 2.3% | Zircon, Tourmaline, Apatite | 3.3% | 7.7% | 1.0% | 1.3% | 0.0% | 9.7% | 1.0% | 5.0% |
| **67** | Emery | LSF (Bio) | 48.0% | 0.7% | 7.3% | 9.3% | 0.3% | 0.0% | 2.0% | Zircon, Tourmaline | 3.0% | 11.0% | 0.3% | 1.3% | 1.3% | 6.0% | 1.0% | 8.3% |
| **68** | Kenilworth | LSF | 42.3% | 1.0% | 5.7% | 5.3% | 0.7% | 0.0% | 0.0% | | 3.7% | 8.7% | 4.0% | 4.3% | 0.0% | 3.0% | 0.7% | 20.7% |
| **69** | Kenilworth | LSF | 34.3% | 0.7% | 9.3% | 6.0% | 1.3% | 0.0% | 0.3% | Tourmaline | 11.7% | 5.7% | 4.0% | 4.7% | 1.0% | 4.7% | 2.7% | 13.7% |
| **70** | Kenilworth | LSF | 38.3% | 0.3% | 8.7% | 5.7% | 1.3% | 0.0% | 1.7% | Zircon, Tourmaline | 5.0% | 4.0% | 5.0% | 3.0% | 0.0% | 4.0% | 2.0% | 21.0% |

| # | Member | Facies association | Quartz | F-spar | Rock fragments | Carbonate -grains | Muscovite | Biotite | Heavy minerals | Heavy minerals | Quartz-cement | Carbonate-cement | Oxide-cement | Alteration products | Silt-grains | Opaque material | Unknown minerals | Porosity |
|---|---|---|---|---|---|---|---|---|---|---|---|---|---|---|---|---|---|---|
| **71** | Kenilworth | MSF | 34.0% | 0.7% | 6.0% | 6.7% | 0.7% | 0.0% | 0.3% | Tourmaline, Apatite, Rutile | 10.7% | 8.3% | 2.3% | 3.7% | 1.3% | 6.7% | 3.7% | 15.0% |
| **72** | Kenilworth | MSF | 38.7% | 0.3% | 6.7% | 9.7% | 0.7% | 0.0% | 1.0% | Zircon, Tourmaline | 7.7% | 9.7% | 1.3% | 4.0% | 0.0% | 3.0% | 2.0% | 15.3% |
| **73** | Kenilworth | MSF | 41.0% | 0.7% | 4.3% | 5.3% | 1.0% | 0.0% | 0.7% | Tourmaline | 6.7% | 8.3% | 1.7% | 4.0% | 0.0% | 4.3% | 1.7% | 20.3% |
| **74** | Kenilworth | USF | 31.7% | 0.3% | 5.3% | 10.7% | 0.0% | 0.0% | 0.3% | Tourmaline | 8.7% | 4.3% | 6.7% | 2.7% | 0.0% | 8.3% | 1.7% | 19.3% |
| **75** | Kenilworth | USF | 35.7% | 0.3% | 2.0% | 12.0% | 0.0% | 0.0% | 0.3% | Tourmaline | 6.3% | 7.3% | 4.3% | 3.0% | 0.7% | 1.0% | 2.0% | 25.0% |
| **76** | Kenilworth | USF- Rip channel | 39.7% | 0.7% | 4.0% | 4.3% | 0.3% | 0.0% | 0.3% | Tourmaline | 7.3% | 9.3% | 1.7% | 5.3% | 0.0% | 4.0% | 1.0% | 22.0% |
| **77** | Kenilworth | USF | 35.7% | 0.7% | 6.7% | 0.0% | 1.0% | 0.0% | 0.0% |  | 9.0% | 0.0% | 1.0% | 21.0% | 0.0% | 1.7% | 1.0% | 22.3% |
| **78** | Kenilworth | FS | 37.7% | 1.0% | 11.0% | 0.0% | 0.7% | 0.0% | 0.3% | Zircon | 10.0% | 0.0% | 1.7% | 7.7% | 0.0% | 2.0% | 3.0% | 25.0% |

# APPENDIX II

## FIGURES

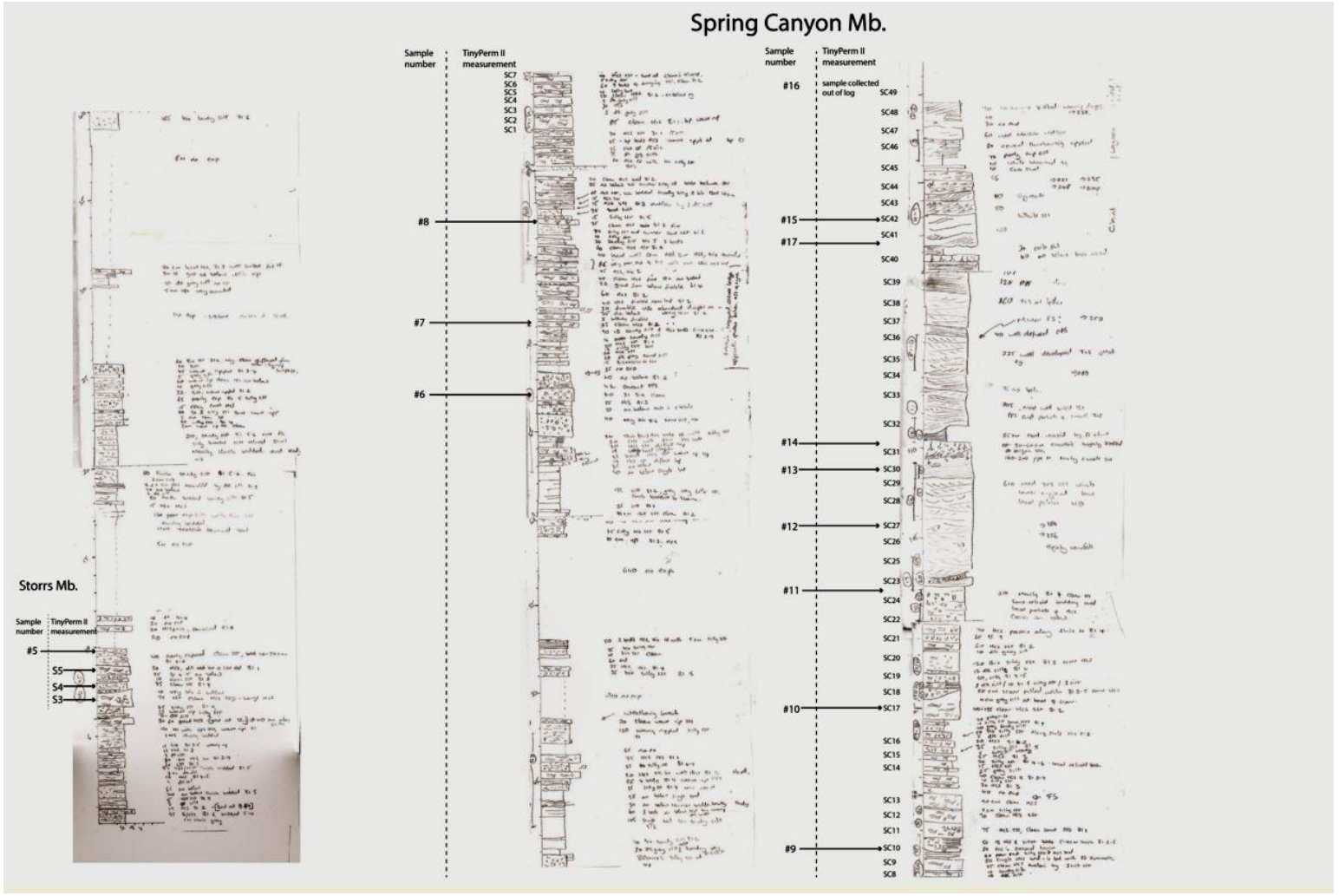


**Fig. 1:** Log by John Howell. The log is of the Storrs Mb. and Spring Canyon Mb. in Gentile Wash location. The position for sampling and permeability measurements are indicated on this log.

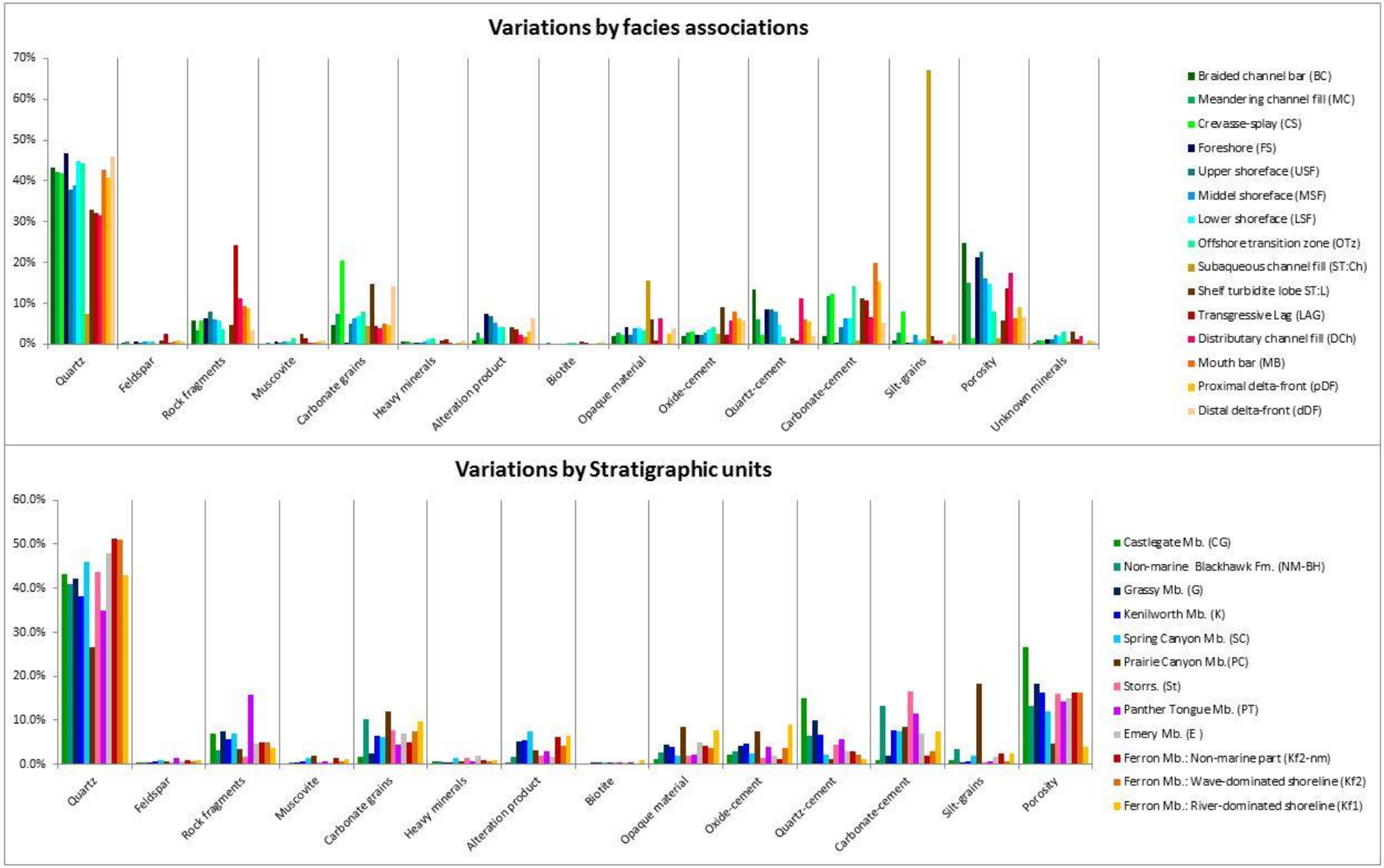


**Fig. 2:** Diagram showing all the point counting data. These diagrams illustrate how the composition of the samples varies with facies associations and stratigraphic units.

# APPENDIX III

## THIN SECTION PHOTOS AND SEM RESULTS

Due to space limitations most of this appendix can be found in this dropbox link:

https://www.dropbox.com/sh/uodl7szv8x6o6rn/AABwOFNG7s0IdFjLVAq20Wb-a?dl=0

This appendix in includes:

- Thin section photos used to navigate the scanning electron microscope
- SEM images
- SEM results for sample 36
- SEM results for sample 40
- SEM results for sample 62
- SEM results for sample 71
- Thin section photos for all the collected samples

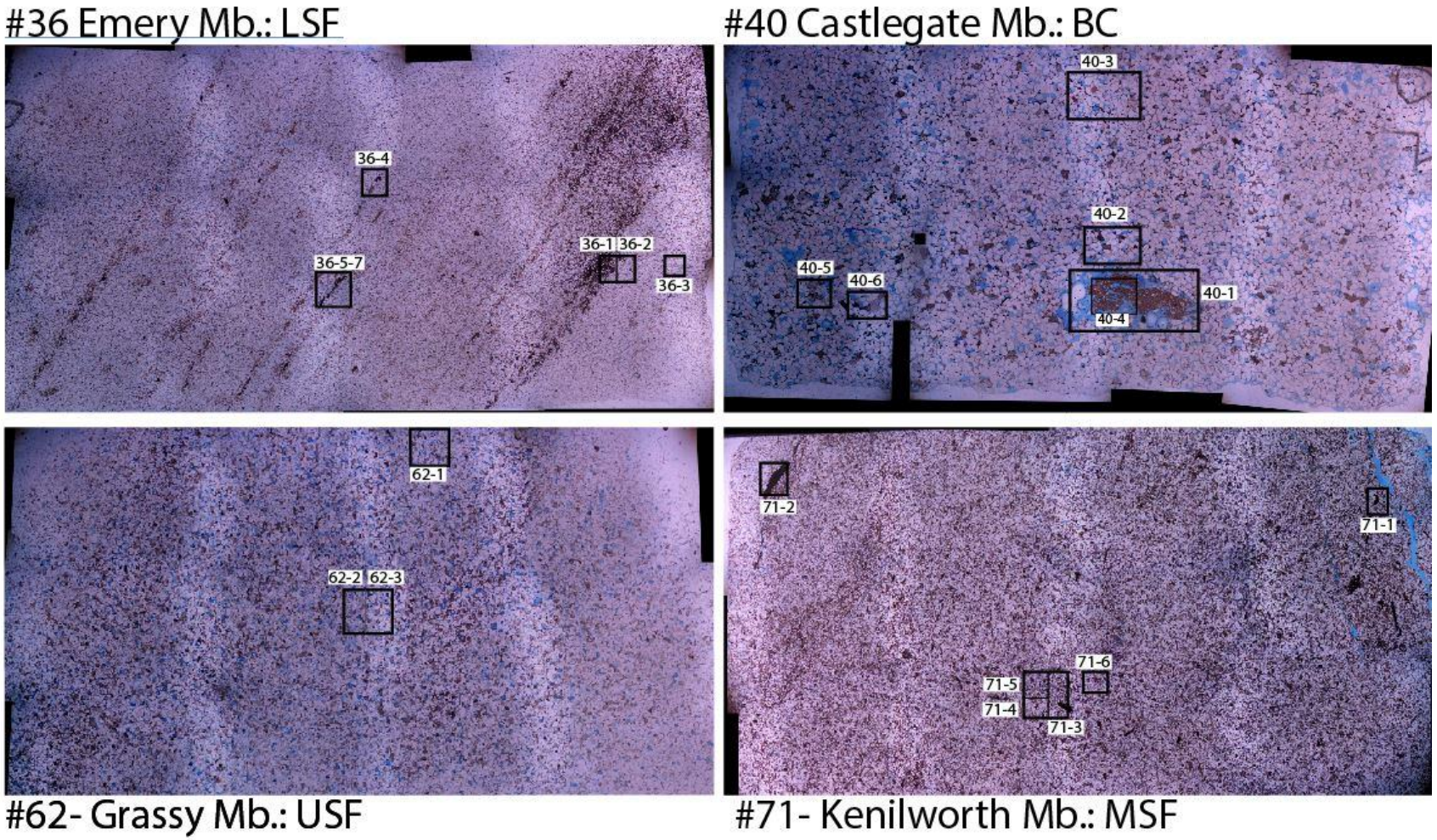


**Fig. 3:** These thin section photos are a product of stitching 12 photos with a magnification of 10 (the 1 X lens was used). The black squares represent the areas where SEM analyses were done, and the number represents the analysis number. The results from these analyses are found in the dropbox appendix: https://www.dropbox.com/sh/uodl7szv8x6o6rn/AABwOFNG7s0IdFjLVAq20Wb-a?dl=0